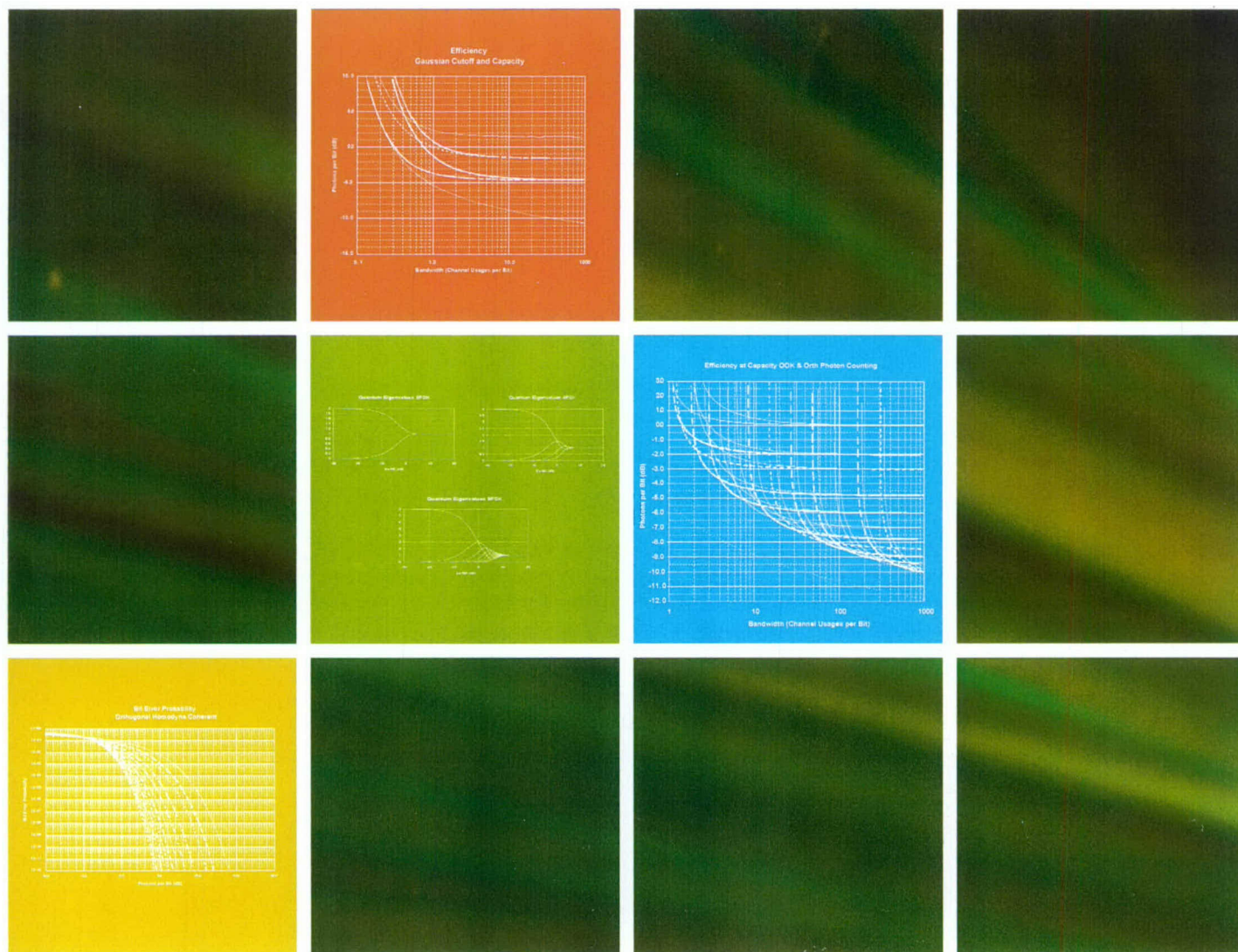


Optical Communications

A Compendium of Signal Formats, Receiver Architectures,
Analysis Mathematics, and Performance Comparisons



Don M. Boroson

Approved for public release; distribution unlimited.

2005


This report is based on studies performed at Lincoln Laboratory, a center for research operated by Massachusetts Institute of Technology. This work was sponsored by NASA under Air Force Contract FA8721-05-C-0002.

This report may be reproduced to satisfy needs of U.S. Government agencies.

The ESC Public Affairs Office has reviewed this report, and it is releasable to the National Technical Information Service, where it will be available to the general public, including foreign nationals.

This technical report has been reviewed and is approved for publication.

FOR THE COMMANDER


Gary Tufungian
Administrative Contracting Officer
Plans and Programs Directorate
Contracted Support Management

Non-Lincoln Recipients

PLEASE DO NOT RETURN

Permission has been given to destroy this document when it is no longer needed.



Massachusetts Institute of Technology
Lincoln Laboratory

OPTICAL COMMUNICATIONS:
A Compendium of Signal Formats, Receiver Architectures,
Analysis Mathematics, and Performance Characteristics

Don M. Boroson

9 September 2005

Approved for public release; distribution is unlimited.

Report 60-1054

Lexington

Massachusetts

ACKNOWLEDGMENTS

My thanks to Michael Yang, who wrote most of the programs used to generate the many curves presented here and then creatively bundled them into a highly useful tool. Along the way, he also caught and corrected many algebraic errors, for which we all thank him. Thanks to Richard Barron who provided many interesting discussions and several of the curves. Thanks also to Chuck Niessen and Jeff Shapiro for reading and commenting on a preliminary draft. Finally, I must certainly acknowledge the sizeable contribution of my editor, Dorothy Ryan, whose talents are responsible for this great-looking document.

TABLE OF CONTENTS

Acknowledgments	iii
List of Illustrations	vii
List of Tables	vii
List of Charts	ix
Preface	xvii
1. INTRODUCTION	1
2. PRELIMINARIES	3
2.1 Communication Systems Options and Requirements	3
2.2 The Classical Receivers	3
Noiseless Photon Counter	3
Heterodyne	4
Homodyne	7
Preamplification	8
Real Detectors	9
2.3 Requirements of the Classical Receivers	9
3. INFORMATION THEORY OF CLASSICAL SYSTEMS	15
3.1 Notation and Basic Error Probability Formulas for Classical Systems	15
3.2 Classical Channel Capacity	17
Definition	17
Capacity Formulas—Hard Decision	17
Capacity Formulas—Soft Decision	19
Measure of Efficiency	20
3.3 Classical Computation Cutoff Rate	21
Definition	21
Cutoff Rate Formulas—Hard Decision	21
Cutoff Rate Formulas—Soft Decision	22
4. INFORMATION THEORY OF QUANTUM SYSTEMS	25
Definitions	25
Quantum Optimum—Hard Decision	26
Quantum Capacity—Maximum Likelihood (Soft Decisions)	28
Quantum Cutoff Rate—Maximum Likelihood (Soft Decisions)	30
The Square-Root Measurement	31
Conclusions	31
5. MODULATION FORMATS	33
5.1 Generalized On-Off Keying (OOK)	33
OOK: Preliminaries	33
OOK: Noiseless Photon-Counting Hard Decisions	33
OOK: Heterodyne and Homodyne Receivers—Coherent Hard Decisions	34

TABLE OF CONTENTS (CONTINUED)

OOK: Preamplified and Heterodyne Receivers—Noncoherent Hard Decisions	36
OOK: Quantum Receiver—Hard Decisions	37
OOK: Photon-Counting Soft Decisions	37
OOK: Heterodyne and Homodyne Receivers—Coherent Soft Decisions	37
OOK: Preamplified and Heterodyne Receivers—Noncoherent Soft Decisions	38
OOK: Quantum Receiver—Maximum-Likelihood Decoding	39
5.2 Orthogonal Modulations—PPM and FSK	39
Orthogonal: Preliminaries	39
Orthogonal: Photon-Counting Hard Decisions	40
Orthogonal: Heterodyne and Homodyne Receivers—Coherent Hard Decisions	42
Orthogonal: Preamplified and Heterodyne Receivers—Noncoherent Hard Decisions	42
Orthogonal: Quantum Receiver—Hard Decisions	43
Orthogonal: Photon-Counting Soft Decisions	44
Orthogonal: Heterodyne and Homodyne Receivers—Coherent Soft Decisions	44
Orthogonal: Preamplified and Heterodyne Receivers—Noncoherent Soft Decisions	46
Orthogonal: Quantum Receiver—Maximum-Likelihood Decoding	46
5.3 <i>M</i> -ary Phase Shift Keying—MPSK	47
PSK: Preliminaries	47
PSK: Photon-Counting Hard Decisions	48
PSK: Heterodyne and Homodyne Receivers—Coherent Hard Decisions	51
PSK: Preamplified and Heterodyne Receivers—Noncoherent Hard Decisions	52
PSK: Quantum Receiver—Hard Decisions	54
PSK: Photon-Counting Soft Decisions	54
PSK: Heterodyne and Homodyne Receivers—Coherent Soft Decisions	55
PSK: Preamplified and Heterodyne Receivers—Noncoherent Soft Decisions	56
PSK: Quantum Receiver—Maximum-Likelihood Decoding	56
6. DISCUSSION AND COMPARISON OF SOME MODULATION FORMATS AND RECEIVERS	57
7. CONCLUSION	61
References	63

LIST OF ILLUSTRATIONS

Figure No.		Page
1	The optical communication system.	2
2	Heterodyne receiver (balanced configuration).	4
3	Heterodyne signal structure.	6
4	Definition of Craig's function.	6
5	Homodyne receiver (balanced configuration).	7
6	Binary receiver options.	11
7	M-ary receiver options.	12
8	Photon-counting DPSK receiver.	48
9	Photon-counting 2PSK receiver—balanced LO version.	49

LIST OF TABLES

Table No.		Page
1	Knowledge Requirements of Communications Receivers	13
2	Event Probabilities for the Bondurant Type I Photon-Counting Receiver for QPSK	50
3	Bit-Error Rate Formulas for Binary Modulations	59

LIST OF CHARTS

Chart No.	Page
1	67
2	69
3	70
4	71
5	73
6	74
7	75
8	76
9	77
10	78
11	79
12	81
13	82
14	83
15	84
16	85
17	87
18	88
19	89
20	90
21	91
22	93
23	94
24	95
25	96
26	97
27	99
28	100
29	101
30	102

LIST OF CHARTS (CONTINUED)

31	Efficiency at classical cutoff OOK heterodyne and preamplified noncoherent hard decision.	103
32	Symbol error probability OOK ($p_0 = p_1 = 1/2$) quantum hard decision.	105
33	Classical capacity OOK quantum hard decision.	106
34	Efficiency at classical capacity OOK quantum hard decision.	107
35	Classical cutoff OOK quantum hard decision.	108
36	Efficiency at classical cutoff OOK quantum hard decision.	109
37	Classical capacity OOK heterodyne coherent soft decision.	110
38	Efficiency at classical capacity OOK heterodyne coherent soft decision.	111
39	Classical cutoff OOK heterodyne coherent soft decision.	112
40	Efficiency at classical cutoff OOK heterodyne coherent soft decision.	113
41	Classical capacity OOK homodyne coherent soft decision.	114
42	Efficiency at classical capacity OOK homodyne coherent soft decision.	115
43	Classical cutoff OOK homodyne coherent soft decision.	116
44	Efficiency at classical cutoff OOK homodyne coherent soft decision.	117
45	Classical capacity OOK heterodyne and preamplified noncoherent soft decision.	118
46	Efficiency at Classical Capacity OOK heterodyne and preamplified noncoherent soft decision.	119
47	Classical cutoff OOK heterodyne and preamplified noncoherent soft decision.	120
48	Efficiency at classical cutoff OOK heterodyne and preamplified noncoherent soft decision.	121
49	Quantum capacity OOK.	122
50	Efficiency at quantum capacity OOK.	123
51	Quantum cutoff OOK.	124
52	Efficiency at quantum cutoff OOK.	125
53	Symbol error (erasure) probability orthogonal photon counting.	126
54	Bit-error probability orthogonal photon counting.	127
55	Classical capacity orthogonal photon counting.	128
56	Efficiency at classical capacity orthogonal photon counting.	129
57	Classical cutoff orthogonal photon counting.	130
58	Efficiency at classical cutoff orthogonal photon counting.	131
59	Symbol error probability orthogonal heterodyne coherent.	132
60	Bit-error probability orthogonal heterodyne coherent.	133
61	Classical capacity orthogonal heterodyne coherent hard decision.	134
62	Efficiency at classical capacity orthogonal heterodyne coherent hard decision.	135

LIST OF CHARTS (CONTINUED)

63	Classical cutoff orthogonal heterodyne coherent hard decision.	136
64	Efficiency at classical cutoff orthogonal heterodyne coherent hard decision.	137
65	Symbol error probability orthogonal homodyne coherent.	138
66	Bit-error probability orthogonal homodyne coherent.	139
67	Classical capacity orthogonal homodyne coherent hard decision.	140
68	Efficiency at classical capacity orthogonal homodyne coherent hard decision.	141
69	Classical cutoff orthogonal homodyne coherent hard decision.	142
70	Efficiency at classical cutoff orthogonal homodyne coherent hard decision.	143
71	Symbol error probability orthogonal heterodyne and preamplified noncoherent.	144
72	Bit-error probability orthogonal heterodyne and preamplified noncoherent.	145
73	Classical capacity orthogonal heterodyne and preamplified noncoherent hard decision.	146
74	Efficiency at classical capacity orthogonal heterodyne and preamplified noncoherent hard decision.	147
75	Classical cutoff orthogonal heterodyne and preamplified noncoherent hard decision.	148
76	Efficiency at classical cutoff orthogonal heterodyne and preamplified noncoherent hard decision.	149
77	Symbol error probability orthogonal quantum.	150
78	Bit-error probability orthogonal quantum.	151
79	Classical capacity orthogonal quantum hard decision.	152
80	Efficiency at classical capacity orthogonal quantum hard decision.	153
81	Classical cutoff orthogonal quantum hard decision.	154
82	Efficiency at classical cutoff orthogonal quantum hard decision.	155
83	Classical capacity orthogonal heterodyne coherent soft decision.	156
84	Efficiency at classical capacity orthogonal heterodyne coherent soft decision.	157
85	Classical cutoff orthogonal heterodyne coherent soft decision.	158
86	Efficiency at classical cutoff orthogonal heterodyne coherent soft decision.	159
87	Classical capacity orthogonal homodyne coherent soft decision.	160
88	Efficiency at classical capacity orthogonal homodyne coherent soft decision.	161
89	Classical cutoff orthogonal homodyne coherent soft decision.	162
90	Efficiency at classical cutoff orthogonal homodyne coherent soft decision.	163
91	Classical capacity orthogonal heterodyne and preamplified noncoherent soft decision.	164
92	Efficiency at classical capacity orthogonal heterodyne and preamplified noncoherent soft decision.	165
93	Classical cutoff orthogonal heterodyne and preamplified noncoherent soft decision.	166

LIST OF CHARTS (CONTINUED)

94	Efficiency at classical cutoff orthogonal heterodyne and preamplified noncoherent soft decision.	167
95	Quantum capacity orthogonal.	168
96	Efficiency at quantum capacity orthogonal.	169
97	Quantum cutoff orthogonal.	170
98	Efficiency at quantum cutoff orthogonal.	171
99	Symbol error probability MPSK photon counting.	172
100	Bit-error probability MPSK photon counting.	173
101	Classical capacity MPSK photon counting hard decision.	174
102	Efficiency at classical capacity MPSK photon counting hard decision.	175
103	Classical cutoff MPSK photon counting hard decision.	176
104	Efficiency at classical cutoff MPSK photon counting hard decision.	177
105	Symbol error probability MPSK heterodyne coherent.	178
106	Bit-error probability MPSK heterodyne coherent.	179
107	Classical cutoff MPSK heterodyne coherent pure hard decision.	180
108	Efficiency at classical cutoff MPSK heterodyne coherent pure hard decision.	181
109	Classical capacity MPSK heterodyne coherent hard decision with ML decoding.	182
110	Efficiency at classical capacity MPSK heterodyne coherent hard decision with ML decoding.	183
111	Classical cutoff MPSK heterodyne coherent hard decision with ML decoding.	184
112	Efficiency at classical cutoff MPSK heterodyne coherent hard decision with ML decoding.	185
113	Symbol error probability MPSK homodyne coherent.	186
114	Bit-error probability MPSK homodyne coherent.	187
115	Classical capacity MPSK homodyne coherent hard decision.	188
116	Efficiency at classical capacity MPSK homodyne coherent hard decision.	189
117	Classical cutoff MPSK homodyne coherent hard decision.	190
118	Efficiency at classical cutoff MPSK homodyne coherent hard decision.	191
119	Symbol error probability MPSK heterodyne and preamplified noncoherent.	192
120	Bit-error probability MPSK heterodyne and preamplified noncoherent.	193
121	Classical cutoff MPSK heterodyne and preamplified noncoherent hard decision pure hard decision.	194
122	Efficiency at classical cutoff MPSK heterodyne and preamplified noncoherent hard decision pure hard decision.	195
123	Classical capacity MPSK heterodyne and preamplified noncoherent hard decision with ML decoding.	196

LIST OF CHARTS (CONTINUED)

124	Efficiency at classical capacity MPSK heterodyne and preamplified noncoherent hard decision with ML decoding.	197
125	Classical cutoff MPSK heterodyne and preamplified noncoherent hard decision with ML decoding.	198
126	Efficiency at classical cutoff MPSK het & preamplified non-coh hard decision with ML decoding.	199
127	Symbol error probability MPSK quantum.	200
128	Bit-error probability MPSK quantum.	201
129	Classical capacity MPSK quantum hard decision.	202
130	Efficiency at classical capacity MPSK quantum hard decision.	203
131	Classical cutoff MPSK quantum hard decision.	204
132	Efficiency at classical cutoff MPSK quantum hard decision.	205
133	Classical capacity 4PSK photon counting hard decision with ML decoding.	206
134	Efficiency at classical capacity 4PSK photon counting hard decision with ML decoding.	207
135	Classical capacity MPSK heterodyne coherent soft decision.	208
136	Efficiency at classical capacity MPSK heterodyne coherent soft decision.	209
137	Classical cutoff MPSK heterodyne coherent soft decision.	210
138	Efficiency at classical cutoff MPSK heterodyne coherent soft decision.	211
139	Classical capacity MPSK homodyne coherent soft decision.	212
140	Efficiency at classical capacity MPSK homodyne coherent soft decision.	213
141	Classical cutoff MPSK homodyne coherent soft decision.	214
142	Efficiency at classical cutoff MPSK homodyne coherent soft decision.	215
143	Classical capacity MPSK heterodyne and preamplified noncoherent soft decision.	216
144	Efficiency at classical capacity MPSK heterodyne and preamplified noncoherent soft decision.	217
145	Classical cutoff MPSK heterodyne and preamplified noncoherent soft decision.	218
146	Efficiency at classical cutoff MPSK heterodyne and preamplified noncoherent soft decision.	219
147	Quantum capacity MPSK.	220
148	Efficiency at quantum capacity MPSK.	221
149	Quantum cutoff MPSK.	222
150	Efficiency at quantum cutoff MPSK.	223
151	Comparison: Capacity and cutoff for classical and quantum Gaussian.	224
152	Comparison: Efficiencies at classical Gaussian capacity, classical Gaussian cutoff, quantum Gaussian capacity, quantum Gaussian cutoff.	225

LIST OF CHARTS (CONTINUED)

153	Comparison: BER, OOK ($p_1 = 1/2$)—preamplified noncoherent, heterodyne coherent, homodyne coherent, photon counting, quantum.	226
154	Comparison: BER, orthogonal ($M = 2$)—preamplified noncoherent, heterodyne coherent, homodyne coherent, photon counting, quantum.	227
155	Comparison: BER, orthogonal ($M = 4$)—preamplified noncoherent, heterodyne coherent, homodyne coherent, photon counting, quantum.	228
156	Comparison: BER, PSK ($M = 2$)—preamplified noncoherent (DPSK), heterodyne coherent, homodyne coherent, photon counting, quantum.	229
157	Comparison: Efficiency at capacity, binary modulations—OOK ($p_1 = 1/2$), PPM, and PSK, each at preamplified noncoherent, heterodyne coherent, and quantum, and Gaussian quantum.	230
158	Comparison: Efficiency at capacity, OOK, $p_1 = 1/2$, soft and hard decisions, preamplified noncoherent, heterodyne coherent, homodyne coherent, photon counting, quantum, and Gaussian quantum.	231
159	Comparison: Efficiency at capacity, OOK, $p_1 = 1/4$, soft and hard decisions, preamplified noncoherent, heterodyne coherent, homodyne coherent, photon counting, quantum, and Gaussian quantum.	232
160	Comparison: Efficiency at capacity, OOK, $p_1 = 1/16$, soft and hard decisions, preamplified noncoherent, heterodyne coherent, homodyne coherent, photon counting, quantum, and Gaussian quantum.	233
161	Comparison: Efficiency at capacity, OOK, $p_1 = 1/64$, soft and hard decisions, preamplified noncoherent, heterodyne coherent, homodyne coherent, photon counting, quantum, & Gaussian quantum.	234
162	Comparison: Efficiency at capacity, OOK, $p_1 = 1/256$, soft and hard decisions, preamplified noncoherent, heterodyne coherent, homodyne coherent, photon counting, quantum, & Gaussian quantum.	235
163	Comparison: Efficiency at capacity, orthogonal, $M = 2$, soft and hard decisions, preamplified noncoherent, heterodyne coherent, homodyne coherent, photon counting, quantum, & Gaussian quantum.	236
164	Comparison: Efficiency at capacity, orthogonal, $M = 4$, soft and hard decisions, preamplified noncoherent, heterodyne coherent, homodyne coherent, photon counting, quantum, and Gaussian quantum.	237
165	Comparison: Efficiency at capacity, orthogonal, $M = 16$, soft and hard decisions, preamplified noncoherent, heterodyne coherent, homodyne coherent, photon counting, quantum, and Gaussian quantum.	238
166	Comparison: Efficiency at capacity, orthogonal, $M = 64$, soft and hard decisions, preamplified noncoherent, heterodyne coherent, homodyne coherent, photon counting, quantum, and Gaussian quantum.	239

LIST OF CHARTS (CONTINUED)

167	Comparison: Efficiency at capacity, orthogonal, $M = 256$, soft and hard decisions, preamplified noncoherent, heterodyne coherent, homodyne coherent, photon counting, quantum, and Gaussian quantum.	240
168	Comparison: Efficiency at capacity, OOK and orthogonal— $M (1/p_1) = 2, 3, 4, 8, 16, 32, 64, 128, 256, 512, 1024$, soft decision, preamplified noncoherent.	241
169	Comparison: Efficiency at capacity, OOK and orthogonal— $M (1/p_1) = 2, 3, 4, 8, 16, 32, 64, 128, 256, 512, 1024$, soft decision—heterodyne-coherent, and classical Gaussian.	242
170	Comparison: Efficiency at capacity, OOK and orthogonal— $M (1/p_1) = 2, 3, 4, 8, 16, 32, 64, 128, 256, 512, 1024$, soft decision—photon counting, and Gaussian quantum.	243
171	Comparison: Efficiency at capacity, OOK and orthogonal— $M (1/p_1) = 2, 3, 4, 8, 16, 32, 64, 128, 256, 512, 1024$, soft decision—quantum ML, and Gaussian quantum.	244
172	Comparison: Efficiency at capacity, MPSK, $M = 2$, soft decision—preamplified DPSK, heterodyne coherent, homodyne coherent, photon counting, quantum, and Gaussian quantum.	245
173	Comparison: Efficiency at capacity, MPSK, $M = 4$, soft decision—preamplified DQPSK, heterodyne coherent, Bondurant photon counting, quantum HD, Gaussian coded, and Gaussian quantum.	246
174	Comparison: Efficiency at capacity, quantum coded.	247
175	Quantum eigenvalues (λ_k): OOK.	248
176	Quantum eigenvalues (v_k): Orthogonal.	249
177	Quantum eigenvalues (v_k): PSK.	250

PREFACE

There are a number of options for modulation formats in optical fiber and free-space lasercom systems. There are a seemingly even greater number of options for receiver architectures. Although most of these possibilities and combinations have been analyzed in journal publications and textbooks, there does not seem to be a *single* place to look for all relevant results concerning these options. Furthermore, comparisons of the options do not seem to have been methodically tabulated.

In this work, then, we will present, describe, analyze, and compare the theoretical communications performance metrics of the most common optical modulation formats paired with the basic classes of receiver types.

Before we start, however, we must warn the reader that this material is not presented in the style of a standard textbook, with the concepts painstakingly developed and derived from first principles. The style we have taken throughout is to present the required mathematical formulas and show the performance curves, but to give only the sketchiest of derivations, if any. Similarly, detailed references are given in only some cases although the more general textbook references listed may help to fill in many missing details. It is hoped that the specific topics discussed, the formulas presented, and the several references given, along with some simple library and web search skills, will lead interested readers to as much extra development and detail as they find interesting or useful.

Despite what this report is *not*, though, we hope that, as a compendium, it will find utility for the communications engineer and analyst. We have also tried to sprinkle throughout comments, observations, and opinions that are not generally found in technical treatises. We hope these are useful to the reader.

1. INTRODUCTION

The most common transmission formats used in optical communications systems include on-off keying (OOK), phase shift keying (PSK), and the so-called orthogonal modulations—pulse position modulation (PPM), frequency shift keying (FSK), and orthogonal polarization shift keying (POLSK). (Of course, optical signaling has at least as many other variants as classical radio and electronic signaling, but we will constrain ourselves in this report to the listed formats, which have been used traditionally.) For each of these, we will examine several receiver architectures, including preamplified, heterodyne, homodyne, photon counting, and optimum quantum. We will examine both coherent and incoherent receivers when applicable. Metrics to be examined include the bit and symbol error rates of uncoded systems and the channel capacity and computation cutoff rate of coded systems. For these, we will examine both hard-decision and maximum-likelihood (soft-decision) algorithms.

We will be assuming that the system is noiseless in that only transmitted photons are received and that additive noise in the receiver can appear only due to imperfect reception mechanisms. Obviously, in a real system, these assumptions would need to be examined and likely relaxed.

Radio frequency (RF) signals are generally modeled with the viewpoint that they would have been perfectly measurable, if only the additive noise at the receiver had not corrupted the measurement. On the other hand, the quantum nature of optical signals—even noiseless signals—means that they are, at their core, not perfectly measurable. Errors are made because of this quantum measurement inadequacy, not because of the corruption of any additive noise (unless, of course, noise is also added at the receiver, such as by an optical amplifier). The best receivers are based on knowledge of this property.

The generic communication system we will be discussing is shown in Figure 1. Bits are presented to the system by an external data source. We may decide to use error-correction coding to improve power efficiency. The encoder maps groups of source bits into groups of encoded “channel bits.” These encoded channel bits may be further mapped into “channel symbols,” which then direct the operation of the modulated optical signal generator. (In fact, the bits-to-symbols mapping may have been done at the input to the encoder or in the encoder itself.)

To increase transmitted power, there may be an optical amplifier. The (lossy) channel is here assumed to include everything—transmitter optics, beam spreading losses, channel attenuation, and receiver optics—between this amplifier and the receiver, which then makes measurements of the channel symbols. Finally, the outputs of this receiver box are fed to a de-mapper and/or decoder, whose outputs are estimates of the original source data bits and which are sent on to the destination. Modern systems may combine certain of these functions in various ways, but we will use this block diagram with the understanding that variants will have obvious analysis extensions.

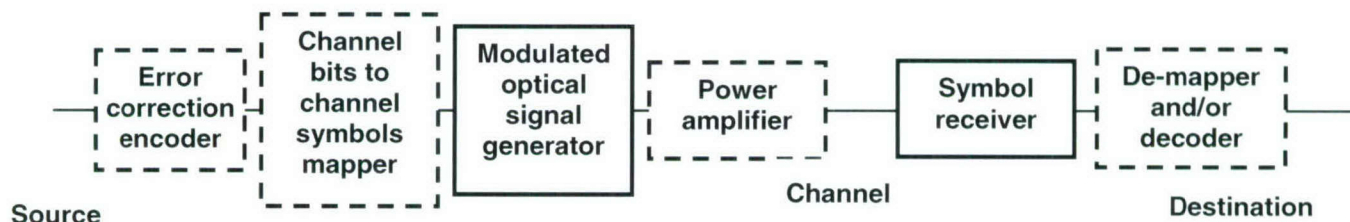


Figure 1. The optical communication system.

The structure of this report is as follows:

Preliminaries

- System Options and Requirements
- The Classical Receivers

Information Theory of Classical Systems

- Notation and Basic Error Probability Formulas for Classical Systems
- Classical Channel Capacity
- Classical Computation Cutoff Rate

Information Theory of Quantum Systems

Modulation Formats

- Generalized On-Off Keying
- Orthogonal Modulations—PPM and FSK
- M -ary Phase Shift Keying (MPSK)

Comparisons

For those readers interested only in the performance results, the Preliminaries sections can be skipped.

2. PRELIMINARIES

2.1 COMMUNICATION SYSTEMS OPTIONS AND REQUIREMENTS

Possibilities for signal generation depend upon the existence of technologies that can vary, at the desired symbol rate, the parameter of interest and then can send the constructed signal, at adequately high power, to the receiver. Thus, the selection of formats will be directed by the availability of, for example, direct laser modulation of amplitude, wavelength, or phase; or of external modulation of amplitude, polarization, or phase. Further, the availability of peak- vs average-limited power generation will favor certain choices.

Once a transmission format has been selected, there exists a hierarchy of receiver structures that can be employed, depending on what is easily known or measurable at the receiver. Selection here will depend upon knowledge of signal frequency (or equivalently wavelength), phase, amplitude, spatial properties, waveform shape, timing, and polarization. This selection is also driven by available receiver technologies with adequate bandwidths.

Each pairing of a modulation format with a receiver structure has its own set of analytical tools and derived performance. To walk through this tree of possibilities, in this work we will first examine the analysis mathematics applicable to the various receivers and then apply them to each major family of modulations.

Therefore, let us first survey the main receiver types.

2.2 THE CLASSICAL RECEIVERS

Noiseless Photon Counter

In this theoretical device, we make the classical assumption of photons being detected with Poisson statistics at a rate proportional to the instantaneous signal power.

$$P_{Pois}(k | N) \equiv \frac{N^k}{k!} e^{-N} \quad k = 0, 1, 2, \dots \quad (1)$$

Here, P_{Pois} is the probability of counting k photons in a measurement period where N is the *average* number of photons (possibly fractional) that could have been expected in such a period. The perfect photon counter has a detection efficiency of 1. (We also assume in this work that there are no noise photons in such a system. Since performance in noise can be shown to depend on two parameters—the signal photons per symbol and the noise photons per symbol—and not just their ratio, as in RF systems, we will not cover this case in this work. Technologies presented here, however, have direct applicability to the noisy case, with noises also modeled as photons counted with Poisson statistics.) Thus, at an average arrival rate of λ photons per second over a time of T seconds, we see that $N = \lambda T$. We can also

see that there is always a finite probability of not detecting a photon (i.e., counting 0 photons) when a signal is actually present, and this probability is given by

$$P_{\text{Pois}}(0 | N) = e^{-N}. \quad (2)$$

(Note that for a signal with a received power such that there is, on average, one photon to be detected per period of time, if we count photons over many such periods of time, we will count zero in 1/e or 37% of them.) In modulations based on the existence or non-existence of pulses, then, errors with such a receiver will be made only if pulses were “supposed to” exist but were not detected. (This fact is sometimes called the quantum limit, but we will see that there are better uses for this term.)

True noiseless photon-counting devices with high detection efficiency and wide bandwidth are difficult to build. Technology for them is rapidly growing, however.

Heterodyne

The architecture for a (balanced) heterodyne front end is shown in Figure 2.

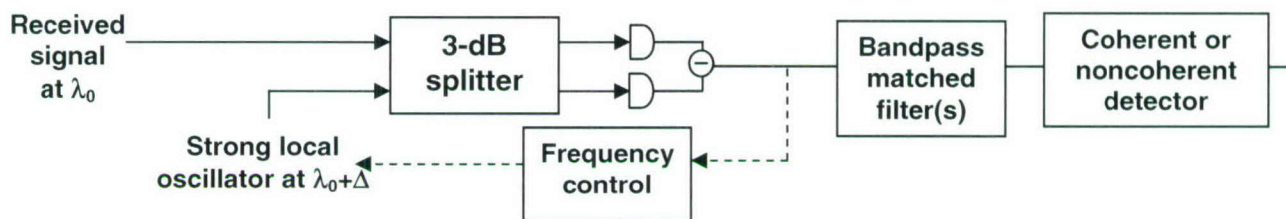


Figure 2. Heterodyne receiver (balanced configuration).

At the receiver, a strong local oscillator (LO) laser beam is combined, in a beam-splitter, with the very small incoming optical signal. The LO is constant amplitude (or constant wave, CW) and its wavelength is selected (or controlled) to be near but not equal to the wavelength of the received signal. (Note: polarization must also be matched in classical heterodyne receivers, but there are variants that do not require polarization [14].) The combined signal is detected at (a differenced pair of balanced) square-law devices whose electrical output can be shown to be a sum of the “beat signal” between the two signals plus the so-called shot noise induced by the photons in the small, received signal. By the selection of the wavelength offset, the electrical beat signal comes out at a desired intermediate frequency. With proper choice of this frequency, standard RF radio receiver techniques, such as electrical filtering, etc., can be employed in further processing. Thus, this heterodyne front end can be followed by a simple square-law detector, by frequency-selective elements, or by coherent receivers, all in the electrical domain.

When the local oscillator power is very large compared to the received signal power, the output electrical signal is well modeled as an undistorted but amplified copy of the input optical signal, now embedded in white Gaussian noise and with its carrier frequency now set at the intermediate frequency. Since phase (relative to the LO) has been preserved, either coherent or noncoherent techniques can be used in further processing and in the detection process.

It is well known that the optimum processing to perform in additive white Gaussian noise is to apply a so-called matched filter, matched to the signal, with the output of the filter then sampled at the point of largest signal-to-noise ratio (SNR). (See, for example, [17].)

This sampled output has an SNR equal to (as described in RF systems) E_s/N_0 (signal symbol energy divided by the noise spectral density). It can be shown that for our heterodyne receiver, this value is equal to the input photons-per-symbol! With this equivalence, we see that all discussions and analyses of classical receivers in this work are applicable to RF systems.

The probability density function of the sampled output signal, properly normalized, at the output of a *coherent* receiver is Gaussian

$$f_G(x - \sqrt{2N_s}) , \quad (3)$$

where

$$f_G(x) \equiv \frac{1}{\sqrt{2\pi}} \exp\left(-\frac{x^2}{2}\right) \quad (4)$$

and its cumulative distribution function is

$$\begin{aligned} \Phi(y) &\equiv \int_y^\infty f_G(x) dx \\ &\equiv \frac{1}{2} \operatorname{erfc}(y/\sqrt{2}) . \end{aligned} \quad (5)$$

There are many algorithms for efficiently calculating this well-known function.

A constraint on heterodyne systems is that the wide bandwidth electrical lasercom signal must appear on a carrier at an intermediate frequency, which means that the detection and the electrical processing must be done with a total bandwidth likely 1.5–3 times as wide as the lasercom signal itself. This is illustrated in Figure 3.

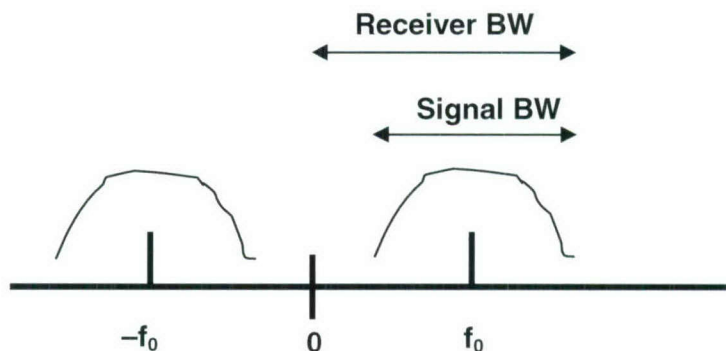


Figure 3. Heterodyne signal structure.

Another constraint is that the local oscillator must be strong enough (a) to allow the output beat signal to well-approximate an undistorted signal in noise and (b) to allow the heterodyne “gain” to be large enough that the Gaussian noise level, set by the incoming signal, is larger than any intrinsic thermal noises in the detection and post-processing electronics.

For so-called quadrature modulations—meaning that the signal varies in the two dimensions, in-phase and quadrature—it turns out we will need to calculate the two-dimensional Gaussian probability of the plane missing a wedge-shaped section, as shown in Figure 4.

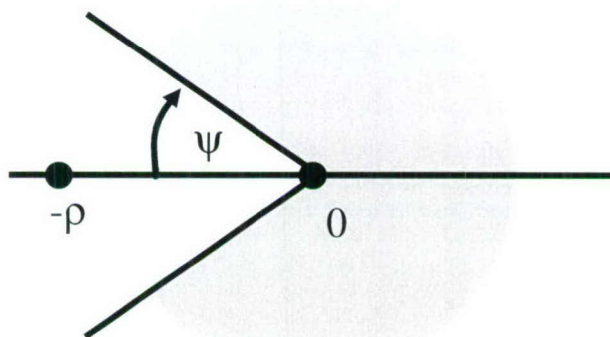


Figure 4. Definition of Craig's function.

Although there have been many versions of formulas defining this probability, Craig's function [7], which can be expressed as

$$f_C(\rho, \psi) \equiv \frac{1}{\pi} \int_0^{\pi-\psi} \exp\left[-\frac{\rho^2 \sin^2(\psi)}{2 \sin^2(\phi)}\right] d\phi, \quad (6)$$

seems to have the best properties, including its ease of numerical integration and the fact that the SNR value is presented linearly in the exponent of the integrand. Here, $\rho^2/2$ is the symbol signal-to-noise ratio.

Homodyne

The architecture for a homodyne front end is shown in Figure 5.

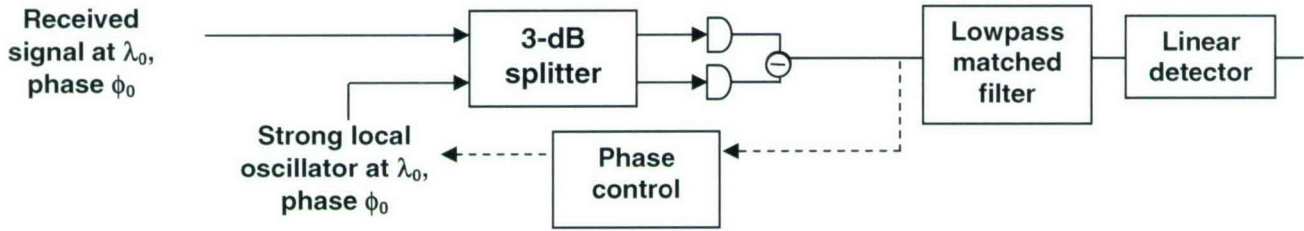


Figure 5. Homodyne receiver (balanced configuration).

The difference between homodyne and heterodyne is that the homodyne local oscillator is at exactly the same wavelength/frequency, polarization, and optical phase as the incoming signal. The output beat signal is thus a coherently derived baseband signal (near DC). There is no intermediate frequency carrier. The expanded-bandwidth requirement of the heterodyne system is thereby avoided. Furthermore, it can be shown mathematically that the signal-to-noise ratio at the output of the filter/sampler is double that of heterodyne—that is, 3 dB better—due to the lack of an “image” signal at minus frequencies. (See Figure 3.) The probability density function of the output of a homodyne receiver is the same as that of heterodyne, but as if the SNR were twice as large.

The drawbacks of homodyne are that (a) an optical phase-locked loop with very tight coupling back to the input is required to keep the LO in phase with the received signal and (b) the “baseband” output really only carries amplitude and sign information and thus supports only one-dimensional signals. Variations of this architecture that try to measure two-dimensional, phase-related modulations (such as QPSK—where a homodyne QPSK receiver splits the signals with an optical hybrid [3]) turn out to give performance that is no better than heterodyne. On the other hand, such a homodyne QPSK receiver allows for a coherent QPSK receiver with only baseband electronics, a significant advantage over QPSK heterodyne with its large receiver bandwidth requirement.

Preamplification

A perfect optical preamplifier is very like an RF amplifier: it takes a very small (noiseless, in this discussion) optical signal and amplifies it with no distortion up to a more usable level, with the cost of the addition of a certain amount of noise. This output signal level is defined as that level such that further electro-optical processing adds only a negligible amount more noise. As in RF amplifiers, noises in the amplifiers we will discuss (e.g., doped fiber amplifiers) are well modeled as additive, white Gaussian processes.

We will assume the most efficient optical amplifiers with 3-dB noise figures. This can be shown to correspond to the fact, as in the heterodyne receiver, that the total signal-energy-to-noise *ratio* in a match-filtered post-amplifier symbol measurement is equivalent to the average number of symbol photons seen at the input [22].

Note that certain properties of an optically amplified signal are the same as those of the electrical heterodyne signal: the desired signal is at a level that is easier to detect with many types of detectors and the otherwise noiseless signal is now embedded in white Gaussian noise. However, the heterodyne signal has been converted to an electrical signal on an IF carrier. The preamplified signal is still optical at its original wavelength. Usually, the detection process is noncoherent because if a coherent method had been available, then a coherent optical receiver would likely have been available. We should also note that optimal matched filtering in an optically amplified system must be in the optical domain since only a certain fraction of the noise effects can be removed post-detection. Usually, it is difficult to achieve true optical matched filtering, although adequate approximations are available [6].

We should make one important note here. The small, noiseless, but inherently unmeasurable input optical signal has properties very different from an amplified version of it, which has had classical Gaussian noise added to it. We will discuss this further in Section 4.

A signal that is preamplified, optically match-filtered, envelope-detected, and sampled has the Rician probability density function

$$f_{Ric}(a, r) \equiv r \exp\left[-\frac{(r^2 + a^2)}{2}\right] I_0(ar) , \quad (7)$$

where r is the envelope of the signal being measured (r^2 is the power) and where the envelope of the desired signal measurement is

$$a = \sqrt{2N_s} . \quad (8)$$

The randomness exists because of the narrowband (due to the matched filtering) Gaussian noise in the signal. When there is no signal, only noise, this density function becomes Rayleigh,

$$\begin{aligned} f_{Ray}(r) &\equiv f_{Ric}(0, r) \\ &= r \exp\left(-\frac{r^2}{2}\right) . \end{aligned} \quad (9)$$

The cumulative distribution function of the Rician density is called the Marcum Q function

$$Q(a, b) \equiv \int_b^{\infty} f_{Ric}(a, r) dr . \quad (10)$$

There are a number of published algorithms for efficiently calculating this function [21].

In the case of quadrature modulations with noncoherent detection, we will need to calculate the probability of measuring phase *differences* over wedge-shaped areas of the 2-D signal plane. With many similarities (by design) to Craig's function above, Pawula [15] showed that the relevant probability can be written as

$$f_P(\rho, \psi) \equiv \frac{1}{\pi} \int_0^{\pi-\psi} \exp\left[-\frac{\rho^2 \sin^2(\psi)}{2[1 + \cos(\psi) \cos(\phi)]}\right] d\phi . \quad (11)$$

This function is also amenable to numerical integration.

Real Detectors

Options discussed so far—photon counting, preamplified, and heterodyne and homodyne—assume perfect, noiseless detectors. Real-world detectors add noise to varying degrees. Avalanche photodiodes (APDs), for example, can operate like photon counters but with appreciable noise. (Generically, systems that make measurements of signal levels, and possibly add noise, are known as Direct Detection systems.) Although real detector models should be used when analyzing real receivers, their performance is not fundamental and depends on device design parameters that trade off certain inherent noise properties. Therefore, we will restrict ourselves to the basic receiver models. For communications system variants that require analyses with other noise or distortion features, it is left to the reader to extrapolate from the results given here.

2.3 REQUIREMENTS OF THE CLASSICAL RECEIVERS

We can see, from the previous discussions, that there exists quite a range of receiver structures that can be employed. Each receiver type has certain requirements for what it needs to know, deduce, or control. In this section, we will examine more closely these requirements.

The one universal requirement is timing. All receivers need to know, or deduce, symbol timing. In fact, in our noiseless system, a photon counting receiver can do without any other knowledge, although practical limitations mean that the wavelength must be within the bandwidth of the detector.

A preamplified receiver requires, in addition, knowledge or control of, to some degree, (a) wavelength—in order to fall in the band of amplification and the matched filter; (b) spatial properties—because many optical amplifiers have single-mode characteristics; (c) polarization—because opposite-polarization amplifier noise, if any, needs to be filtered out for best performance; and (d) baseband waveform shape—because optimal filtering of the post-amplifier Gaussian noise requires a matched filter based on this shape.

Heterodyne and preamplified receivers require knowledge and/or control of wavelength, polarization, and spatial properties in order to generate a local oscillator that mixes with the signal. Homodyne receivers require, in addition, knowledge and/or control of the optical phase. As in the preamplified receiver, the added Gaussian noise requires a filter matched to the baseband waveform, although in the heterodyne and homodyne cases, as mentioned above, the filter is electrical.

We will assume throughout our analyses that fully matched local oscillators and matched filters are available in our receivers, in addition to perfect symbol timing.

Because the homodyne receiver uses the phase of the incoming signal and measures only signal amplitude, it is a so-called coherent receiver, to be analyzed later. Since the output of the heterodyne system is an electrical IF signal, its follow-on electronics can employ either coherent detection techniques—using the deduced electrical phase of the IF carrier—or noncoherent techniques—measuring only electrical power using square-law detectors. Once again, both of these coherent techniques require electrical matched filters.

We must next decide how we wish to make and process our measurements. If the modulation requires deducing the presence or absence of a pulse, there are several possibilities. In a noiseless, photon-counting system, counting any photons vs counting no photons makes the decision simple. In preamplified, heterodyne, and homodyne systems, the added Gaussian noise means that optimum detection of a pulse requires both a matched filter and a threshold that divides outputs into those announced as “pulse” and those announced as “no pulse.” The optimum threshold must be based on knowledge of the signal and noise levels, which both must be either measured or known *a priori*.

Optimum quantum receivers, to be discussed at length later, will be seen to require knowledge of all of the parameters discussed so far.

Finally, once the signal has been “received,” a receiver can then select one of several types of measurements, summarized in Figures 6 and 7. If there is no decoding to be done, bits or symbols must be decided upon, in so-called “hard decisions.” If there is a decoder, a number of options are possible.

For a decoder to make maximum-likelihood (ML) decisions, it uses all the information it gets from the receiver. If hard decisions are all it receives, then the decoder’s ML decision is equivalent to assuming a

constant *average* signal-to-noise ratio (SNR) through all the symbols. If the receiver can make other measurements of the received waveform, then the decoder's goal is to use this information in its ML decisions.

The optimum receiver calculates the likelihood of *all* possible code words (possibly a huge number), each of which may last many bits. The decoding decision is made by choosing that code word that had the greatest (maximum) likelihood.

In classical communications systems, these likelihoods can be built up by first making amplitude and/or phase measurements independently on each channel symbol. (These are sometimes called "soft decisions" because they are measurements of information concerning the symbols, without actually making the "hard" bit decision.). Then, a processor constructs, usually implicitly via complex mathematics, the likelihood estimates of *all* possible received code words and then finally makes its code word decoding decision. Both hard- and soft-decision techniques are available to us for photon-counting, heterodyne, homodyne, and preamplified systems. We will see, however, that quantum optimum systems have different properties in each of these steps.

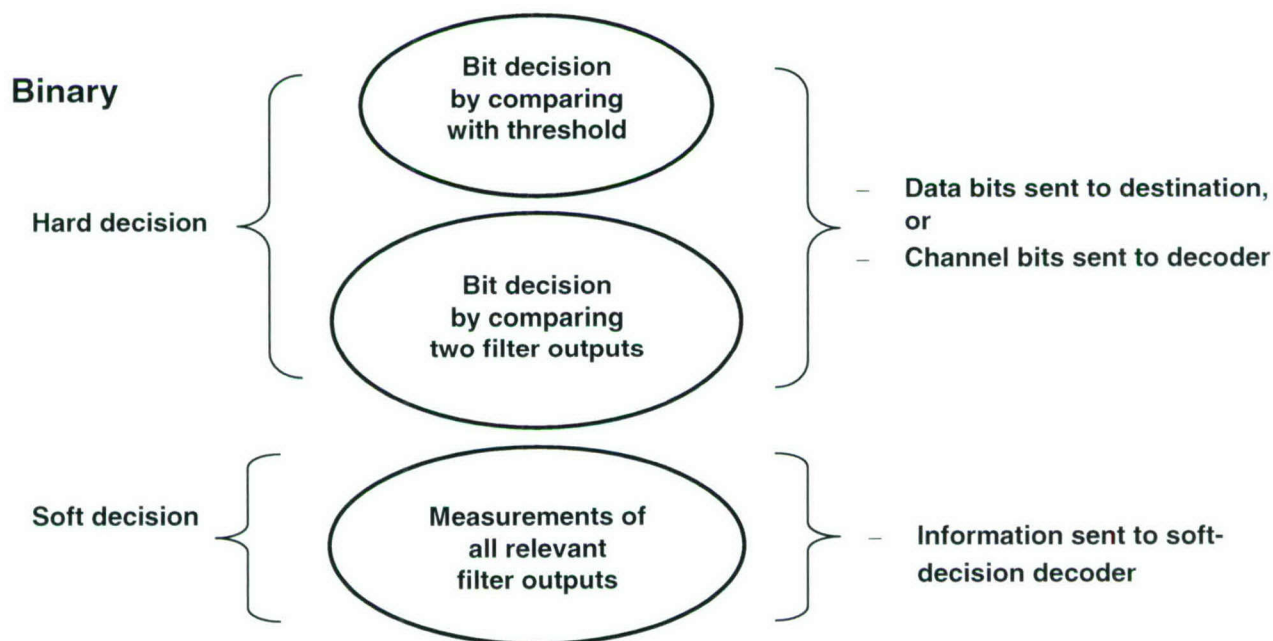


Figure 6. Binary receiver options.

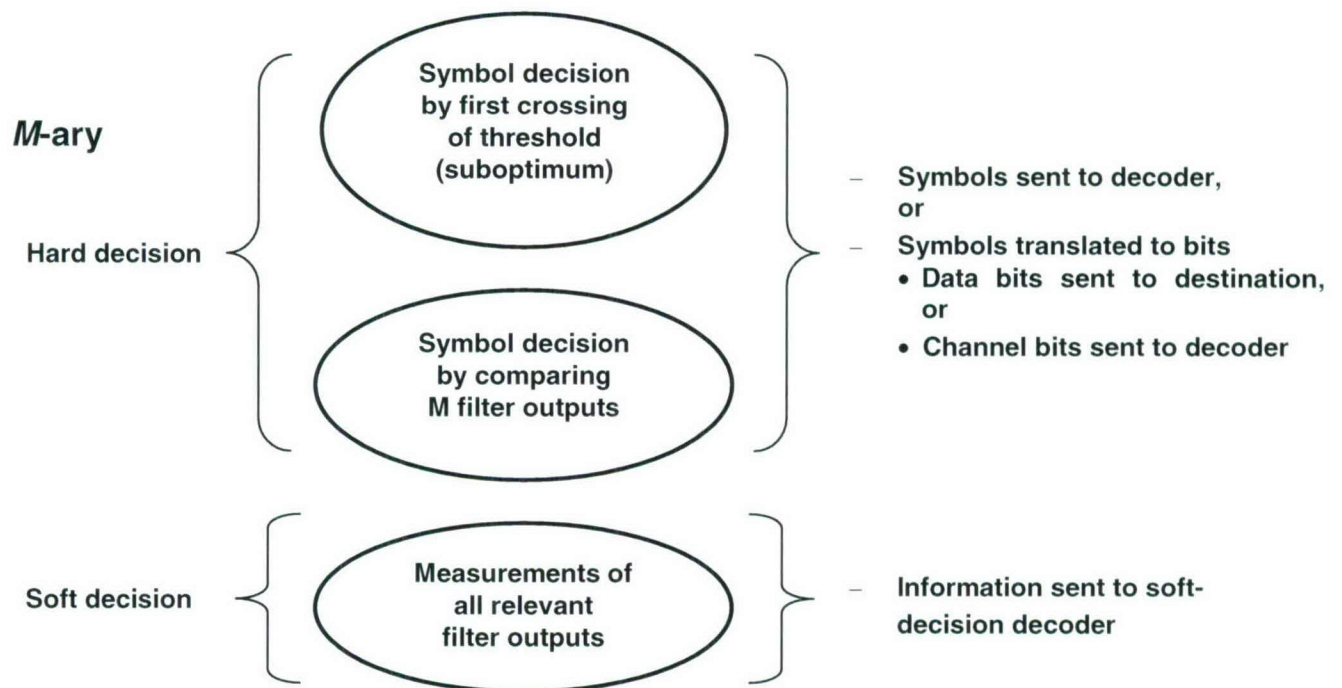


Figure 7. *M-ary receiver options.*

All of the requirements for the different receivers are summarized in Table 1. The table shows which receiver types need knowledge or control of which parameters. It also lists the subsystems typically used to estimate the parameters. The modulations assumed include OOK, orthogonal modulations, and PSK, all of which will be described in Section 5.

Table 1
Knowledge Requirements of Communications Receivers

Feature	Symbol Timing	Waveform Shape	Signal Amplitude	Receiver Noise Power	Optical Frequency/Wavelength	Subcarrier/IF Phase	Optical Phase	Polarization State	Spatial Properties
Noiseless Photon Counting Hard Decision	X								
Noiseless Photon Counting Soft Decision	X								
Heterodyne Coherent Hard Decision	X	X	A	A	X	X		X	X
Heterodyne Coherent Soft Decision	X	X	X	X	X	X		X	X
Homodyne Coherent Hard Decision	X	X	A	A	X		X	X	X
Homodyne Coherent Soft Decision	X	X	X	X	X		X	X	X
Heterodyne/Pre-Amp Non-Coherent Hard Decision	X	X	A	A	X			X	X
Heterodyne/Pre-Amp Non-Coherent Soft Decision	X	X	X	X	X			X	X
(Noiseless) Quantum Hard Decision	X	X	X		X		X	X	X
(Noiseless) Quantum Max Likelihood	X	X	X		X		X	X	X
Means to obtain knowledge	Time tracking loop	a priori knowledge	Power monitor	Out-of-band monitor; Demodulator/decoder outputs	Freq-tracking loop; a priori via calibration	IF phase lock loop	Optical phase lock loop	Polarization tracker/controller	WF sensor; camera

(A = OOK only)

Now that we have finished this whirlwind tour of receivers and have introduced the mathematical functions needed for their analyses, we will examine the metrics of communication system performance.

3. INFORMATION THEORY OF CLASSICAL SYSTEMS

3.1 NOTATION AND BASIC ERROR PROBABILITY FORMULAS FOR CLASSICAL SYSTEMS

We will need to distinguish between peak and average powers as well as energy per pulse, bit, and symbol, so we propose the following notation throughout: Whether a channel symbol corresponds to a single bit or multiple bits, we will call it "channel symbol." Let N_p be the *average* number of photons in a received pulse, N_s the *average* number in a channel symbol, and N_b the *average* number in the time corresponding to a source bit. Let T_p be the time duration of a pulse, T_s the time duration of a channel symbol, and T_b the time duration of a source bit. We thus have that N_p/T_p is the (pulse-averaged) peak received power and N_s/T_s is the average received power. Relationships between the various parameters will be explained for each format.

For soft-decision systems, we use the notation $P_{Y|X}(y|k)$ to represent the probability density function of receiving the (sampled) random quantity $Y = y$ given that the k th symbol at the input X was sent. (We can also see that an even more general case allows nonquantized inputs, X). We may drop the subscripts X and Y when the variables are obvious. The value y may be the single voltage sample at the output of a matched filter, or it may correspond to a vector of measurements of M sampled filter outputs. We number these symbols from 0 to $M - 1$. For hard decision systems, we use the notation $P_{Y|X}(i|k)$ to represent the probability that symbol i is announced by the receiver when symbol k is sent. For M -ary and coded systems, we use the notation p_i to mean the input probability (or frequency, or prior probability) that symbol i is sent.

The average probability of a hard decision M -ary symbol error is given by the formula

$$\begin{aligned} P_S &\equiv \sum_{j=0}^{M-1} \sum_{k=0, \neq j}^{M-1} p_k P_{Y|X}(j|k) \\ &= 1 - \sum_j p_j P_{Y|X}(j|j), \end{aligned} \tag{12}$$

which, for binary systems, is equivalent to

$$P_S = p_1 P(0|1) + p_0 P(1|0). \tag{13}$$

Note that, if $p_0 = p_1$, then a symbol error is equivalent to a bit error, P_b , where we let P_S and P_b be, respectively, the symbol and bit-error probabilities.

Remember from basic probability theory that

$$\sum_{j=1}^M P_{Y|X}(j|k) = 1 \quad (14)$$

and

$$\sum_{k=1}^M P_{Y|X}(j|k)p_k = P_Y(j), \quad (15)$$

where we let $P_Y(j)$ define the unconditional probability density function of the output, $Y = j$.

In Section 5, we will investigate two basic classes of modulations: binary, and nonbinary. The nonbinary modulations we will investigate will all have a certain symmetry in that each of the M signals is related to the set of remaining signals in the same way. That is,

$$\begin{aligned} P(j|k) &= P(j+1|k+1) \\ &= P(j-k|0), \end{aligned} \quad (16)$$

where the sum and difference are taken modulo M . Since no signal's relative properties are different from any other's, we will be assuming that the prior (i.e., the input) probabilities are equivalent, i.e., $p_k = 1/M$ for all k in the symmetric M -ary system. In this case, Equation (12) would reduce to

$$P_s \equiv 1 - P(0|0). \quad (17)$$

Furthermore, Equation (15) would reduce to

$$P(j) = 1/M, \quad (18)$$

which means that, in such symmetric systems, the outputs are also equiprobable.

One last topic regarding M -ary symbols is the mapping of bits into symbols and the symmetrical problem of mapping received symbol decisions into source bits. It is of interest to know the error probability of the final bits when it was the symbol error probabilities that are usually calculated. Of course, every system's unique mapping needs to be examined on its own merits. However, in many mappings—in particular so-called Gray-code mapping, where there is exactly one bit difference between subsequent symbols—it can be shown that the probability of a bit error is

$$P_b = \frac{M}{2(M-1)} P_s. \quad (19)$$

3.2 CLASSICAL CHANNEL CAPACITY

Definition

Channel capacity is the theoretical maximum rate at which source data can be transmitted *error-free* over a noisy or quantum channel to the destination. ***It is the modern metric against which all communications system performance should be compared.*** Capacity, C , is a function of the average number of photons per channel symbol that is available at the destination. It is usually calculated in (source) bits per channel symbol time, a rate, but can also be specified in source bits per second or some related, correctly normalized quantities.

It is known that certain long, complex coding schemes exist that can allow a communication system to approach this performance limit. A code at rate $R < 1$ means that the code transmits 1 channel bit for every R source bits. If we employ a capacity-achieving code, i.e., a highly efficient code at code rate, C , then, by definition, it will be able to achieve error-free transmission through the channel at the theoretical minimum power per original source bit.

The error probability of a coded system is lower-bounded by the following formula [17],

$$P_b \geq H^{-1} \left[1 - \frac{C(R N_b)}{R} \right], \quad (20)$$

where the binary entropy function is defined as,

$$H(p) \equiv -[p \log(p) + (1-p) \log(1-p)]. \quad (21)$$

We will use only base-2 logarithms throughout. This entropy function is plotted in Chart 1.

In Equation (20), $C(N_s)$ is the capacity in source bits per channel symbol as a function of photons per symbol, N_s , and R is the code rate employed. (Thus, $R N_b = N_s$). Since $H(p)$ is positive, we see that the error rate cannot go to zero if $R > C$.

Capacity Formulas—Hard Decision

In this section, we will give the basic formulas for classical channel capacity. We will present the formulas for both hard- and soft-decision systems. We will also provide some special cases, which we will refer to later.

Classical channel capacity for hard-decision systems can be calculated as [11]

$$C_c \equiv \max_{\{p_k\}} \sum_{i,j} p_i P_{Y|X}(j|i) \log \frac{P_{Y|X}(j|i)}{P_Y(j)} \quad (22)$$

$$P_Y(j) = \sum_k p_k P_{Y|X}(j|k), \quad (23)$$

where $P_Y(j)$ is the average probability that output j is produced.

(We are using the term “classical” here to distinguish it from the optical quantum systems, to be described in the next section). This value has units of source bits per channel symbol. The formula is shown as a maximum over all choices of prior probabilities since this is usually a free parameter for the system designer.

The formula can also be written in a way that shows the symmetry between the input and the output. (Capacity is based on the average mutual information between the inputs and the outputs.) The following equation is equivalent to Equation (22):

$$C_C \equiv \max_{\{p_k\}} \sum_{i,j} P_{XY}(i,j) \log \frac{P_{XY}(i,j)}{P_X(i)P_Y(j)} \quad (24)$$

$$P_{XY}(i,j) = P_{Y|X}(j|i)P_X(i) \quad (25)$$

$$P_X(i) = p_i \quad (26)$$

For a binary input/output channel, we can rearrange Equation (22) to be

$$C_C = \max_{p_1} \left\{ H[p_1 P(1|1) + p_0 P(1|0)] - p_0 H[P(1|0)] - p_1 H[P(0|1)] \right\}. \quad (27)$$

In the case of symmetric M -ary modulations, the formula for channel capacity reduces to

$$C_C = \log(M) + \sum_j P(j|0) \log P(j|0), \quad (28)$$

which, when describing the binary *symmetric* channel (BSC; $M = 2$, $p_1 = p_0 = 1/2$) further reduces to

$$C_C = 1 - H[P(1|0)]. \quad (29)$$

Channel capacity for the BSC as a function of symbol error probability, $P(0|1)$, is plotted in Chart 2. This curve shows us the symbol error probability at which a channel capacity-achieving code will “operate.” Notice that the lowest rate capacity-achieving codes can operate with quite high crossover probabilities.

Capacity Formulas—Soft Decision

For a soft-decision system, classical channel capacity is calculated as (with the most general, analog transmitted inputs, X)

$$C_C \equiv \sup_{\{p_X(x)\}} \int p_X(x) p_{Y|X}(y|x) \log \frac{p_{Y|X}(y|x)}{p_Y(y)} dx dy \quad (30)$$

$$p_Y(y) = \int p_{Y|X}(y|x) p_X(x) dx \quad (31)$$

or, for a more typical M -ary input alphabet,

$$C_C \equiv \max_{\{p_k\}} \sum_i \int p_i p_{Y|X}(y|i) \log \frac{p_{Y|X}(y|i)}{p_Y(y)} dy \quad (32)$$

$$p_Y(y) = \sum_i p_i p_{Y|X}(y|i). \quad (33)$$

Perhaps a more useful way to write Equation (32) is

$$C_C \equiv \max_{\{p_k\}} \left\{ - \sum_i \int p_i p_{Y|X}(y|i) \log \sum_k p_k \frac{p_{Y|X}(y|k)}{p_{Y|X}(y|i)} dy \right\}. \quad (34)$$

From this, the special case of binary systems reduces to

$$\begin{aligned} C_C \equiv & -p_0 \int p(y|0) \log \left[p_0 + p_1 \frac{p(y|1)}{p(y|0)} \right] dy \\ & - p_1 \int p(y|1) \log \left[p_1 + p_0 \frac{p(y|0)}{p(y|1)} \right] dy \end{aligned} \quad (35)$$

or, equivalently,

$$C_C = p_1 \int p(y|1) \log p(y|1) dy + p_0 \int p(y|0) \log p(y|0) dy - \int p(y) \log p(y) dy, \quad (36)$$

where

$$p(y) = p_1 p(y|1) + p_0 p(y|0). \quad (37)$$

The soft-decision capacity using M -ary symmetric signals reduces to

$$C_C = \log(M) - \int p(y|0) \log \left[1 + \sum_{k=1}^{M-1} \frac{p(y|k)}{p(y|0)} \right] dy . \quad (38)$$

We should note that the measurement, y , here may actually correspond to a vector of measurements (such as the outputs of several different filters), and thus the integration over y may be a multiple integration.

Except in very special cases, we will find that soft-decision channel capacity needs to be calculated via numerical integration because of the log inside the integral. For the even more complex multiple-integral version, a technique often used is to notice that the integral is a kind of expected value. Thus, a Monte Carlo simulation using computer-generated random variables can be used.

It can be shown (and was shown by Shannon in his seminal work) that starting with Equation (30) and in an otherwise unconstrained additive Gaussian noise channel, the channel capacity is [18, 19]

$$C_C = \log(1 + N_S) . \quad (39)$$

(For the receivers we will examine, this formula will be relevant to the coherent heterodyne architecture.)

As discussed in an earlier section, the noise in a homodyne receiver is also Gaussian but at half the level. Since homodyne systems do not allow for quadrature information, however, they are only half as bandwidth efficient as heterodyne.

The capacity curves for heterodyne and homodyne unconstrained signals are plotted in Chart 3. (Sometimes the heterodyne equation is shown with other factors of 2, when the normalization is with respect to *dimensions*. Equation (39) is correct for source bits per channel usage.) This ultimate capacity can be achieved using Gaussian-distributed, i.e., not quantized to M levels, source signal values.

Measure of Efficiency

Although the basic value of channel capacity—source bits per channel symbol at a given symbol photon count—is highly useful, we sometimes want to know the cost of achieving a certain data rate as opposed to knowing the data rate achievable at a certain cost (signal power). A way to do this is to calculate the photons required per *source* bit as a function of some speed or redundancy property of the code. We will present this efficiency at channel capacity vs bandwidth expansion, where bandwidth expansion is a combination of the expansion due to the code parity check overhead plus the expansion due to modulation.

Since N_S = average photons per channel symbol, and C_C = source bits per channel symbol, we see that N_S / C_C = average photons per source bit. That is, N_S / C_C is the number of photons required at the receiver

in order for a system to reliably deliver source bits using a channel-capacity-achieving code of rate C_C . The bandwidth expansion due to coding is just $1/C_C$, and the bandwidth expansion from modulation must be calculated on a case-by-case basis. As an example of efficiency at channel capacity, see Chart 4, in which we have plotted the efficiency of the Gaussian channel capacity for both heterodyne and homodyne systems. Notice that heterodyne efficiency bottoms out at $\ln 2$, or -1.59 dB (with homodyne 3 dB lower). Thus, with a (high bandwidth, low code rate) capacity-achieving code, we should be able to transmit source bits at rate R_b by delivering to the heterodyne receiver $R_b \ln 2$ photons per second. We can also see that heterodyne becomes more efficient than homodyne for normalized bandwidths less than about 0.631.

3.3 CLASSICAL COMPUTATION CUTOFF RATE

Definition

For many years, the computation cutoff rate (sometimes called computational cutoff rate or even just cutoff rate) was considered the maximum rate achievable by buildable codes. With the advent of turbo-codes and their progeny, classical channel capacity (which is greater than cutoff rate) is now known to be essentially achievable, although the cutoff rate, R_C (sometimes called R_0) is still a good upper bound for many classical coding schemes. It is similarly parameterized as source bits per channel symbol.

Cutoff Rate Formulas—Hard Decision

The classical computation cutoff rate for hard-decision systems is defined by the formula [11]

$$R_C \equiv -\log \left\{ \min_{\{p_k\}} \sum_j \left[\sum_k p_k \sqrt{P_{Y|X}(j|k)} \right]^2 \right\}. \quad (40)$$

For a general binary channel, this formula is

$$R_C = -\log \left\{ 1 - 2p_1 p_0 \left[\frac{1 - \sqrt{P(1|0)(1 - P(0|1))}}{-\sqrt{P(0|1)(1 - P(1|0))}} \right] \right\}. \quad (41)$$

For our symmetric M -ary channel, we find

$$R_C = \log(M) - 2 \log \left[\sum_k \sqrt{P(k|0)} \right], \quad (42)$$

which, for the BSC, further reduces to

$$R_C = 1 - \log \left[1 + 2\sqrt{P(1|0)P(0|0)} \right]. \quad (43)$$

The cutoff rate for the BSC is shown in Chart 5.

Cutoff Rate Formulas—Soft Decision

For a soft-decision decoder, the classical computation cutoff rate is

$$R_C \equiv -\log \left\{ \inf_{p_X} \int \left[\int p_X(x) p_{Y|X}(y|x)^{1/2} dx \right]^2 dy \right\} \quad (44)$$

for the most general analog input case. For the more typical discrete, M -ary input case, it is

$$R_C \equiv -\log \left\{ \min_{\{p_k\}} \int \left[\sum_k p_k \sqrt{p(y|k)} \right]^2 dy \right\} . \quad (45)$$

For a binary input system, this reduces to

$$R_C = -\log \left\{ 1 - 2p_0p_1 + 2p_0p_1 \int \sqrt{p(y|0)p(y|1)} dy \right\} . \quad (46)$$

As in the capacity calculation, we should note that the measurement, y , may be a vector of measurements and thus the integration over y may actually be a multiple integration.

We can see that the soft-decision cutoff rate is made up of the log of sums of integrals, each integral being the geometric mean of two density functions. Such an integral is called a Bhattacharya coefficient. Let us define this integral, with a nonstandard but easily understood notation, as

$$\mathcal{B}(f(y), g(y)) \equiv \int \sqrt{f(y)g(y)} dy . \quad (47)$$

In the M -ary symmetric case, the cutoff rate can be reduced to

$$R_C = \log(M) - \log \left[\sum_k \mathcal{B}[p(y|0), p(y|k)] \right]. \quad (48)$$

For the BSC, the soft-decision cutoff rate further reduces to

$$R_C = 1 - \log [1 + \mathcal{B}[p(y|0), p(y|1)]] . \quad (49)$$

It can be shown, starting with Equation (44), that in an otherwise unconstrained additive Gaussian noise channel, the cutoff rate for our heterodyne system is [20]

$$\begin{aligned} R_0 &= \frac{1}{\ln(2)} \left[1 + \frac{N_s}{2} - \sqrt{1 + \left(\frac{N_s}{2} \right)^2} \right] + \log_2 \left[\frac{1}{2} \left(1 + \sqrt{1 + \left(\frac{N_s}{2} \right)^2} \right) \right] \\ &\equiv R_0(N_s) . \end{aligned} \quad (50)$$

As in our capacity calculations, the version for homodyne is 3 dB better, but half as bandwidth efficient. These formulas are plotted in Chart 6. The efficiencies at these Gaussian channel cutoff rates are plotted in Chart 7. We see that they bottom out at $2 \ln 2$, or 1.42 dB, and $\ln 2$ or -1.59 dB, exactly 3 dB higher than the efficiencies at Gaussian channel capacity for heterodyne and homodyne.

Calculation of these cutoff formulas is much simpler than those of the soft-decision channel capacity. Very often, Bhattacharya coefficients even have a closed form.

4. INFORMATION THEORY OF QUANTUM SYSTEMS

It has been known since the 1960s that the optimum approach to optical signal detection is based on quantum state descriptions and projection operators. As we are interested only in optical systems in which there is a large loss between the transmitter and receiver, we will be considering only so-called pure, coherent states. In these cases, solutions to the mathematical optimizations have been found for most relevant formats.

Interpretation of the mathematically optimum receivers as implementable physical systems is still largely unknown and the topic of much research.

The following section is an extremely cursory introduction to the relevant theory and mathematics. (See [12] or [13] for more.)

Definitions

Quantum states are described using infinite-dimensional vectors $|\psi\rangle$ in a Hilbert space over the field of complex numbers, with Hermitian conjugate vectors $\langle\psi|$, inner products $\langle\psi|\eta\rangle$, outer products $|\psi\rangle\langle\psi|$, and matrix trace $\text{Tr}(\cdot)$ defined in the obvious ways. It is the outer product that describes a so-called pure state.

A coherent state has the further description

$$|\alpha\rangle = \exp(-|\alpha|^2/2) \sum_{n=0}^{\infty} \frac{\alpha^n}{(n!)^{1/2}} |n\rangle \quad (51)$$

for some complex number, α , where $|n\rangle$ are orthonormal, so-called number eigenstates. (It is straightforward to deduce the Poisson counting statistics from this model.) Thus, the inner product between two coherent states can be calculated to be

$$|\langle\alpha|\beta\rangle|^2 = \exp(-|\alpha - \beta|^2) \quad (52)$$

and so

$$\langle\alpha|\alpha\rangle = 1. \quad (53)$$

Notice that, by Equation (52), there cannot be truly orthogonal coherent states.

As in the classical description, transmitters can select a coherent state signal to transmit with prior probability p_i .

Measurements at the receiver are described by so-called probability operator measures, which are sets of nonnegative-definite Hermitian operators, summing to the identity. For the optical systems we are interested in, the signal states are coherent, pure, and linearly independent [12]. In this case, the operators can be shown to take the form of outer products, called projection operators, of orthonormal vectors, $|\eta_k\rangle$, which sum to the identity

$$\sum |\eta_k\rangle\langle\eta_k| = I . \quad (54)$$

It is the task of the receiver designer to find the set of $|\eta_k\rangle$ to optimize the relevant metric. Unfortunately, measurements described by operators do not (yet) have simple physical interpretations. Thus, most of the results in this quantum section are of theoretical interest only although the excellent performance they predict will provide a great incentive to find such physical interpretations.

As discussed in Section 1.0, noiseless quantum systems incur errors not because of intrinsic added noise but because the signals themselves are not completely measurable. Furthermore, a particular physical measurement on a quantum signal means that the signal is then no longer available for making further *arbitrary* measurements. This is the major difference between quantum systems and RF systems. In an RF system, by including a low-noise front-end amplifier, the RF signal plus noise can be made large enough so that it can be split into many replicas, each of which can be measured by a different matched filter.

We could try the same approach with optical signals, i.e., put the optical signal through an optical amplifier so that we could make multiple measurements at its output. Unfortunately, as we mentioned earlier, this signal in Gaussian noise would have substantially different properties from the original noiseless signal. Optimum processing requires a very different approach for multiple measurements that must be based on operator theory.

We can see that the fact that the operators sum to the identity specifies how any set of multiple measurements must be related. Changing one operator element (“matched” to a zero signal, say) means that the other elements (“matched” to the other signals) must also change. Remember that in an RF system, each of the post-preamplifier filters may be selected independently.

Quantum Optimum—Hard Decision

Hard symbol decisions can be made with these quantum operators. We choose them to minimize the probability of symbol error, defined as in Equation (12).

Although the quantum mechanical mathematics is infinite-dimensional, it can be shown that the coherent problem can be reduced to one in many fewer dimensions. We only need to consider the variables

$$x_{jk} = \langle\eta_j|\psi_k\rangle \quad (55)$$

for the pure state,

$$\rho_k = |\psi_k\rangle\langle\psi_k| \quad k = 0, 1, 2, \dots, M-1 \quad (56)$$

with prior probabilities p_k , and the operator

$$\Pi_j = |\eta_j\rangle\langle\eta_j| \quad j = 0, 1, 2, \dots, L-1 \quad (57)$$

with the property

$$\sum_{j=0}^{L-1} \Pi_j = I. \quad (58)$$

The basic property of projection operators is that

$$\begin{aligned} P(j|k) &= |x_{jk}|^2 \\ &= |\langle\eta_j|\psi_k\rangle|^2. \end{aligned} \quad (59)$$

That is, the receiver announces signal j when k is true with probability $P(j|k)$ defined here.

Notice that the dimensionality of the operators does not need to be the same as the dimensionality of the signals. If $L = M$, then it is a true hard decision, with announcements of the signal decision. However, we can choose $L > M$ under some soft-decision-like metric, if we like. (Analogously, in classical systems, we can perform hard decisions, or describe the outputs, y , with 2, 3, or more bits. The more bits we choose, the closer we get to soft decisions.) For our quantum hard-decision calculations, we will use only $L = M$. We will discuss the $L > M$ case in the next section.

It has been shown (See [12] for a summary.) that to minimize the probability of symbol error, the solution must satisfy the following set of nonlinear equations:

$$p_j x_{kj} x_{jj}^* = p_k x_{kk} x_{jk}^*, \quad (60)$$

where it is simple also to find that

$$\sum_k x_{kj} x_{ki}^* = \langle\psi_i|\psi_j\rangle. \quad (61)$$

Even these equations are difficult to solve in general in closed form although solutions have been found for our binary and M -ary symmetric cases.

These hard symbol decisions can be used as is, or can be fed to a classical decoder with performance described using the formulas of classical channel capacity Equation (22) or classical computation cutoff rate Equation (40) with $P(j/k)$ from Equation (59). This approach is sometimes called “semiclassical” because the hard symbol decisions are made using optimum quantum techniques, but the decoding is done classically.

Because of the property mentioned at the end of the previous section, the operators that optimize the probability of error are not necessarily the same as those that optimize semiclassical channel capacity or semiclassical computation cutoff rate. In other words, the optimum hard symbol decisions derived above for minimization of the symbol error probability may not be the same decisions that optimize capacity or cutoff.

It turns out that, for binary (and M -ary symmetric) systems, it is known that the two (or M) measurements that make up the P_S -optimizing solutions do, in fact, satisfy necessary conditions for semiclassical capacity optimization. (As of this work’s writing, sufficient conditions are not known.) Cutoff optimization has similar properties. It has been shown, however, that the optimum capacity-achieving solution has $d \leq L \leq d^2$, where d is the dimension of the Hilbert space in which the signals can be defined [8].

Quantum Capacity—Maximum Likelihood (Soft Decisions)

As discussed in the previous section, we can choose L , the number of operators in Equation (57) to be greater than M , the number of symbols. This is analogous to soft decisions in RF systems, where each of M measurements might have 2 or more bits of resolution in them, resulting in more than M possible outputs. All these bits of descriptions can then be fed to a soft-decision decoder. We will see that some M -ary quantum receivers do, indeed, perform better in coded systems when $L > M$.

In the correct analogy with the classical maximum-likelihood decoder, though, the fully optimum quantum decoder tries to make ML decisions between all the possible received codewords. As an example, for an (n, k) block code with 2^k codewords, each constructed of $n > k$ binary channel symbols, the quantum decoder views the problem as an $M = 2^k$ -ary problem. As mentioned earlier, in classical systems, this is done implicitly by measuring each channel symbol and then computing the 2^k ML estimates after the fact in a processor. In quantum systems, however, this estimate cannot be built up by measuring each sequential symbol independently, but must be done by making measurements on the complete codeword as if it were a much more complex quantum state. This is sometimes known as an “entangled” quantum receiver.

It will be seen that such an optimum quantum receiver has a strictly better performance than any other receiver, including the optimized semiclassical decoding receiver. Its performance is described thus:

Calculate the following description (density operator) of the quantum information source

$$\hat{\rho}_p \equiv \sum_{k=1}^M p_k |\psi_k\rangle\langle\psi_k|, \quad (62)$$

where we use the subscript p to remind us that it is a function of the prior probabilities, which can be selected to optimize performance. The quantum channel capacity can be shown to take the form [13]

$$C_Q \equiv \max_{\{p_k\}} -Tr[\hat{\rho}_p \log \hat{\rho}_p] \quad (63)$$

(which is known as the von Neumann entropy). It is usually calculated by first finding the eigenvalues, λ_i , of $\hat{\rho}_p$. By Equation (62) we see that these are nonnegative and sum to 1, and are thus a lot like probabilities. Using these eigenvalues, we can equivalently calculate

$$C_Q = -\sum_{k=1}^M \lambda_k \log \lambda_k, \quad (64)$$

where we have suppressed the maximization over the priors.

For M -ary modulations with the symmetry property, we will find it useful to use the related quantity

$$v_k \equiv M\lambda_k, \quad (65)$$

which leads to

$$C_Q = \log M - \frac{1}{M} \sum_{k=1}^M v_k \log v_k. \quad (66)$$

It can also be shown that, for this M -ary symmetric case, the symbol error probability described by Equation (60) can be written explicitly as

$$P_S = 1 - \frac{1}{M^2} \left[\sum_{k=1}^M \sqrt{v_k} \right]^2. \quad (67)$$

Similar to the classical case of unconstrained signals in Gaussian noise, there is a so-called ‘‘Gaussian’’ quantum capacity for unconstrained coherent signals, given by [13]:

$$C_Q = (1 + N_S) \log(1 + N_S) - N_S \log N_S. \quad (68)$$

This formula is plotted in Chart 8. It is the *ultimate performance* of all the methods we will have examined.

We have also plotted the efficiency at Gaussian quantum capacity in Chart 9. The most interesting feature of this curve is that it does not bottom out as does efficiency at Gaussian classical capacity. Instead, it continues to improve as more and more bandwidth is used—that is, as the error-correction coding rate gets smaller and smaller. Theoretically, the channel capacity can be shown to become *infinite*, i.e., the efficiency approaches an infinite number of bits per photon, although, of course, real-world (and perhaps even model validity) constraints prevent this. Practical limits on efficiency seem to be about 10, or perhaps 20, bits per photon.

The fact that channel capacity (in source bits per channel symbol) increases as the receiver entangling increases from 1 to 2 to n consecutive channel symbols is sometimes called *superadditivity*.

Quantum Cutoff Rate – Maximum Likelihood (Soft Decisions)

The quantum computation cutoff rate is described similarly. Using the same source description as in Equation (62), it can be shown that [1, 13]

$$\begin{aligned} R_Q &\equiv -\max_{\{p_k\}} \log [Tr \hat{\rho}_p^2] \\ &= -\max_{\{p_k\}} \log \sum_{k=1}^M \lambda_k^2. \end{aligned} \tag{69}$$

For symmetric modulations, we have

$$R_Q = \log M - \log \frac{1}{M} \sum_{k=1}^M v_k^2. \tag{70}$$

Similar to the classical case of unconstrained signals in Gaussian noise, there is a “Gaussian” quantum cutoff rate, given by [13]:

$$R_Q = \frac{1}{\ln(2)} \left[1 + 2N_s - \sqrt{1 + 4N_s^2} \right] + \log_2 \left[\frac{1}{2} \left(1 + \sqrt{1 + 4N_s^2} \right) \right] \tag{71}$$

$$= R_0(4N_s). \tag{72}$$

[Compare Equation (50).]

The Gaussian quantum cutoff rate is plotted in Chart 10, and the efficiency at Gaussian quantum cutoff rate is plotted in Chart 11. We see that this efficiency is exactly 6 dB lower than that of Gaussian (heterodyne) cutoff, and thus bottoms out at -4.6 dB. Thus, there is a big incentive (more than 5 dB) to find coding schemes that achieve quantum capacity and not just quantum cutoff rate.

The Square-Root Measurement

Although Equations (60) and (61) are difficult to solve in general, a set of solutions has been proposed that satisfies these equations in many cases. Let us define measurements as

$$|\eta_j\rangle = \sqrt{p_j} [\hat{\rho}_p]^{-1/2} |\psi_j\rangle,$$

where the matrix inverse may need to be a generalized inverse. This has come to be known as the square-root measurement and has been investigated in several works as good approximations to optimum solutions. In fact, it was recently shown [10] to be symbol-error-rate optimum for a wide class of modulations, including all binary modulations, as well as equal-priors orthogonal and MPSK.

Conclusions

We end this section by reminding the reader once again that *physical implementations of quantum optimum receivers, demodulators, and decoders are still unknown, as are codes that might use them. These are all topics of much research.*

(It would be fair to note that some years ago Sam Dolinar at MIT invented a nearly implementable receiver that achieves the optimum quantum bit-error probability for any binary modulation. (See [12] for a simplified description.) This receiver has certain similarities to homodyne systems in that it requires a phase-coherent LO. Unfortunately, neither Dolinar nor subsequent researchers have successfully generalized this method in an implementable form to M -ary symbol decisions or, especially, to ML decoding.)

5. MODULATION FORMATS

In this section, we will apply the general formulas from the previous sections to specific modulations. For the most part, we will *assume* prior probabilities and then calculate the “capacity” one could achieve given those assumptions. Sometimes, we will find that, in certain regions of the curves, selecting a different set of priors would have given better efficiency or throughput. In the true spirit of maximizing capacity, one would choose the optimizing prior at each signal level as long as the selection did not violate some other system constraint.

5.1 GENERALIZED ON-OFF KEYING (OOK)

OOK: Preliminaries

During a symbol period, T_S , the transmitter sends either nothing (corresponding to a 0 and with probability p_0) or a pulse (corresponding to a 1, with probability p_1) such that an average of N_P photons is detected by the receiver during the pulse. Note that this is a *binary* modulation even when $p_1 \neq p_0$. The *average* received number of photons per symbol is

$$N_S = p_1 N_P. \quad (73)$$

We thus see that the peak-to-average ratio of photon flux (and power) is $1/p_1$. Traditional OOK uses the values $p_1 = p_0 = 1/2$ with a peak-to-average ratio of 2. We call the case $p_i \neq 1/2$ generalized OOK.

We note that the pulse can actually be of arbitrary shape although, in this analysis, we assume that the pulses do not overlap. (Note that the instantaneous peak-to-average ratio would change for non-flat pulses.) As discussed in Section 2.3, this shape must be known for optimum performance in receiver types that need to separate the signal from additive noises.

OOK: Noiseless Photon-Counting Hard Decisions

Whatever the (classical) measurement type, a hard decision on whether a pulse is present or not requires a comparison threshold. The receiver declares “1” if the measurement is greater than this threshold and “0” if it is less. The threshold must be chosen to optimize the desired criterion.

A photon counter in a noiseless system has the easiest task of all the OOK hard-decision receiver types. If it detects any photons at all, it correctly declares “1.” If it detects none, it declares “0” and makes an error only if a pulse was actually transmitted. Thus, with the Poisson model, we see that error probabilities are

$$P(1|0) = 0 \quad (74)$$

$$P(0|1) = \exp(-N_P). \quad (75)$$

Symbol (bit) error probabilities can be calculated using Equation (13)

$$P_S = p_1 \exp(-N_p) = p_1 \exp(-N_s / p_1) . \quad (76)$$

This bit-error probability is plotted in Chart 12 for the symmetric case, $p_1 = 1/2$.

We can also insert Equations (74) and (75) into Equations (27) and (41) to find that capacity and cutoff, for the generalized case, are

$$C_C = H[p_1(1 - \exp(-N_s / p_1))] - p_1 H[\exp(-N_s / p_1)] \quad (77)$$

$$R_C = -\log[1 - 2p_1 p_0(1 - \exp(-N_s / 2p_1))] . \quad (78)$$

These results are all plotted in Charts 13–16 for a variety of p_i .

We can note here that generalized OOK can achieve higher and higher efficiency as the peak-to-average power ratio increases. On the other hand, as this ratio increases, there are certain higher data rates that become unattainable for fixed pulse widths. For instance, for $p_1 = 1/32$, the system cannot transmit more than about 0.2 bits per OOK symbol.

OOK: Heterodyne and Homodyne Receivers—Coherent Hard Decisions

Heterodyne and homodyne coherent receivers (again, assuming sampled outputs of matched filters) produce a signal, y , in Gaussian noise with normalized density function description

$$p(y|0) = f_G(y) \quad (79)$$

and

$$p(y|1) = f_G(y - \sqrt{2s N_p}) , \quad (80)$$

where $s = 1$ for heterodyne and $s = 2$ for homodyne. (Functions here were defined in Section 2.2.)

With these, and basing decisions upon a threshold, T , we find

$$\begin{aligned}
P(1|0) &= \int_T^{\infty} p(y|0) dy \\
&= \Phi(T)
\end{aligned} \tag{81}$$

$$\begin{aligned}
P(0|1) &= \int_{-\infty}^T p(y|1) dy \\
&= 1 - \Phi(T - \sqrt{2sN_p}).
\end{aligned} \tag{82}$$

Inserting these into the formula for symbol error, Equation (13), we can optimize over T to find that the optimum T satisfies

$$p_1 p(T|1) = p_0 p(T|0). \tag{83}$$

For this coherent case, the result is

$$T = \frac{sN_p + \ln \frac{p_0}{p_1}}{\sqrt{2sN_p}}. \tag{84}$$

In the most-used symmetric case of $p_0 = p_1$, we see that

$$T = \sqrt{sN_p / 2}, \tag{85}$$

which, when inserted into Equation (13), produces

$$\begin{aligned}
p_b &= \Phi(\sqrt{sN_p / 2}) \\
&= \Phi(\sqrt{sN_s}).
\end{aligned} \tag{86}$$

Notice that optimum performance is achieved only if the receiver selects the threshold optimally, an action which requires knowledge of the signal power at the receiver. A system that deduces this level in real time is known as an Automatic Gain Control (AGC).

These heterodyne and homodyne probabilities for $p_0 = p_1$ are plotted in Charts 17 and 22. We can also use Equations (81), (82), and (85) in Equations (27) and (41) to calculate channel capacity and computation cutoff rate for hard decisions with general p_i . Unfortunately, the values of the threshold, T , that optimize

capacity and cutoff are different from that derived in Equation (84). These values are best calculated numerically. All these results are plotted in Charts 18–21 and Charts 23–26.

OOK: Preamplified and Heterodyne Receivers—Noncoherent Hard Decisions

In the preamplified and heterodyne noncoherent receivers, we use, instead of the Gaussian density, the Rician density (defined in Equation (7)):

$$p(y|1) = f_{Ric}(\sqrt{2N_s}, y) \quad (87)$$

$$p(y|0) = f_{Ric}(0, y). \quad (88)$$

Using a threshold, T , as in Equations (81) and (82), we find, using Equation (10)

$$P(1|0) = Q(0, T) \quad (89)$$

$$P(0|1) = 1 - Q(\sqrt{2N_p}, T). \quad (90)$$

Inserting these into the formula for symbol error, Equation (13), and optimizing over T , we find that T is defined by (for the symmetric case of $p_0 = p_1$)

$$\exp(N_p) = I_0(T\sqrt{2N_p}) \quad (91)$$

or

$$T = \frac{1}{\sqrt{2N_p}} I_0^{-1}(\exp(N_p)), \quad (92)$$

which must be solved numerically although it has a good approximate solution as

$$T \approx \sqrt{2 + N_p / 2}. \quad (93)$$

Inserting this back into Equation (13), we can calculate the error probability, which is shown in Chart 27. We can also use Equations (89), (90), and (92) in Equations (27) and (41) to calculate channel capacity and computation cutoff rate for these hard decisions. As in the coherent hard decision section, the thresholds must be numerically reoptimized for capacity and cutoff. The results are plotted in Charts 28–31.

OOK: Quantum Receiver—Hard Decisions

The two-dimensional optimization problem described by Equations (60) and (61) can be solved using polar coordinates with solutions given as trigonometric equations. These will not be presented here. However, the result can be shown to provide performance described by [12]:

$$P(1|0) = 1/2 \left\{ 1 - \frac{1}{\sqrt{1 - 4p_1 p_0 \exp(-N_p)}} [1 - 2p_1 \exp(-N_p)] \right\} \quad (94)$$

$$P(0|1) = 1/2 \left\{ 1 - \frac{1}{\sqrt{1 - 4p_1 p_0 \exp(-N_p)}} [1 - 2p_0 \exp(-N_p)] \right\}, \quad (95)$$

from which we can calculate

$$P_s = 1/2 \left(1 - \sqrt{1 - 4p_1 p_0 \exp(-N_p)} \right). \quad (96)$$

These have been plotted in Chart 32 for $p_0 = p_1 = 1/2$. We can also use Equations (94) and (95) in Equations (27) and (41) to calculate semiclassical channel capacity and semiclassical computation cutoff rate for these hard decisions. These results are shown in Charts 33–36.

OOK: Photon-Counting Soft Decisions

In the noiseless case, we can see that there is no more information if we receive 2 or 3 or 10 photons than if we receive 1. Thus, the soft decision capacity and cutoff are the same as for hard decisions. This would not be the case, however, if there were noise mixed in with the signal.

OOK: Heterodyne and Homodyne Receivers—Coherent Soft Decisions

To calculate capacity using coherent soft decisions, we insert Equations (79) and (80) into Equation (36). We find

$$C_c = -\frac{1}{2} \log(2\pi e) - \int_{-\infty}^{\infty} p(y) \log p(y) dy \quad (97)$$

with

$$p(y) = p_0 f_G(y) + p_1 f_G(y - \sqrt{2sN_p}), \quad (98)$$

which requires numerical integration. (Remember, $s = 1$ for heterodyne and $s = 2$ for homodyne.) Computation cutoff is similarly found to be

$$R_C = -\log \left[1 - 2p_0p_1 + 2p_0p_1 \mathcal{B}(f_G(y - \sqrt{2sN_p}), f_G(y)) \right], \quad (99)$$

where the Bhattacharya distance for Gaussian densities has the closed form solution

$$\mathcal{B}(f_G(y - \sqrt{2sN_p}), f_G(y)) = \exp(-sN_p / 4). \quad (100)$$

These results are plotted in Charts 37–44.

OOK: Preamplified and Heterodyne Receivers—Noncoherent Soft Decisions

To calculate capacity using noncoherent soft decisions, we insert Equations (87) and (88) into Equation (35). We find

$$\begin{aligned} C_C = & -p_0 \int f_{Ric}(0, y) \log \left[p_0 + p_1 \frac{f_{Ric}(\sqrt{2N_p}, y)}{f_{Ric}(0, y)} \right] dy \\ & - p_1 \int f_{Ric}(\sqrt{2N_p}, y) \log \left[p_1 + p_0 \frac{f_{Ric}(0, y)}{f_{Ric}(\sqrt{2N_p}, y)} \right] dy. \end{aligned} \quad (101)$$

Computation cutoff is similarly found to be

$$R_C = -\log \left[1 - 2p_0p_1 + 2p_0p_1 \mathcal{B}(f_{Ric}(\sqrt{2N_p}, y), f_{Ric}(0, y)) \right], \quad (102)$$

where the Bhattacharya distance

$$\mathcal{B}(f_{Ric}(\sqrt{2N_p}, y), f_{Ric}(0, y)) = \exp(-N_p / 2) \int_0^\infty y \exp(-y^2 / 2) \sqrt{I_0(y\sqrt{2N_p})} dy \quad (103)$$

does not have a closed-form solution and so must be calculated numerically. Capacity and cutoff results are plotted in Charts 45–48.

OOK: Quantum Receiver—Maximum-Likelihood Decoding

For quantum decoding, we need to calculate the eigenvalues of the density operator of Equation (62). For coded OOK, it can be shown that [12]

$$\lambda_i = 1/2 \left[1 \pm \sqrt{1 - 4 p_1 p_0 (1 - \exp(-N_p))} \right] \quad (104)$$

and thus

$$C_Q = H(\lambda_0) = H(\lambda_1) \quad (105)$$

and

$$\begin{aligned} R_Q &= -\log(\lambda_0^2 + \lambda_1^2) \\ &= -\log[1 - 2 p_1 p_0 (1 - \exp(-N_p))] \end{aligned} \quad (106)$$

These results are plotted in Charts 49–52.

5.2 ORTHOGONAL MODULATIONS—PPM AND FSK

Orthogonal: Preliminaries

An orthogonal modulation is one such that the integral of the product of any two different waveforms in the set is zero. Orthogonal modulations can be either binary or M -ary for integer M . The orthogonal dimensions can be time, frequency, polarization, or other features. The most popular time-orthogonal waveform for lasercom is the pulse position modulation (PPM) set. Here, time is divided up into M consecutive, non-overlapping timeslots. Exactly one of the M carries a pulse, while the others are empty. Usually, M is selected to be a power of 2, $M = 2^K$. This way, an M -ary channel symbol represents exactly K channel bits.

Notice that orthogonal modulations have the symmetry property discussed earlier. Thus, we will assume equiprobable prior probabilities, $p_i = 1/M$.

We note here that PPM is very much like OOK with $p_1 = 1/M$. That is, they both have the same peak-to-average ratio and the same probability of sending a pulse. The difference is that PPM requires that there be exactly one pulse every M , where OOK has no such restriction.

Frequency shift keying (FSK) has a single pulse per symbol, but it is a pulse of one of M wavelengths, or frequencies. These are selected so that the time integral of the product of two of the sinusoids, over the period of the pulse, is zero. This property is true when, for instance, the tones are separated by a frequency $1/T_p$, where T_p is the time duration of the tone pulse.

We can also send a pulse of one polarization or the orthogonal polarization (e.g., left-hand circular and right-hand circular). Although the modulation called polarization shift keying (POLSK) is more general, its simple, binary orthogonal form is in the class of orthogonal modulations.

Finally, we will see later that binary DPSK has the orthogonality property, too, although over two bits at a time.

The reason we group together these disparate waveforms is that they will be seen to have the same analysis and performance.

Relationships between pulse, bit, and symbol photon counts for uncoded orthogonal signals are thus

$$N_p = N_s \quad (107)$$

$$= N_b \log(M). \quad (108)$$

Hard decisions for orthogonal signals are different from OOK in that no threshold is required. The receiver first losslessly separates the M orthogonal dimensions—with different time slots for PPM, different band pass filters for FSK, and so on. Measurements are then made on the M components. The receiver selects the one that maximizes the likelihood of choosing the correct signal, usually the largest measurement value.

We will plot capacity and cutoff as source bits per channel usage (i.e., PPM slot) even though the formulas given are per channel symbol. These are then plotted versus average photons per usage as well. These choices simplify the comparisons with OOK.

When we plot efficiencies achievable at channel capacity and cutoff rates, we would like to plot them versus the total bandwidth expansion that the coding plus the modulation requires. The coding expansion we know to be $1/C$. However, orthogonal modulation dimensions require extra bandwidth. M -ary uncoded PPM time slots, for $M = 2^K$, require M times the bandwidth of a single slot (channel usage) to deliver K bits. Thus, the PPM modulation expansion is $M/\log_2(M)$. This value is then multiplied by the expansion due to the coding. For instance, uncoded binary orthogonal requires 2 times the bandwidth of a single slot. Notice that uncoded 4-ary also requires this expansion.

M -ary FSK sends only one pulse per symbol, but the M optical frequencies must be separated by multiples of $1/T_s$. For M -ary, we have M tones to deliver K bits, with a similar bandwidth expansion to PPM. (Actually, the expansion is more like $M-1$ because that is how many frequency spaces there are between M tones. Nevertheless, using the $M/\log_2(M)$ expansion formula for FSK is indicative of the trades involved. For exact measurements of the bandwidth expansion, one would need to know the exact spectrum of the transmitted pulses.) (If the system designer is more interested in the required speed of electronics rather than in signal bandwidth, he might find it useful to normalize all these charts in some other way.)

Orthogonal: Photon-Counting Hard Decisions

A photon counter is used to make the M measurements on the losslessly separated components of the noiseless signal. If any detector sees a photon, then the signal is correctly announced, and no error is made. An error is made only if no photon is counted. This is known as an *erasure* because the receiver knows it doesn't know the answer. Thus, there are really $M + 1$ possible outputs— M correct ones, plus an erasure. Sometimes, the information that an erasure has taken place is useful to the subsequent signal processing, and sometimes it is not. If it is not, the receiver can flip an M -sided coin to make a guess.

The probability of getting an erasure is seen to be

$$P(\text{erasure} | k) = \exp(-N_p) \quad (109)$$

and we then have

$$P(k | k) = 1 - \exp(-N_p) . \quad (110)$$

Thus, the probability of a symbol error, really an erasure, is

$$P_s = \exp(-N_p) , \quad (111)$$

which is shown in Chart 53.

If the decoder does not allow erasures, then the probability of a symbol error, after the coin flip, is

$$P_s = \frac{M-1}{M} \exp(-N_p) \quad (112)$$

since it will map an erasure into a correct symbol only one time out of M . Using Equation (19) we see that such symbol errors map into bit errors as

$$P_b = \frac{1}{2} \exp(-N_b \log M), \quad (113)$$

shown in Chart 54.

We can calculate capacity and cutoff, assuming the decoder knows how to make use of erasures. The results are

$$C_c = (1 - \exp(-N_p)) \log(M) \quad (114)$$

$$R_c = \log M - \log[1 + (M-1) \exp(-N_p)] . \quad (115)$$

Results are plotted in Charts 55–58.

Orthogonal: Heterodyne and Homodyne Receivers—Coherent Hard Decisions

Similar to OOK, we need to calculate the probability density function of outputs with and without signals in them. Let us call them *correct* and *incorrect* outputs, with output densities denoted $p_C(y)$, and $p_I(y)$. A symbol will be incorrectly announced if any of the *incorrect* outputs is larger than the *correct* output. Equivalently, an error will be made if it is not true that the *correct* output is the largest. This hard-decision symbol error probability is thus

$$P_S = 1 - \int p_C(y) \left[\int_0^y p_I(x) dx \right]^{M-1} dy. \quad (116)$$

For our heterodyne and homodyne receivers, we have seen in the previous section that

$$p_I(y) = f_G(y) \quad (117)$$

and

$$p_C(y) = f_G(y - \sqrt{2sN_p}), \quad (118)$$

where $s = 1$ for heterodyne and $s = 2$ for homodyne. In general, the integrals in Equation (116) need to be calculated numerically, although for $M = 2$, they can be shown to simplify to

$$\Phi(\sqrt{sN_p}). \quad (119)$$

The results are shown in Charts 59, 60, 65, and 66. Capacity and cutoff can be calculated by using this formula for P_S and observing symmetries:

$$C_C = \log M - H(P_S) - P_S \log(M-1) \quad (120)$$

$$R_C = \log M - 2 \log \left[\sqrt{1-P_S} + \sqrt{(M-1)P_S} \right] \quad (121)$$

These results are plotted in Charts 61–64 and Charts 67–70.

Orthogonal: Preamplified and Heterodyne Receivers—Noncoherent Hard Decisions

For noncoherent receivers, we saw in the last section that

$$p_I(y) = f_{Ric}(0, y) \quad (122)$$

$$p_C(y) = f_{Ric}(\sqrt{2N_s}, y). \quad (123)$$

We use these functions in Equation (116) to find the symbol error probability

$$P_s = 1 - \int_0^{\infty} \exp[-(x + sN_s)] I_0(\sqrt{4sN_s x}) [1 - \exp(-x)]^{M-1} dx. \quad (124)$$

The term in the square brackets can be further expanded and the M terms integrated separately, to get the final result

$$P_s = \sum_{k=1}^{M-1} \frac{(-1)^{k+1}}{k+1} \binom{M-1}{k} \exp\left(-\frac{kN_s}{k+1}\right). \quad (125)$$

This formula is good for small and medium-sized M . The formula with large M , however, ends up with numerical problems, and then Equation (124) needs to be integrated numerically.

These results are shown in Charts 71 and 72. The formulas for capacity and cutoff are the same as Equations (120) and (121), with these new values of P_s inserted. These results are shown in Charts 73–76.

Orthogonal: Quantum Receiver—Hard Decisions

To calculate symbol error probabilities using Equation (67), it can be shown that the eigenvalues of Equations (64) and (65) are given by

$$\nu_i \equiv 1 + e^{-N_s} \left[\sum_{k=1}^M \exp(-2\pi k i / M) \right], \quad (126)$$

which simplifies to

$$\nu_0 = [1 + e^{-N_s} (M-1)] \quad (127)$$

and

$$\nu_i = [1 - e^{-N_s}] \quad i = 1, 2, \dots, M-1. \quad (128)$$

We can insert these values into the formulas for symbol error probability to deduce

$$P(i|i) = \frac{1}{M^2} \left\{ \sqrt{1 + (M-1)e^{-N_s}} + (M-1)\sqrt{1 - e^{-N_s}} \right\}^2 \quad (129)$$

and also

$$P(i|k) = \frac{1}{M^2} \left\{ \sqrt{1 + (M-1)e^{-N_s}} - \sqrt{1 - e^{-N_s}} \right\}^2, \quad k \neq i. \quad (130)$$

Together, these give the result

$$P_s = \frac{(M-1)}{M^2} \left[\sqrt{1 + (M-1)e^{-N_s}} - \sqrt{1 - e^{-N_s}} \right]^2. \quad (131)$$

The symbol and bit-error rates are shown in Charts 77 and 78. The formulas for semiclassical capacity and semiclassical cutoff are the same as Equations (120) and (121), with this new value of P_s inserted. It can be shown that the formula for cutoff reduces to

$$R_c = \log M - \log v_0. \quad (132)$$

These results are shown in Charts 79–82.

Orthogonal: Photon-Counting Soft Decisions

As in the case of OOK, we observe that, in the noiseless case, detecting one signal photon has the same information as detecting more than one signal photon. Thus, soft-decision capacity and cutoff are the same as for hard decisions, with the understanding that erasures are kind of a special case.

Orthogonal: Heterodyne and Homodyne Receivers—Coherent Soft Decisions

To calculate soft-decision performance, we need to find the probability density function of the group (vector) of M measurements. We can see that the y variable of our output is a vector made up of $\{y_0, y_1, \dots, y_{M-1}\}$. Its probability density function can be written

$$p(\underline{y}|k) = \left(\prod_{i=0}^{M-1} p_I(y_i) \right) \frac{p_C(y_k)}{p_I(y_k)}. \quad (133)$$

We repeat Equation (38) here with explicit notation of the vectors:

$$C_C = \log(M) - \int p_{Y|X}(\underline{y} | 0) \log \left[1 + \sum_{k=1}^{M-1} \frac{p_{Y|X}(\underline{y} | k)}{p_{Y|X}(\underline{y} | 0)} \right] d\underline{y} \quad (38)$$

Inserting Equation (133) into Equation (38), we find

$$C_C = \log(M) - \int p_{Y|X}(\underline{y} | 0) \log \left[1 + \sum_{k=1}^{M-1} \frac{p_C(y_k) p_I(y_0)}{p_I(y_k) p_C(y_0)} \right] d\underline{y} . \quad (134)$$

Using the density formulas in Equations (117) and (118), we can show that the term in the summation reduces to

$$\exp \left[(y_k - y_0) \sqrt{2sN_p} \right] , \quad (135)$$

where the y variables are Gaussian, the 0^{th} variable having the signal as mean. [See Equation (118).]

For M larger than 2, we resort to Monte Carlo simulations to calculate this integral. The results are shown in Charts 83 and 84, and in Charts 87 and 88.

Cutoff rate is simpler. Repeating Equation (48) with explicit notation of the vectors,

$$R_C = \log(M) - \log \left[\sum_k \mathcal{B} \left[p(\underline{y} | 0), p(\underline{y} | k) \right] \right] , \quad (136)$$

observing the symmetries, and using Equation (133), we can show

$$R_C = \log(M) - \log \left(1 + (M-1) \mathcal{B}^2 \left[p_C, p_I \right] \right) . \quad (137)$$

For this coherent case, we find

$$\mathcal{B} \left[p_C, p_I \right] = \exp(-sN_p / 4) . \quad (138)$$

These results are shown in Charts 85 and 86, and in Charts 89 and 90.

Orthogonal: Preamplified and Heterodyne Receivers—Noncoherent Soft Decisions

For noncoherent soft-decision capacity, we follow the development of the coherent case, but use the density functions of Equations (122) and (123). The summation term in Equation (134) then becomes [5]

$$\frac{I_0(y_k \sqrt{2N_p})}{I_0(y_0 \sqrt{2N_p})}, \quad (139)$$

and once again, we use a Monte Carlo simulation to calculate the integral. The result is shown in Charts 91 and 92.

For cutoff, we use Equation (137), where, for this noncoherent case, we can calculate

$$\mathcal{B}[P_C, P_I] = \exp(-N_p/2) \int_0^\infty r \exp(-r^2/2) \sqrt{I_0(r\sqrt{2N_p})} dr \quad (140)$$

[which was shown in Equation (103)]. The cutoff result is shown in Charts 93 and 94.

Orthogonal: Quantum Receiver—Maximum-Likelihood Decoding

For quantum decoding, we again use the eigenvalues of the density operator, which were shown in Equations (127) and (128). We can insert these values into the formulas for capacity and cutoff to find

$$C_Q = \log M - \frac{1}{M} [v_0 \log v_0 + (M-1)v_1 \log v_1] \quad (141)$$

and

$$R_Q = \log(M) - \log(1 + (M-1)e^{-2N_s}) . \quad (142)$$

We can see that this is exactly 3 dB better than the semiclassical cutoff rate shown in Equation (132).

These results are all plotted in Charts 95–98.

5.3 M -ARY PHASE SHIFT KEYING—MPSK

PSK: Preliminaries

Phase shift keying uses a single pulse per symbol, but the pulse's optical phase is one of M phases, equally spaced around the unit circle. Thus, binary PSK uses $0, \pi$; ternary PSK uses $0, \pm 2\pi/3$; 4-ary PSK (known as QPSK) uses $0, \pi, \pm\pi/2$; and so forth. We see that $P_S = P_P$. We also note that the pulses need not be constant amplitude. In fact, any pulse shape can be used to send PSK information, with peak-to-average properties, as well as matched filter designs, having straightforward extensions.

We can note that the MPSK signal is created in two dimensions only—in-phase and quadrature of a single carrier in a single timeslot. (2PSK uses only one dimension.) We saw that orthogonal modulations use M dimensions. Since only two dimensions are used to send more than two bits, MPSK for $M > 2$ is particularly bandwidth efficient. Thus, it is usually employed to achieve high bandwidth efficiency rather than the highest power efficiency, although at M between 3 and 8, one can have some of both.

The MPSK receiver needs to deduce which phase was sent in each pulse. As in the previous modulations, the best performance is usually achieved when the carrier's phase is known or deduced at the receiver (i.e., it is coherent or quantum optimum.) However, noncoherent techniques exist for phase modulations, too. By measuring the *difference* in phase between subsequent pulses, we can deduce properties of the phase without having an absolute coherent reference. These differential phase shift keying (DPSK) techniques will be discussed in the photon-counting and noncoherent sections.

There is another interesting facet about PSK communication that makes its analysis and receivers different from OOK and orthogonal. Since the possible signals are not orthogonal, it will be seen that some errors are more likely than others. That is, even though MPSK has the symmetry property shown in Equation (16), when a particular phase is sent, the receiver is more likely to make the error of choosing a nearby phase than a farther away phase. Soft-decision receivers, of course, implicitly make intelligent use of this fact by measuring the exact received phase and then requiring the decoder to make the best maximum-likelihood use of that information.

Hard-decision receivers, for orthogonal signals, are just as likely to choose ANY incorrect signal as any other. Thus, if a hard decision is made, the decoder for such a system performs its maximum-likelihood calculation with no information other than the symbol decision. For MPSK, however, if a hard decision is made, we see that we have two choices. First, the decoder can always be built like the one for orthogonal signaling—it just takes the symbol or bit decisions and makes algebraic or other simple decisions. The second option is to take the hard symbol decisions and then require that the decoder take into account the structure of the signal constellation. That is, it makes a real maximum-likelihood decision on what it knows about which symbols, if there are errors, are the most likely to have been substituted. (In reality, this extra information requires the knowledge of the probabilities of symbols being in error, and this is a function of the signal and noise levels. However, knowledge of these values does not require symbol-by-symbol measurements and can be gotten by much slower and simpler AGC-type circuits. It is also likely that a very coarse approximation can be made for these two values with very little loss in performance.)

One really needs to weigh the costs and benefits of building each of these structures. The main reason one builds a simple hard-decision receiver is that the technology for making voltage or other soft-decision measurements at that symbol rate is either unavailable or perhaps just too expensive. However, even to make a so-called M -ary hard decision, one still needs to build a circuit to compare the M voltages and choose the largest. This may turn out to be almost as difficult as making the soft decisions in the first place.

A decoder, too, is selected not only to be paired with the selected receiver, but also because of the availability of its own technology. Maximum-likelihood decoders will always require more calculations per bit than algebraic or other simpler decoders.

Selecting a receiver architecture thus requires a careful trade of all the available technologies. For completeness, then, in this PSK section, we will present, in addition to the soft-decision receivers, both kinds of hard-decision systems: the true hard decision receiver, in which the decoder is not required to make use of signal constellation knowledge, and the maximum-likelihood decoder based on the hard decisions, but which DOES make use of the signal structure. We will see that this latter option often gives quite good performance but, as we have stated, may be an impractical option.

PSK: Photon-Counting Hard Decisions

Photon counters cannot discern the phase of the carrier, so these detectors are not applicable to direct measurements of phase. However, there are at least two ways to turn 2PSK into pulses that can be detected using photon counters—differentially and coherently. In Figure 8 we show an architecture for differential photon counting of 2PSK.

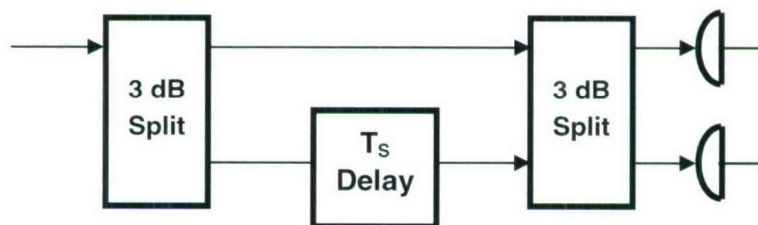


Figure 8. Photon-counting DPSK receiver.

This receiver splits the signal, sends the signals through two arms whose lengths differ by one symbol time, and then interferes the two signals. (That is, it coherently adds and subtracts the two signals at the output ports.) The output is seen to be the same as binary orthogonal—one arm or the other has all the signal. Each output pulse is made up of the sum of two pulses, each at half the power. Thus, this receiver has all the same efficiency properties as photon-counting binary orthogonal. (It does NOT have the well-known 3-dB advantage that heterodyne or preamplified DPSK has over heterodyne or preamplified binary orthogonal—as we will see soon—because of the power split. Also, it should be noted that this system

has twice the bandwidth efficiency of orthogonal because this receiver puts out one bit after every pulse, whereas PPM, for instance, needs two time slots per bit.)

Notice that this receiver really produces the change in phases between two bits. Thus, if we want the original bits at the receiver, we need to have performed pre-encoding at the transmitter. The required encoder is a rate-one coder whose output is the (mod-2) sum of all the source bits transmitted so far. Then, at the receiver, the difference between two phases turns out to be an original source bit. This encoder is called, equivalently, a differential encoder or an accumulator.

There are at least two methods for performing coherent photon counting. The first is shown in Figure 9.

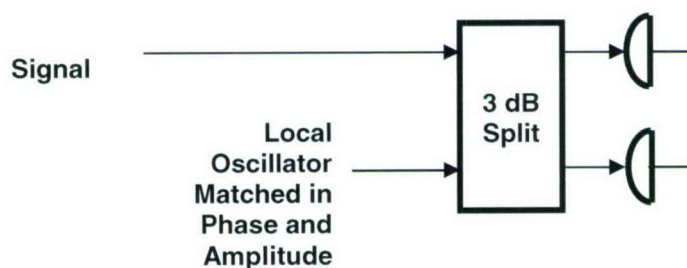


Figure 9. Photon-counting 2PSK receiver—balanced LO version.

This local oscillator is very special: it not only has exactly the same optical phase as the signal, as in a homodyne LO, but also has exactly the same amplitude. Thus, we see that all the power from both arms goes to either one or the other output. This is another binary orthogonal system [see Equation (110)] but this time with 3 dB more power than the DPSK version.

An even better coherent-photon-counting method was invented by Kennedy [12] as an approximation to quantum hard decision. On a $K:1$ splitter, with K approaching infinity, we place the signal and a very large LO. The LO is such that, at the output where most of the signal emerges, the LO has the same amplitude as the signal. Thus, this output is either zero or twice the input amplitude. (The waste port has almost no signal and a very large amount of LO.) It therefore has OOK performance [Equation (76)] but with 4 times the energy in an *on* pulse, which is 3 dB better than photon-counting OOK.

An interesting method of using photon counting for 4PSK was proposed by Bondurant [4]. It uses a configuration like the Kennedy configuration. The LO starts out with the phase of any of the four possible signals. If the selected phase turns out to be the negative of the transmitted phase, then that signal is nulled out and no photons will be counted at the output.

If the selected phase is one of the three other phases, then a signal appears at the output. This may or may not lead to the counting of a photon. If a photon is counted, then we know that the phase of the LO is not the negative of that of the true signal, and we immediately change it to be one of the other possible phases. The idea is that we keep changing phases as we learn which signal it is NOT. Wherever we stop, either because we are right or because we ran out of time, we announce that phase as the negative of the actual transmitted signal.

Bondurant proposes two different rules for deciding on the subsequent phases. They have only slightly different performance, so we will analyze only his so-called Type I receiver.

He shows, assuming Gray coding, that the probabilities of counting 0 or 1 or 2 or 3 photons in succession, assuming the various true signals, are given by the formulas in Table 2. Note that the columns must sum to 1.

Table 2
Event Probabilities for the Bondurant Type I Photon-Counting Receiver for QPSK

	S_{00}	S_{01}	S_{11}	S_{10}
0	1	e^{-2N_s}	e^{-4N_s}	e^{-2N_s}
1	0	$1 - e^{-2N_s}$	$2(e^{-2N_s} - e^{-4N_s})$	$e^{-2N_s} - e^{-4N_s}$
2	0	0	$1 - 2e^{-2N_s} + e^{-4N_s}$	$2(2N_s - 1)e^{-2N_s} + 2e^{-4N_s}$
3	0	0	0	$1 - 4N_s e^{-2N_s} - e^{-4N_s}$

Here, we assume that the user starts with the nulling signal for S_{00} , followed by S_{01} , S_{11} , and finally S_{10} , the signals walking around the circle. By symmetry, we need only analyze one starting point, S_{00} , especially if each new symbol at the receiver gets a randomly chosen starting point.

For hard decisions, we assume that “no counts” is announced as S_{00} , “one count” as S_{01} , and so on. From this table, we can deduce that the probability of making a 2-bit error is

$$[P(0|S_{11}) + P(1|S_{10})] / 4 = (1/4) \exp(-2N_s) \quad (143)$$

and the probability of choosing one bit correct and one incorrect is

$$[P(0|S_{01}) + P(0|S_{10}) + P(1|S_{11}) + P(2|S_{10})] / 4 = (N_s + 1/2) \exp(-2N_s) . \quad (144)$$

From these formulas, we can calculate symbol and bit-error probabilities. To calculate classical capacity and cutoff, we have two choices. The true hard-decision analysis assumes that the decoder is given just the symbol decision, with no information about the path it took to get there. Thus, the hard-decision calculations of capacity and cutoff use only Equations (143) and (144). We will examine a more soft-decision approach in a later section.

Error-rate performances of all these (coherent) photon-counting PSK systems are shown in Charts 99 and 100. (We have also included symbol error probability for the Type II receiver, as calculated by Bondurant.) The capacity and cutoff results are shown in Charts 101–104. (As an aside, we can note here that the cutoff formula for photon-counting orthogonal $M = 2$ and photon-counting OOK $p_1 = 1/2$ turn out to be exactly the same, as can be seen from the noncoherent and coherent/Kennedy cutoff curves.)

PSK: Heterodyne and Homodyne Receivers—Coherent Hard Decisions

If, in a homodyne receiver, the local oscillator has the phase of the 0 (or the 1) signal of a binary PSK input, then that receiver's output is a baseband signal corresponding to the 1's and 0's, which can be baseband matched filtered. As mentioned in Section 2.2, an optical hybrid can be used to make homodyne-like measurements of QPSK. These are at baseband, but do not achieve the 3-dB improvement the binary homodyne receiver sees. Finally, a heterodyne receiver uses a heterodyne front end, and then follows it with a classical (RF-style) coherent MPSK matched-filter receiver.

It can be shown that the hard-decision error probability for homodyne 2PSK is

$$p_b = \Phi(\sqrt{4N_s}) . \quad (145)$$

For coherent heterodyne, MPSK has the symbol probability

$$P_{SM} = f_c(\sqrt{2N_s}, \frac{\pi}{M}) , \quad (146)$$

where we let P_{SM} be the M -ary symbol error probability, and where Craig's function f_c was defined in Equation (6). It has the properties that

$$P_{s2} = \Phi(\sqrt{2N_s}) \quad M = 2 \quad (147)$$

$$P_{s4} = 1 - (1 - P_{s2})^2 \quad M = 4 . \quad (148)$$

Interestingly, the bit-error probability from Gray-coded 4PSK is the same as the bit (symbol) error probability from 2PSK.

For the true hard-decision receiver, as discussed in the introductory PSK section, we need to analyze a decoder that assumes only that a symbol is either correct or incorrect. Thus, the error probabilities for each of the $(M - 1)$ incorrect symbols is assumed to be

$$P_E = P_{SM} / (M - 1) \quad (149)$$

and the probability of the correct symbol choice is

$$P_C = 1 - P_{SM} . \quad (150)$$

Symbol error probabilities are shown in Chart 105 for heterodyne and Chart 113 for homodyne. Bit-error probabilities are shown in Charts 106 and 114.

Using these formulas, we can also calculate the pure hard-decision coded performance. We only show cutoff for this case because any decoding technique that could have achieved capacity would have used a maximum-likelihood algorithm, for which the added complexity of signal structure knowledge would certainly have been worth it. We show cutoff results for this heterodyne MPSK case in Charts 107 and 108.

To calculate capacity and cutoff for hard decisions with maximum-likelihood decoding, we need to calculate the probabilities, not just of symbol errors, but of choosing each output symbol given each possible input symbol. By the equal phase-spacing property, we see that we need only find the probabilities of declaring each $k \neq 0$, given that 0 was sent. Let us number the symbols $0, 1, \dots, M-1$ as we travel around the unit circle. That is, symbol k is declared if the phase is measured as being between

$$\frac{(2k-1)\pi}{M} \quad \text{and} \quad \frac{(2k+1)\pi}{M} .$$

Using Craig's probability function [Equation (6)], it can be shown that the probability of choosing symbol k is

$$\begin{aligned} P(k | 0) &= \frac{1}{2} \left[f_c \left(\sqrt{2N_s}, \frac{(2k-1)\pi}{M} \right) - f_c \left(\sqrt{2N_s}, \frac{(2k+1)\pi}{M} \right) \right] \quad 1 \leq k \leq \frac{M-1}{2} \\ &= P(M-k | 0) \end{aligned} \quad (151)$$

and, for M even, the center ($M/2$) term is given by

$$P\left(\frac{M}{2} | 0\right) = f_c \left(\sqrt{2N_s}, \frac{(M-1)\pi}{M} \right) . \quad (152)$$

We first use these formulas to calculate the heterodyne bit-error probabilities by weighting each multi-bit-error pattern with its probability. These probabilities are shown in Chart 106.

Using these probability formulas in Equations (28) and (42), we can also calculate the capacity and cutoff curves, whose results are shown in Charts 109–112 for heterodyne and Charts 115–118 for binary homodyne.

PSK: Preamplified and Heterodyne Receivers—Noncoherent Hard Decisions

As mentioned briefly above, the noncoherent techniques for MPSK measure differences in phase between subsequent symbols. (Although we will not pursue them here, there are more efficient noncoherent MPSK receivers that examine more than two symbols in a row [9, 16].) A particularly efficient architecture for

binary systems that has found much utility in wideband systems is an optical preamplifier, followed by the interferometer-based demodulator shown in Figure 8. As discussed earlier, such a DPSK system requires a precoding at the transmitter with a differential encoder.

For larger M , one would need to make phase measurements in the two symbols and then deduce which phase transition was most likely, although there are sometimes architectural tricks to simplify this structure.

The symbol error probability of a differential MPSK receiver (sometimes called MDPSK or some other variant) can be shown to be

$$P_s = f_p(\sqrt{2N_s}, \frac{\pi}{M}), \quad (153)$$

where f_p is Pawula's function, defined in Equation (11). This symbol error probability is plotted in Chart 119 with the related, Gray-coded bit-error probability in Chart 120.

As in the coherent case, we first calculate the true hard-decision cutoff using this symbol error probability along with an analog of Equations (149) and (150). These results are shown in Charts 121 and 122.

Also following the coherent case, in order to calculate capacity and cutoff for hard decisions with maximum-likelihood decoding, we need to find specific symbol error probabilities. Exactly paralleling the coherent case, we find that the probability of choosing symbol k when symbol 0 is correct is

$$\begin{aligned} P(k|0) &= \frac{1}{2} \left[f_p\left(\sqrt{2N_s}, \frac{(2k-1)\pi}{M}\right) - f_p\left(\sqrt{2N_s}, \frac{(2k+1)\pi}{M}\right) \right] \quad 1 \leq k \leq \frac{M-1}{2} \\ &= P(M-k|0) \end{aligned} \quad (154)$$

and for M even, we have

$$P\left(\frac{M}{2}|0\right) = f_p\left(\sqrt{2N_s}, \frac{(M-1)\pi}{M}\right). \quad (155)$$

Using these functions, we can calculate capacity and cutoff, with the results shown in Charts 123–126.

We can note here briefly that binary DPSK compares the sequences (1, 1) and (1, -1), which are seen to be orthogonal two-bit sequences. Thus, all the performance equations (in heterodyne, homodyne, and preamplified receivers) for binary DPSK are the same as binary orthogonal except that the DPSK decision uses the energy from two sequential symbols. Thus, binary DPSK is exactly 3 dB better than binary orthogonal in every metric (except the noncoherent photon-counting variant, as mentioned earlier).

PSK: Quantum Receiver—Hard Decisions

Without performing the derivation here, it can be shown that the optimized quantum measurement operators result in performance described by [12]

$$\begin{aligned} P(j|k) &= \left| \frac{1}{M} \sum_{i=0}^{M-1} \sqrt{v_i} \exp[-j\pi 2(j-k)i/M] \right|^2, \\ &= P(j-k|0) \end{aligned} \quad (156)$$

where

$$v_i = \sum_{k=0}^{M-1} \exp[-2N_s \sin^2\left(\frac{\pi k}{M}\right)] \exp[jN_s \sin\left(\frac{2\pi k}{M}\right)] \exp[j2\pi ki/M]. \quad (157)$$

Note that both these formulas involve discrete Fourier transforms. Also note the explicit satisfaction of the symmetry property in Equation (156).

Using these formulas, we can calculate the symbol probability using Equation (67). Results are shown in Charts 127 and 128.

We reason that one who works hard enough to build a quantum optimum receiver would not settle for the “pure” hard-decision decoder. Thus, we will only calculate the maximum-likelihood decoding performance. Using Equation (156) in Equations (28) and (42), we can calculate semiclassical capacity and semiclassical cutoff for quantum hard decisions (for the $L = M$ case, as discussed earlier). Care must be taken with the complex nature of the x_{jk} values defined in Equations (55) through (59).

These results are all shown in Charts 129–132.

PSK: Photon-Counting Soft Decisions

As in the cases of OOK and orthogonal, we observe that, in the noiseless *binary* cases, detecting one signal photon has the same information as detecting more than one signal photon. Thus, soft-decision capacity and cutoff are the same as for hard decisions. This applies to all the *binary* photon-counting methods presented earlier.

The Bondurant photon-counting 4PSK approach, however, has a kind of soft metric that comes along with the hard decision—namely, how many counts were counted. We would know, for example, that if we announced “01” after one count, the answer is likely 01, but might also be 11 or 10. However, it could NOT be 00, since that hypothesis was rejected by counting the first photon. Thus, the decoder can make use of this information.

The symbol error probabilities were given in Table 2 earlier. Assuming that each starting phase is randomly chosen, we can calculate classical capacity for this hard-decision-plus-ML decoding system. The results are shown in Charts 133 and 134.

We should also note that Bondurant designed this receiver for uncoded, hard-decision use. Hence, its performance is less good for low code rates. It is likely that a variant on his decision rule could give better coded performance.

There is one more observation to be made here. It has been shown [2] that the likelihood function for any photon-counting scheme is more correctly a function of the actual times of the photon arrivals. In fact, in his Type II, Bondurant used these times to try to improve QPSK hard-decision performance. Using either Type I or Type II, the exact likelihood functions for receiving 0 or 1 or 2 photons in succession can be calculated, using the arrival times. We will not perform this calculation here.

PSK: Heterodyne and Homodyne Receivers—Coherent Soft Decisions

To calculate capacity and cutoff rate for coherent, soft-decision PSK, we need to find the distances between the signal points around the unit circle. These can be found using straightforward geometry. The results, when inserted into the formulas of Equations (38) and (48) can be shown to be

$$C_c = \log(M) - \int f_G(x) \int f_G(y) \log \left[\sum_{k=0}^{M-1} \exp \left\{ -2 \left\{ N_s \sin^2 \left(\frac{\pi k}{M} \right) + \sqrt{N_s} \sin \left(\frac{\pi k}{M} \right) \left[x \sin \left(\frac{\pi k}{M} \right) - y \cos \left(\frac{\pi k}{M} \right) \right] \right\} \right\} \right] dy dx \quad (158)$$

and

$$R_c = \log(M) - \log \left\{ 1 + \sum_{k=1}^{M-1} \exp \left[-N_s \sin^2 \left(\frac{\pi k}{M} \right) \right] \right\} . \quad (159)$$

Since the capacity is a simple (two-dimensional) expected value, it can be calculated using either numerical integration or Monte Carlo techniques.

These results are shown in Charts 135–138.

For homodyne 2-PSK, replace N_s by $2N_s$ in these formulas. For other M , homodyne is not generally attempted. (See the discussion in Section 2.2.)

The results for binary homodyne are shown in Charts 139–142.

PSK: Preamplified and Heterodyne Receivers—Noncoherent Soft Decisions

To calculate the performance of noncoherent MPSK, we need to find the probability density of the complex components of the two adjacent symbol times, but averaged over the unknown phase angle, assumed to be uniformly distributed. This is kind of a generalization of the Rician density [Equation (7)] and is given by

$$p(\underline{y}|k) = \frac{1}{2\pi} \exp\left[-(2N_s + \frac{|y_0|^2 + |y_1|^2}{2})\right] I_0\left[\sqrt{2N_s} |y_0 + y_1 e^{jk2\pi/M}|\right], \quad (160)$$

where \underline{y} is the two-dimensional complex vector of the two symbols. We can see the phase relationship between the two symbols is $2\pi k/M$, which implies a differential encoding. We insert this formula in Equation (38) to find the capacity. Similarly, we insert it into Equation (48) to find the cutoff. These results are shown in Charts 143–146. As mentioned above, there are more efficient receivers that make use of multiple sequential symbols [16]. Also as mentioned earlier, binary (noncoherent, 2-bit observation interval) DPSK has exactly the same form as binary orthogonal, but with 3 dB better performance.

PSK: Quantum Receiver—Maximum-Likelihood Decoding

We can use the eigenvalues of Equation (157) in Equation (66) to calculate quantum capacity. We can also use them in Equation (70) to find quantum cutoff explicitly (using Parseval's theorem to simplify the formula)

$$R_Q = \log(M) - \log\left(1 + \sum_{k=1}^{M-1} \exp\left[-4N_s \sin^2\left[\frac{\pi k}{M}\right]\right]\right), \quad (161)$$

which is seen to be exactly 3 dB better than cutoff using homodyne soft decision. These results are shown in Charts 147–150.

6. DISCUSSION AND COMPARISON OF SOME MODULATION FORMATS AND RECEIVERS

In this section, we will make explicit comparisons of some of the results we have shown in order to see the benefits and drawbacks of employing the different methods.

First, in Charts 151 and 152, we compare the theoretical optimum coded performance for unconstrained classical and quantum systems. At low code rates (high bandwidth, low signal power) there is a 3-dB jump from classical cutoff to classical capacity, then another 3 dB to quantum cutoff. Quantum optimum capacity is seen to have a very different quality in that it continues to improve as the bandwidth increases.

In Chart 153, we plot BER for symmetric OOK using all the different receiver structures we have investigated. We can see that in uncoded systems at high signal powers where the BER is low, there is about a 3-dB gain going from heterodyne to homodyne receivers and another 3 dB going to either photon-counting or quantum optimum. For hard-decision coded systems, however, where we would operate at high BER, the efficiency gains are not so clear-cut.

In Charts 154 and 155, we can see the BER for orthogonal signals with various receivers, for $M = 2$ and 4.

In Chart 156, we see the BER for all the receivers for 2PSK, including the several photon-counting variants. Once again, optimum quantum hard-decision and (coherent) photon-counting variants do the best at high signal powers.

In Chart 157, we compare many different binary coded systems. It is quite clear where the gains are.

In Charts 158–162, we compare the performance at capacity of generalized OOK for the different receivers at various peak-to-average ratios. Interestingly, for high ratios, noiseless photon counting does just about as well as quantum optimum hard decision. We can also see that at fairly high bandwidths (i.e., low FEC code rates), this family essentially achieves optimum hard-decision capacity performance.

In Charts 163–167, we compare the performance at capacity of orthogonal modulation for various alphabet sizes, M . Here, it is interesting to see that at high M , photon counting does better than the so-called quantum optimum hard decision. This is because the hard-decision system had been constrained to make a decision between the M possibilities, while our photon-counting receiver was allowed an $M + 1$ th output, the erasure. Although we will not derive it here, an optimum [choose $L > M$, with the notation of Equation (57)] symbol measurement would do better than this $L = M$ measurement, although for high M , it is doubtful that the optimum would be much better than the photon-counting receiver.

In Charts 168–171, we compare generalized OOK and orthogonal for several receiver types. We can see that OOK is quite a bit better at low peak-to-average ratios (M), but that the differences become less at high M and high bandwidth (low code rate). In general, we can see that these pulsed formats are very near

their theoretical optimum channel capacities for many M in heterodyne (and homodyne) soft-decision and quantum optimum systems.

In Charts 172 and 173, we compare coded performance of 2-ary and 4-ary PSK for various receivers. We can see that there is a big gap between all the symbol-by-symbol hard-decision systems and the quantum optimum system. The potential gain here certainly justifies investigation into code and receiver construction for the quantum optimum.

In Chart 174, we compare optimum quantum coded performance for many of the modulation formats.

For completeness, we show in Charts 175–177 the forms of the eigenvalues of the quantum density operators [see Equations (63) to (65)]. The eigenvalues for PSK have a quite different shape from those of OOK and orthogonal.

We conclude with Table 3 (variants of which can be found in many references), which gathers the bit-error rate performance formulas for all the binary formats we have presented, using each of the receivers we have analyzed. Although it is of interest, we have seen that the more complex channel capacity formulas are really the ones that show the performance we seek.

Table 3
Bit-Error Rate Formulas for Binary Modulations

Modulation Format	Receiver Type	Bit-Error Probability	Comments
OOK	Photon Counting	$\frac{1}{2} \exp(-2N_b)$	Only error type is by missing a '1'
	Heterodyne Coherent	$\Phi(\sqrt{N_b})$	Requires threshold
	Homodyne Coherent	$\Phi(\sqrt{2N_b})$	Requires threshold
	Heterodyne Noncoherent	$\frac{1}{2} [1 + Q(0, T) - Q(2\sqrt{N_b}, T)]$	Requires threshold, T [see Equation (92)]
	Quantum Optimum	$\frac{1}{2} (1 - \sqrt{1 - \exp(-2N_b)})$	
Orthogonal	Photon Counting	$\frac{1}{2} \exp(-N_b)$	Error from coin flip when erasure
	Heterodyne Coherent	$\Phi(\sqrt{N_b})$	
	Homodyne Coherent	$\Phi(\sqrt{2N_b})$	
	Heterodyne Noncoherent	$\frac{1}{2} \exp(-N_b/2)$	
	Quantum Optimum	$\frac{1}{2} (1 - \sqrt{1 - \exp(-2N_b)})$	
PSK	Photon Counting Noncoherent	$\frac{1}{2} \exp(-N_b)$	Error from coin flip when erasure
	Photon-Counting Coherent Symmetric	$\frac{1}{2} \exp(-2N_b)$	Error from coin flip when erasure
	Photon Counting Coherent Kennedy	$\frac{1}{2} \exp(-4N_b)$	Only error type is by missing a '1'
	Heterodyne Coherent	$\Phi(\sqrt{2N_b})$	
	Homodyne Coherent	$\Phi(\sqrt{4N_b})$	
	Heterodyne Noncoherent	$\frac{1}{2} \exp(-N_b)$	
	Quantum Optimum	$\frac{1}{2} (1 - \sqrt{1 - \exp(-4N_b)})$	

7. CONCLUSION

It is hoped that this collection might serve several functions:

- Act as a single place for finding many relevant equations for many communications analyses
- Serve as a reminder of all the design possibilities there are for the lasercom system designer
- Act as a repository of basic references, explicit and implicit, that may serve as a jumping-off point for the interested reader

However, the main hope of the author is that these side-by-side presentations and comparisons will motivate the reader to invent efficient systems that can achieve the theoretical possibilities.

REFERENCES

- [1] Ban, M., Kurokawa, K., and Hirota, O., "Cut-off rate performance of quantum communication channels with symmetric signal states," *J. Opt. B: Quantum Semiclass. Opt.*, 1999, pp. 206–218.
- [2] Bar-David, I., "Communication Under the Poisson Regime," *IEEE Transactions on Information Theory*, Vol. 15, No. 1, January 1969, pp. 31–37.
- [3] Barry, J.R. and Lee, E.A., "Performance of coherent optical receivers," *Proceedings of the IEEE*, Vol. 78, No. 8, August 1990, pp. 1369–1394.
- [4] Bondurant, R. S., "Near-Quantum Optimum Receivers for the Phase-Quadrature Coherent-State Channel," *Optics Letters*, Vol. 18, No. 22, November 15, 1993, pp. 1896–1898.
- [5] Butman, S., Bar-David, I., Levitt, B. Lyon, R., and Klass, M., "Design Criteria for Noncoherent Gaussian Channels with MFSK Signaling and Coding," *IEEE Transactions on Communications*, Vol. 24, No. 10, October 1976.
- [6] Chinn, S.R., Boroson, D.M., and Livas, J.C., "Sensitivity of optically preamplified DPSK receivers with Fabry-Perot filters," *Journal of Lightwave Technology*, Vol. 14, No. 3, March 1996, pp. 370–376.
- [7] Craig, J.W., "A new, simple and exact result for calculating the probability of error for two-dimensional signal constellations," *Military Communications Conference*, 1991. MILCOM '91, Conference Record, 4–7 November 1991, Vol. 2, pp. 571–575.
- [8] Davies, E.B., "Information and Quantum Measurement," *IEEE Transactions on Information Theory*, Vol. IT-34, No. 5, September 1978, pp. 596–599.
- [9] Divsalar, D. and Simon, M.K., "Multiple-symbol differential detection of MPSK," *IEEE Transactions on Communications*, Vol. 38, March 1990, pp. 300–308.
- [10] Eldar, Y.C. and Forney, G.D., Jr., "On Quantum Detection and the Square-Root Measurement," *IEEE Transactions on Information Theory*, Vol. 47, No. 3, March 2001, pp. 858–872.
- [11] Gallager, R.G., *Information Theory and Reliable Communication*, New York: John Wiley and Sons, 1968.
- [12] Helstrom, C.W., *Quantum Detection and Estimation Theory*, New York: Academic Press, 1976.
- [13] Holevo, A.S., "Coding Theorems for Quantum Channels," eprint arXiv:quant-ph/9809023, September 1998.

- [14] Kazovsky, L.G., "Phase- and Polarization-Diversity Coherent Optical Techniques," *IEEE/OSA Journal of Lightwave Technology*, Vol. LT-7, No. 2, pp. 279-92, February, 1989.
- [15] Pawula, R.F., "Generic error probabilities," *IEEE Transactions on Communications*, Vol. 47, No. 5, May 1999, pp. 697-702.
- [16] Peleg, M. and Shamai, S., "On the Capacity of the Blockwise Incoherent MPSK Channel," *IEEE Transactions on Communications*, Vol. 46, No. 5, May 1998, pp. 603-609.
- [17] Proakis, J.G., *Digital Communications*, New York: McGraw-Hill, 1983.
- [18] Shannon, C.E., "A Mathematical Theory of Communications," *Bell Syst. Tech. J.*, Vol. 27, July 1948, pp. 379-423.
- [19] Shannon, C.E., "A Mathematical Theory of Communications," *Bell Syst. Tech. J.*, Vol. 27, October 1948, pp. 623-656.
- [20] Shannon, C.E., "Probability of Error for Optimal Codes in a Gaussian Channel," *Bell Syst. Tech. J.*, Vol. 38, May 1959, pp. 611-656.
- [21] Shnidman, D.A., "The calculation of the probability of detection and the generalized Marcum Q-Function," *IEEE Transactions on Information Theory*, Vol. 35, No. 2, March 1989, pp. 389-400.
- [22] Tonguz, O.K. and Kazovsky, L.G., "Theory of Direct-Detection Lightwave Receivers Using Optical Amplifiers," *IEEE/OSA Journal of Lightwave Technology*, Vol. 9, No. 2, February, 1991, pp. 174-81.
- [23] Wyner, A.D., "Capacity and error exponent for the direct detection photon channel—part 1," *IEEE Trans. Information Theory*, Vol. 34 (6), November 1988, pp.1449-1461.

CHARTS

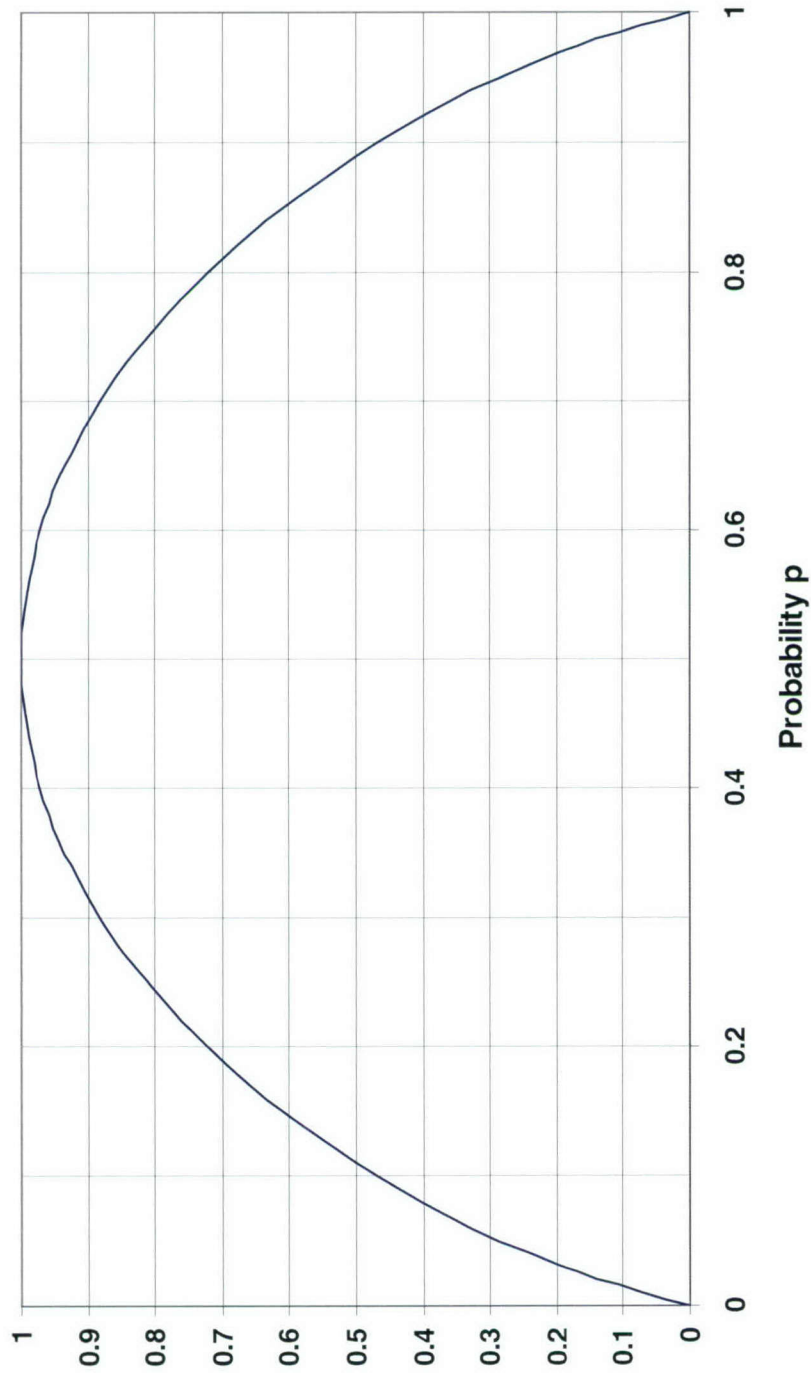


Chart 1. Binary entropy function.

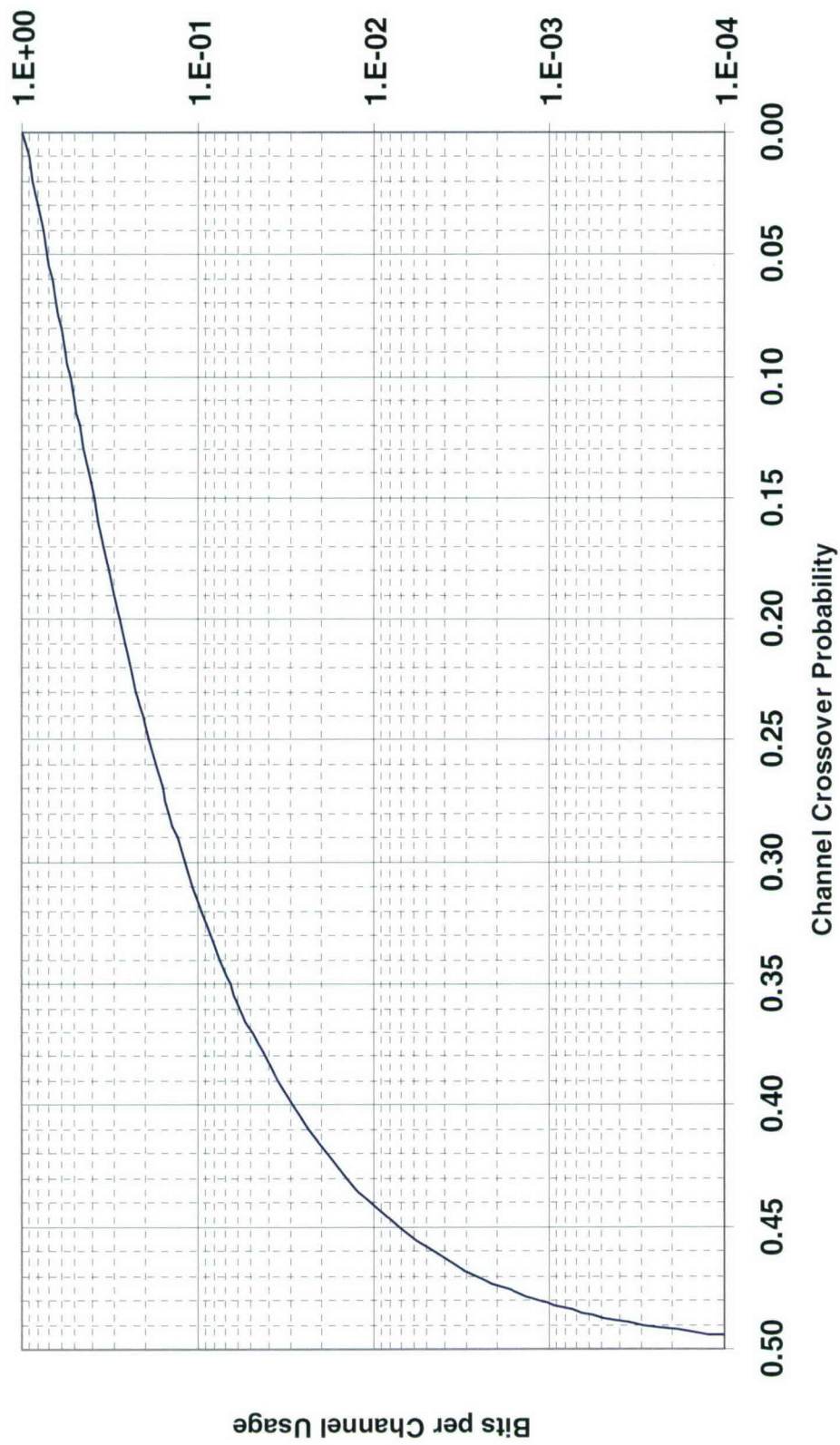


Chart 2. Classical capacity: BSC (hard decisions).

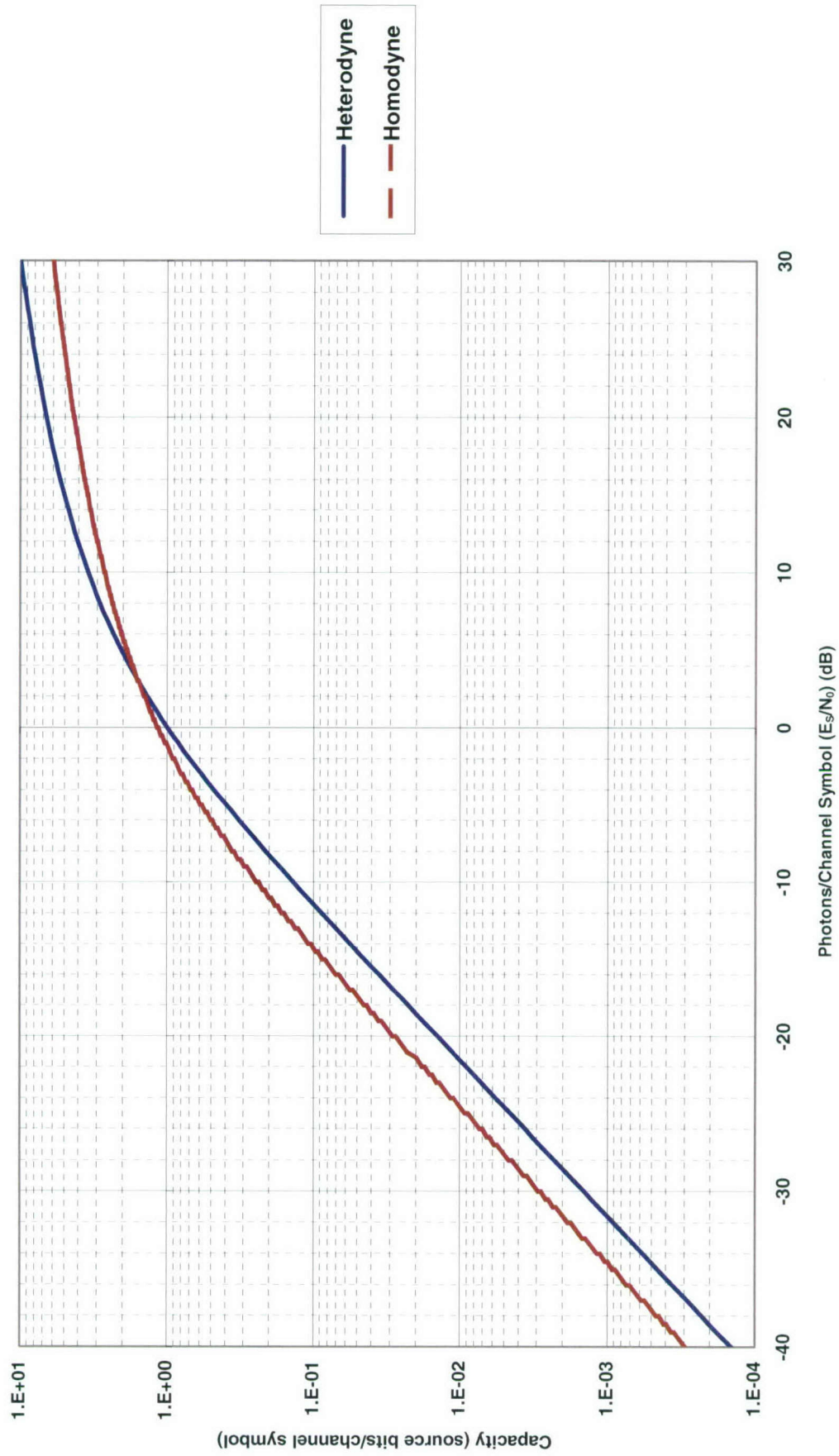


Chart 3. Classical capacity: Coherent Gaussian.

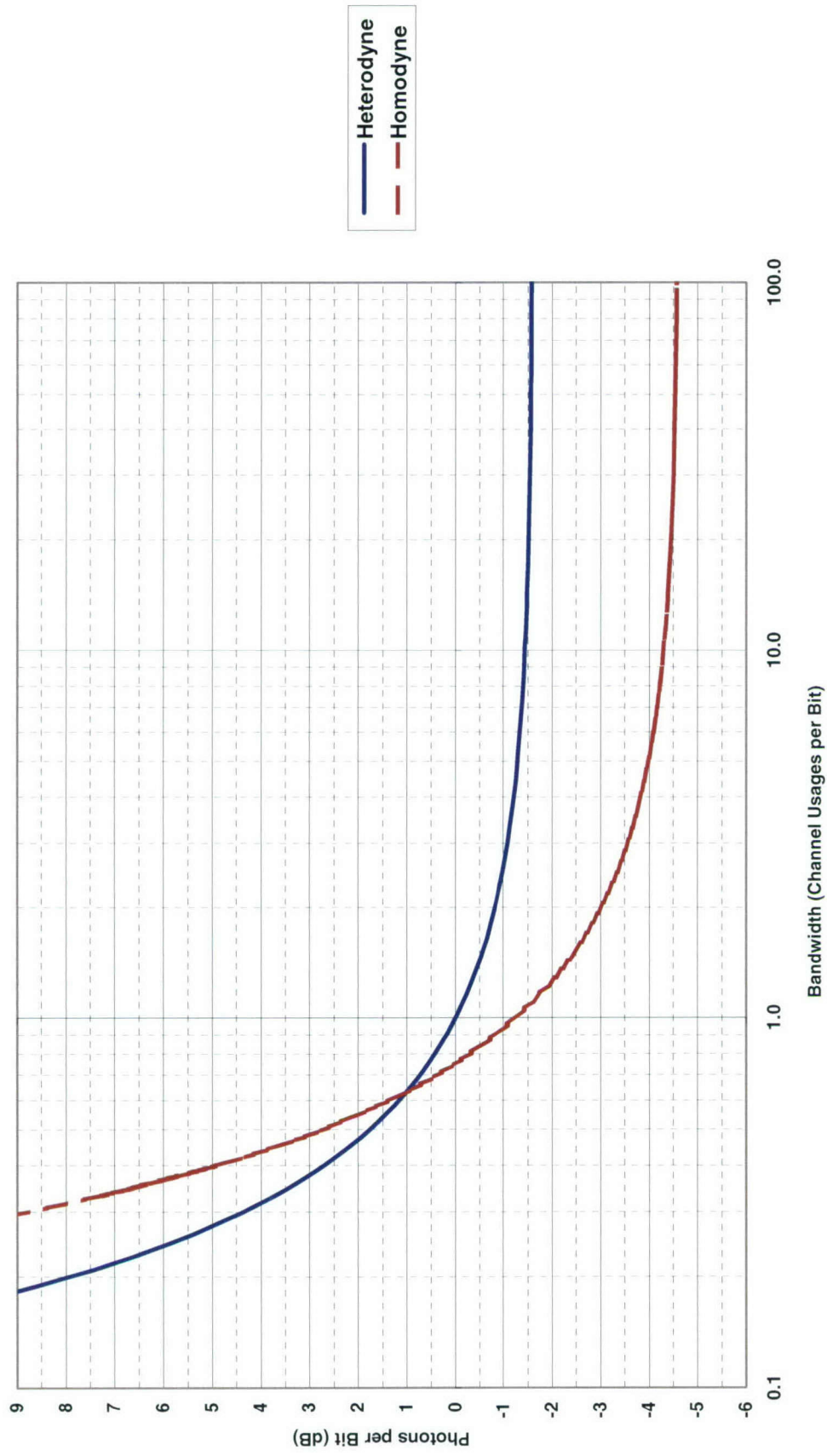


Chart 4. Efficiency at classical capacity: Coherent Gaussian.

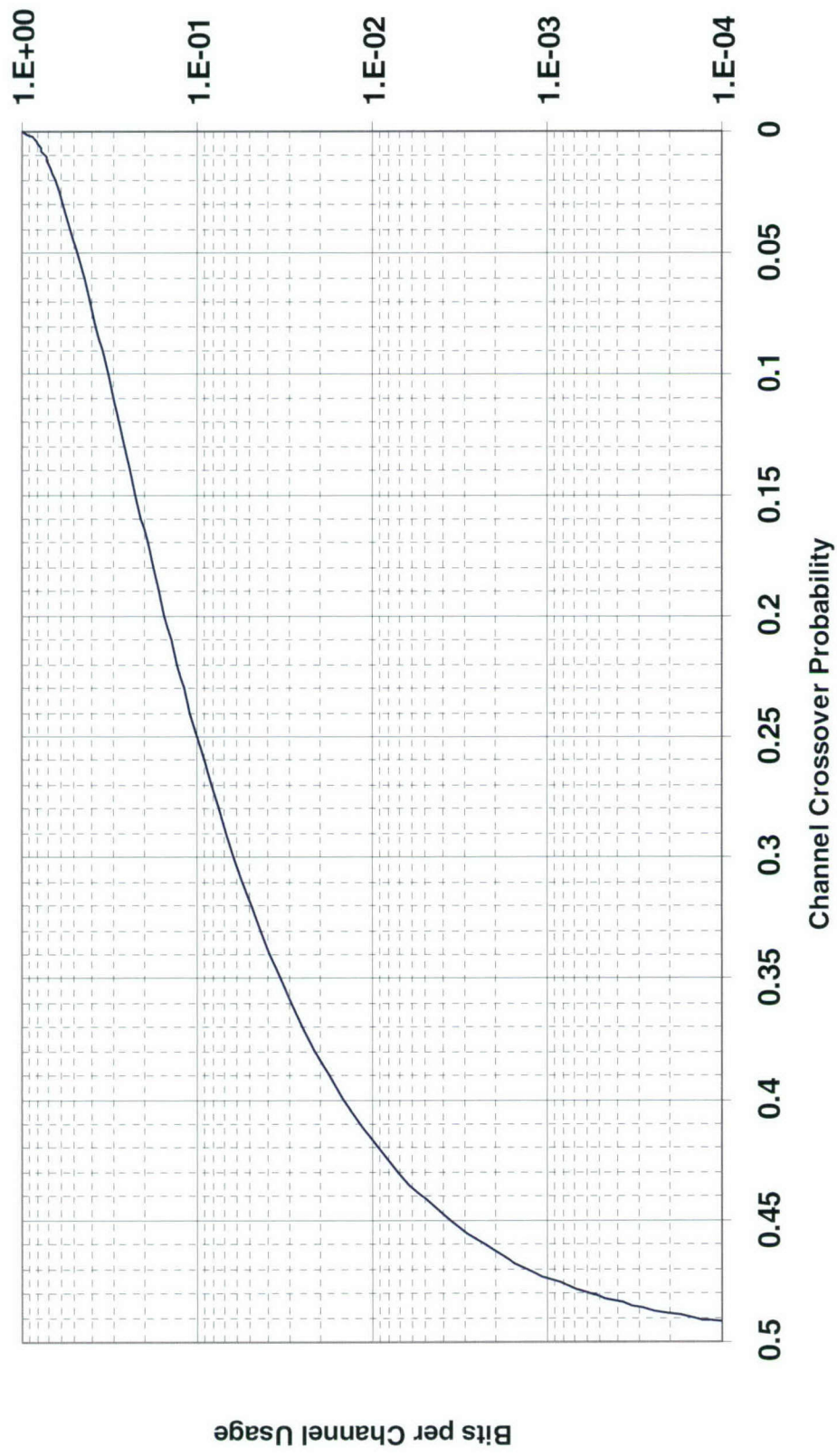


Chart 5. Classical cutoff: BSC (hard decision).

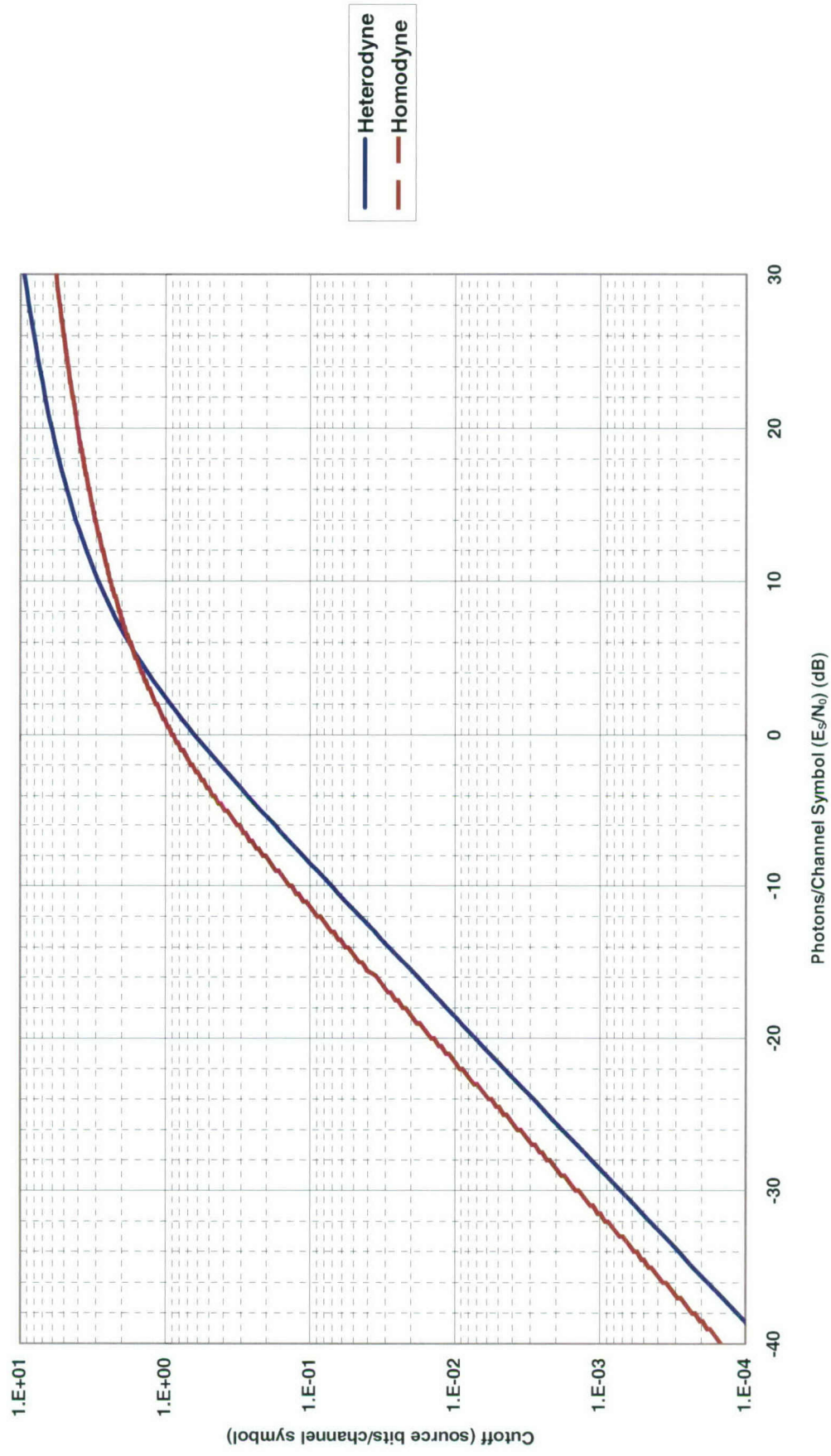


Chart 6. Classical cutoff: Coherent Gaussian.

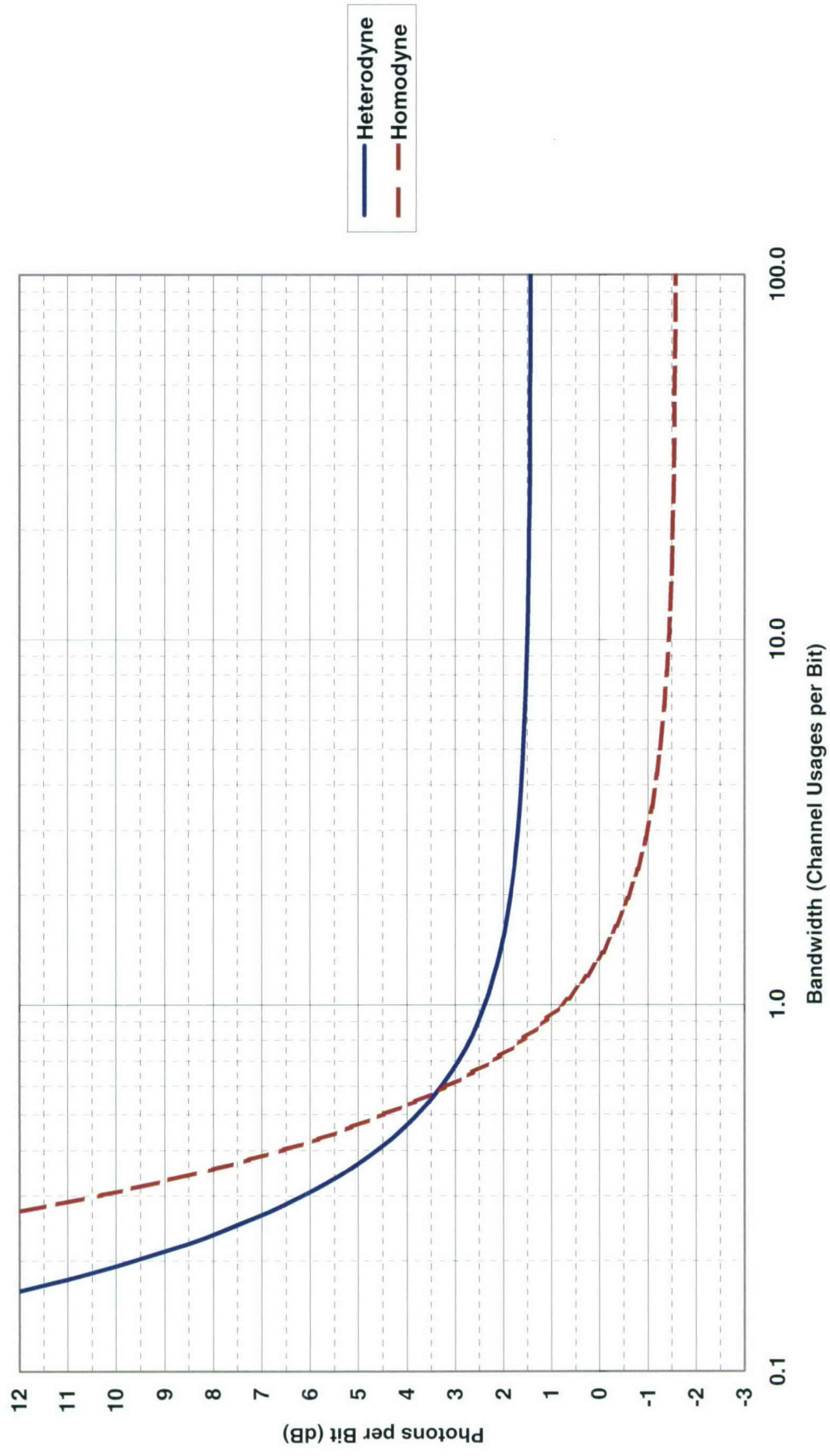


Chart 7. Efficiency at classical cutoff: Coherent Gaussian.

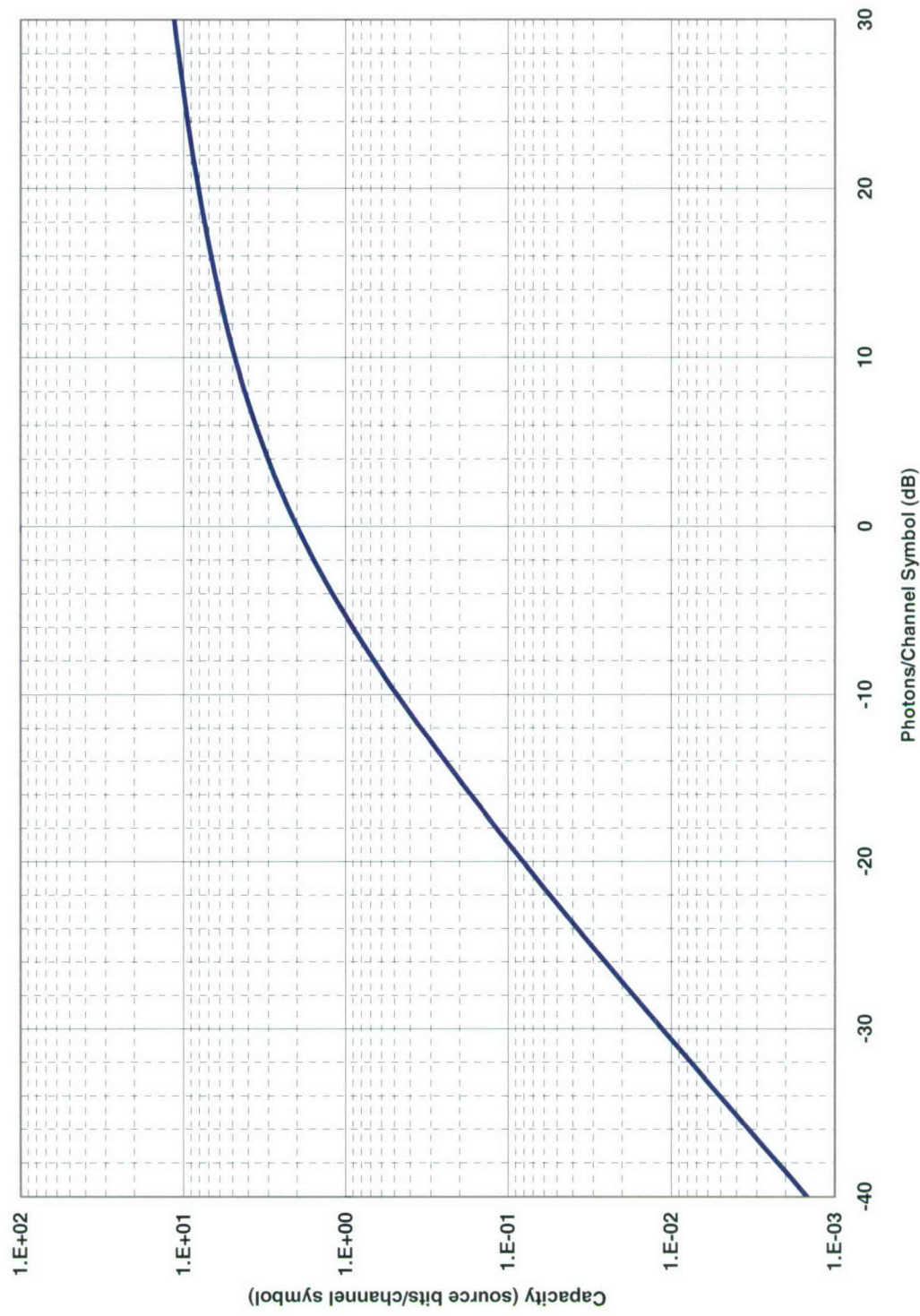


Chart 8. Quantum capacity: Gaussian.

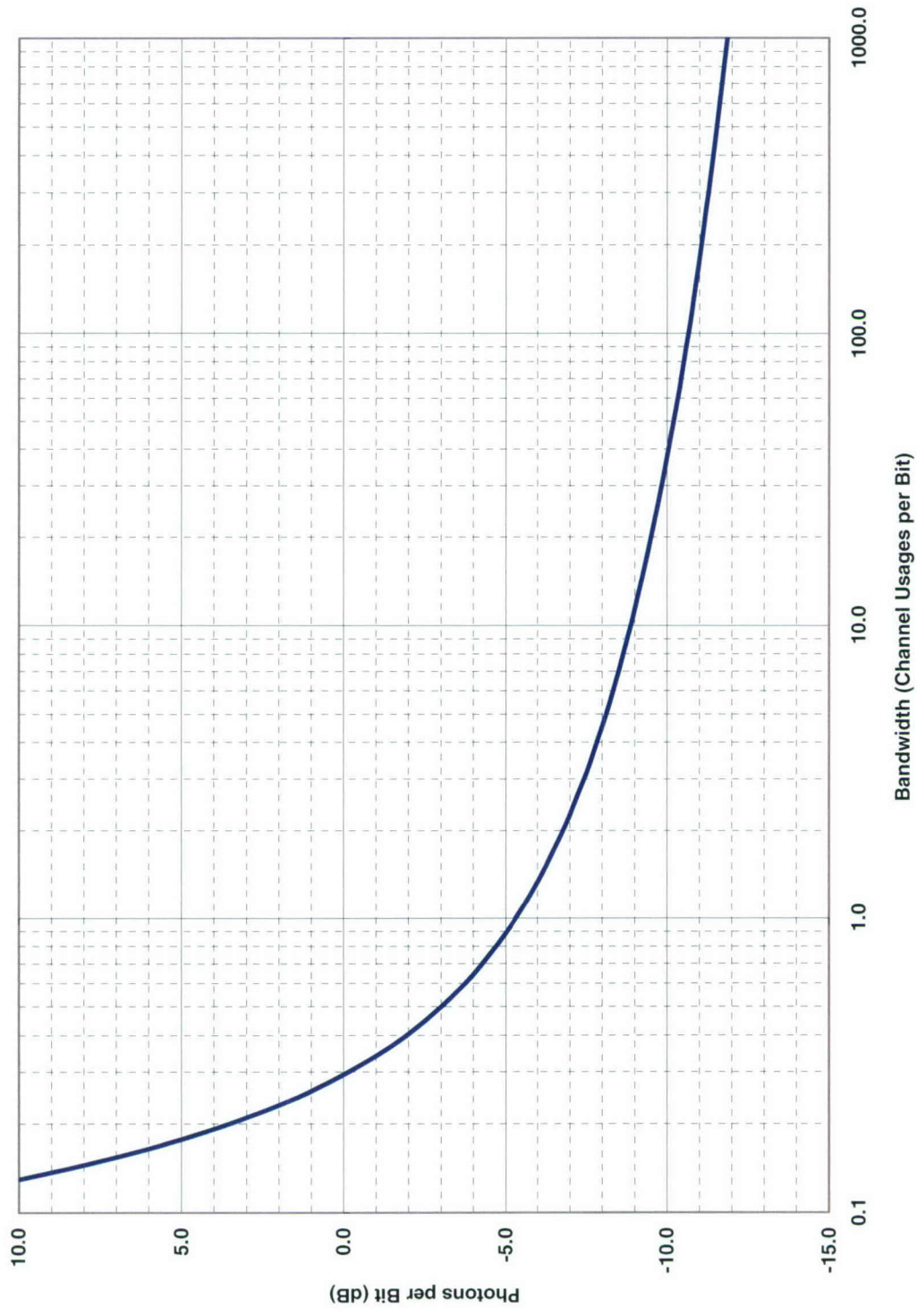


Chart 9. Efficiency at quantum capacity: Gaussian.

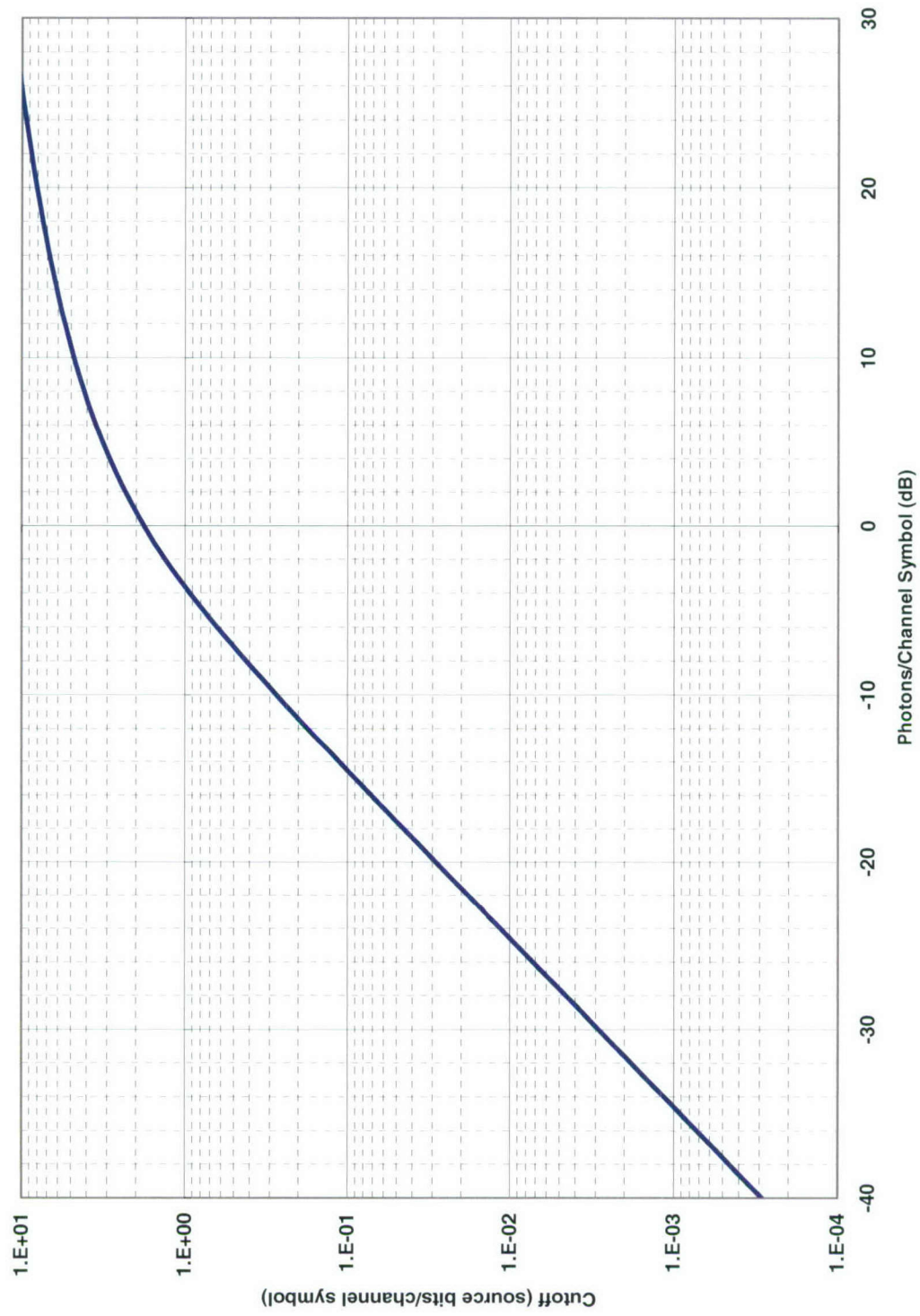


Chart 10. Quantum cutoff: Gaussian.

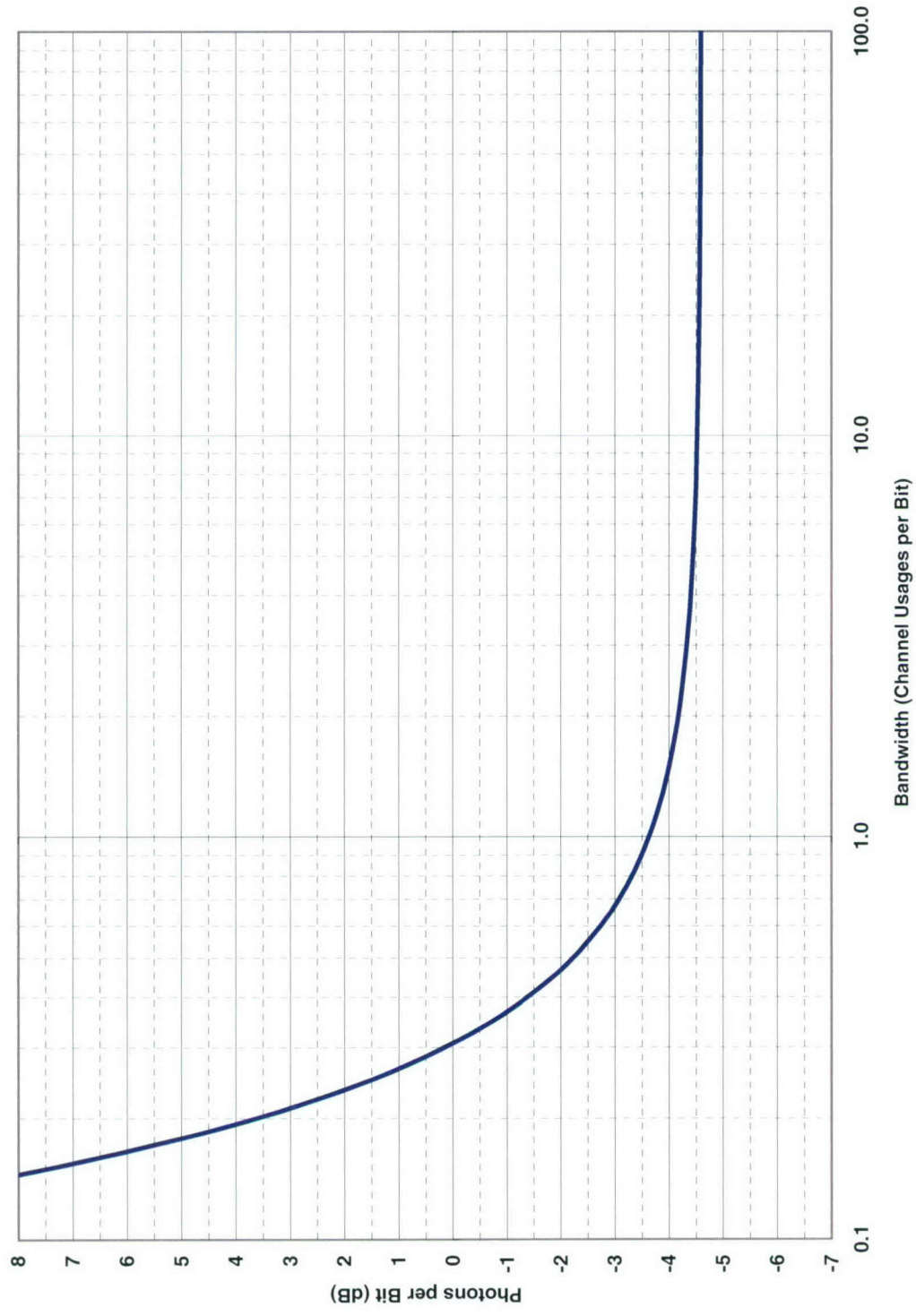


Chart 11. Efficiency at quantum cutoff: Gaussian.

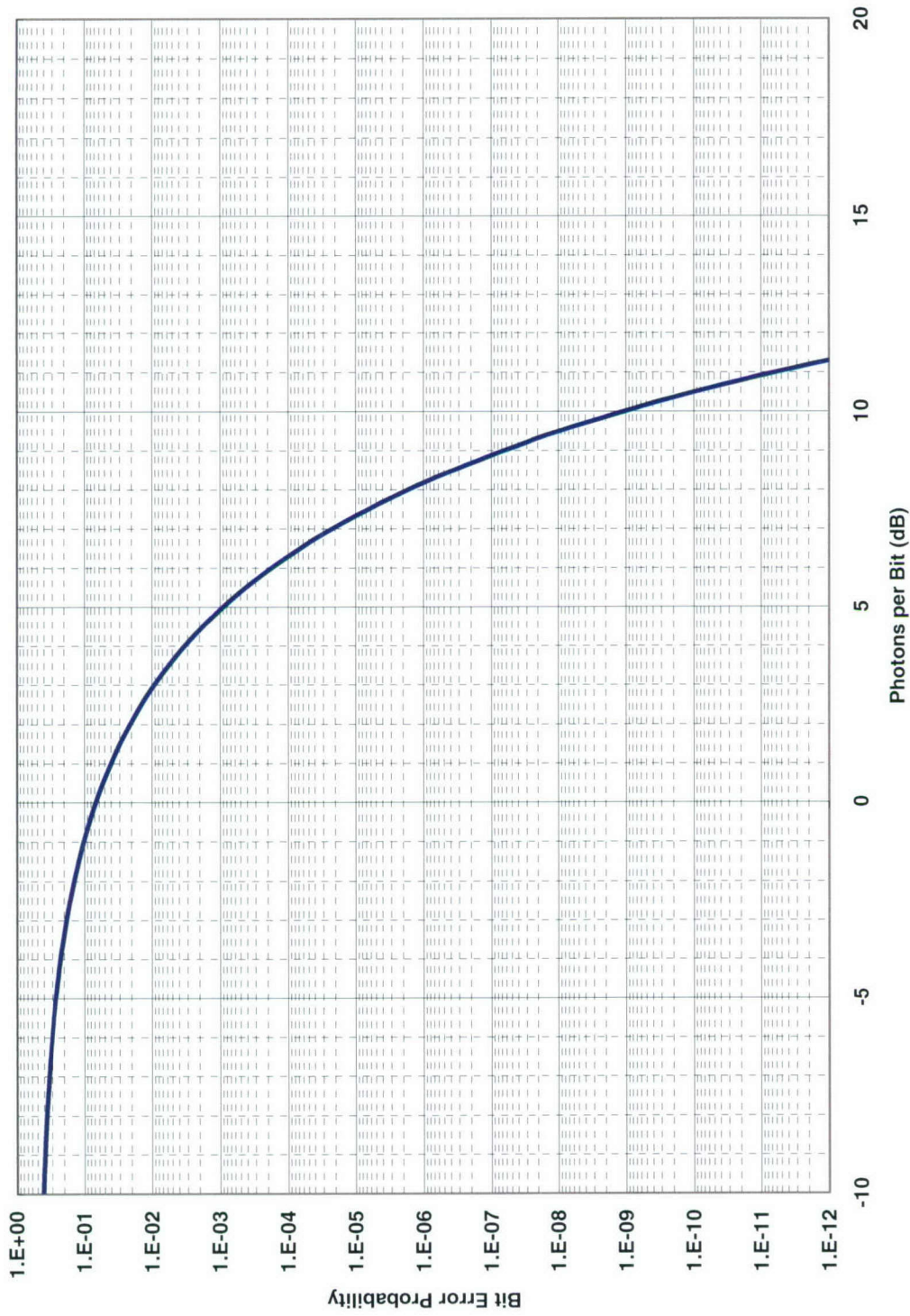


Chart 12. Bit-error probability: OOK ($p_0 = p_1 = 1/2$) photon counting.

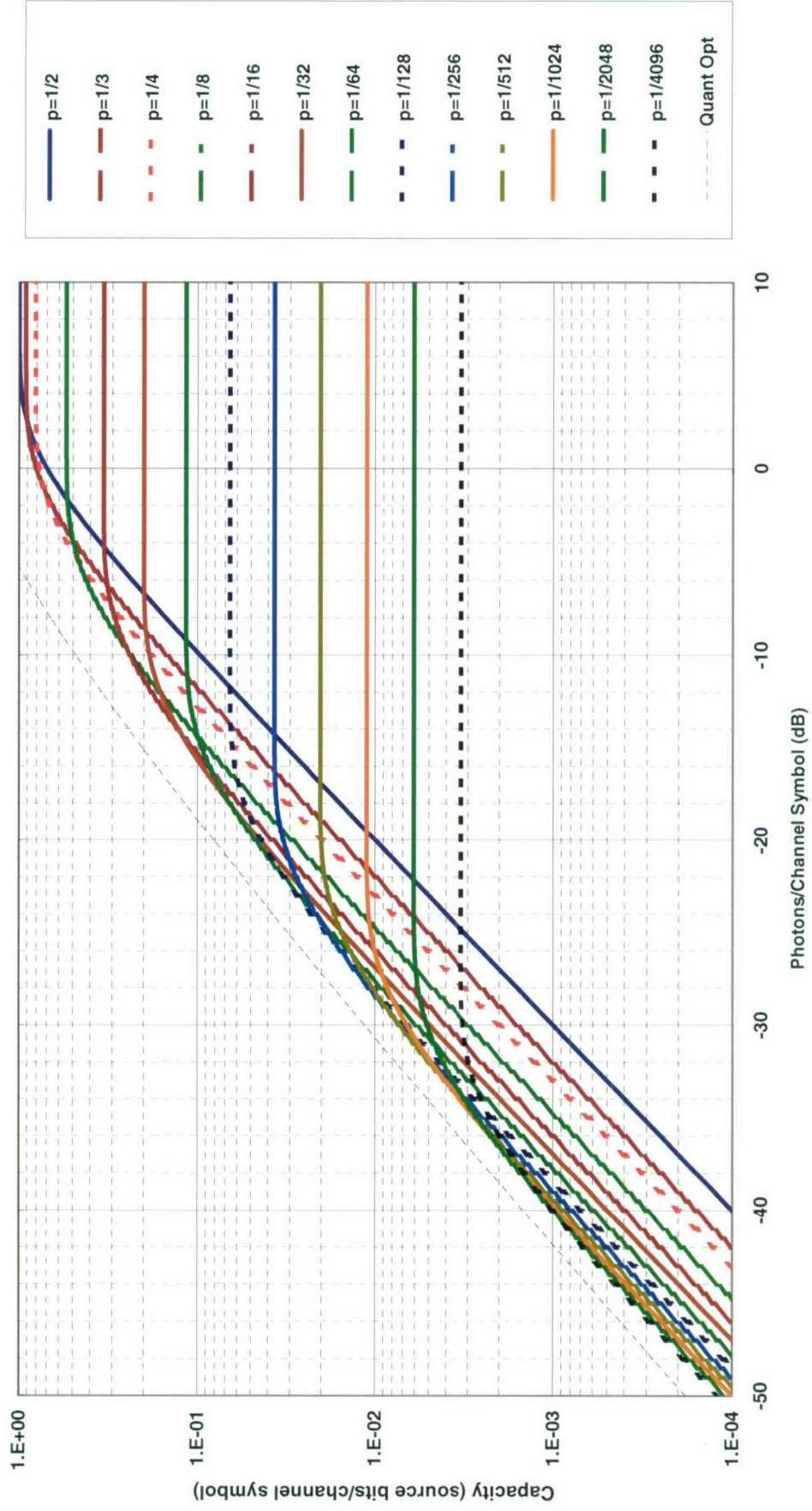


Chart 13. Classical capacity: OOK photon counting.

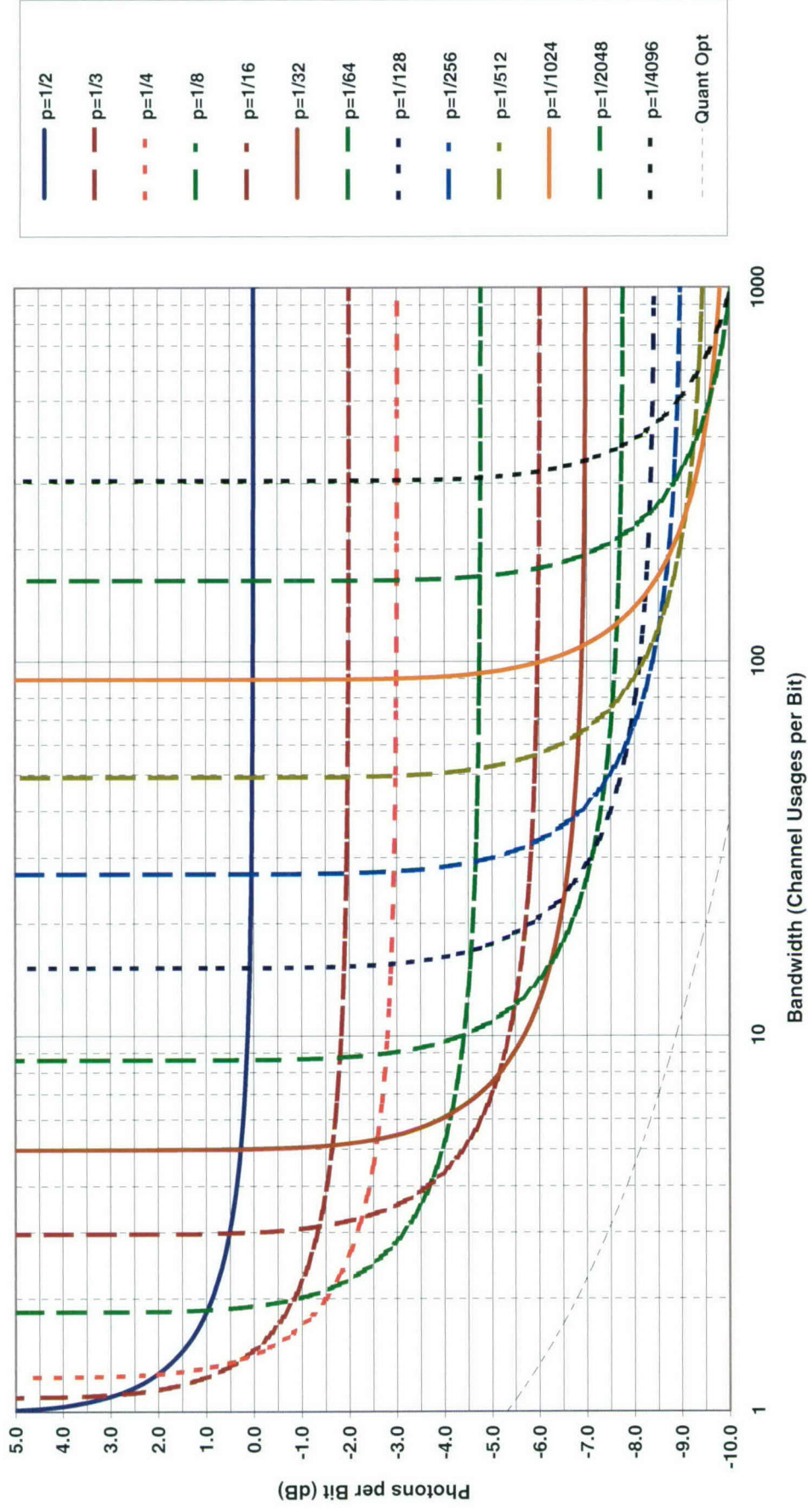


Chart 14. Efficiency at classical capacity: OOK photon counting.

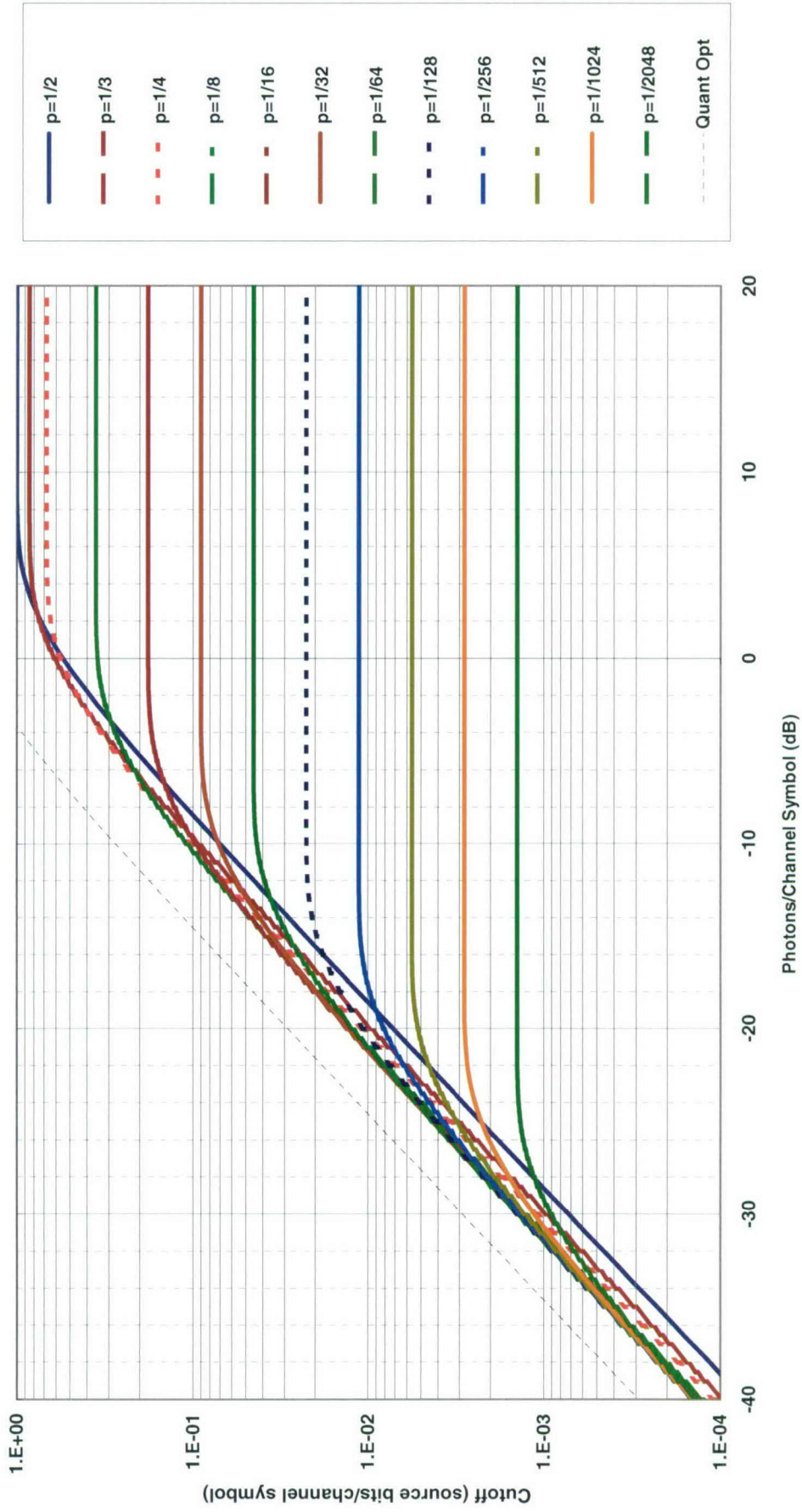


Chart 15. Classical cutoff: OOK photon counting.

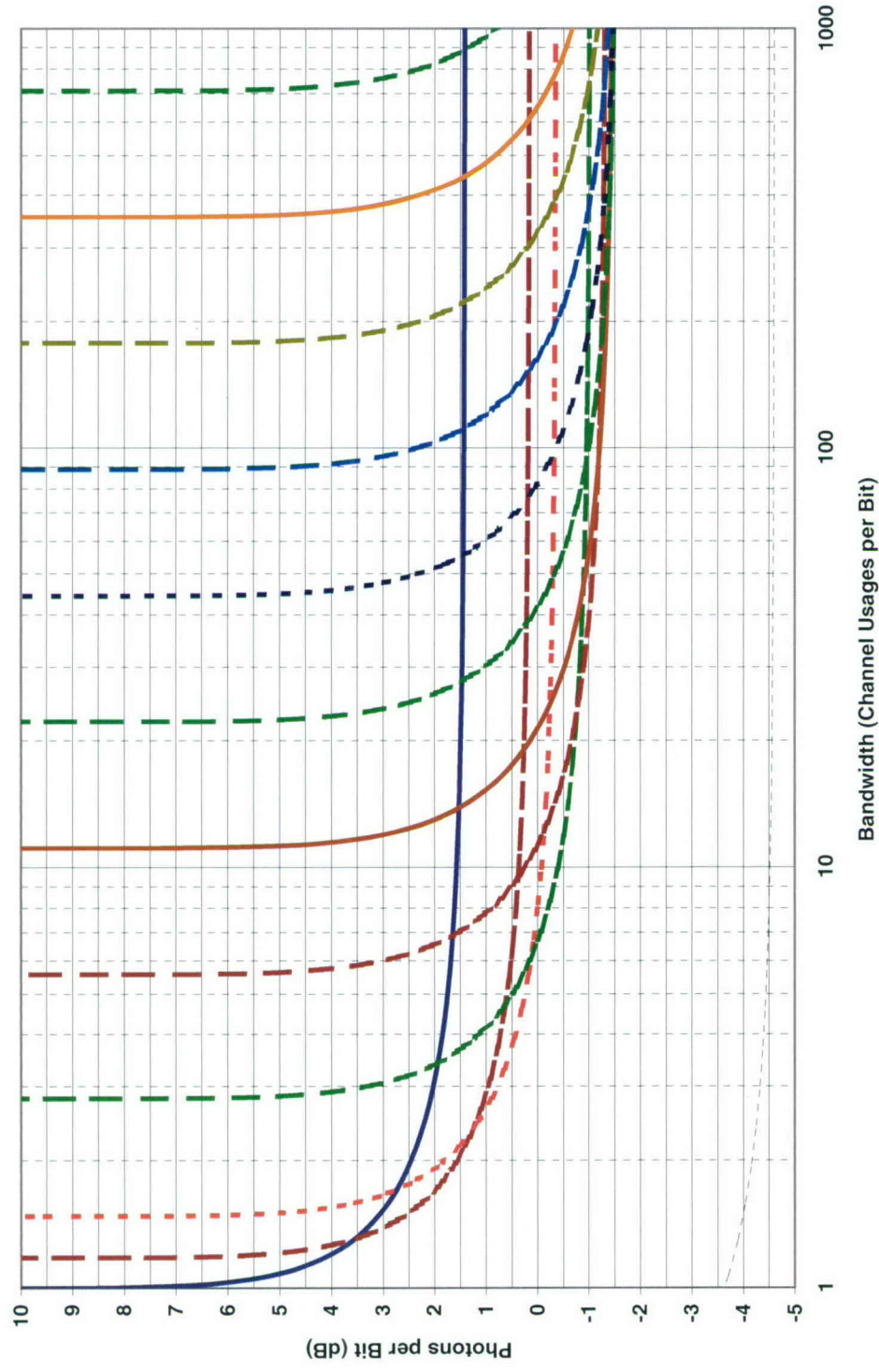


Chart 16. Efficiency at classical cutoff: OOK photon counting.

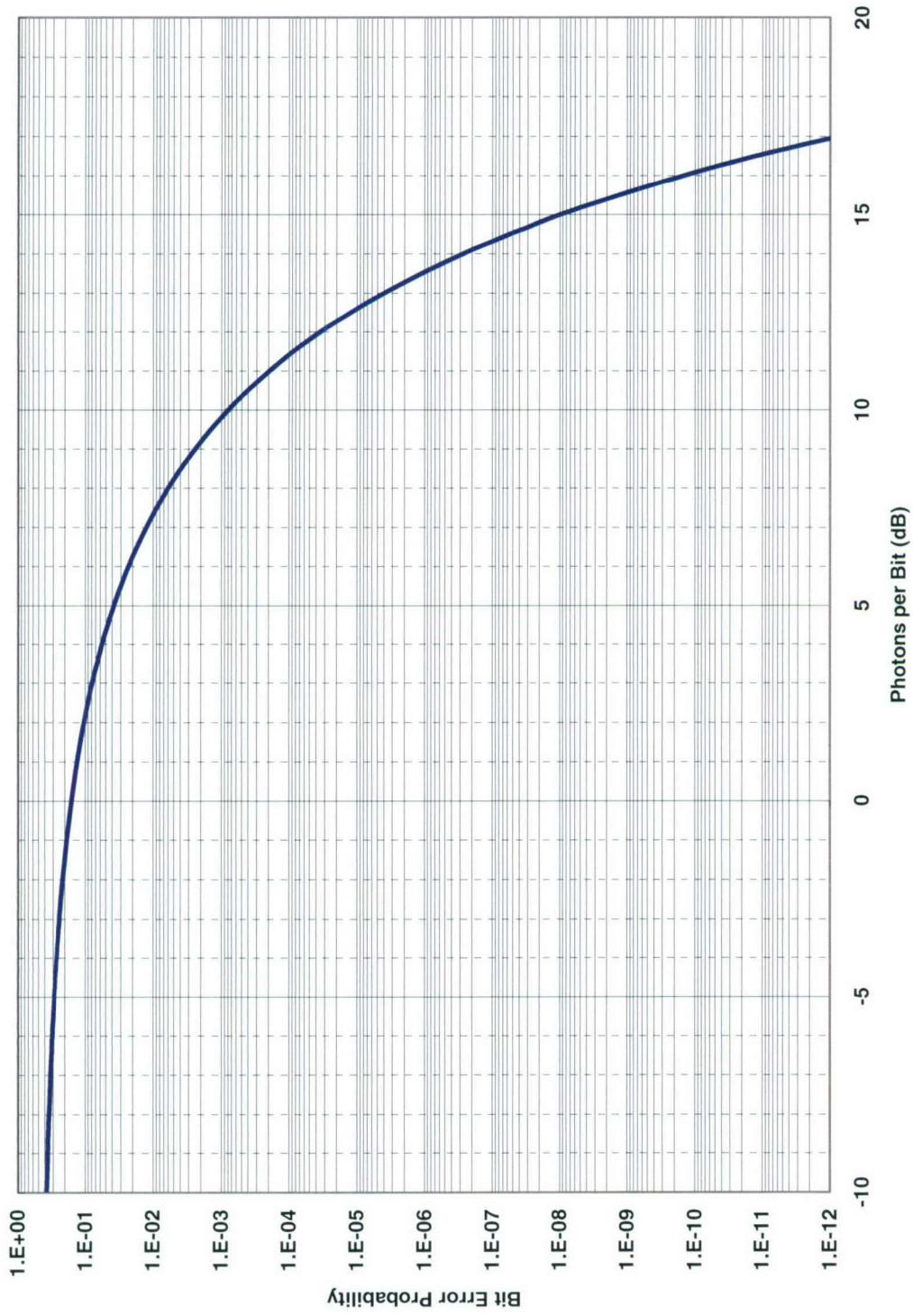


Chart 17. Symbol error probability: OOK ($p_0 = p_1 = 1/2$) heterodyne or preamplified coherent.

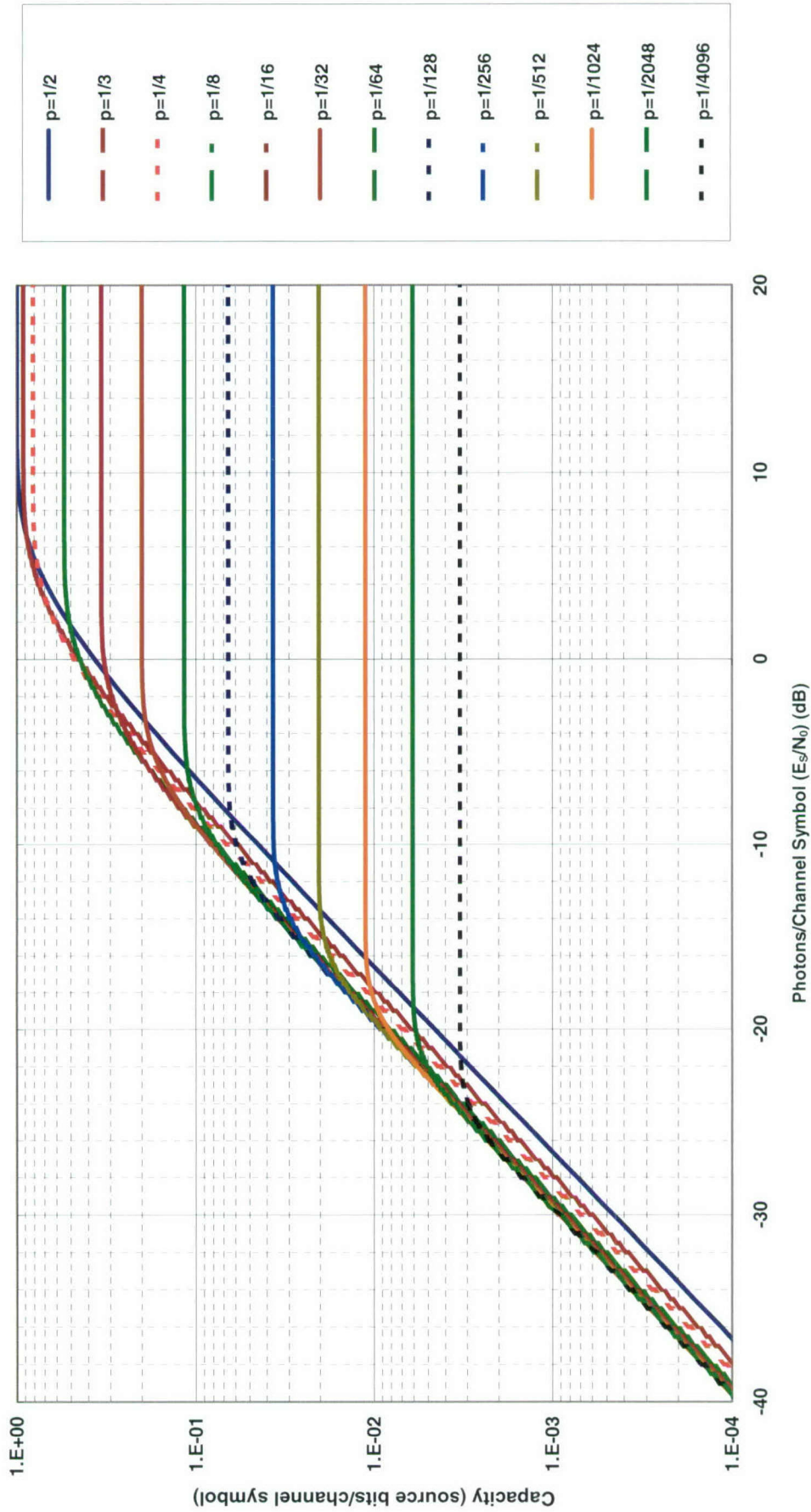


Chart 18. Classical capacity: OOK heterodyne or preamplified coherent hard decision.

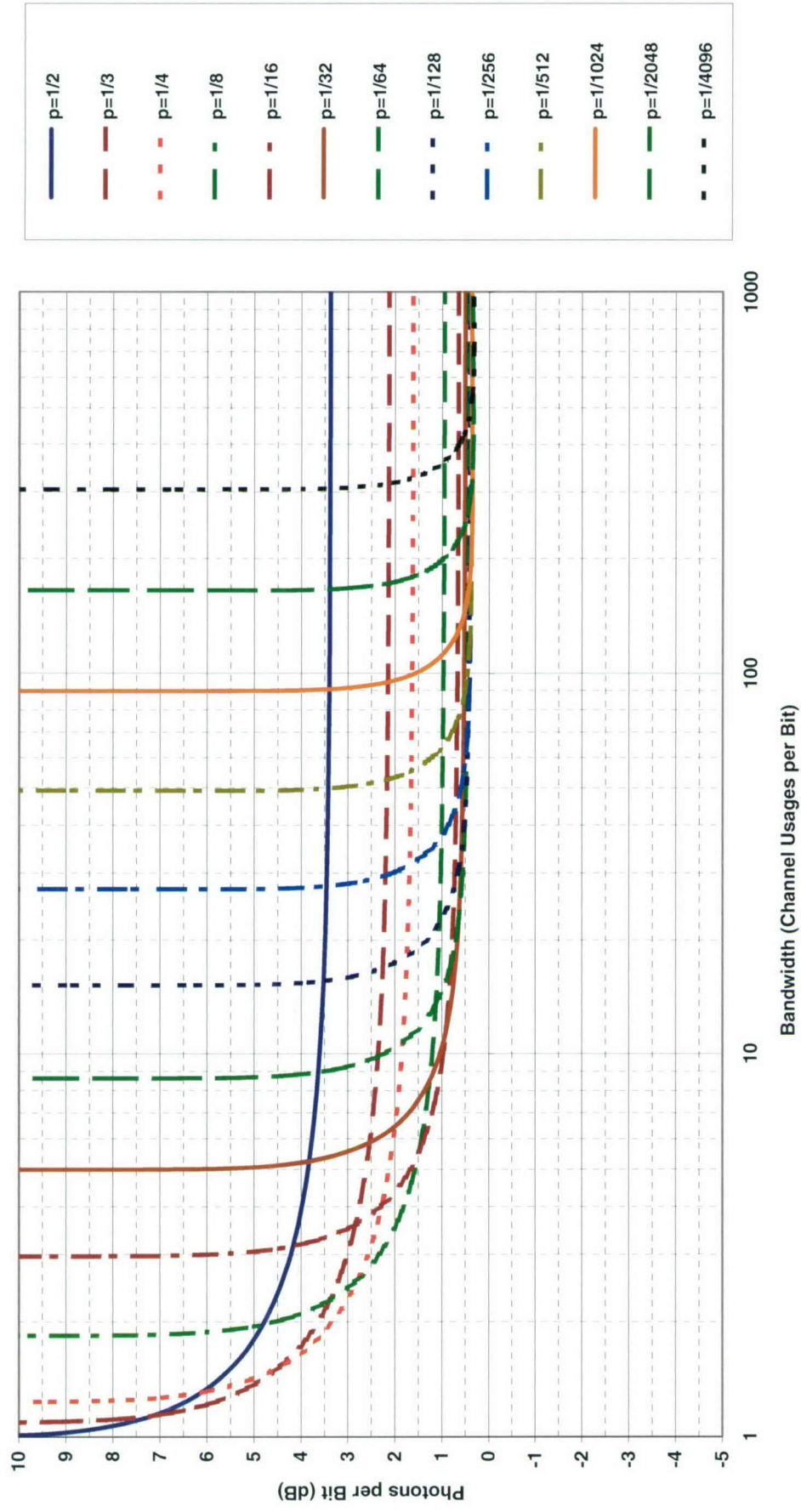


Chart 19. Efficiency at classical capacity: OOK heterodyne or preamplified coherent hard decision.

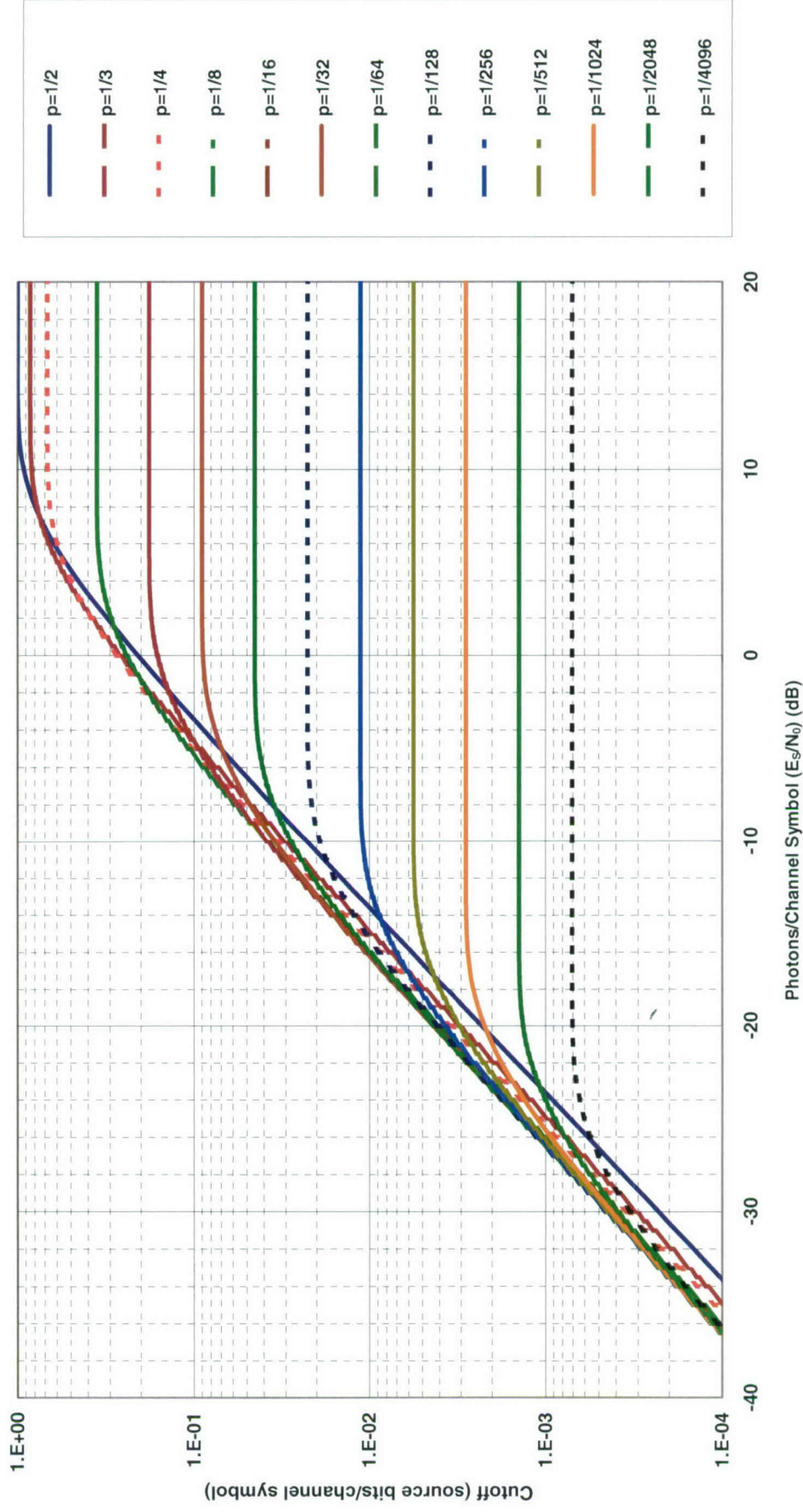


Chart 20. Classical cutoff: OOK heterodyne or preamplified coherent hard decision.

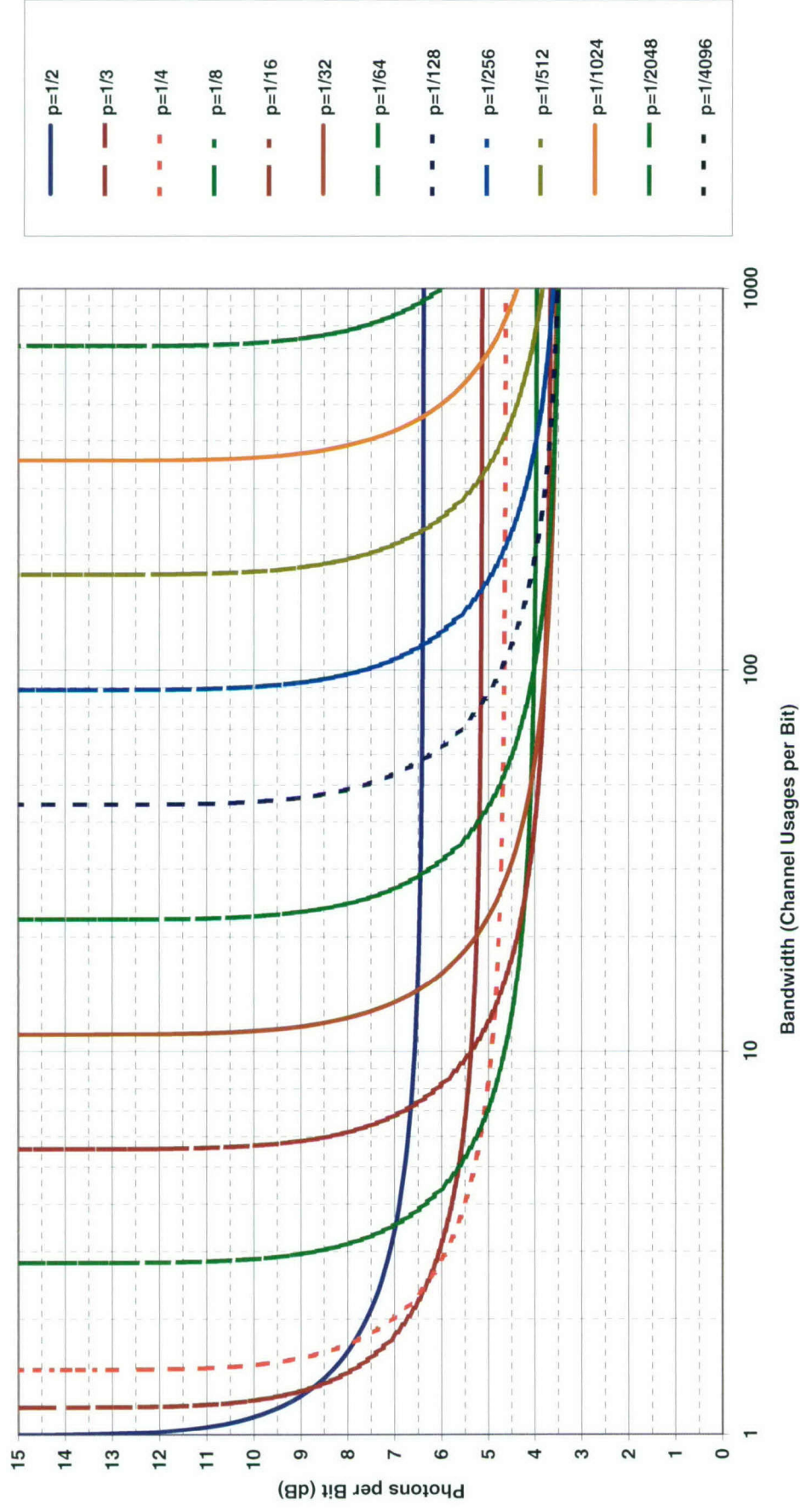


Chart 21. Efficiency at classical cutoff: OOK heterodyne or preamplified coherent hard decision.

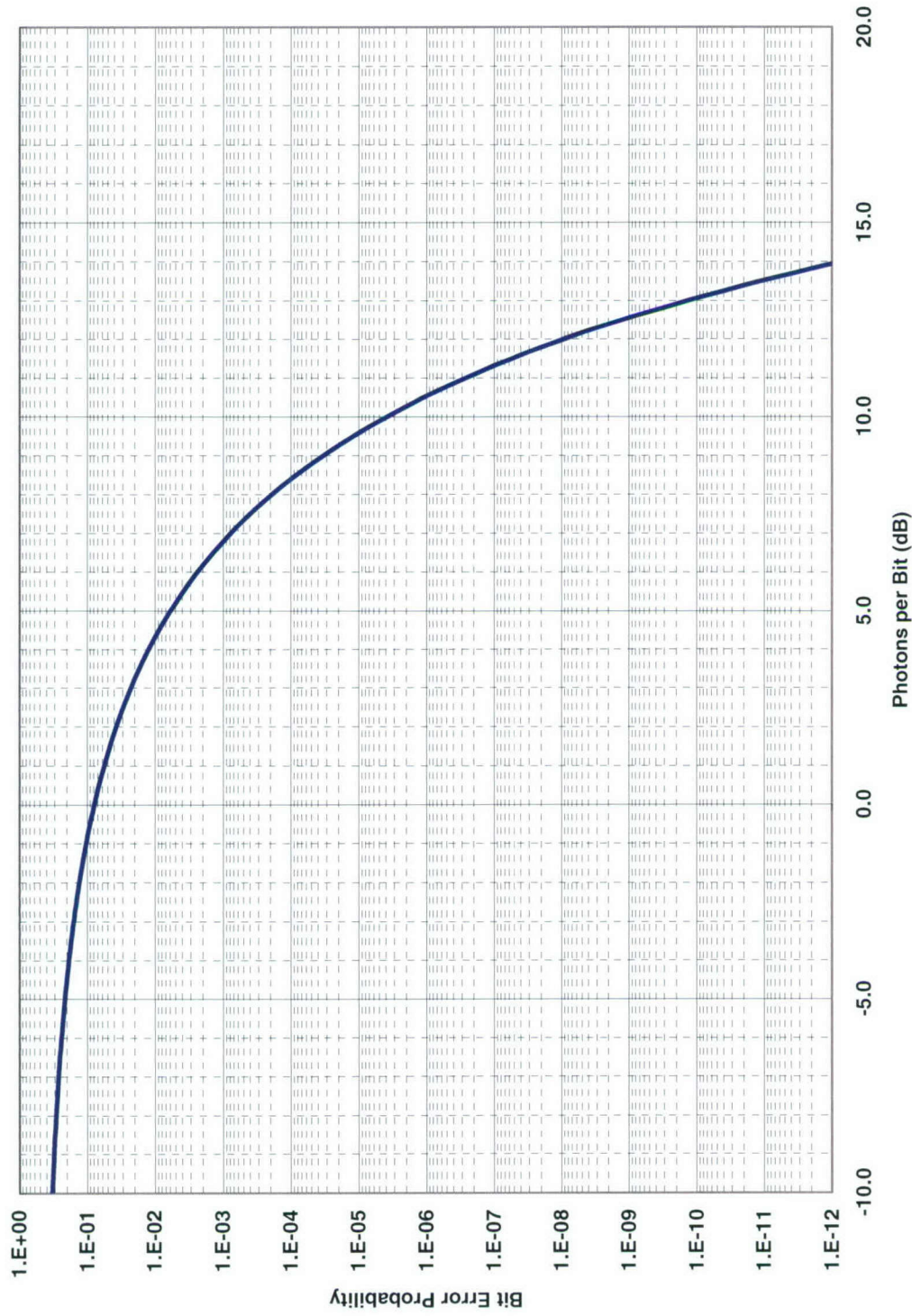


Chart 22. Symbol error probability: OOK ($p_0 = p_1 = 1/2$) homodyne coherent.

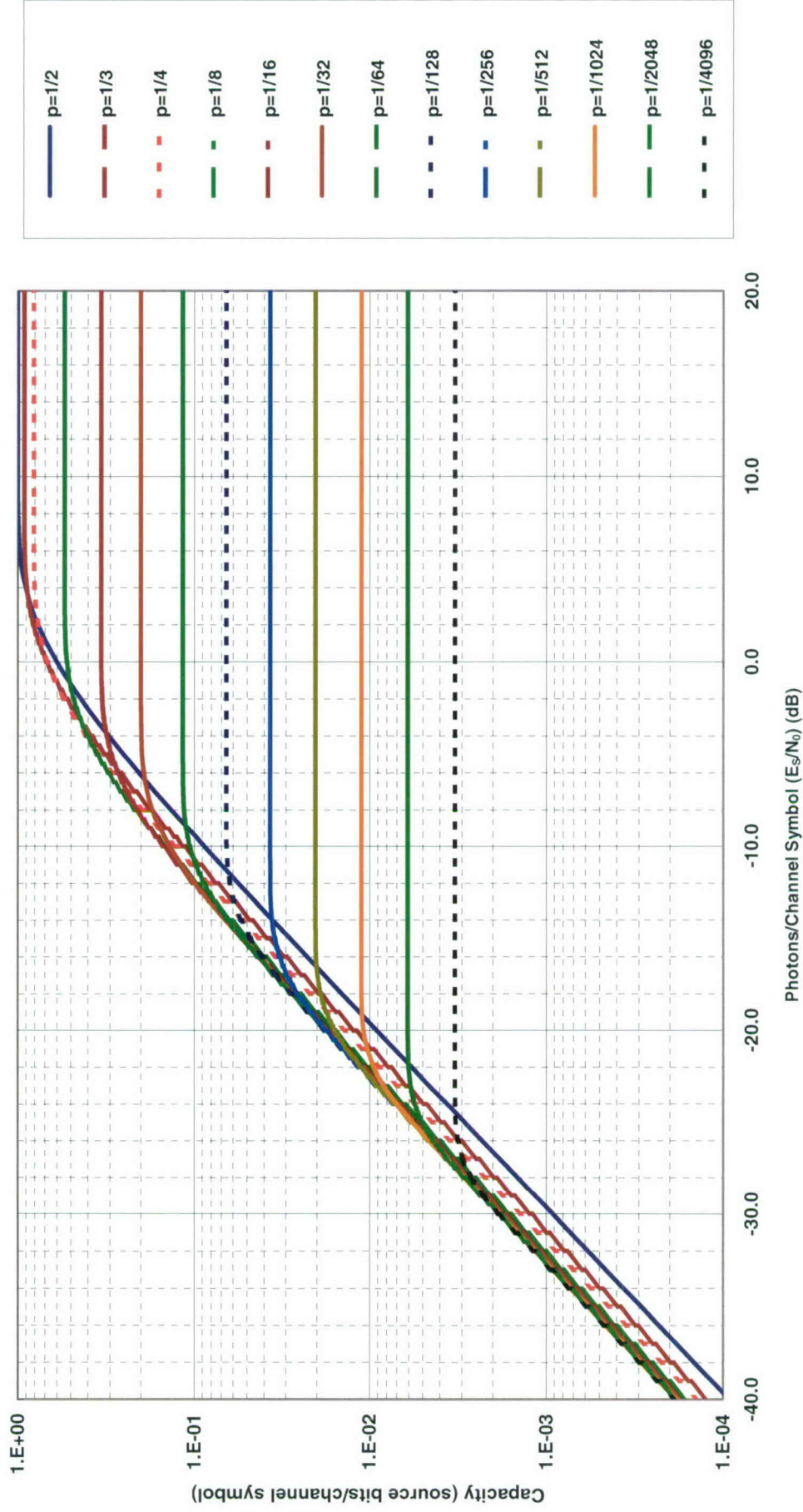


Chart 23. Classical capacity: OOK: homodyne coherent hard decision.

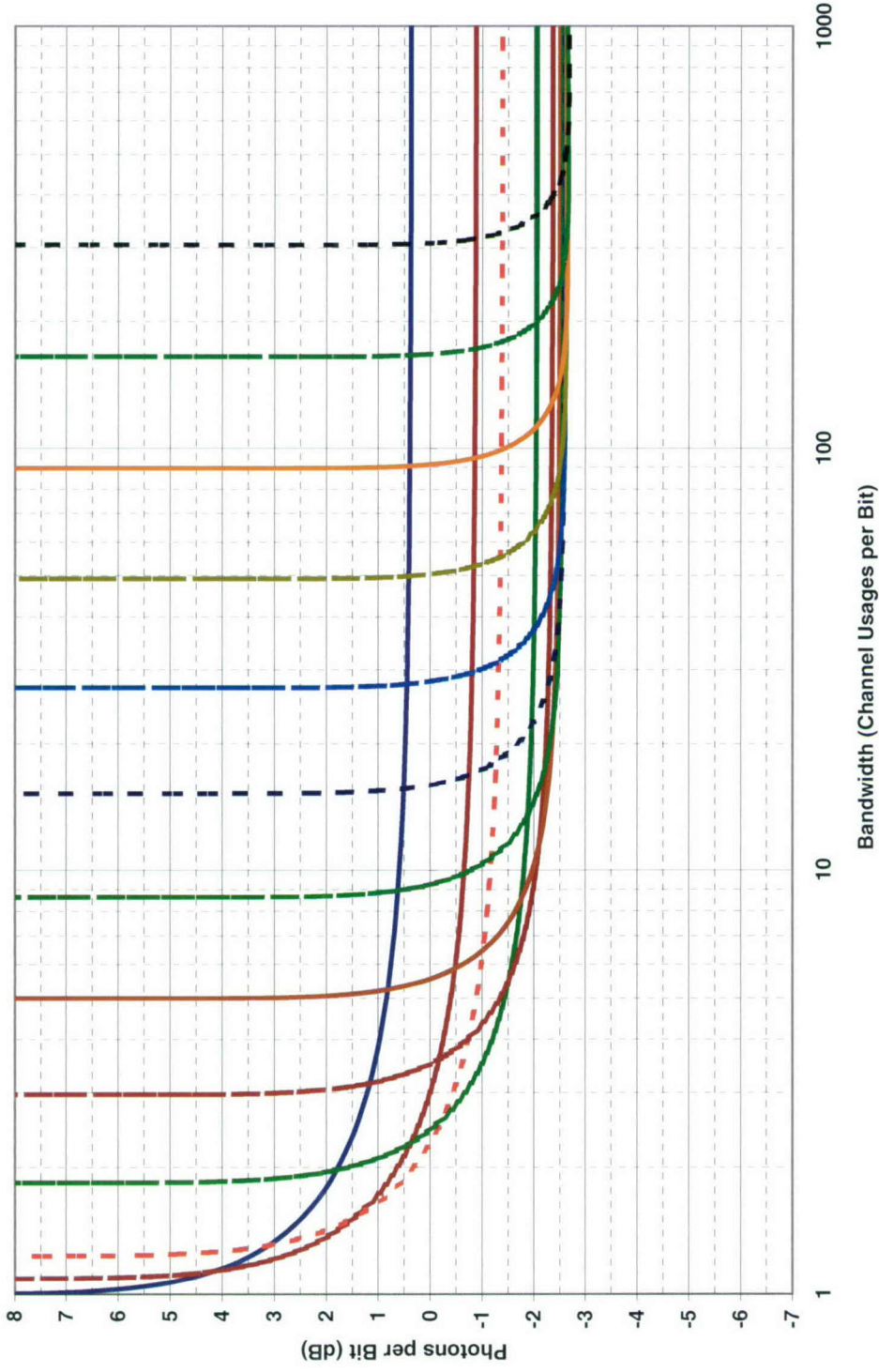


Chart 24. Efficiency at classical capacity: OOK homodyne coherent hard decision.

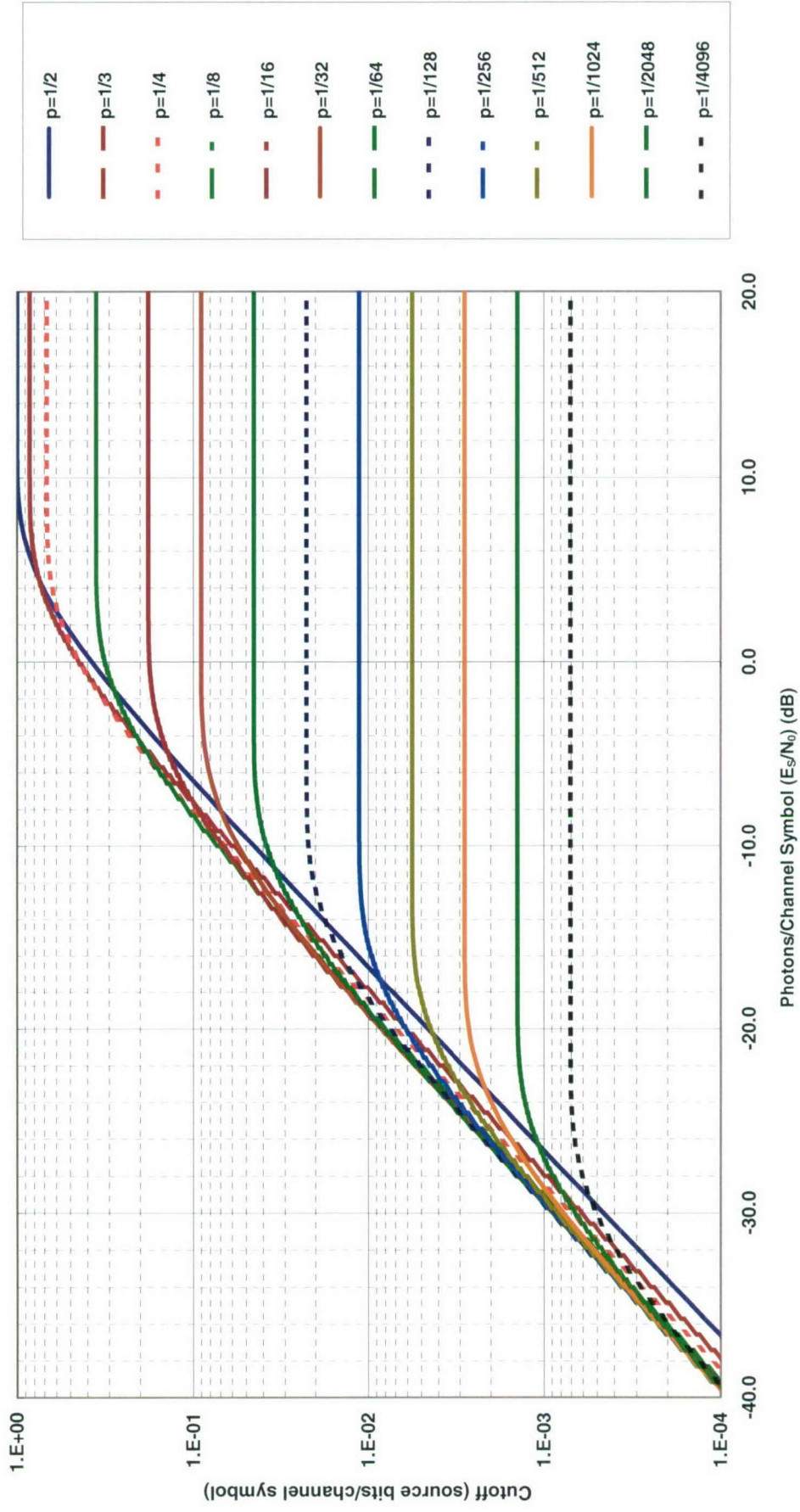


Chart 25. Classical cutoff: OOK homodyne coherent hard decision.

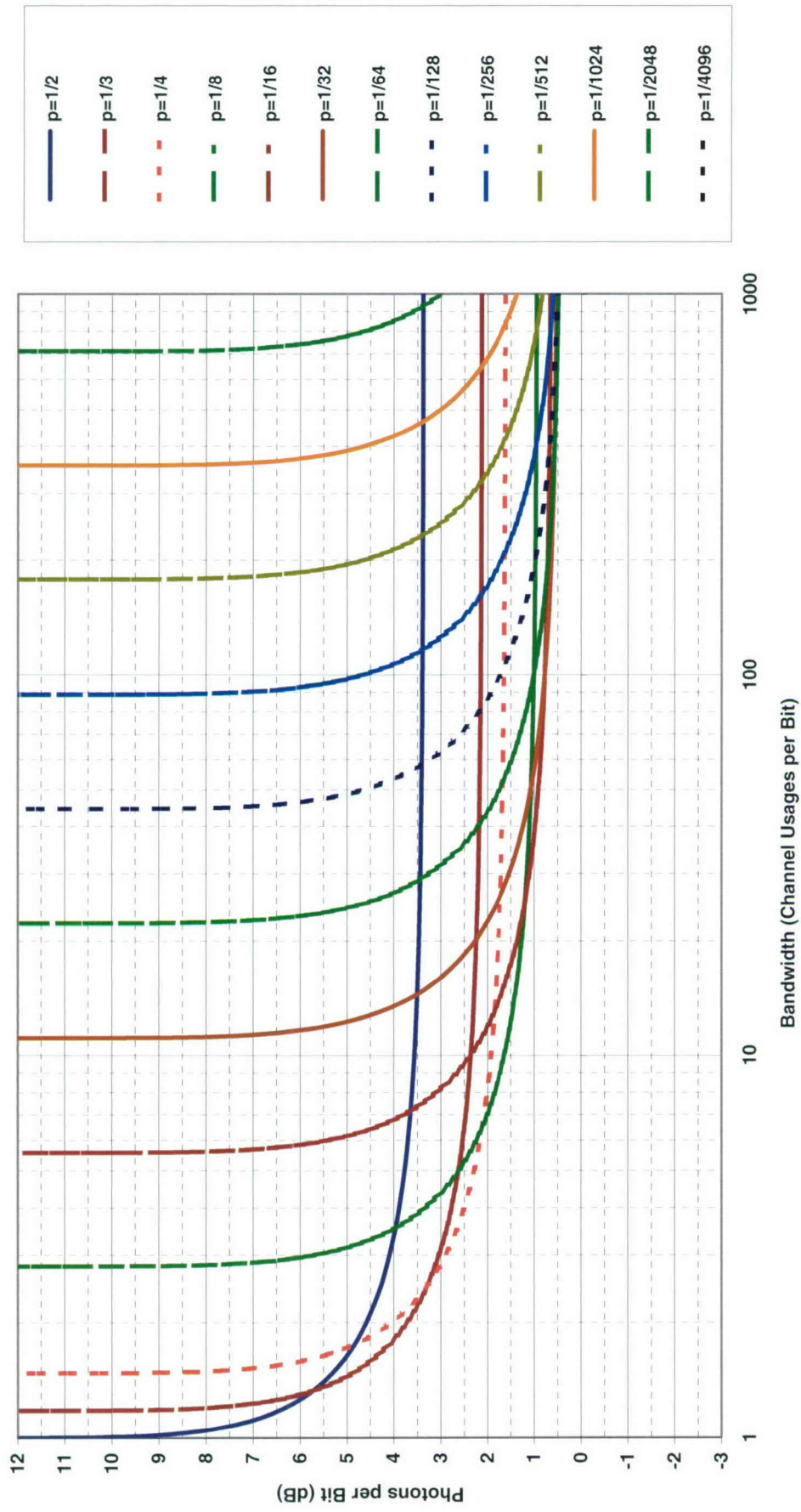


Chart 26. Efficiency at classical cutoff: OOK homodyne coherent hard decision.

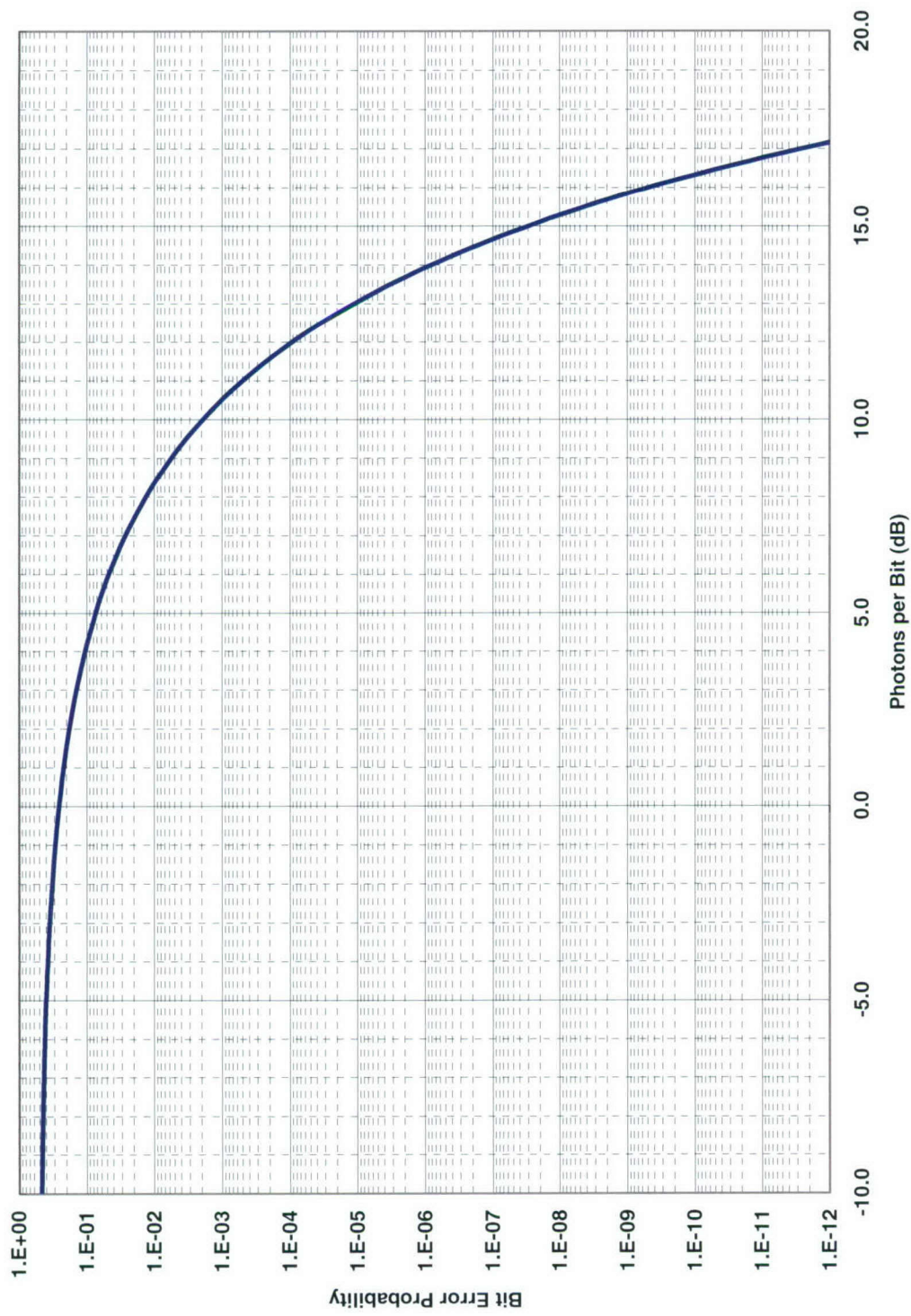


Chart 27. Symbol error probability: OOK ($p_0 = p_1 = 1/2$) heterodyne or preamplified noncoherent.

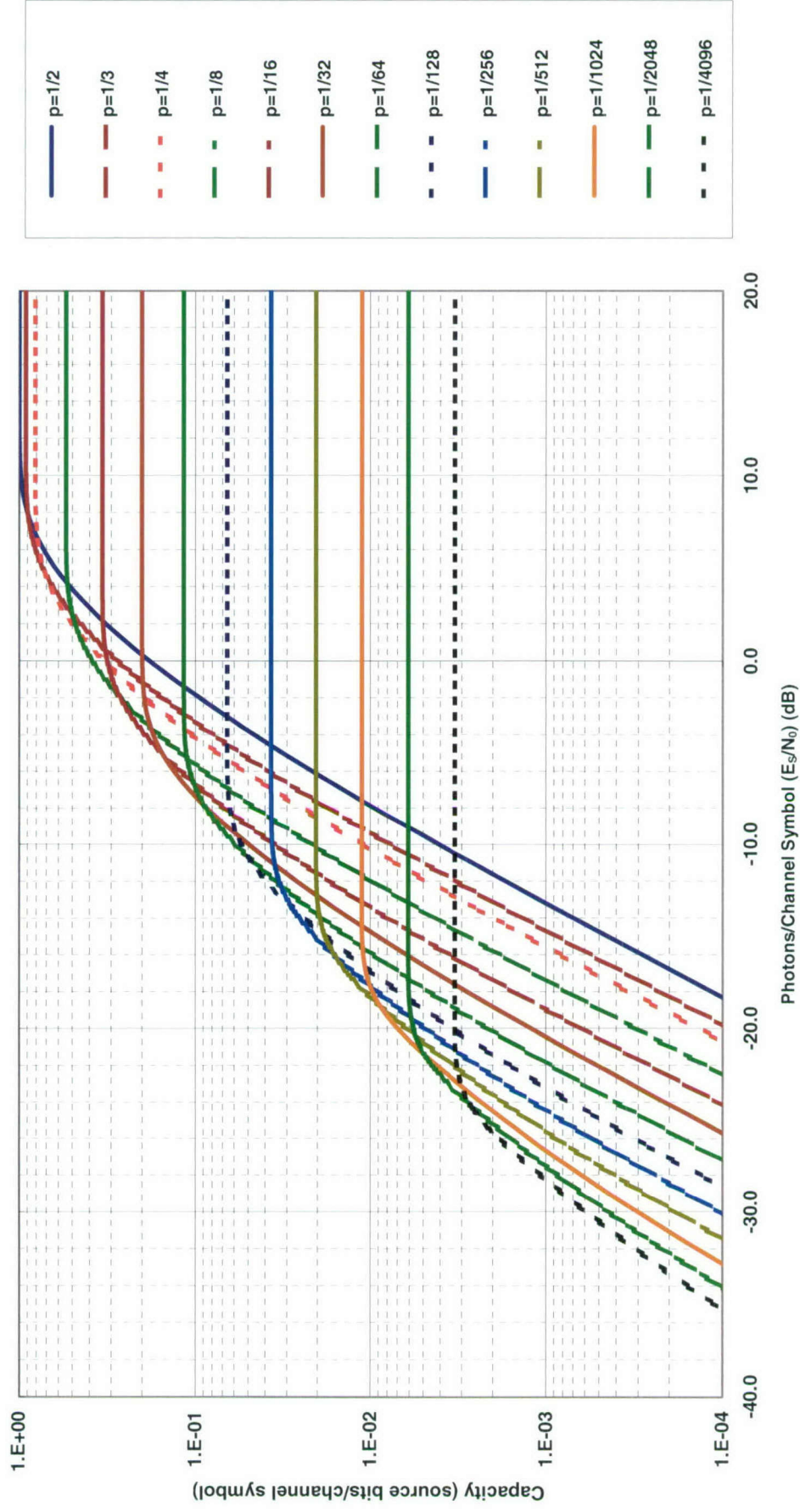


Chart 28. Classical capacity: OOK heterodyne or preamplified noncoherent hard decision.

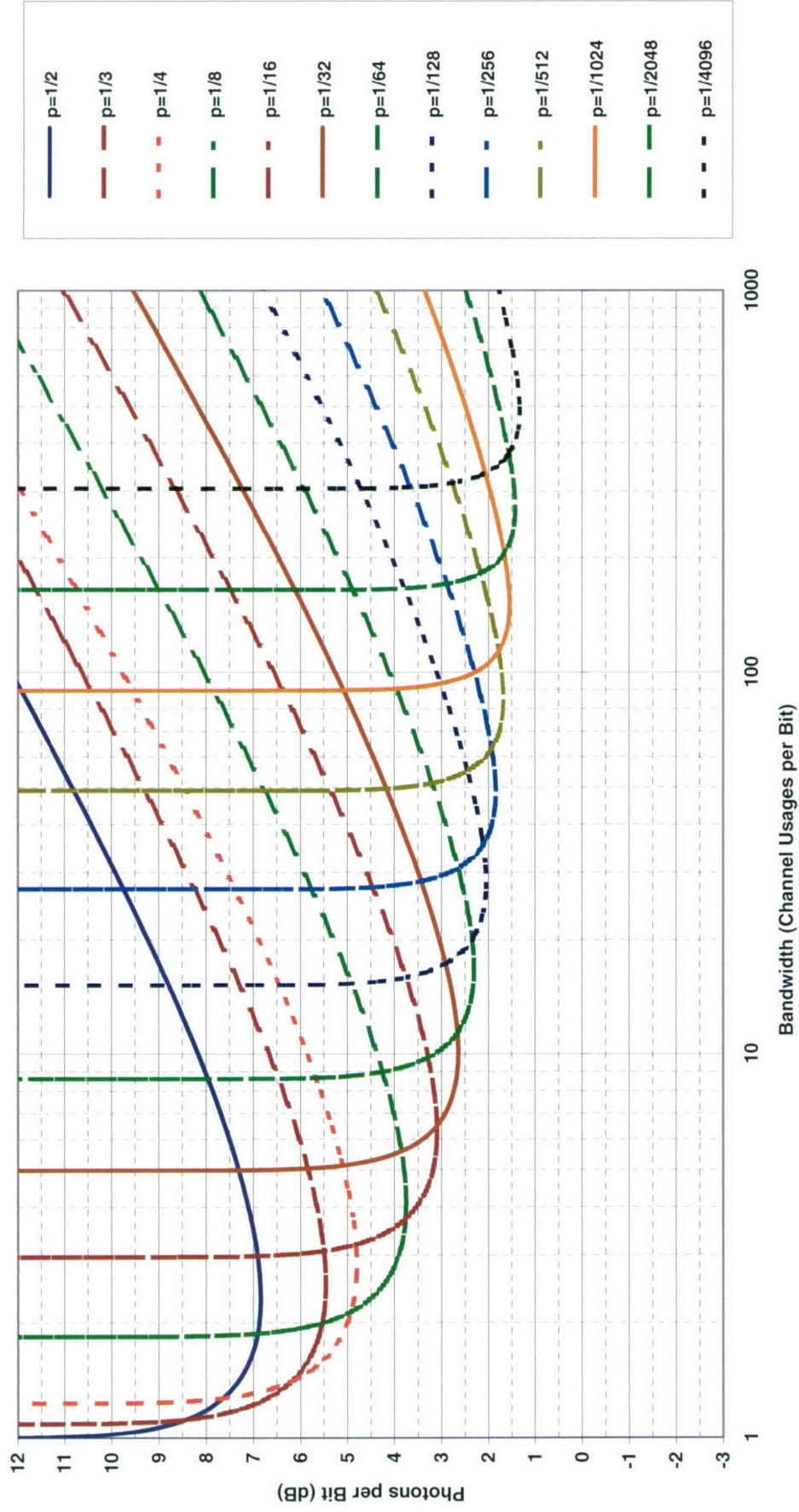


Chart 29. Efficiency at classical capacity: OOK heterodyne or preamplified noncoherent hard decision.

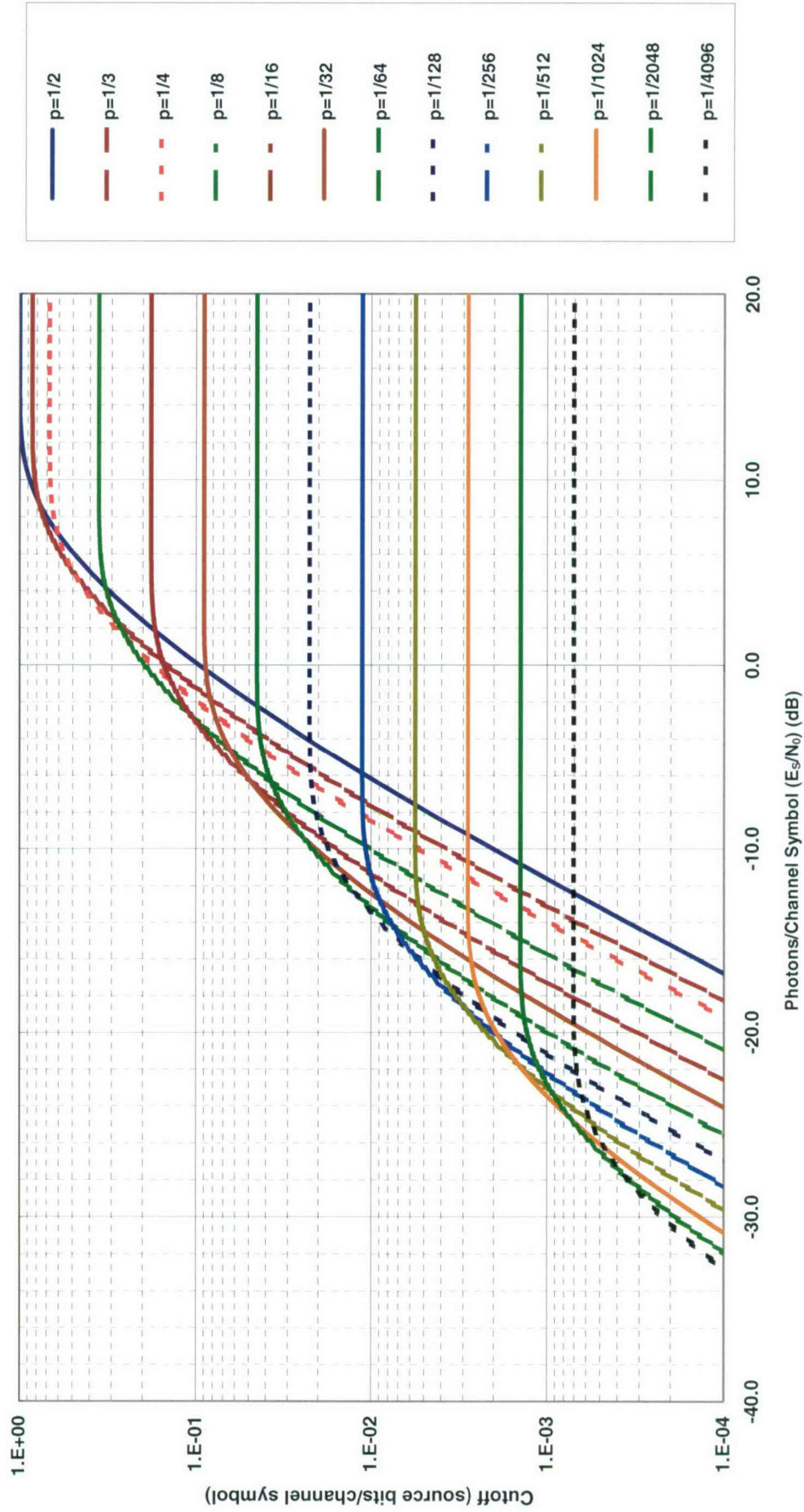


Chart 30. Classical cutoff: OOK heterodyne or preamplified noncoherent hard decision.

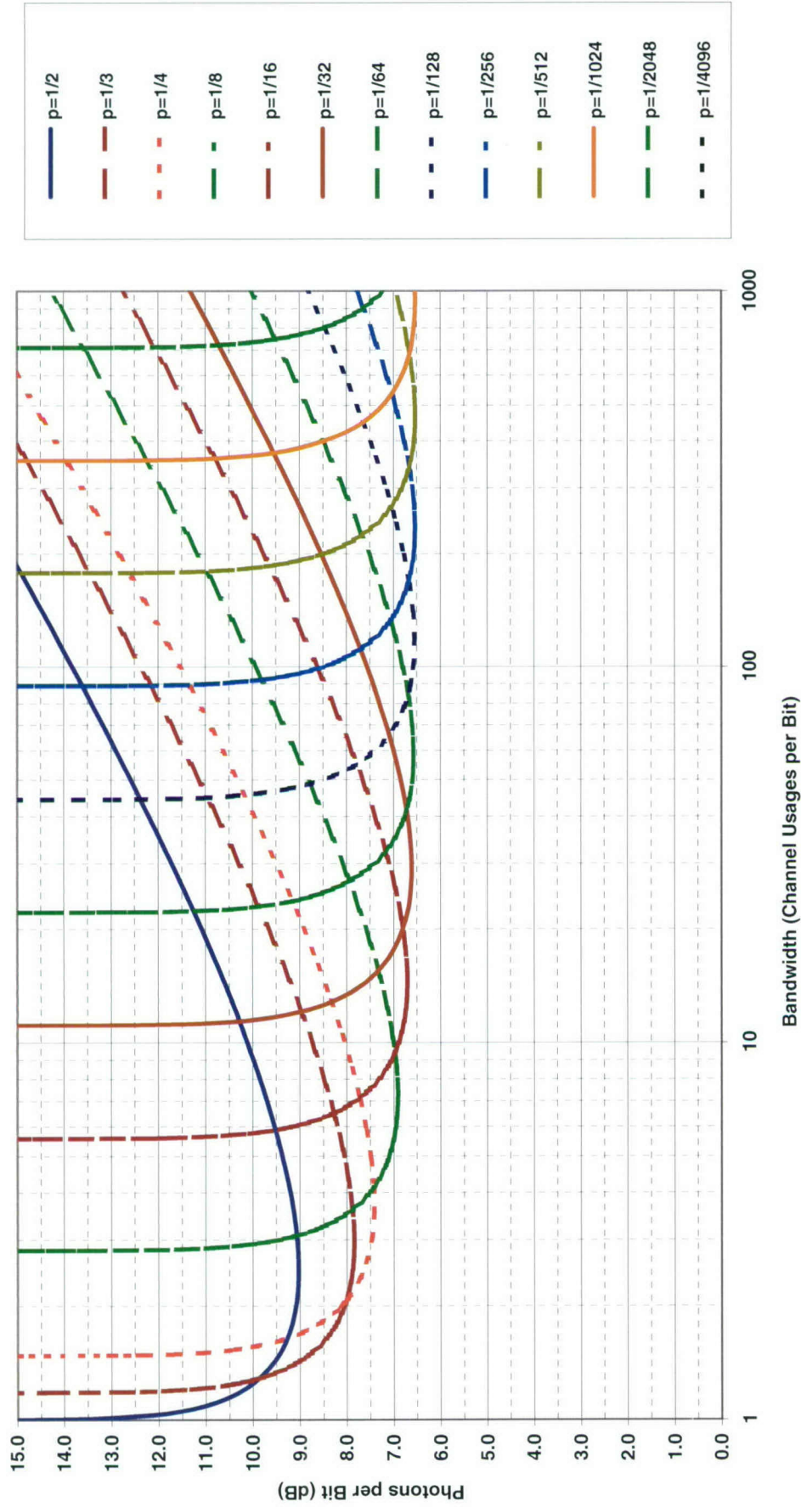


Chart 31. Efficiency at classical cutoff: OOK heterodyne or preamplified noncoherent hard decision.

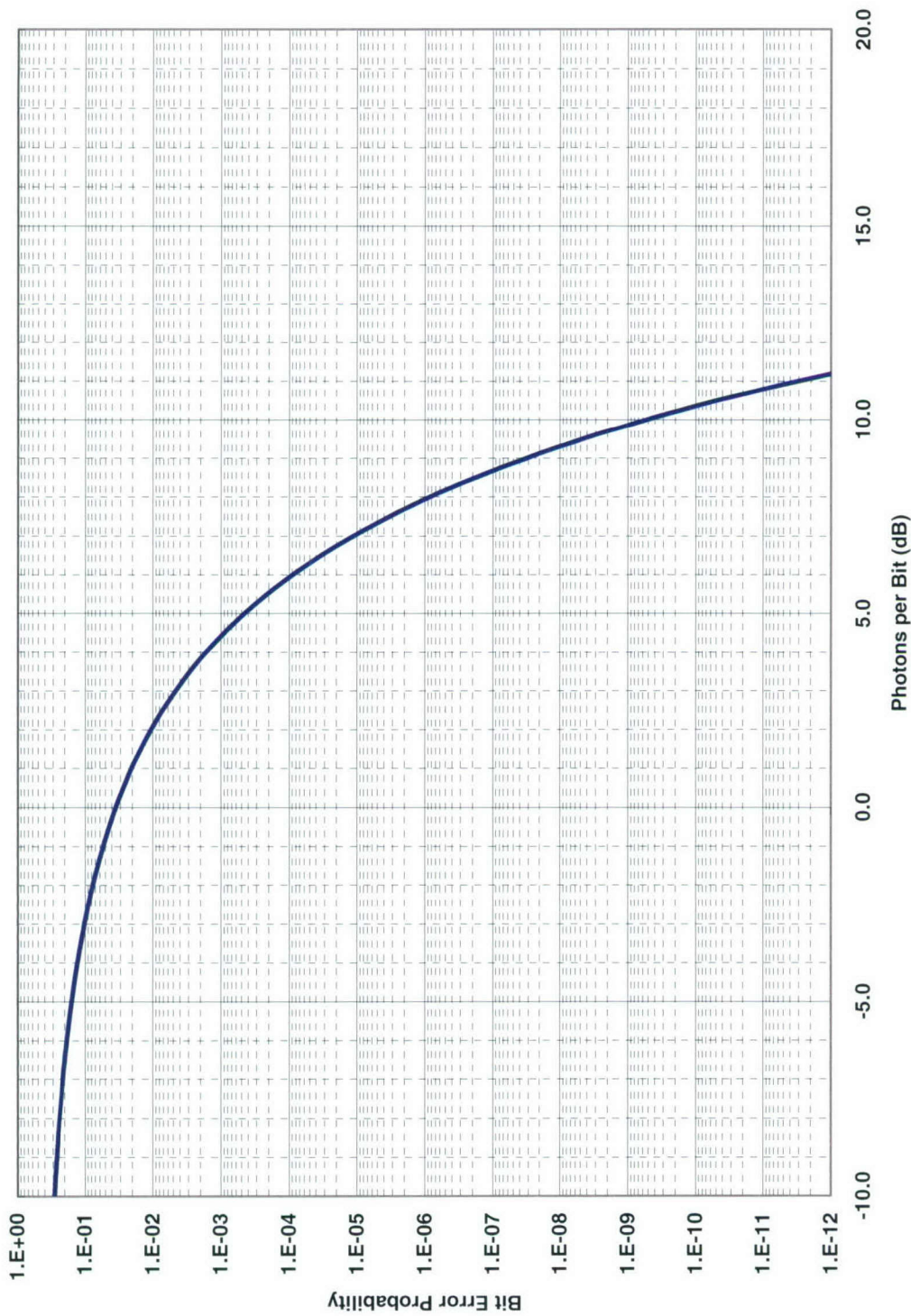


Chart 32. Symbol error probability: OOK ($p_0 = p_1 = 1/2$) quantum hard decision (semiclassical).

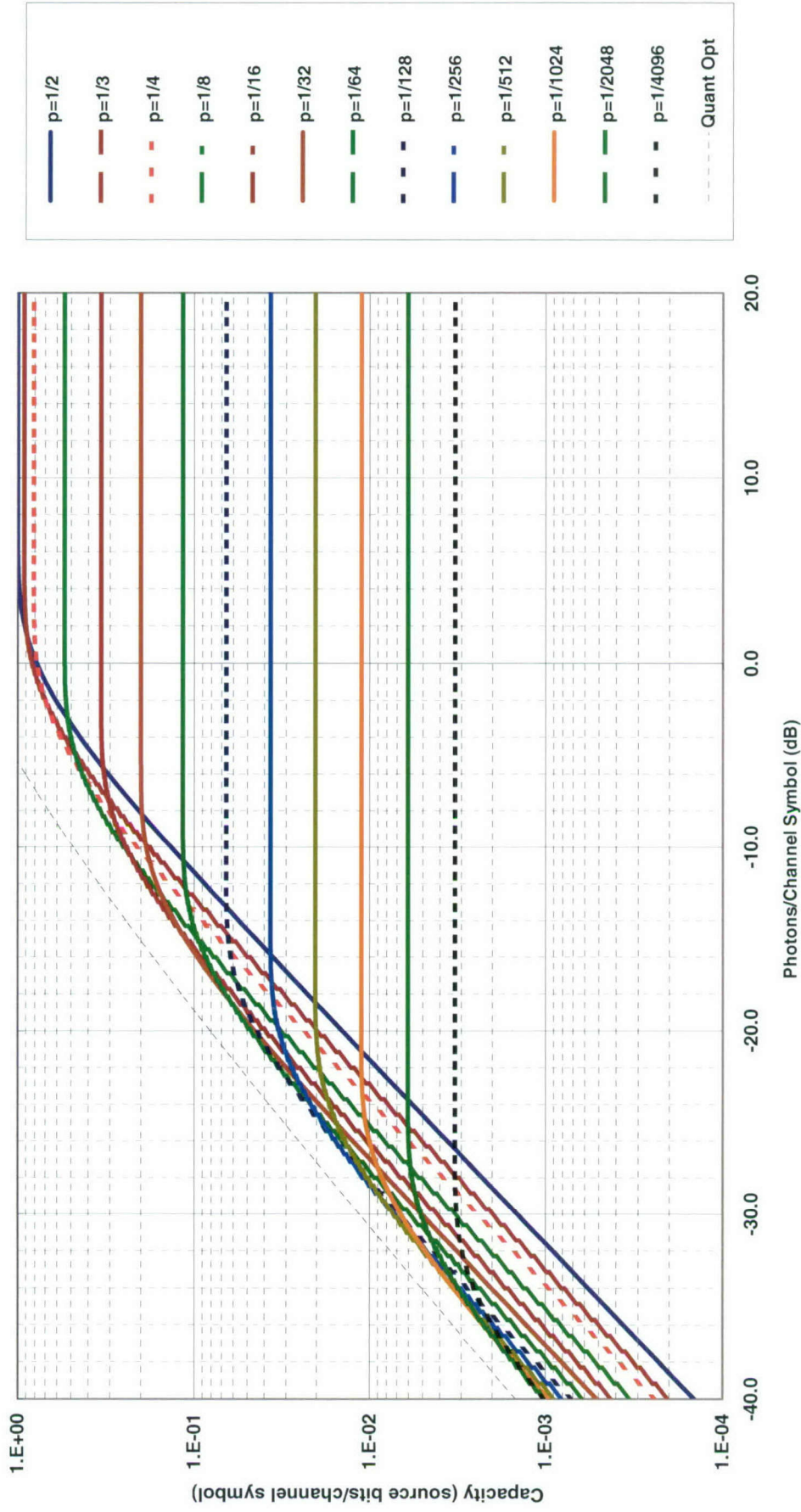


Chart 33. Classical capacity: OOK quantum hard decision (semiclassical).

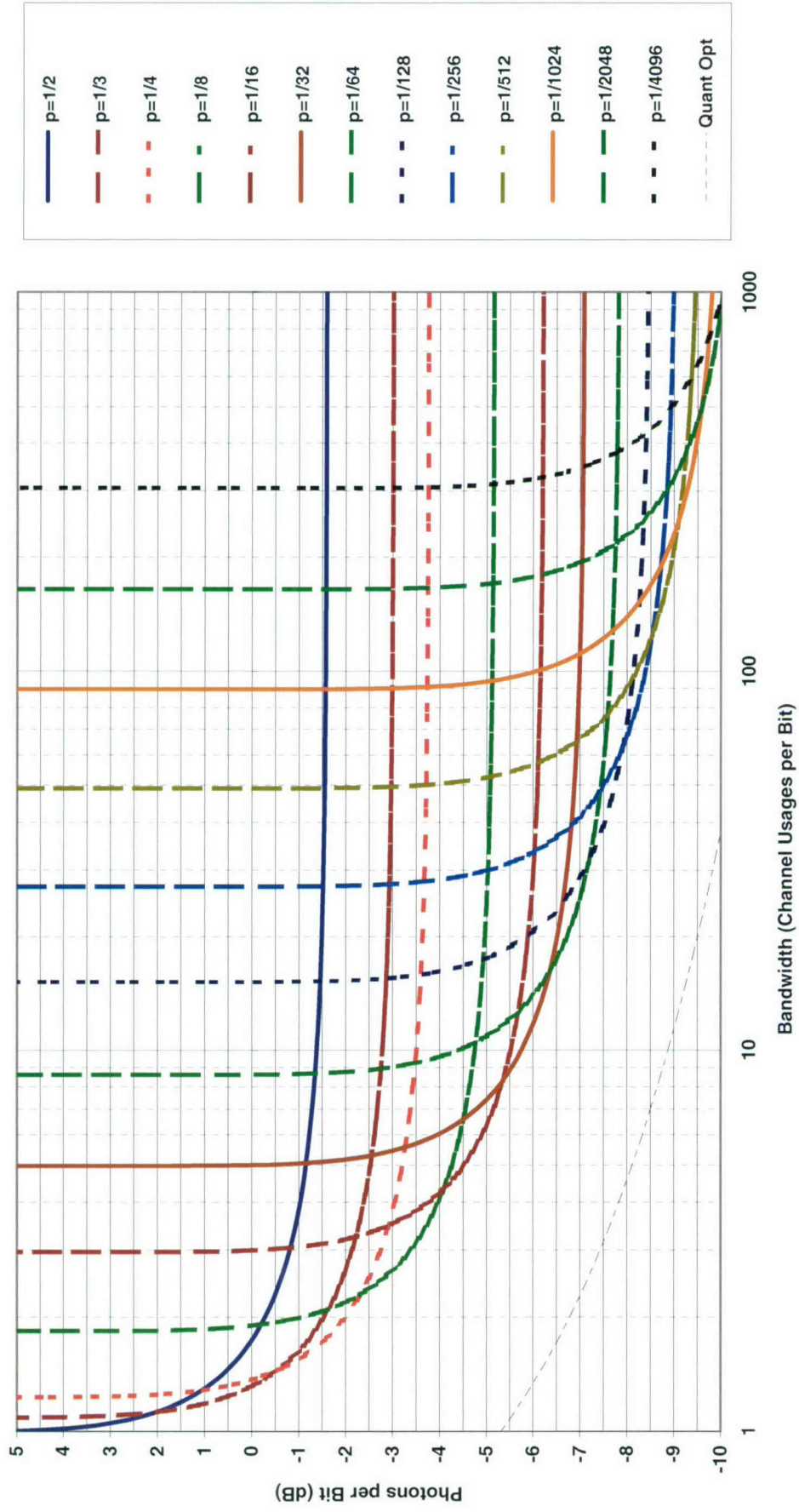


Chart 34. Efficiency at classical capacity: OOK quantum hard decision (semiclassical).

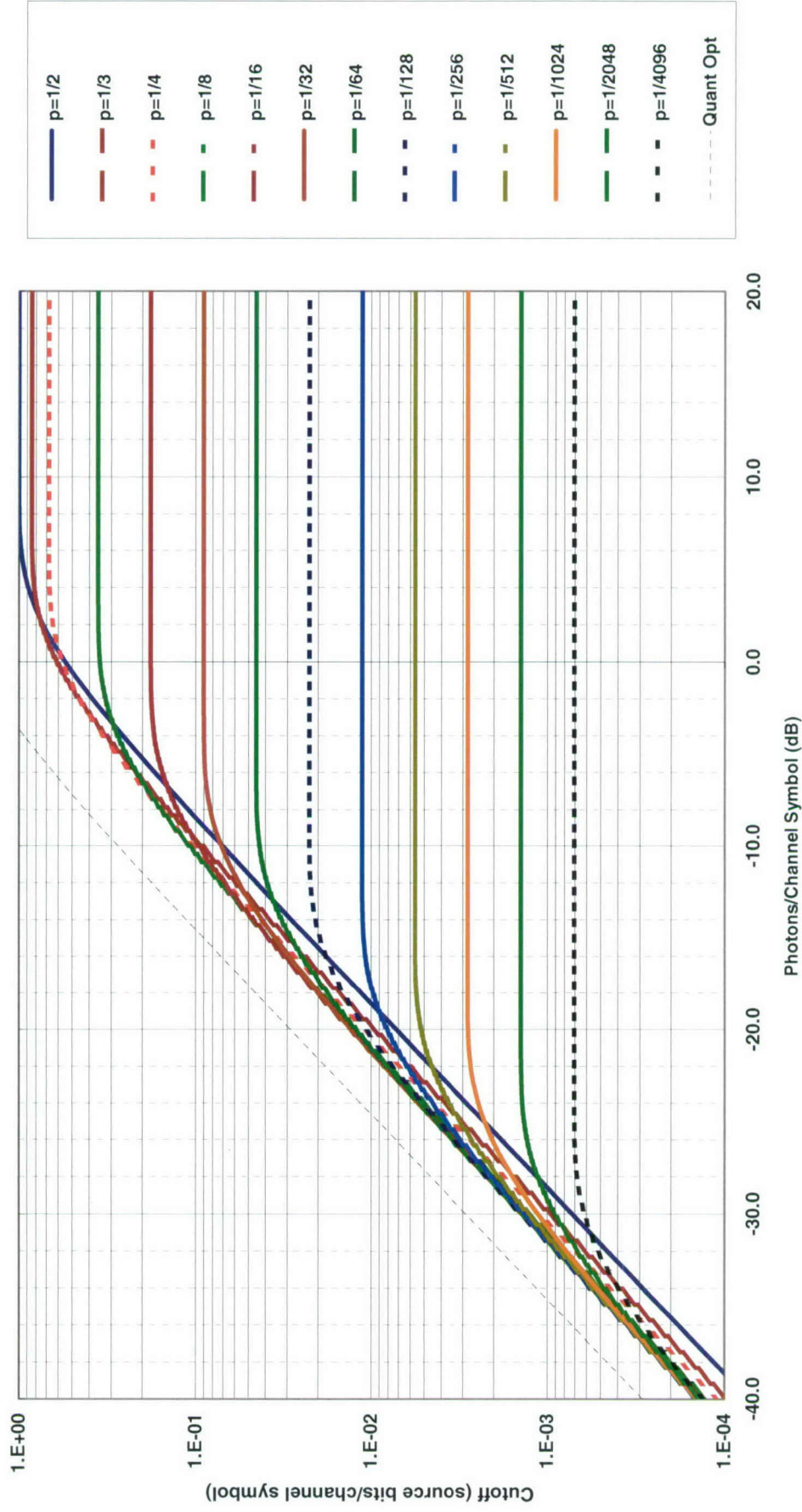


Chart 35. Classical cutoff: OOK quantum hard decision (semiclassical).

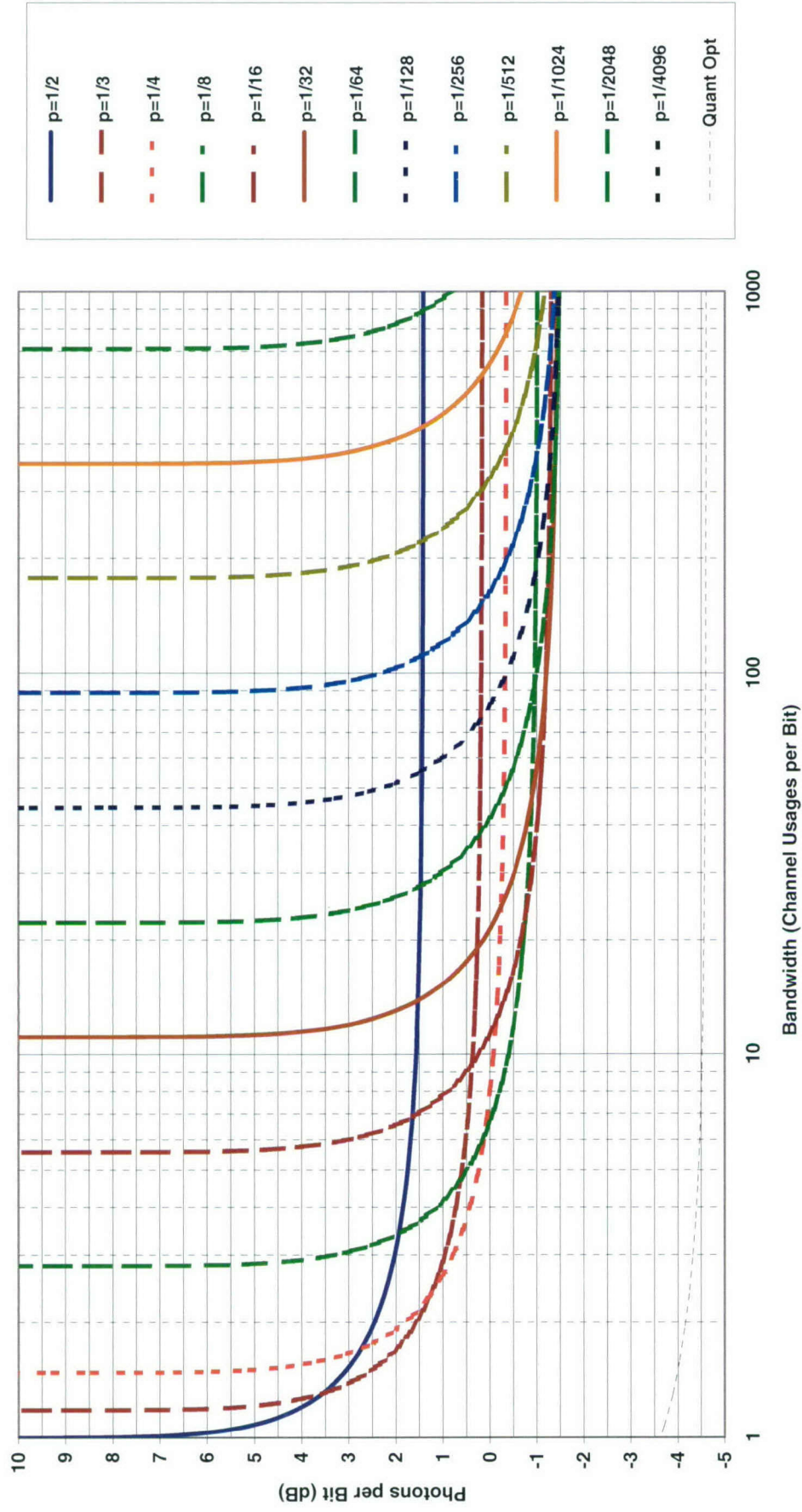


Chart 36. Efficiency at classical cutoff: OOK quantum hard decision (semiclassical).

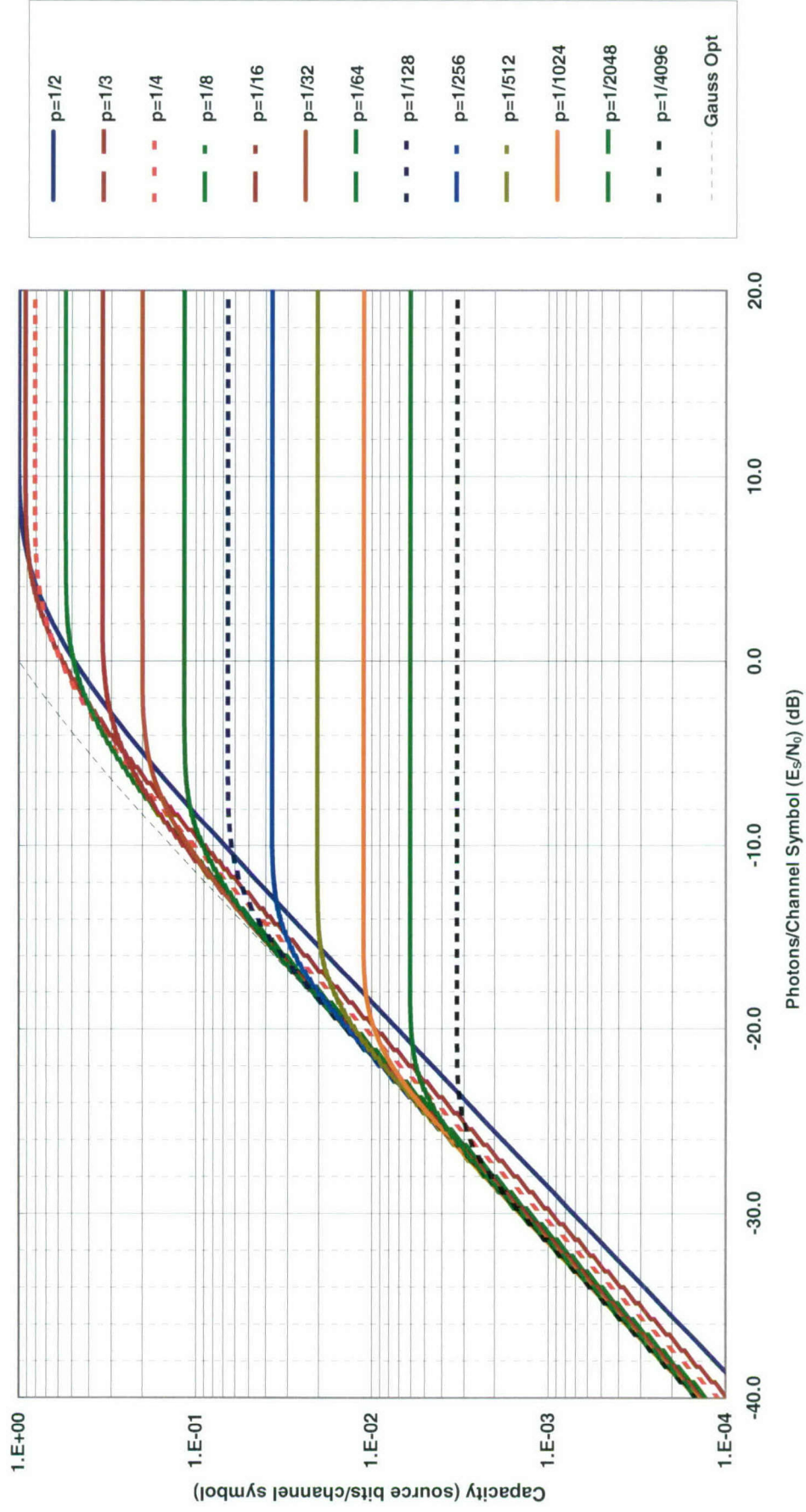


Chart 37. Classical capacity: OOK heterodyne or preamplified coherent soft decision.

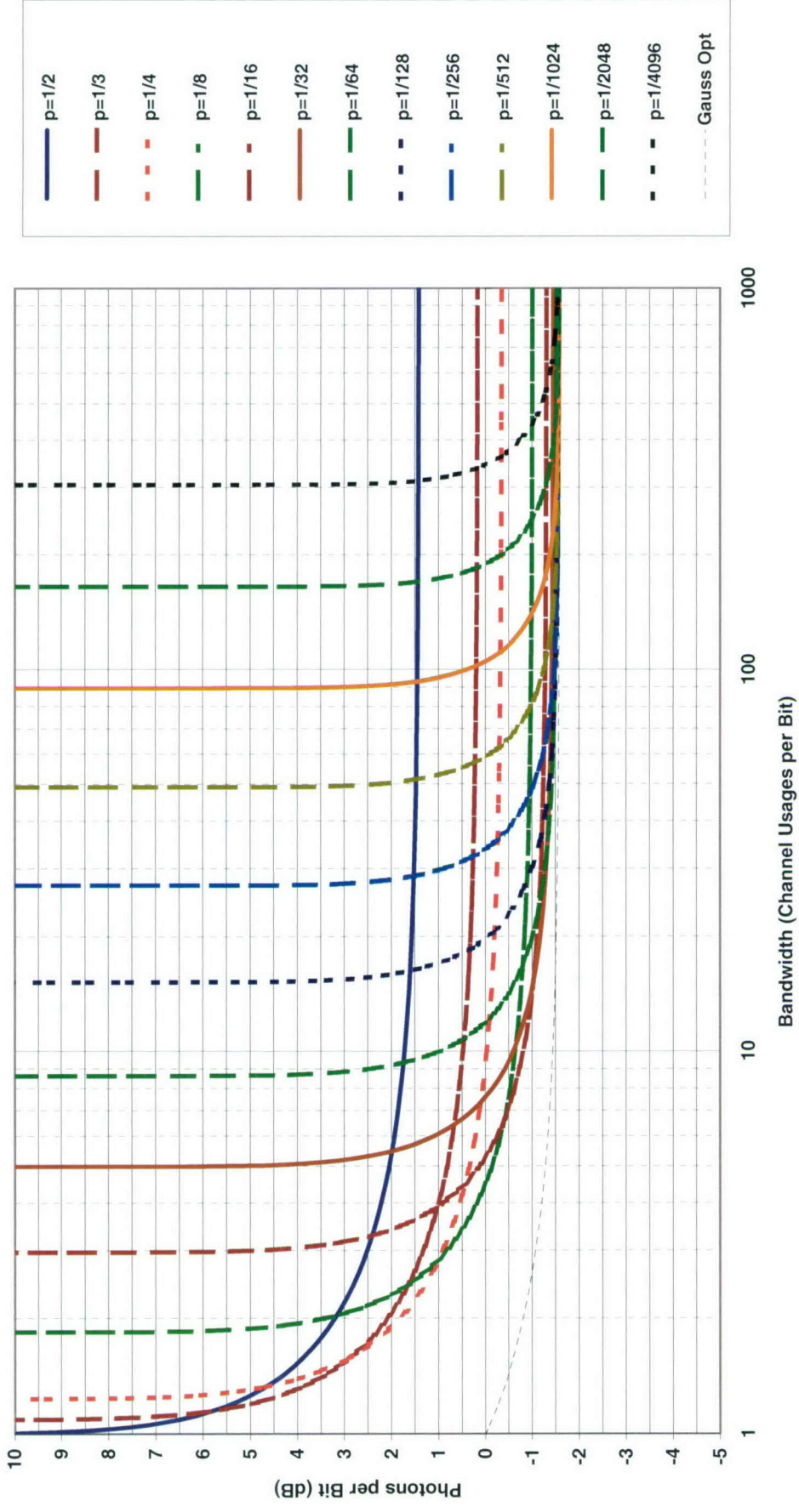


Chart 38. Efficiency at classical capacity: OOK heterodyne or preamplified coherent soft decision.

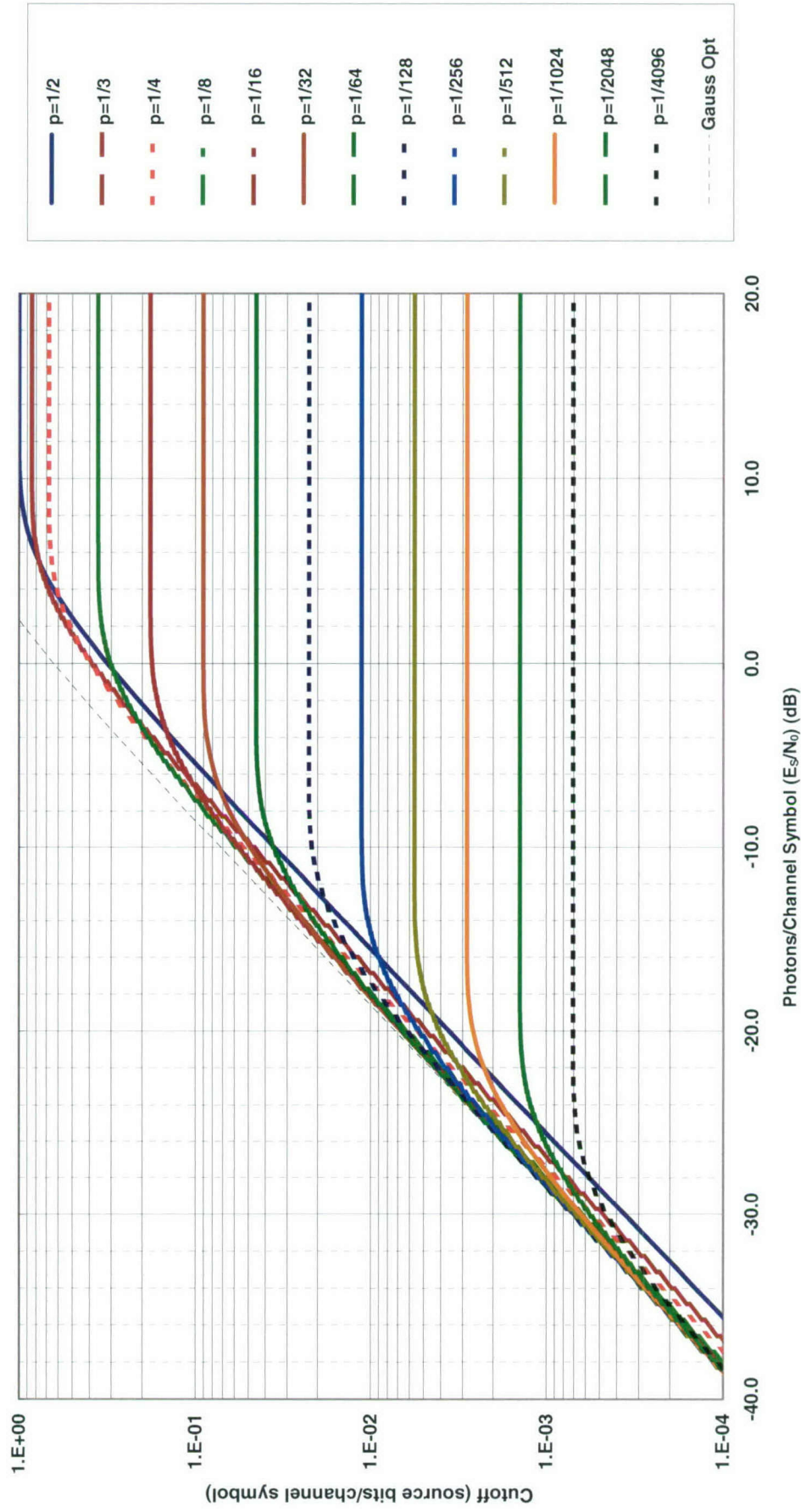


Chart 39. Classical cutoff: OOK heterodyne or preamplified coherent soft decision.

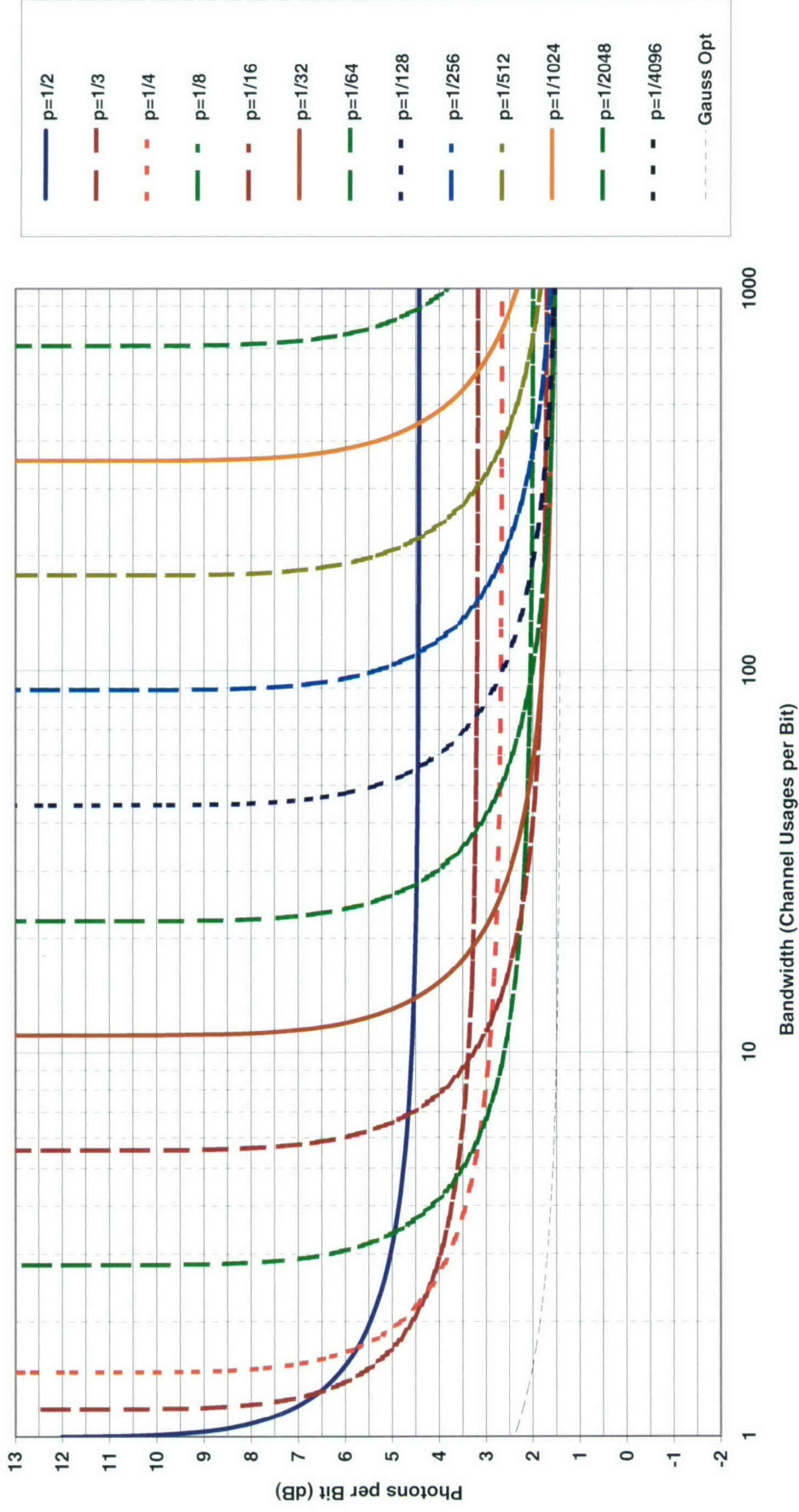


Chart 40. Efficiency at classical cutoff: OOK heterodyne or preamplified coherent soft decision.

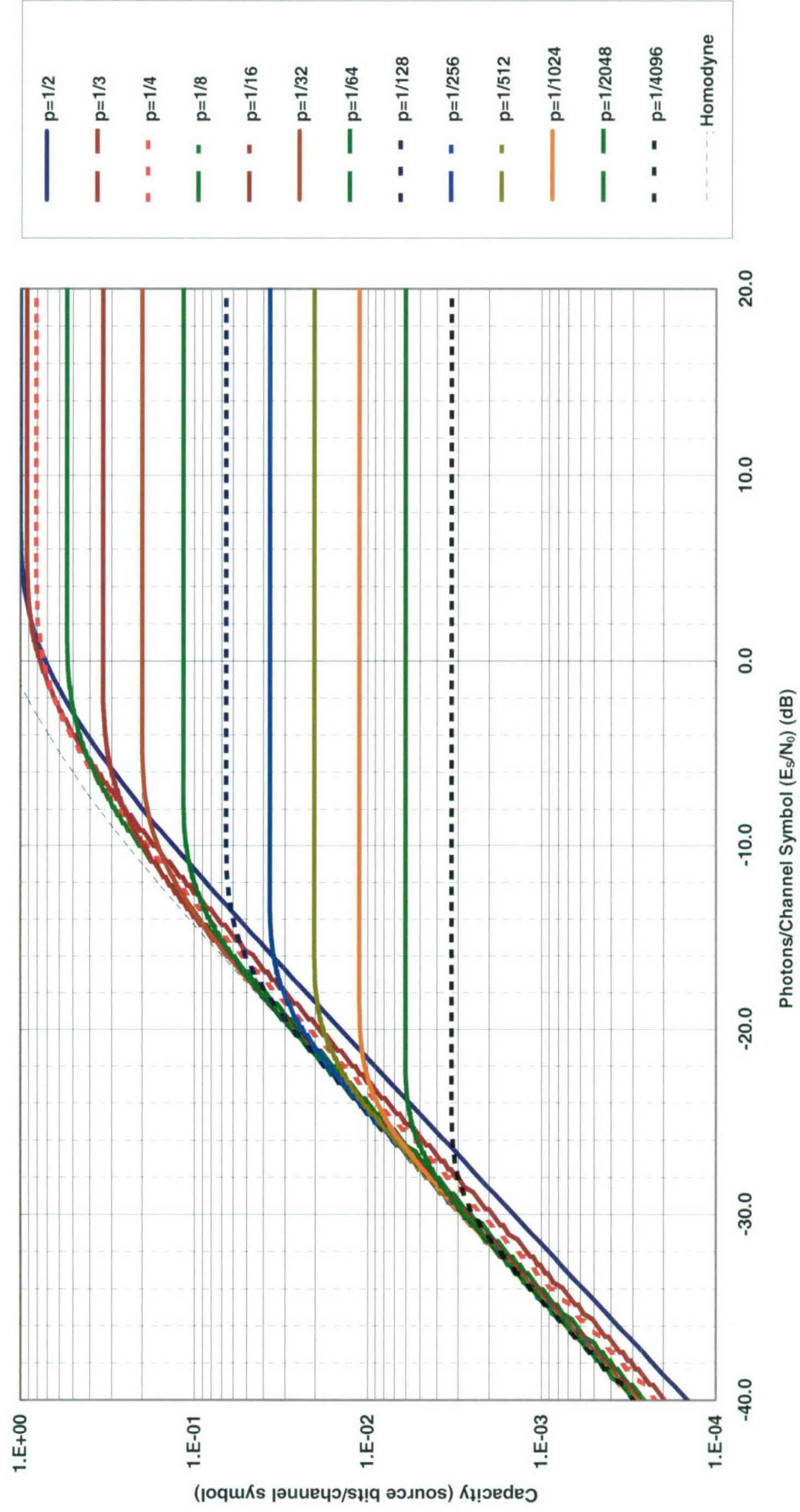


Chart 41. Classical capacity: OOK homodyne coherent soft decision.

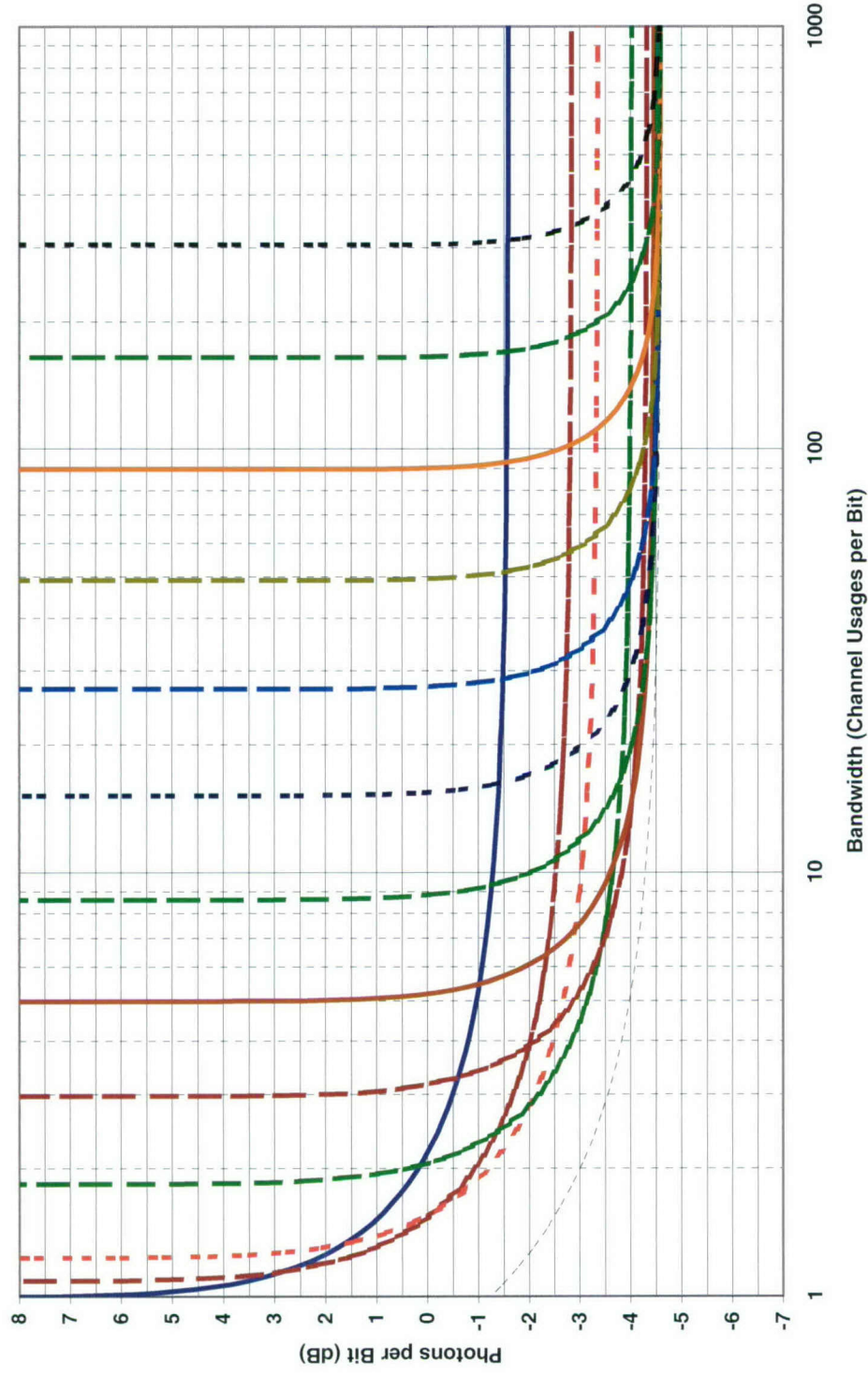


Chart 42. Efficiency at classical capacity: OOK homodyne coherent soft decision.

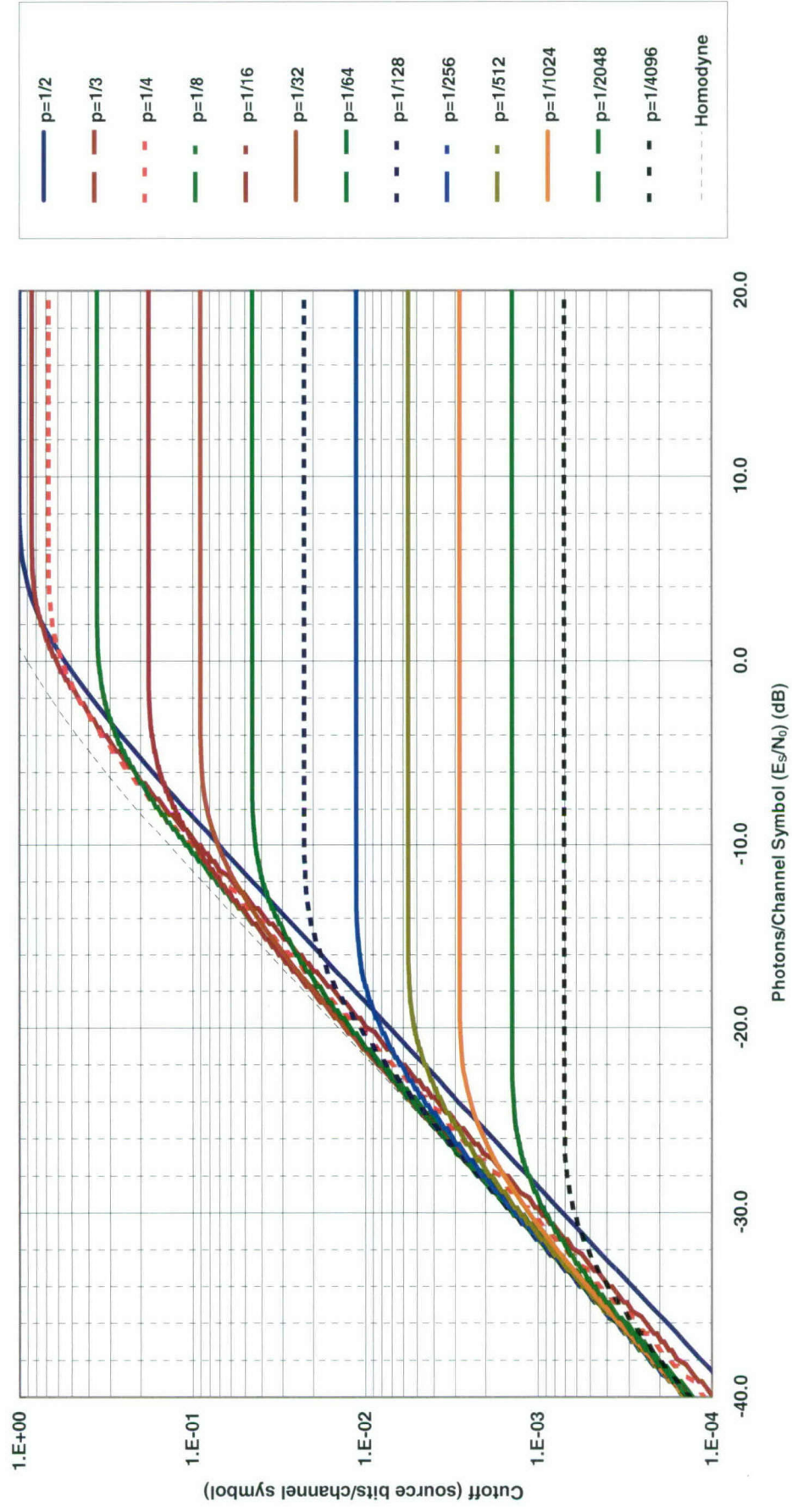


Chart 43. Classical cutoff: OOK homodyne coherent soft decision.

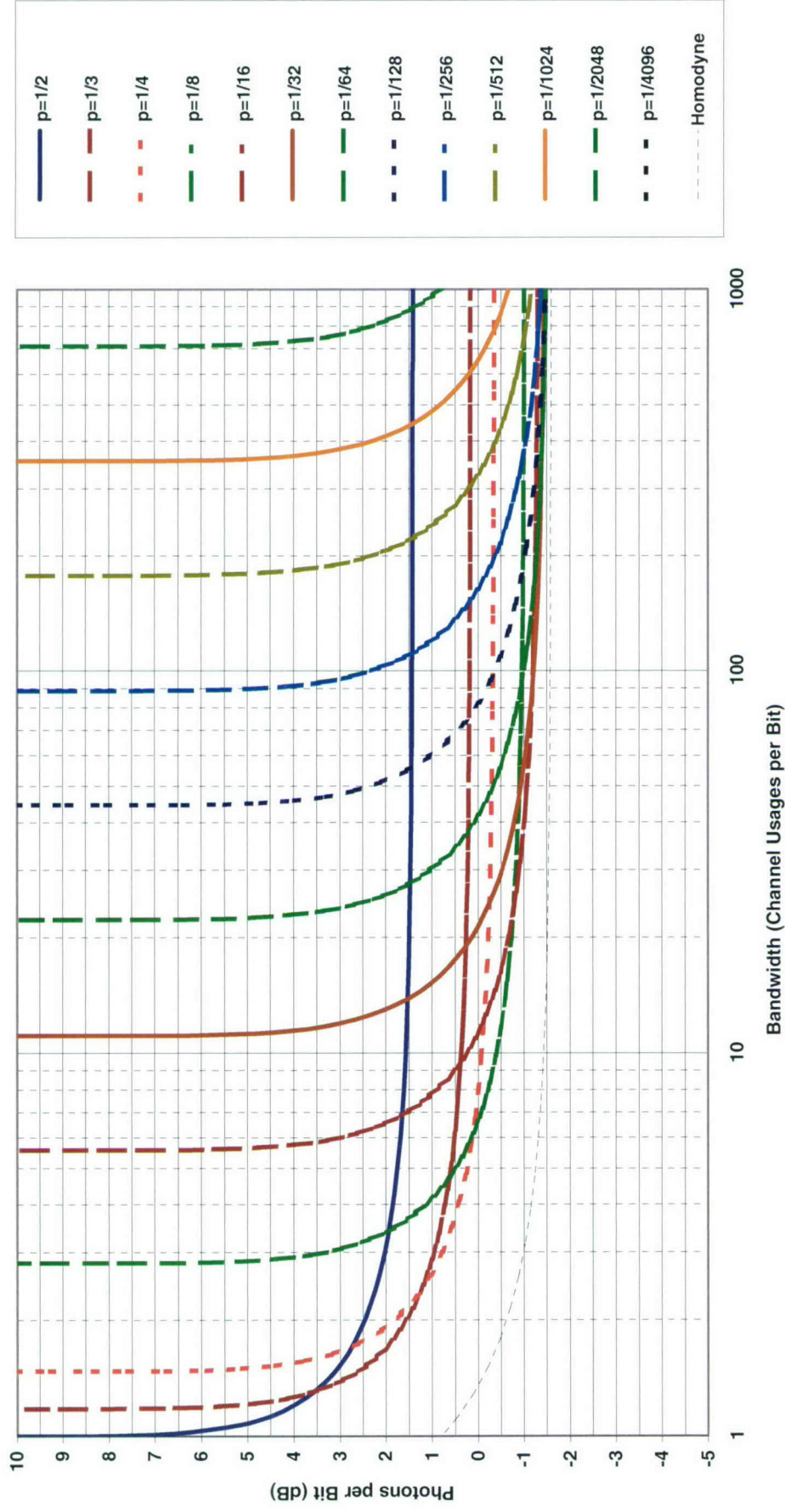


Chart 44. Efficiency at classical cutoff: OOK homodyne coherent soft decision.

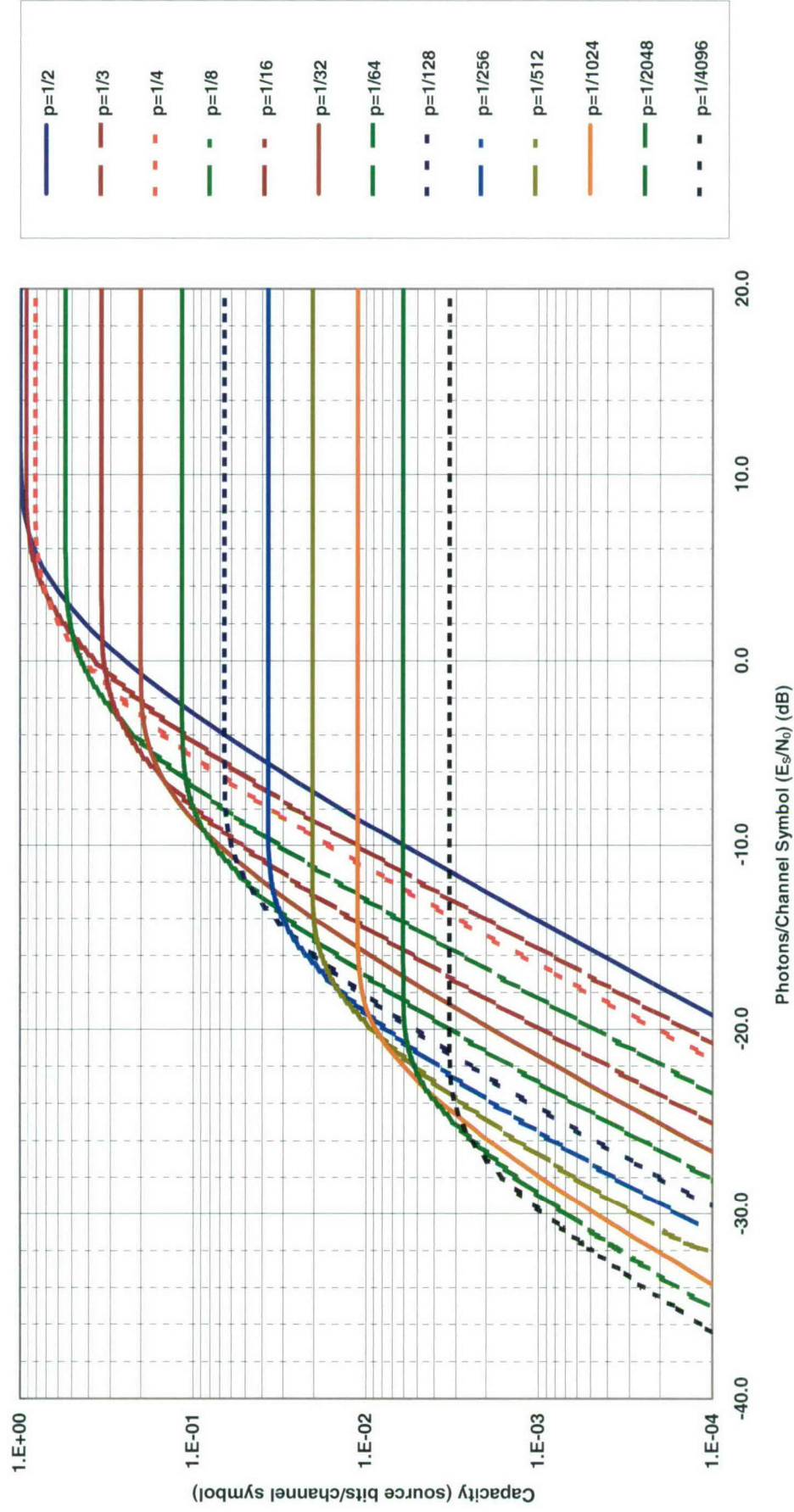


Chart 45. Classical capacity: OOK heterodyne or preamplified noncoherent soft decision.

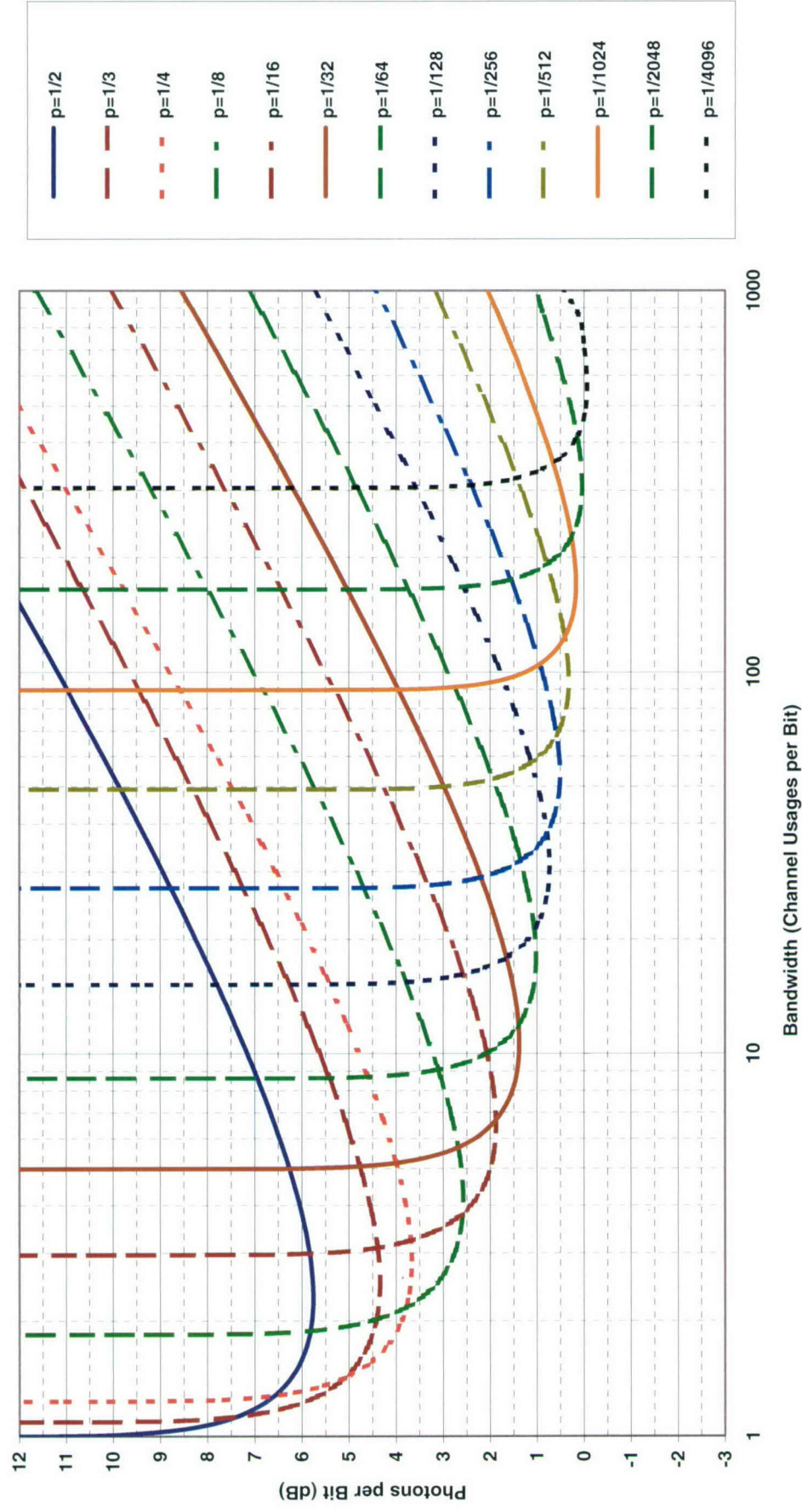


Chart 46. Efficiency at classical capacity: OOK heterodyne or preamplified noncoherent soft decision.

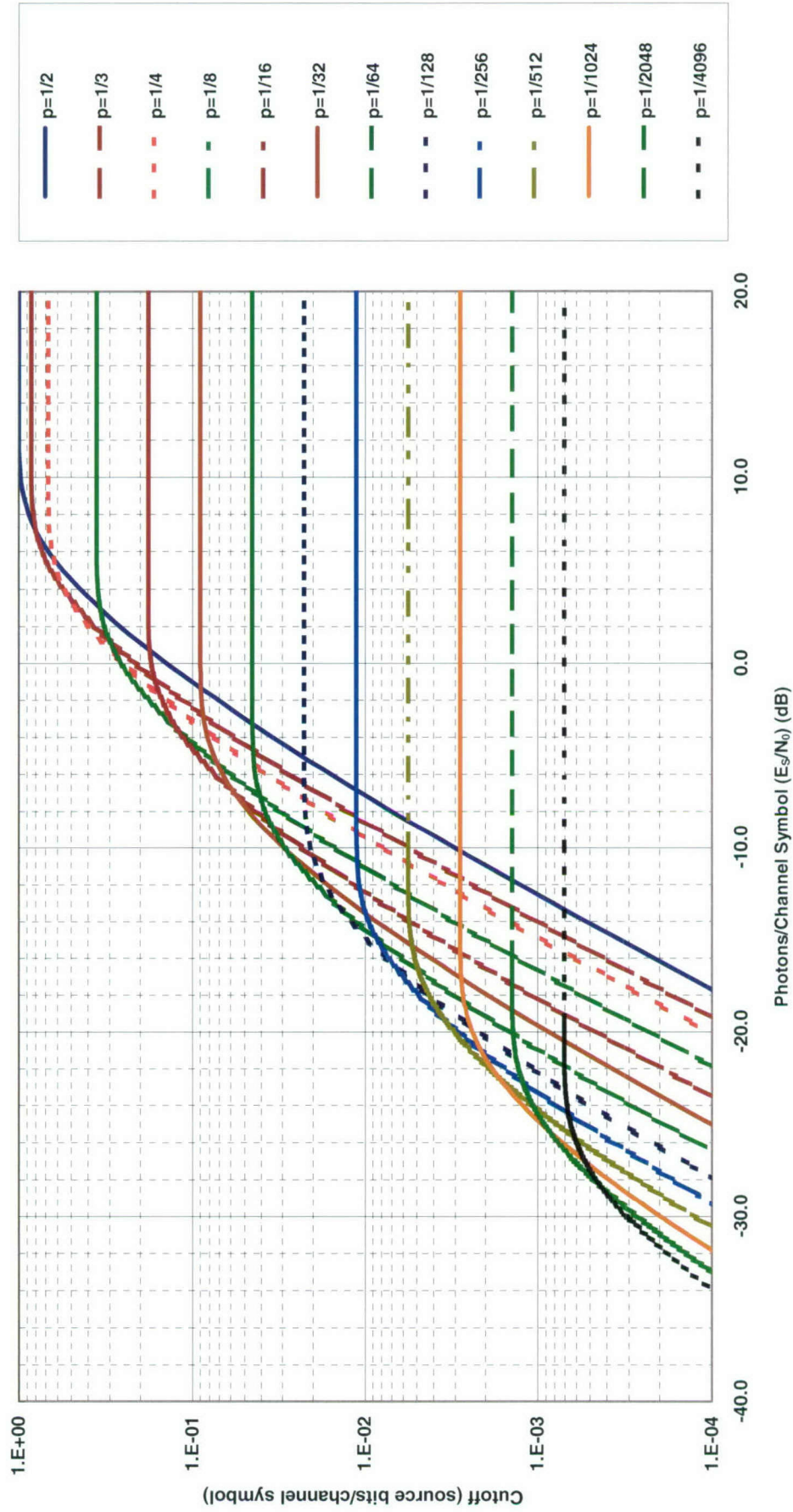


Chart 47. Classical cutoff: OOK heterodyne or preamplified noncoherent soft decision.

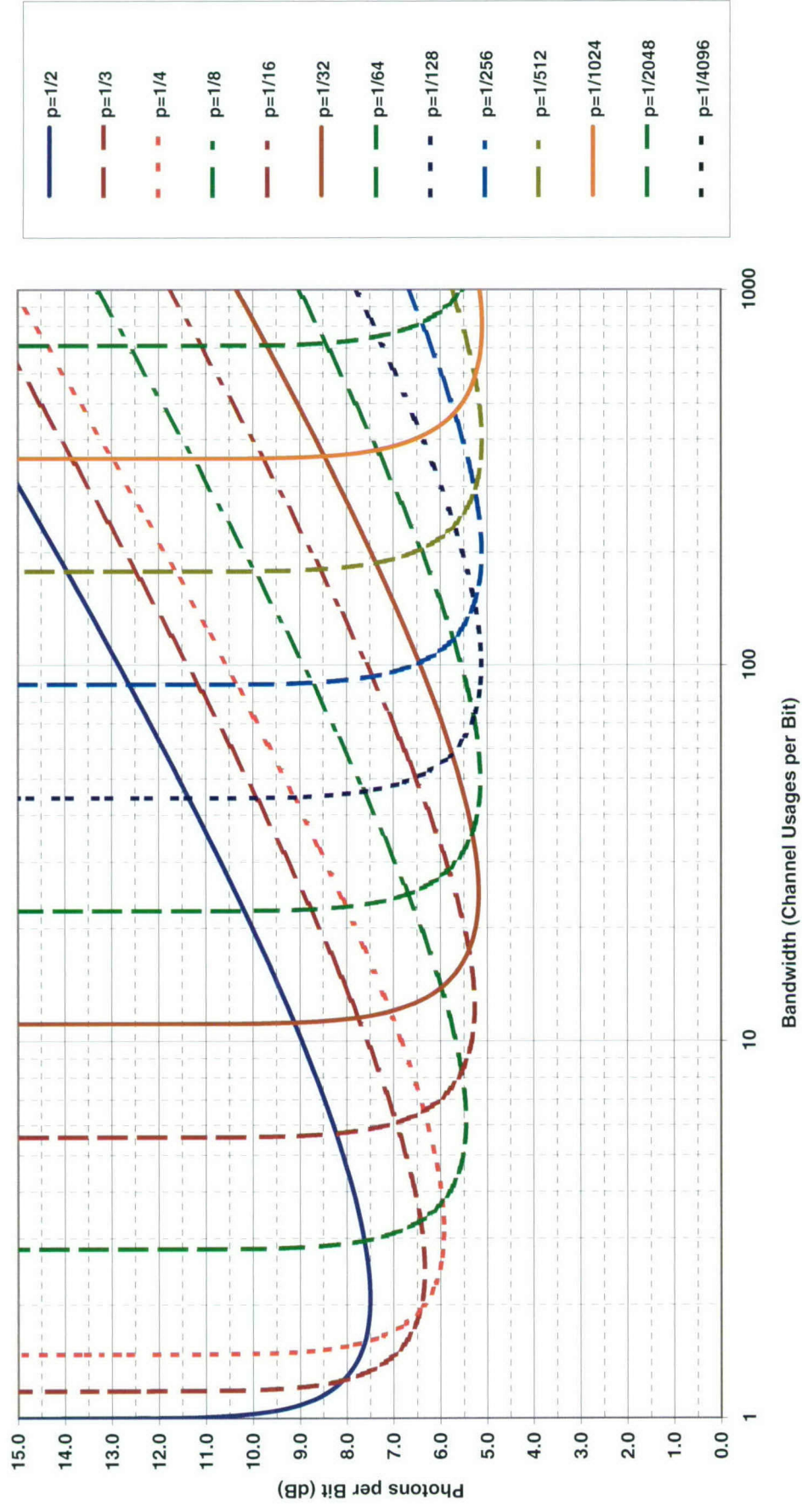


Chart 48. Efficiency at classical cutoff: OOK heterodyne or preamplified noncoherent soft decision.

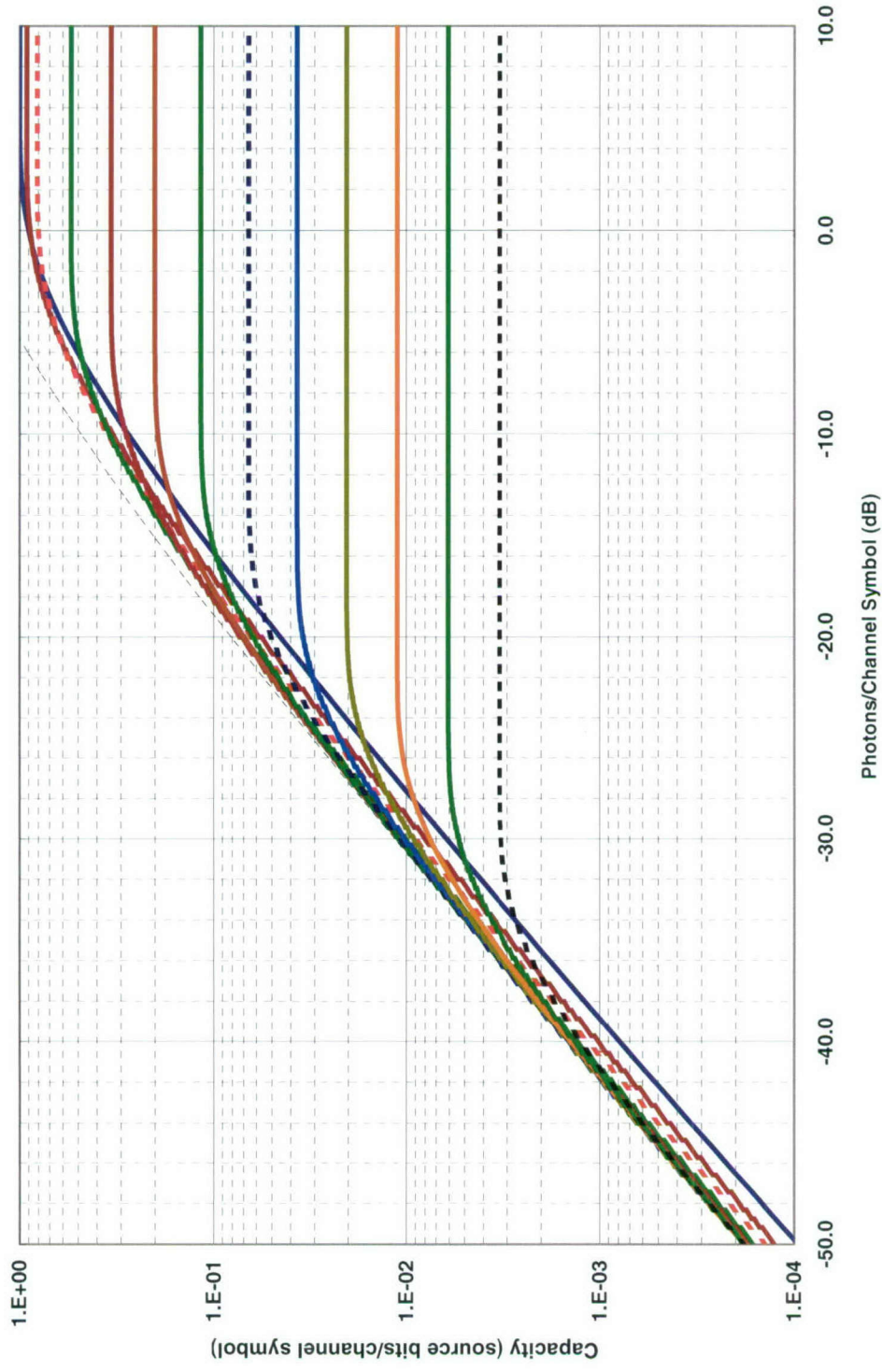


Chart 49. Quantum capacity: OOK.

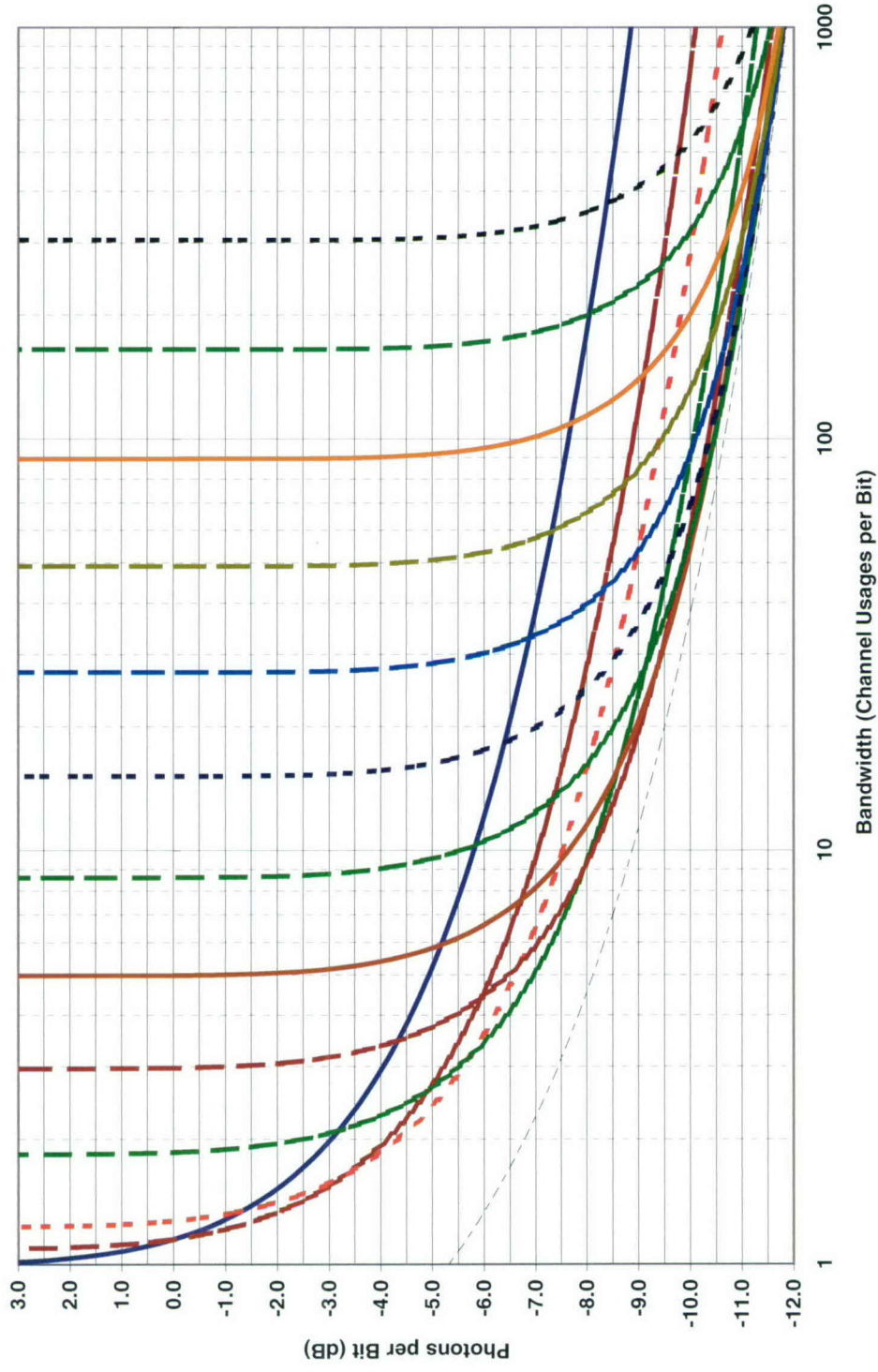


Chart 50. Efficiency at quantum capacity: OOK.

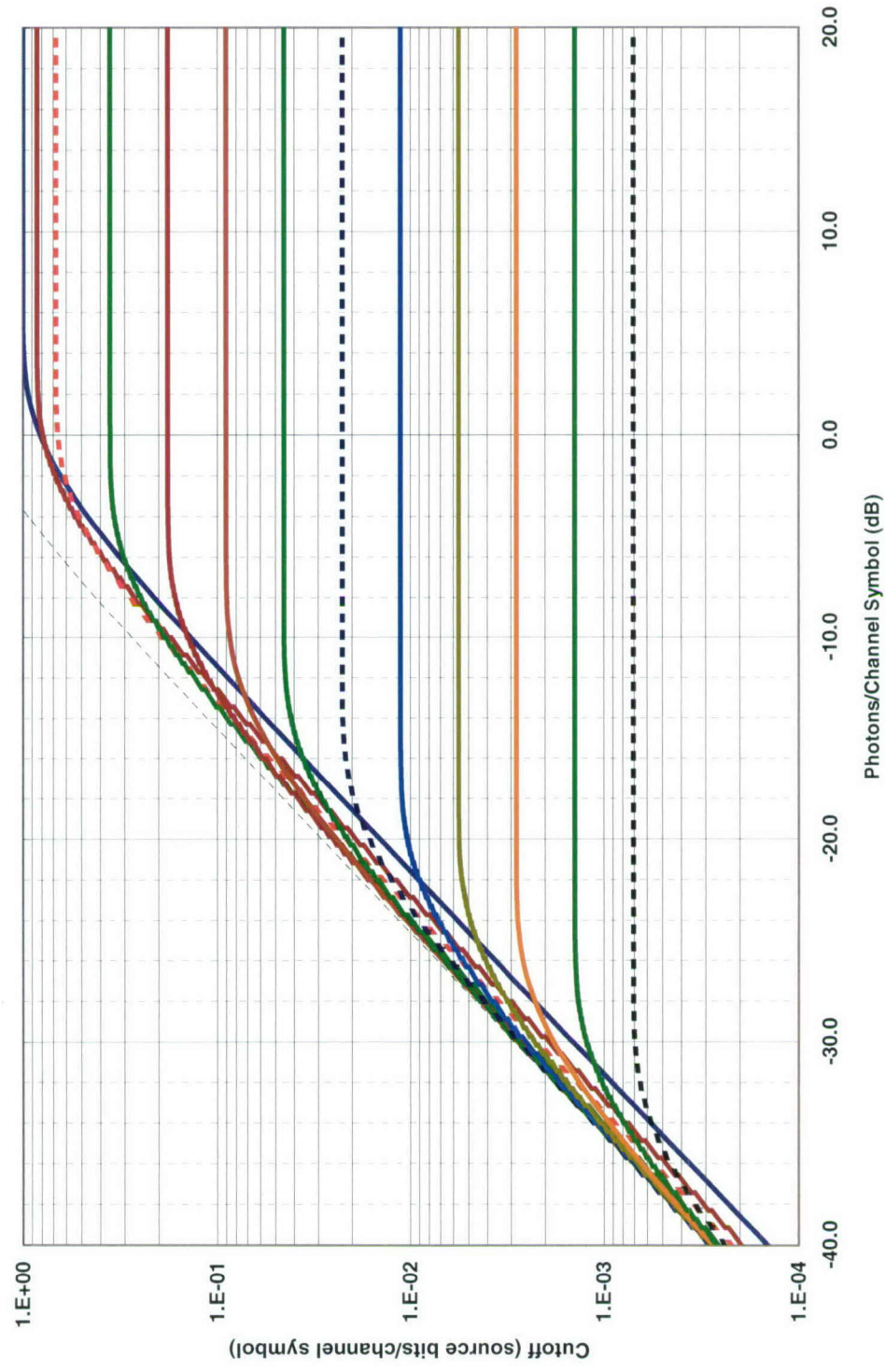


Chart 51. Quantum cutoff: OOK.

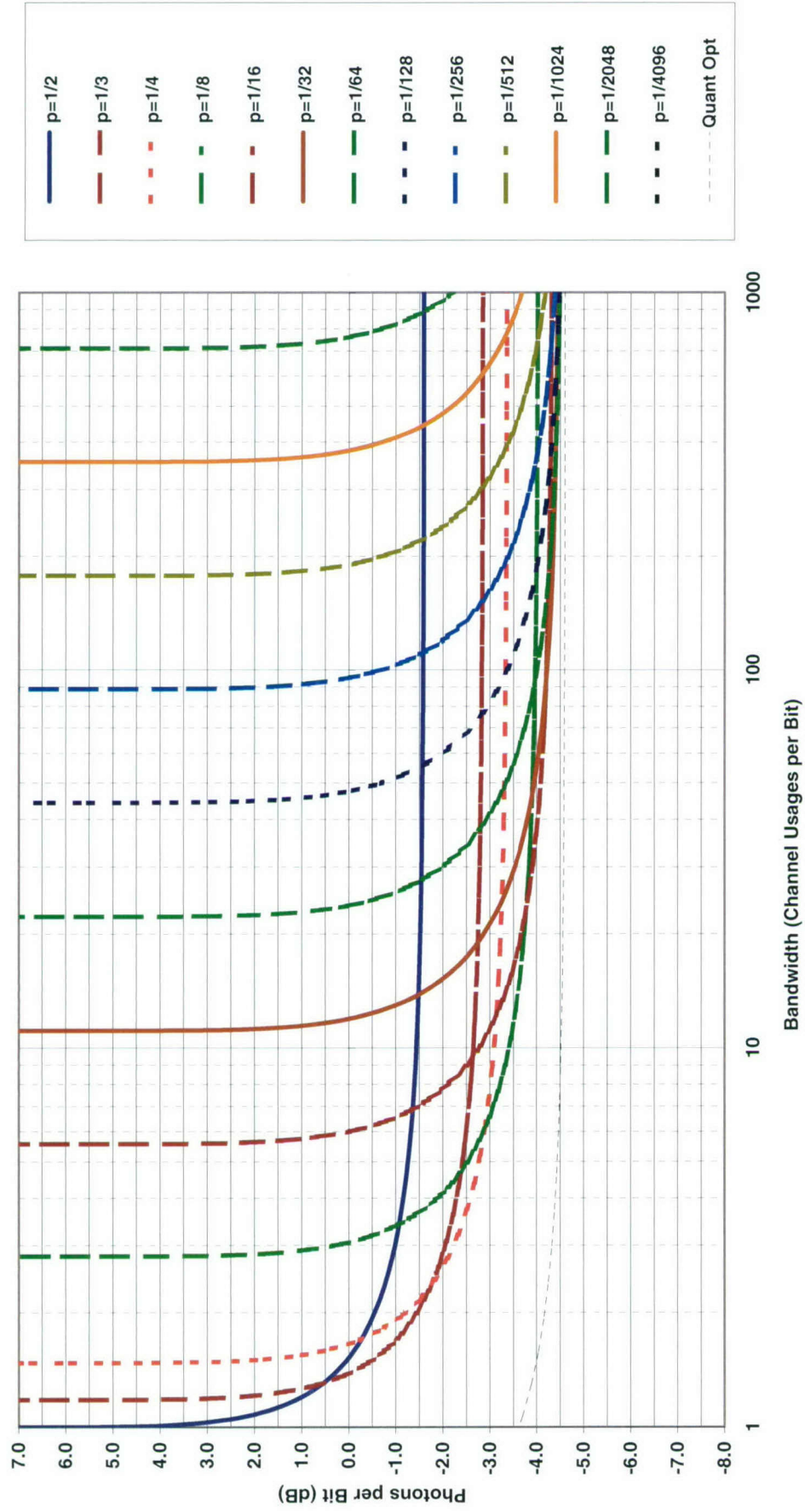


Chart 52. Efficiency at quantum cutoff: OOK.

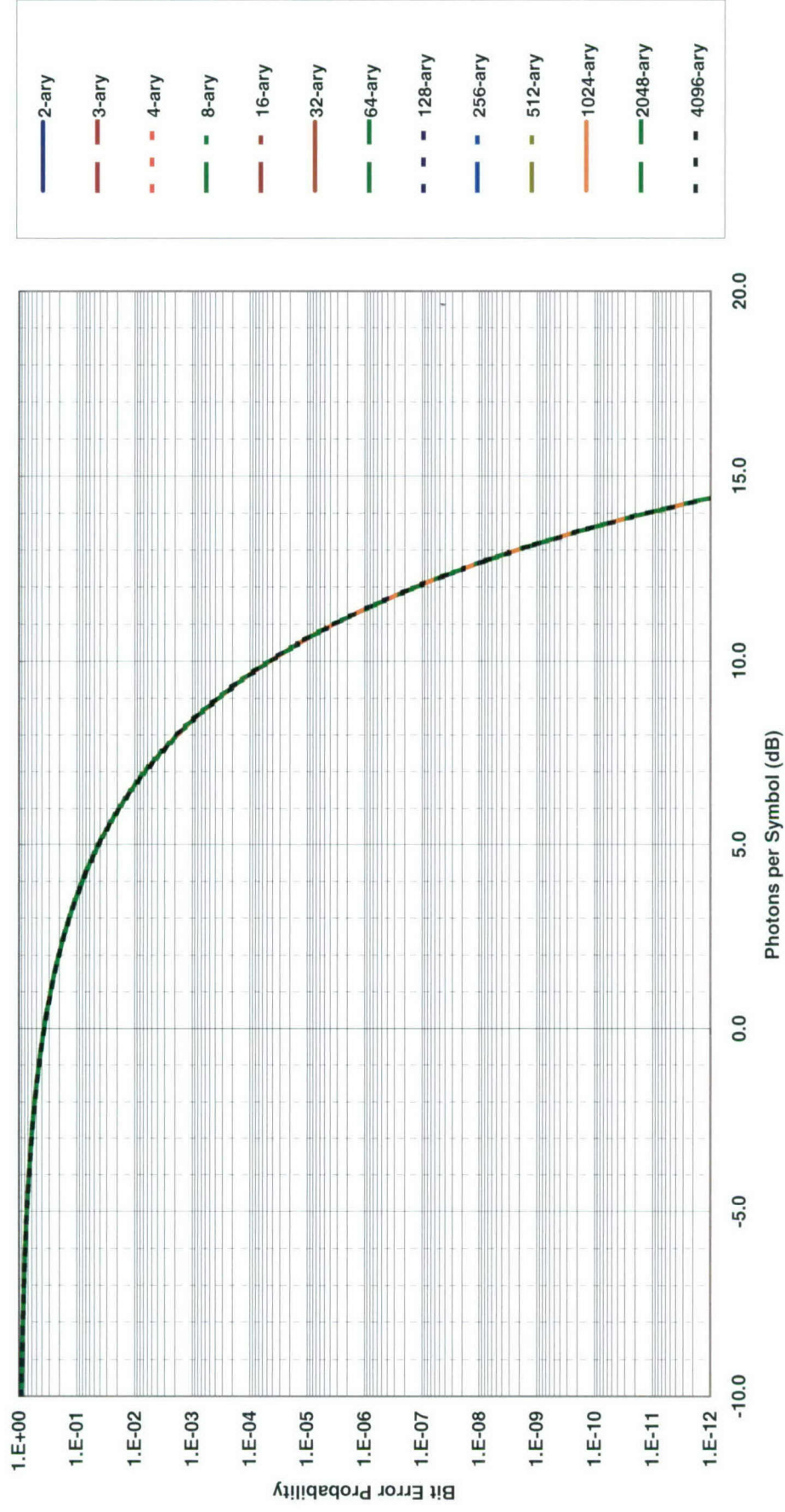


Chart 53. Symbol error (erasure) probability: orthogonal photon counting.

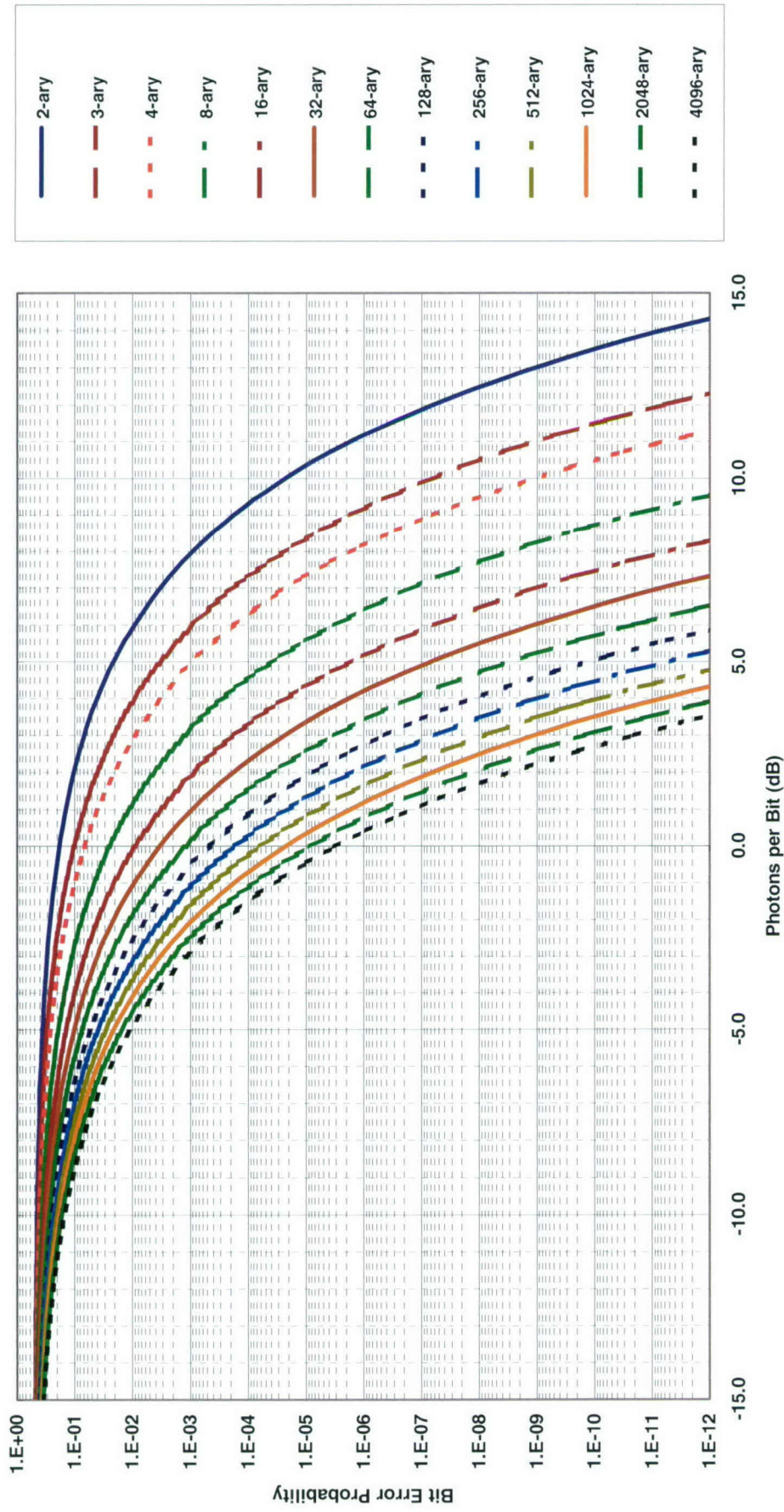


Chart 54. Bit-error probability (erasure with coin flip): orthogonal photon counting.

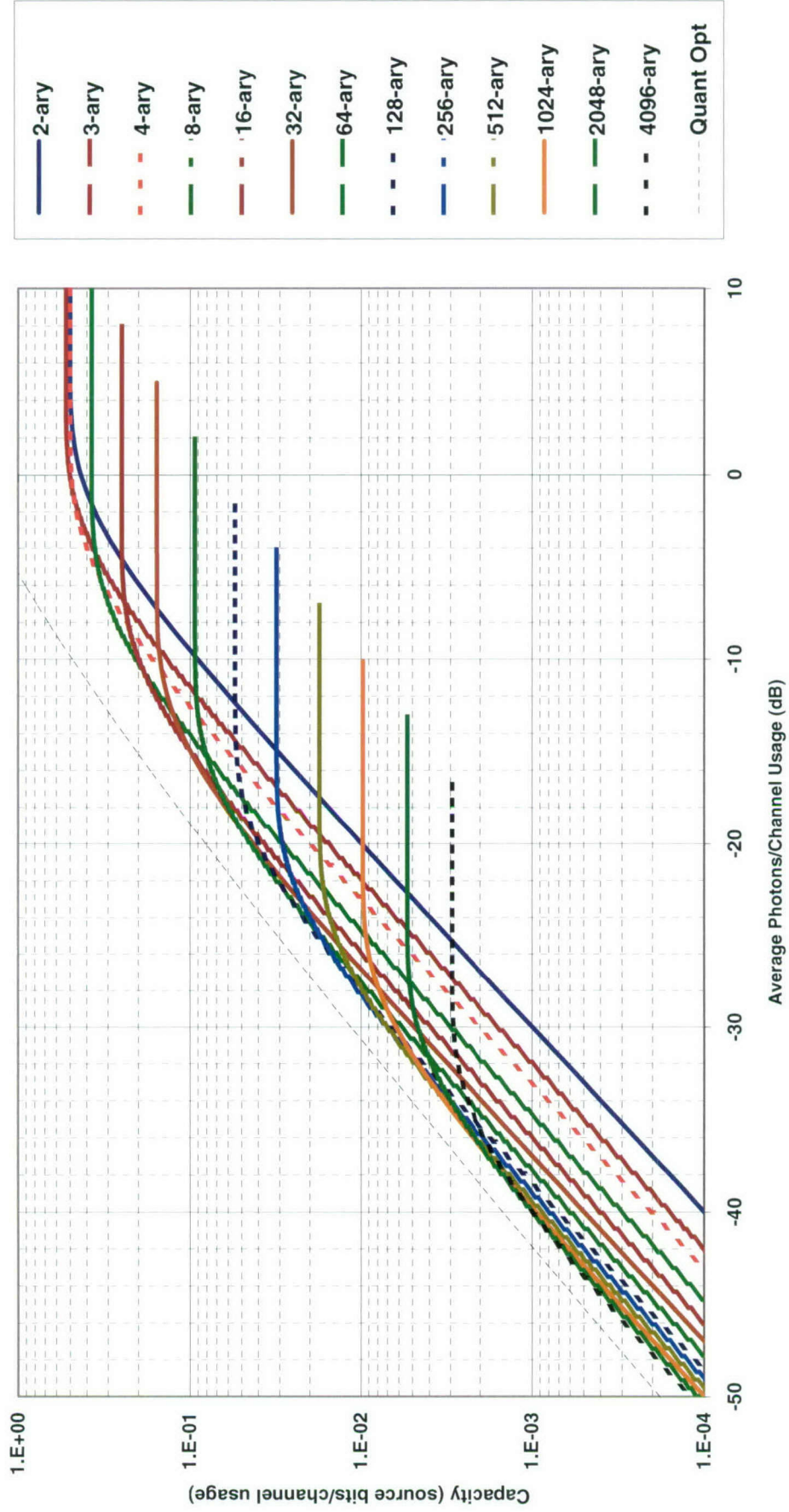


Chart 55. Classical capacity: orthogonal photon counting.

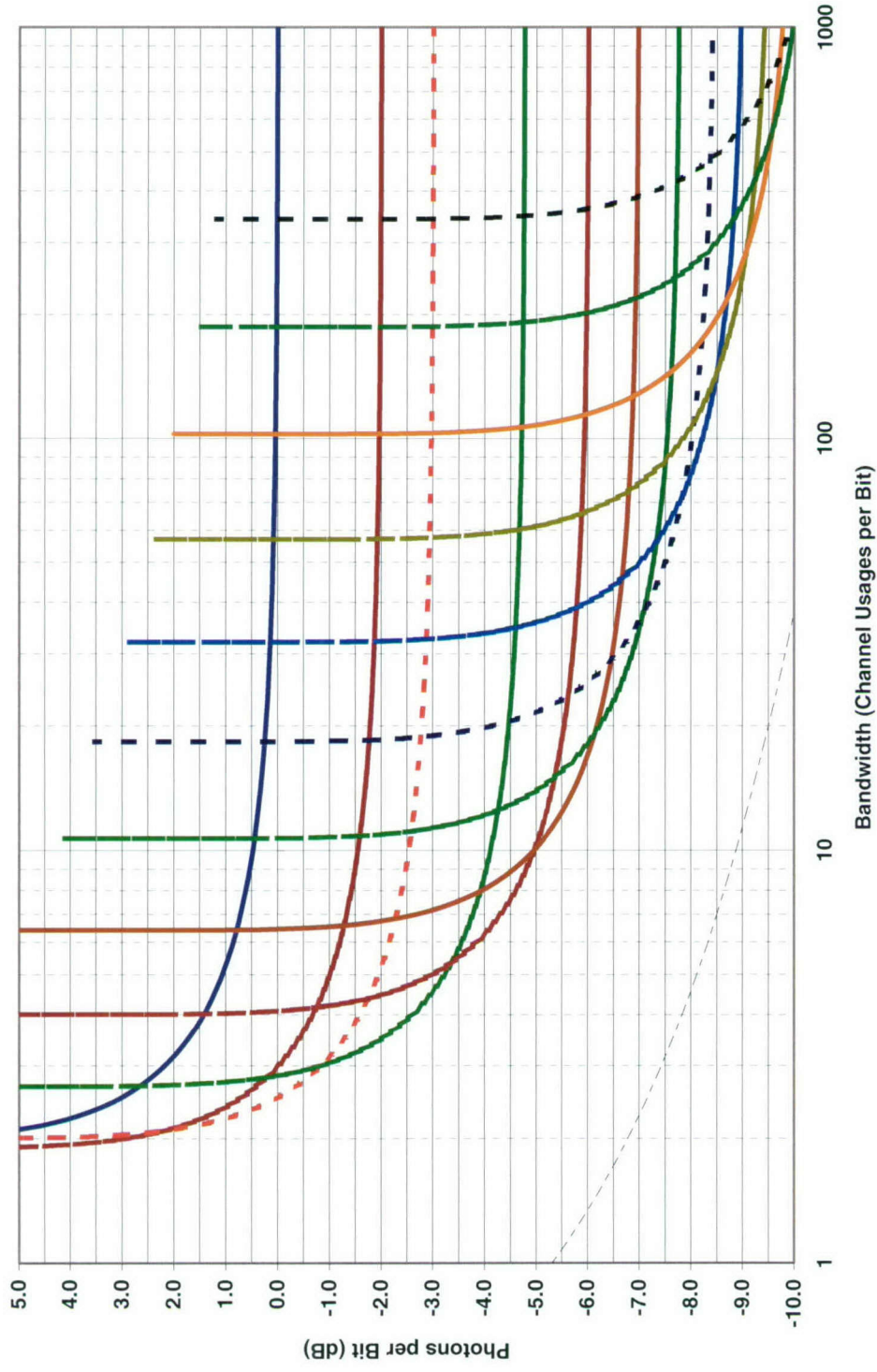


Chart 56. Efficiency at classical capacity: orthogonal photon counting.

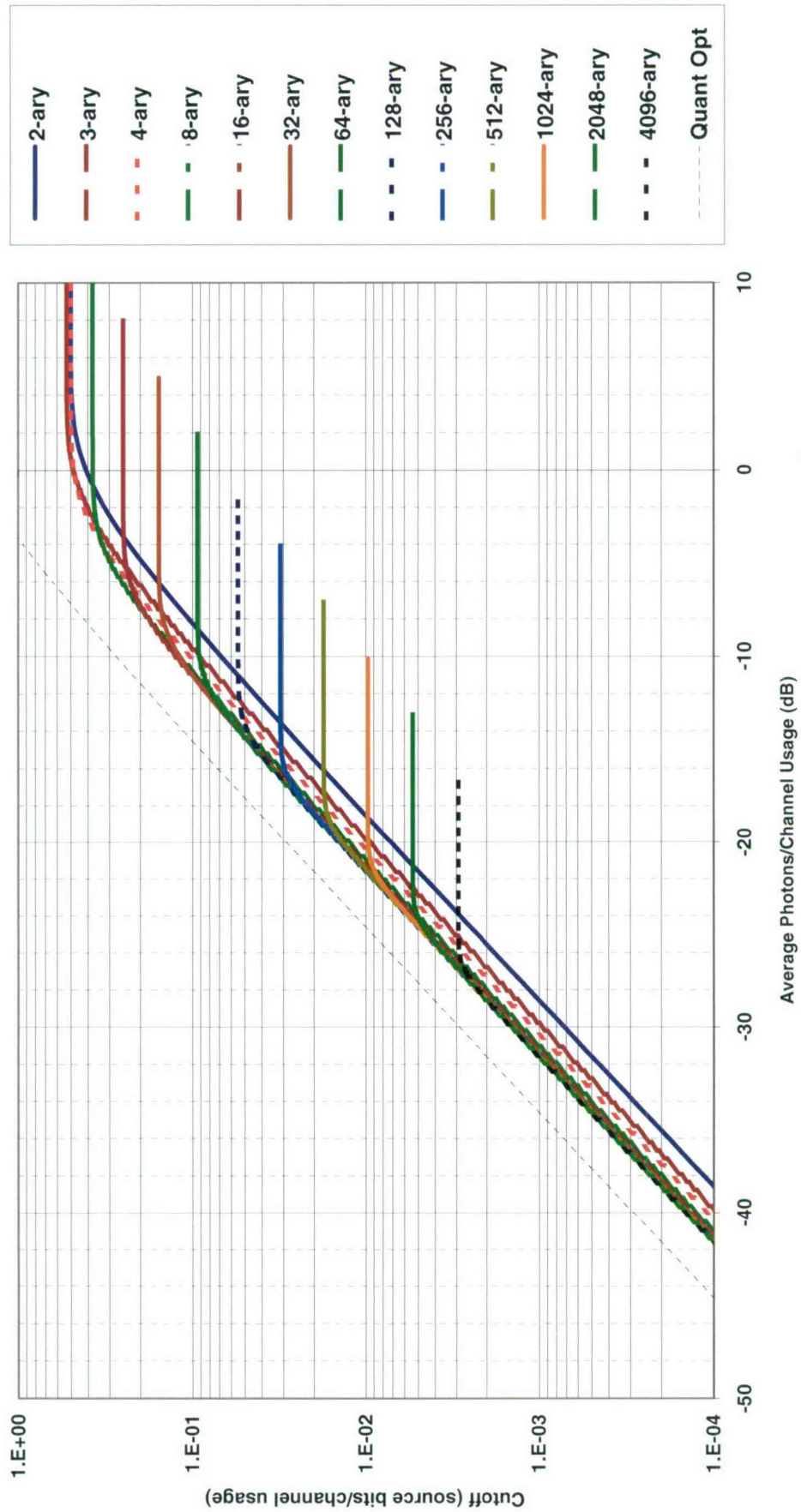


Chart 57. Classical cutoff: orthogonal photon counting.

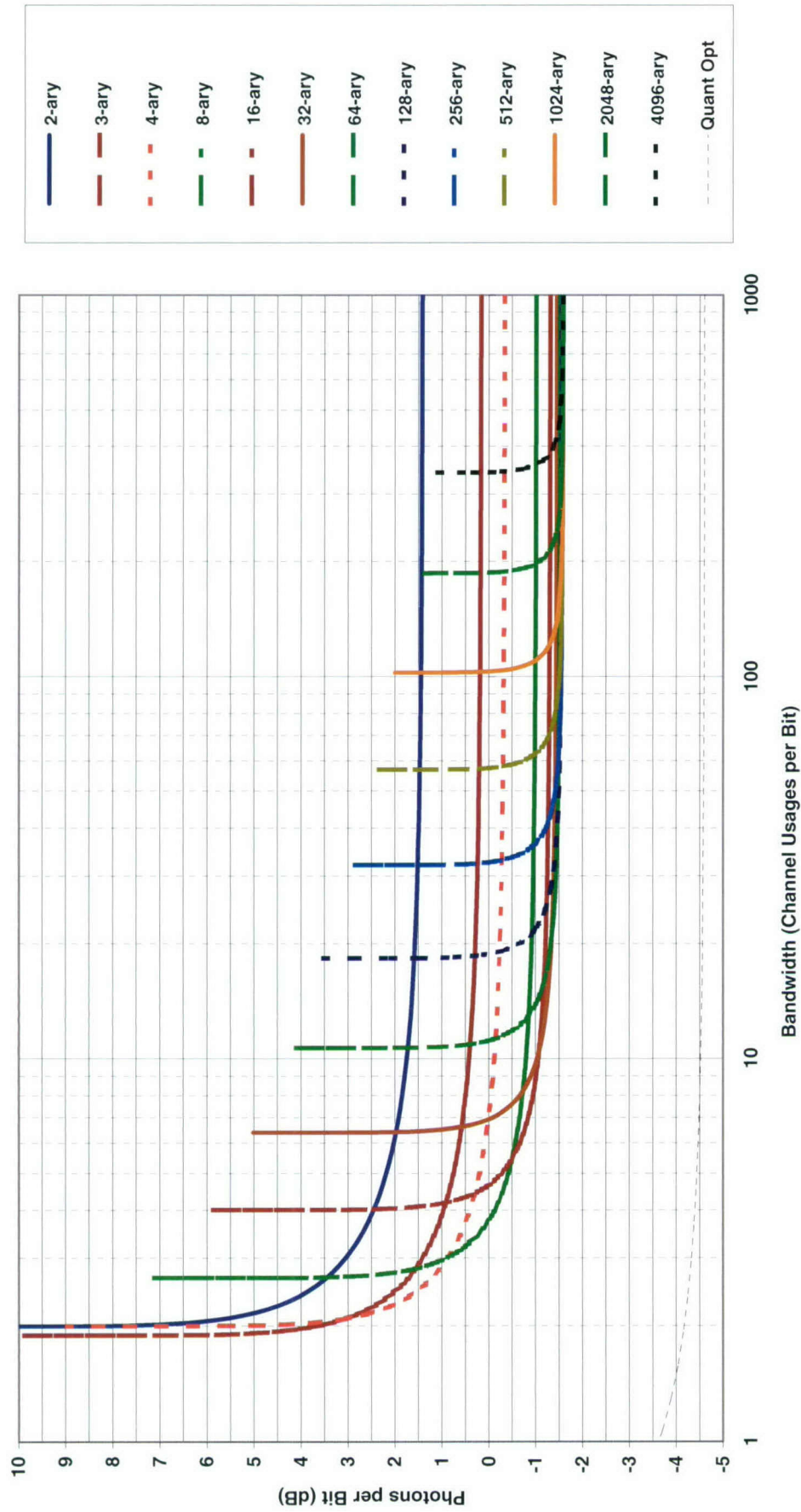


Chart 58. Efficiency at classical cutoff: orthogonal photon counting.

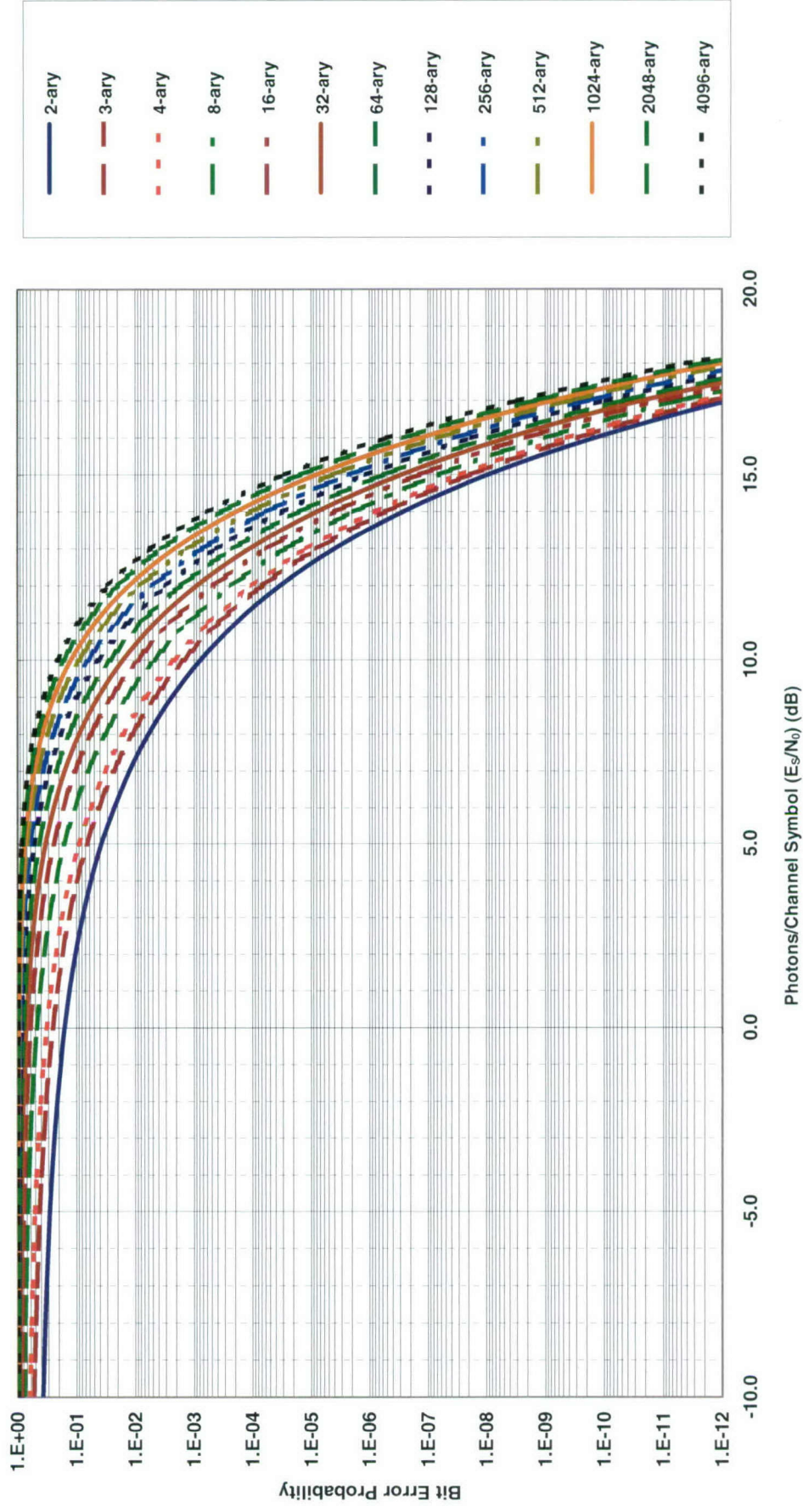


Chart 59. Symbol error probability: orthogonal heterodyne or preamplified coherent.

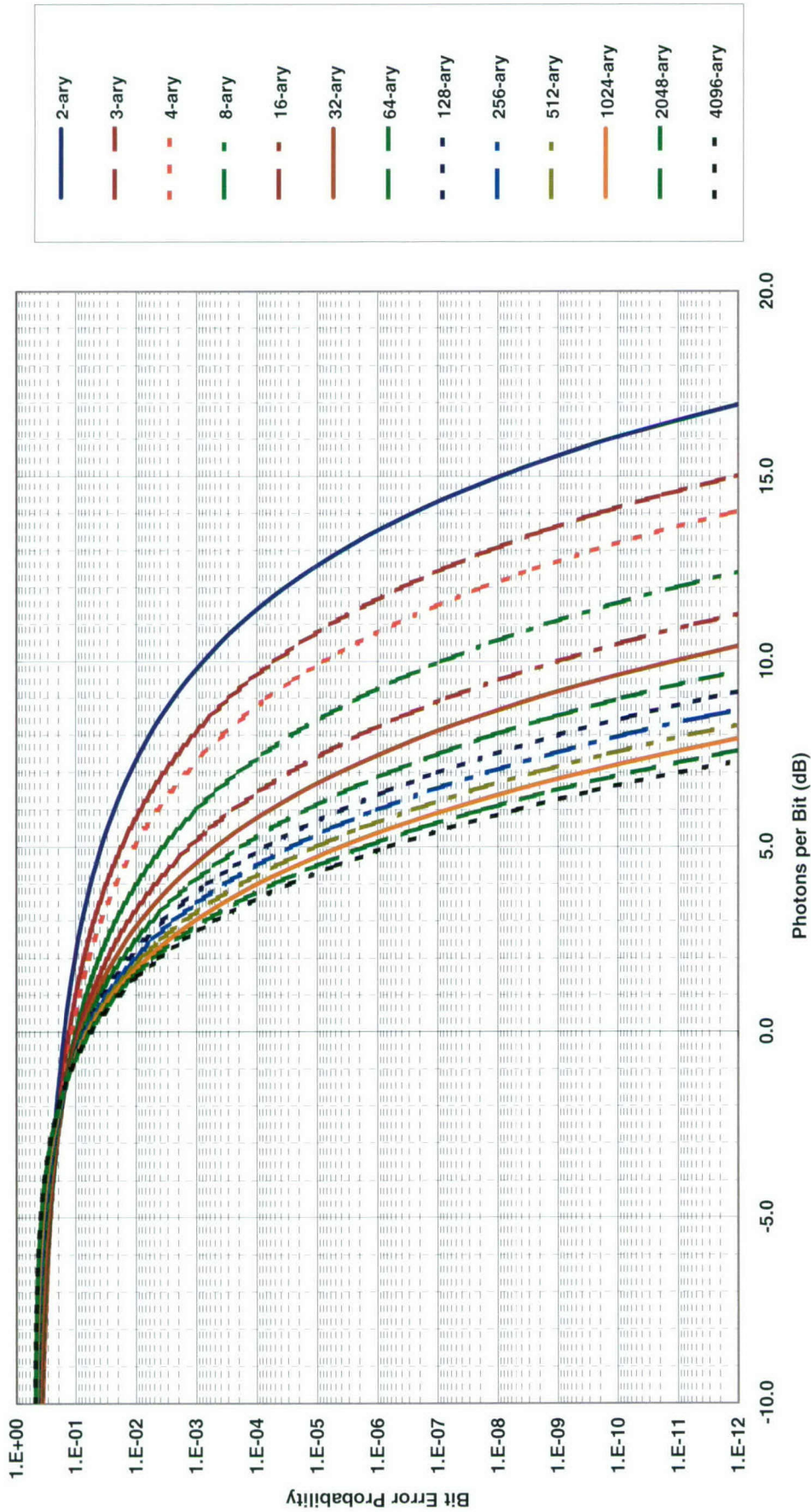


Chart 60. Bit-error probability: orthogonal heterodyne or preamplified coherent.

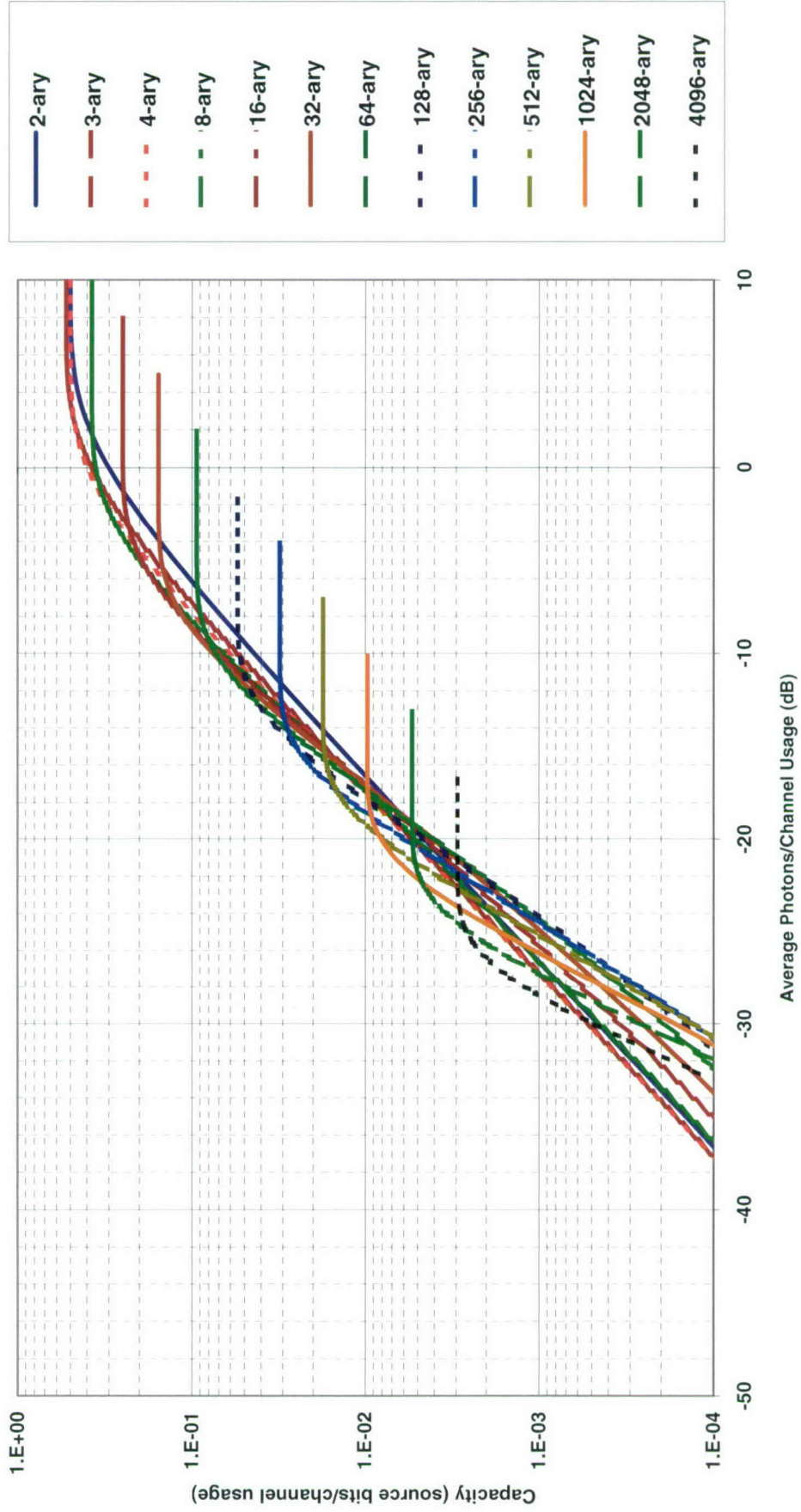


Chart 61. Classical capacity: orthogonal heterodyne or preamplified coherent hard decision.

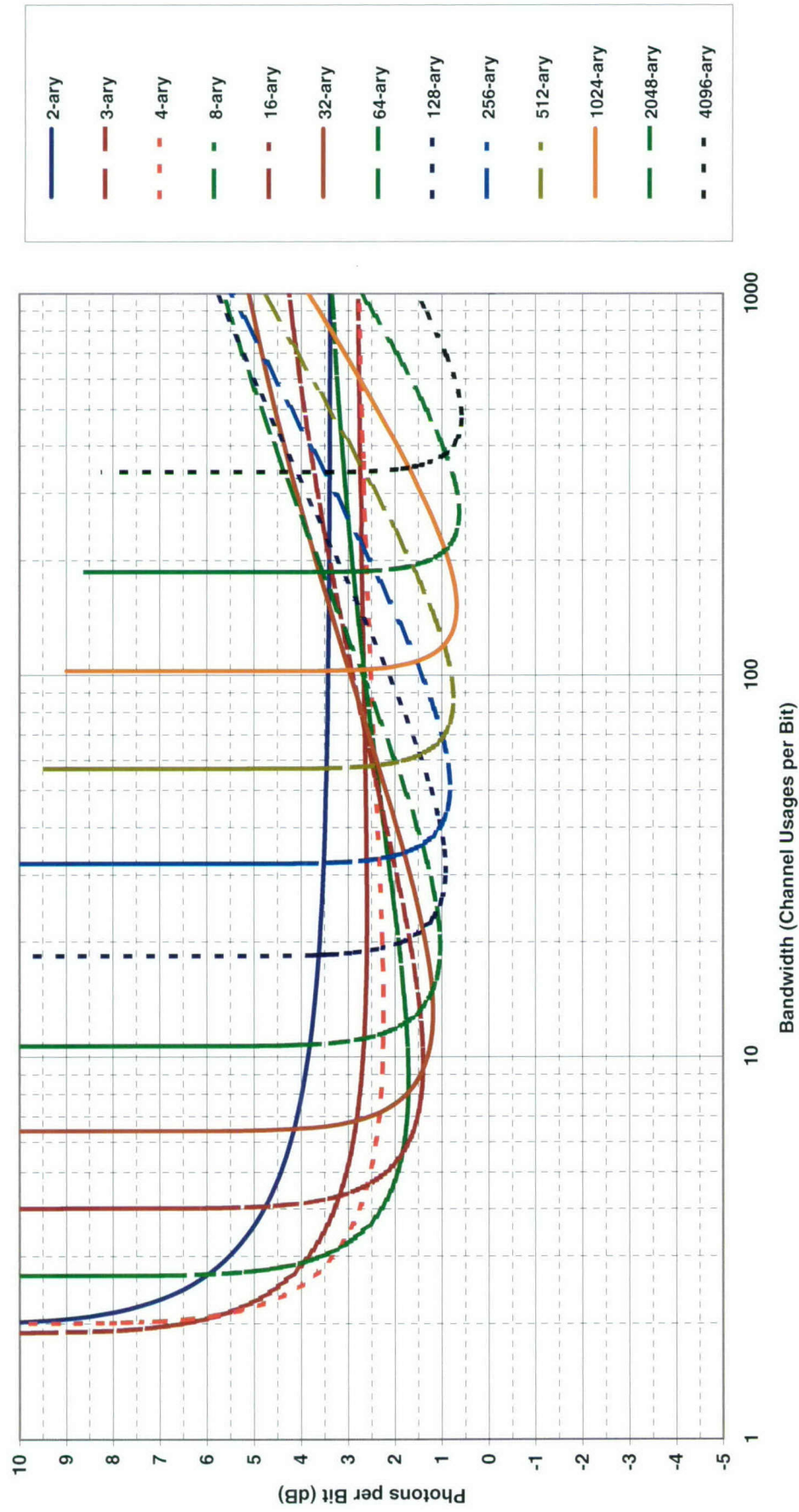


Chart 62. Efficiency at classical capacity: orthogonal heterodyne or preamplified coherent hard decision.

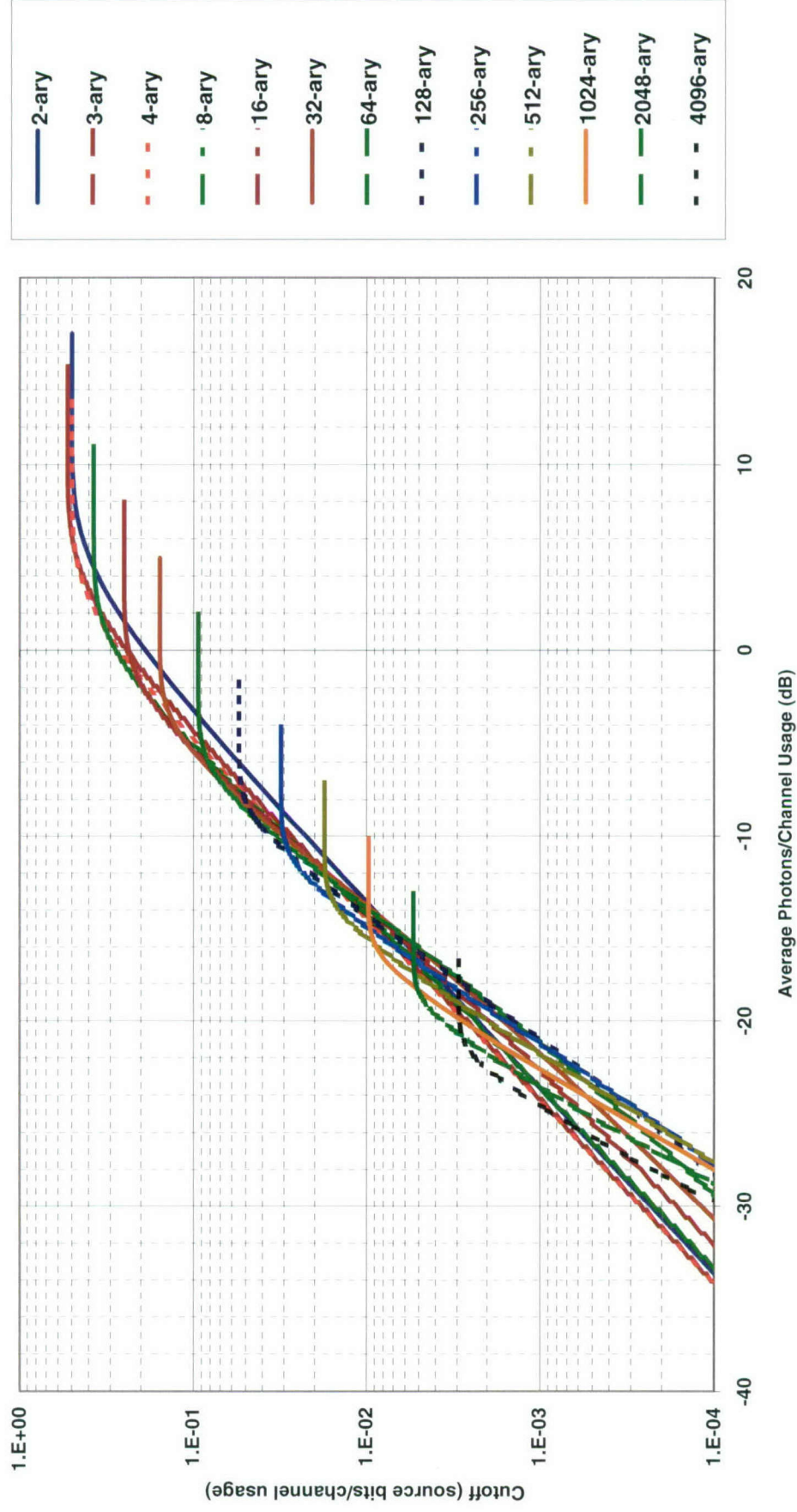


Chart 63. Classical cutoff: orthogonal heterodyne or preamplified coherent hard decision.

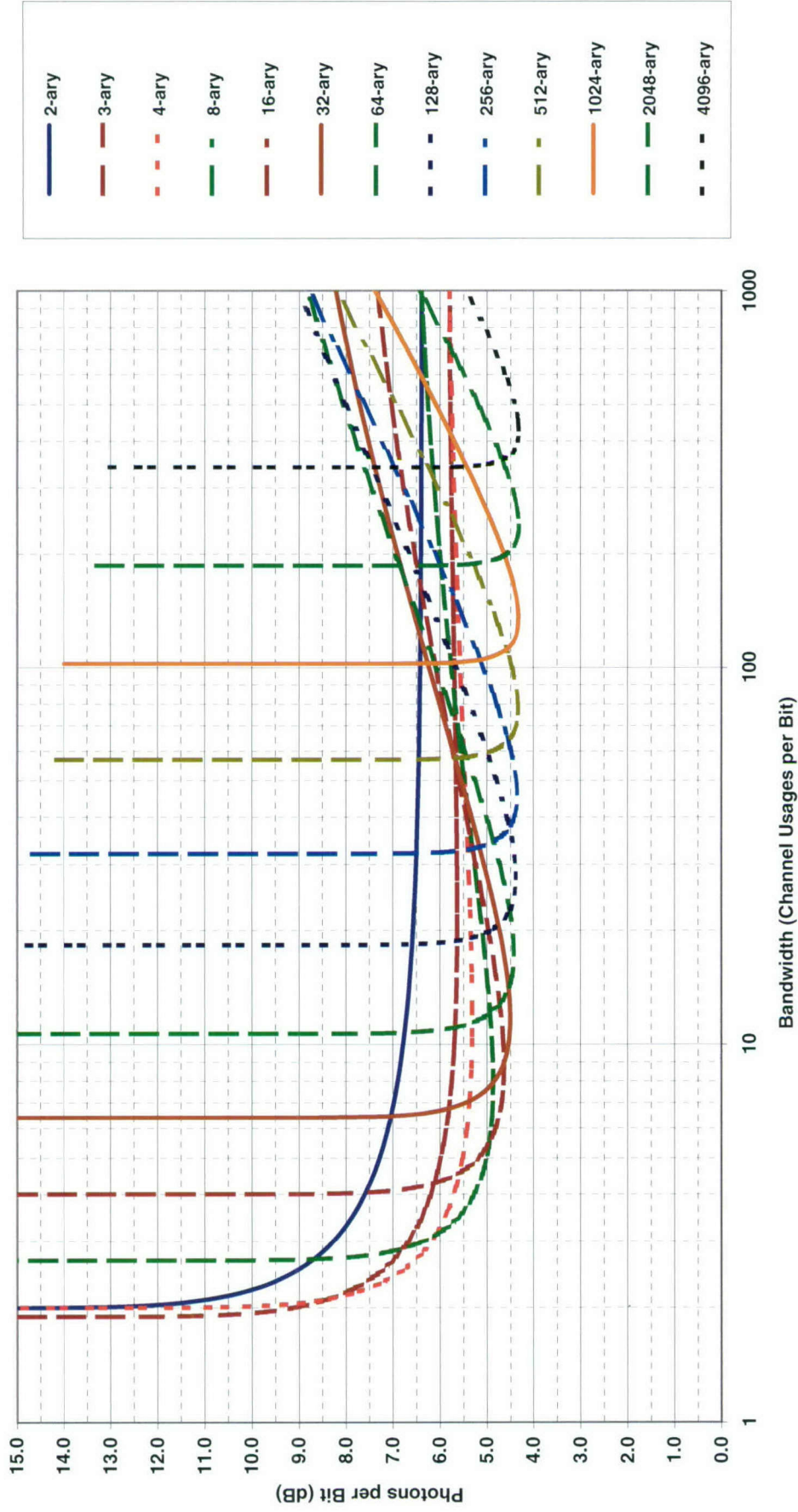


Chart 64. Efficiency at classical cutoff: orthogonal heterodyne or preamplified coherent hard decision.

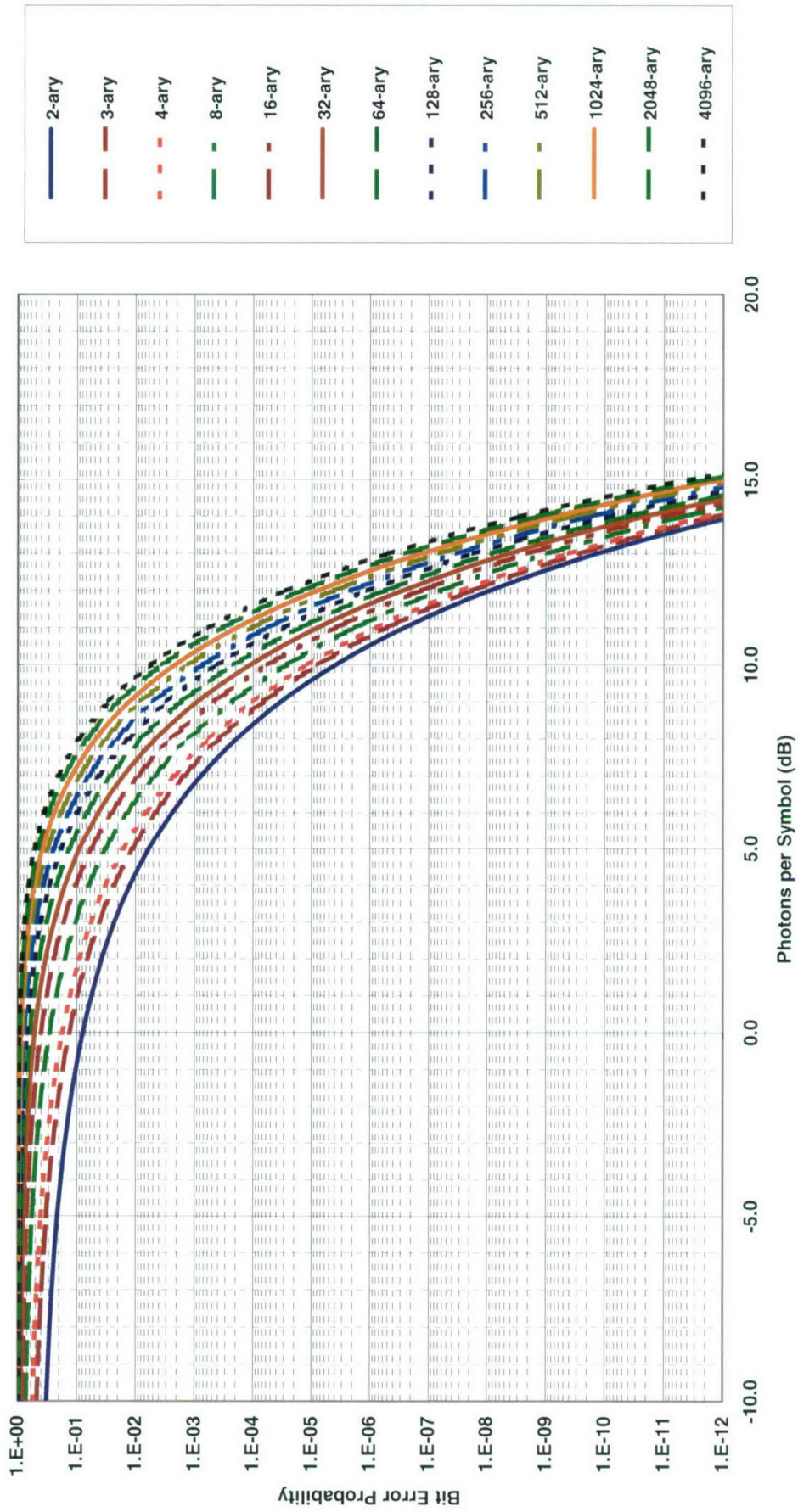


Chart 65. Symbol error probability: orthogonal homodyne coherent.

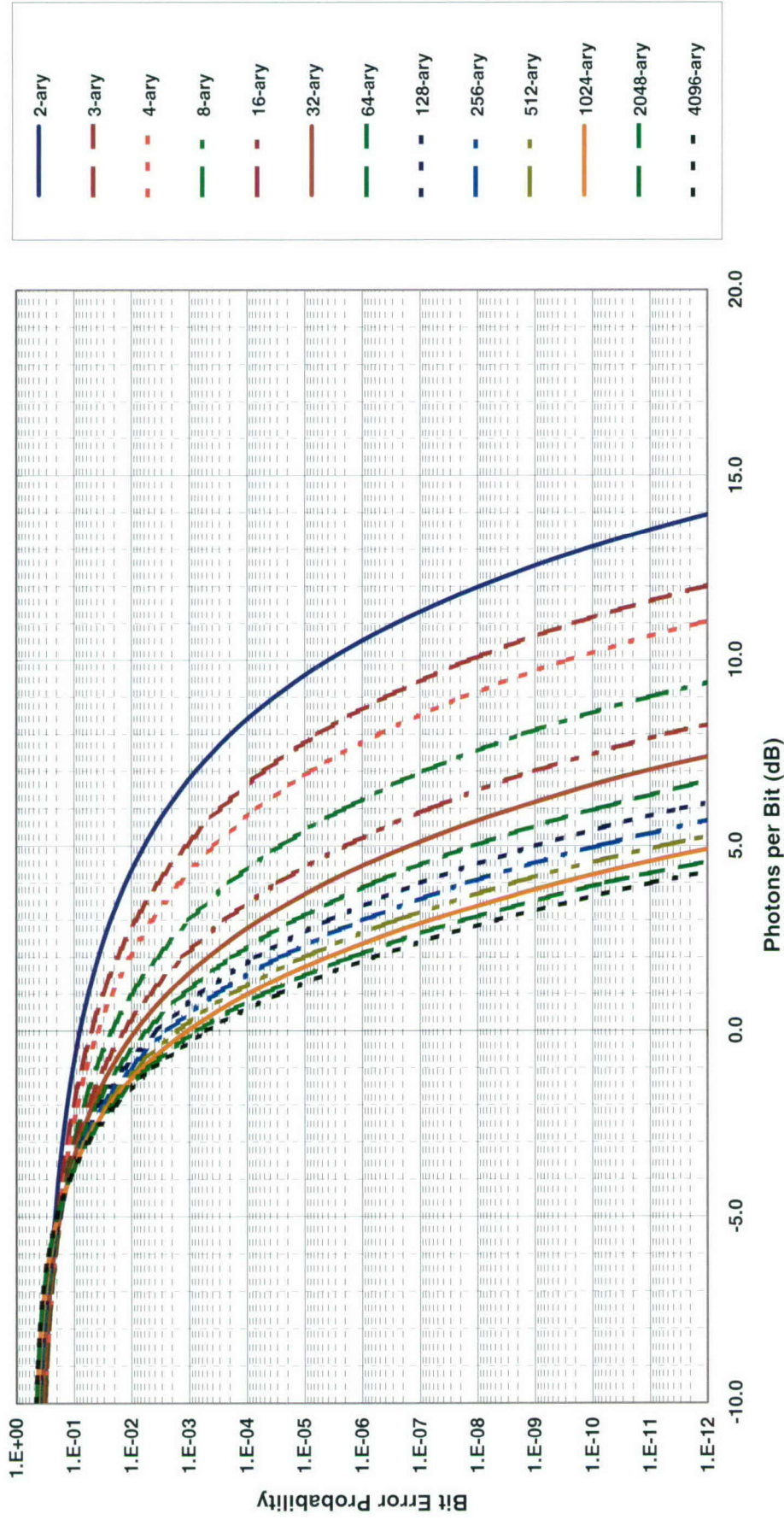


Chart 66. Bit-error probability: orthogonal homodyne coherent.

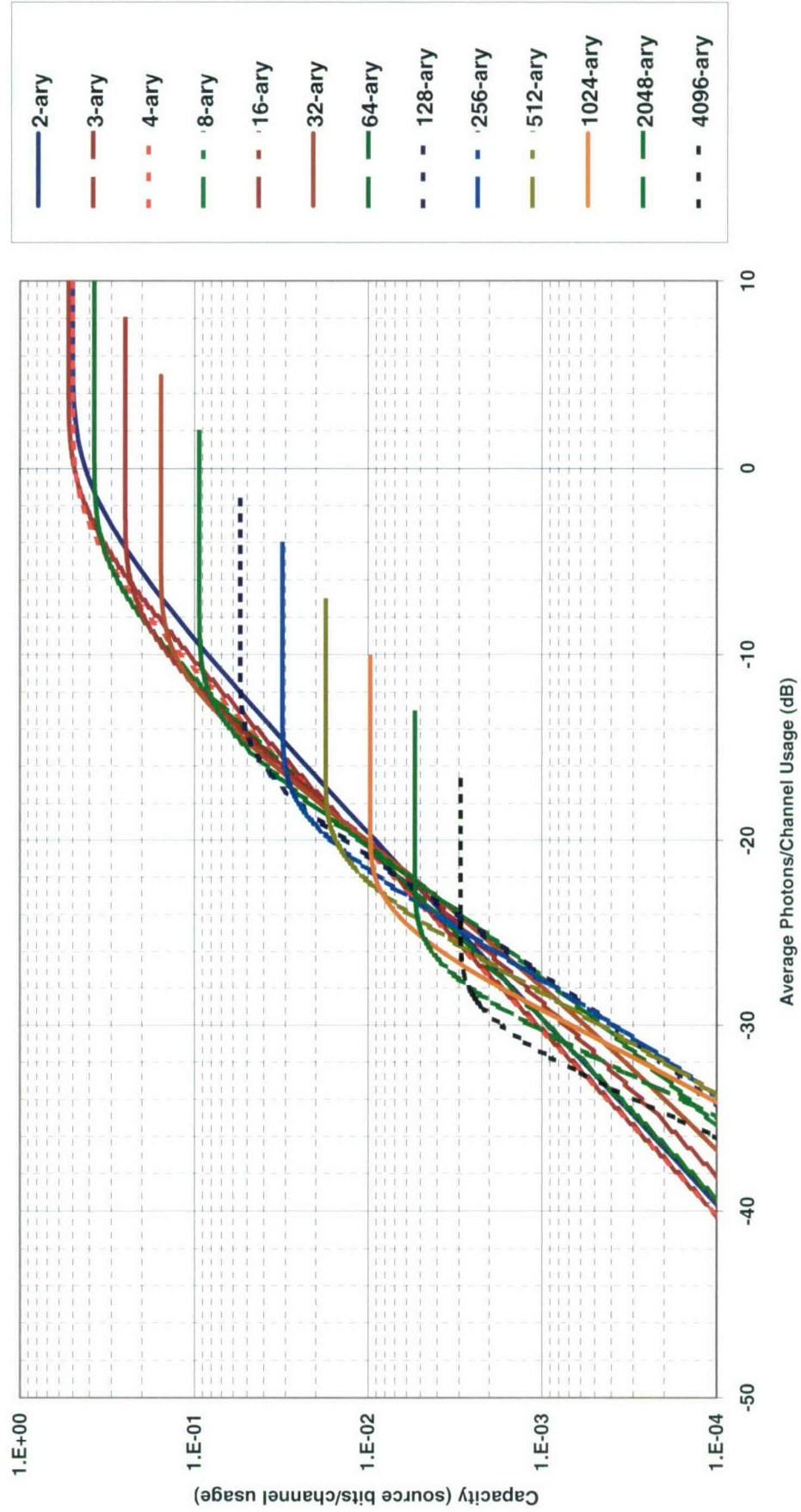


Chart 67. Classical capacity: orthogonal homodyne coherent hard decision.

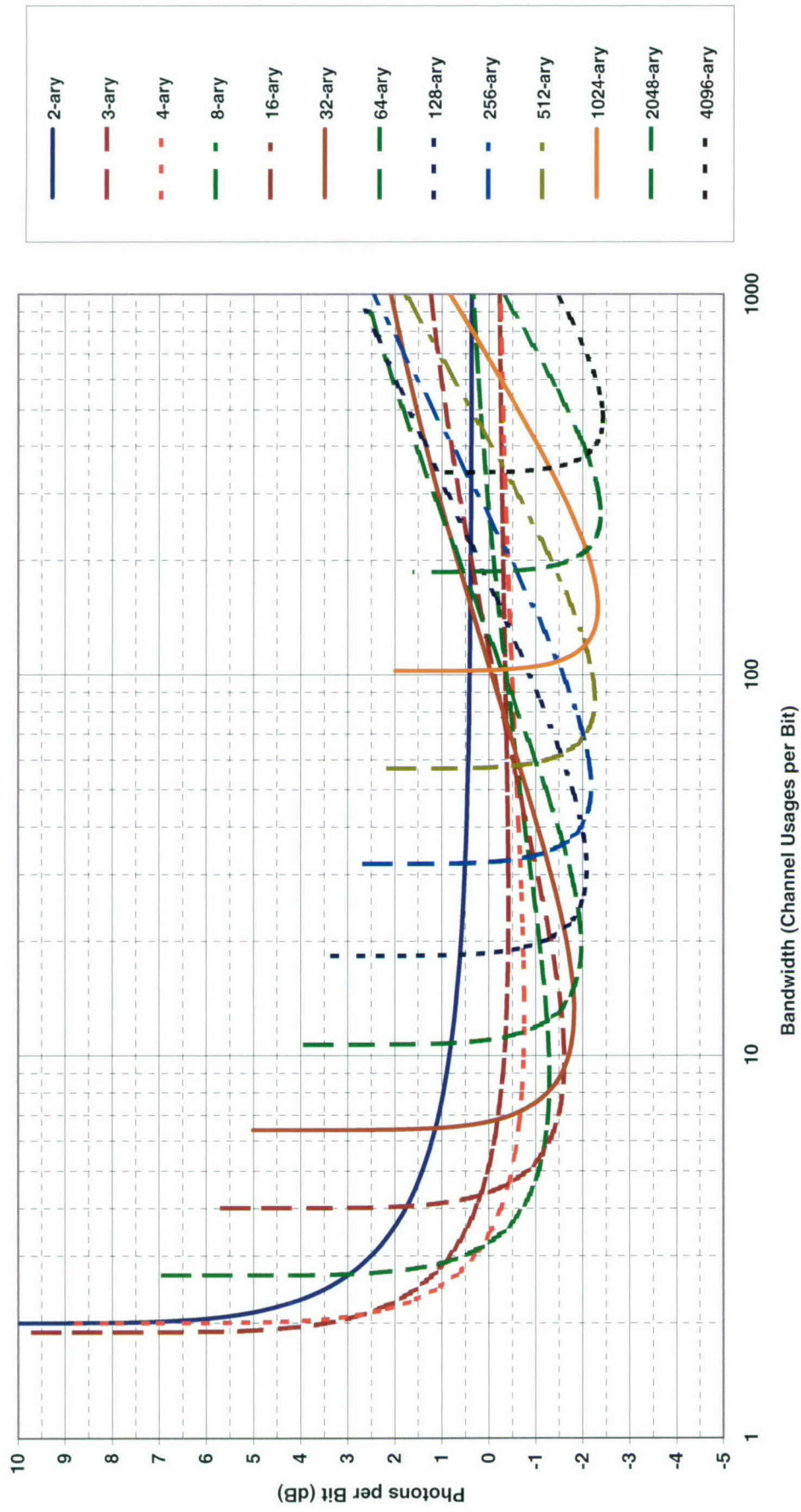


Chart 68. Efficiency at classical capacity: orthogonal homodyne coherent hard decision.

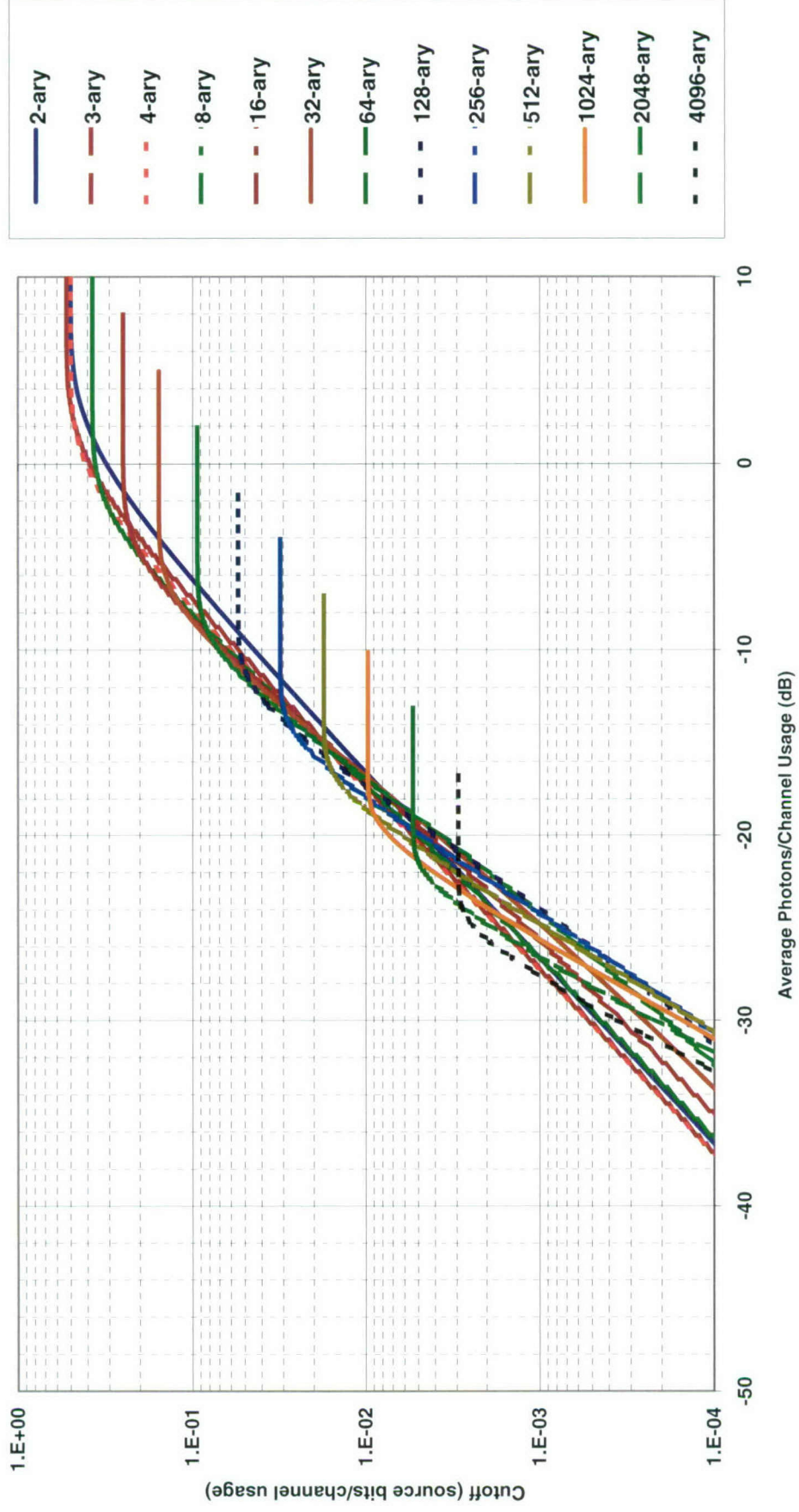


Chart 69. Classical cutoff: orthogonal homodyne coherent hard decision.

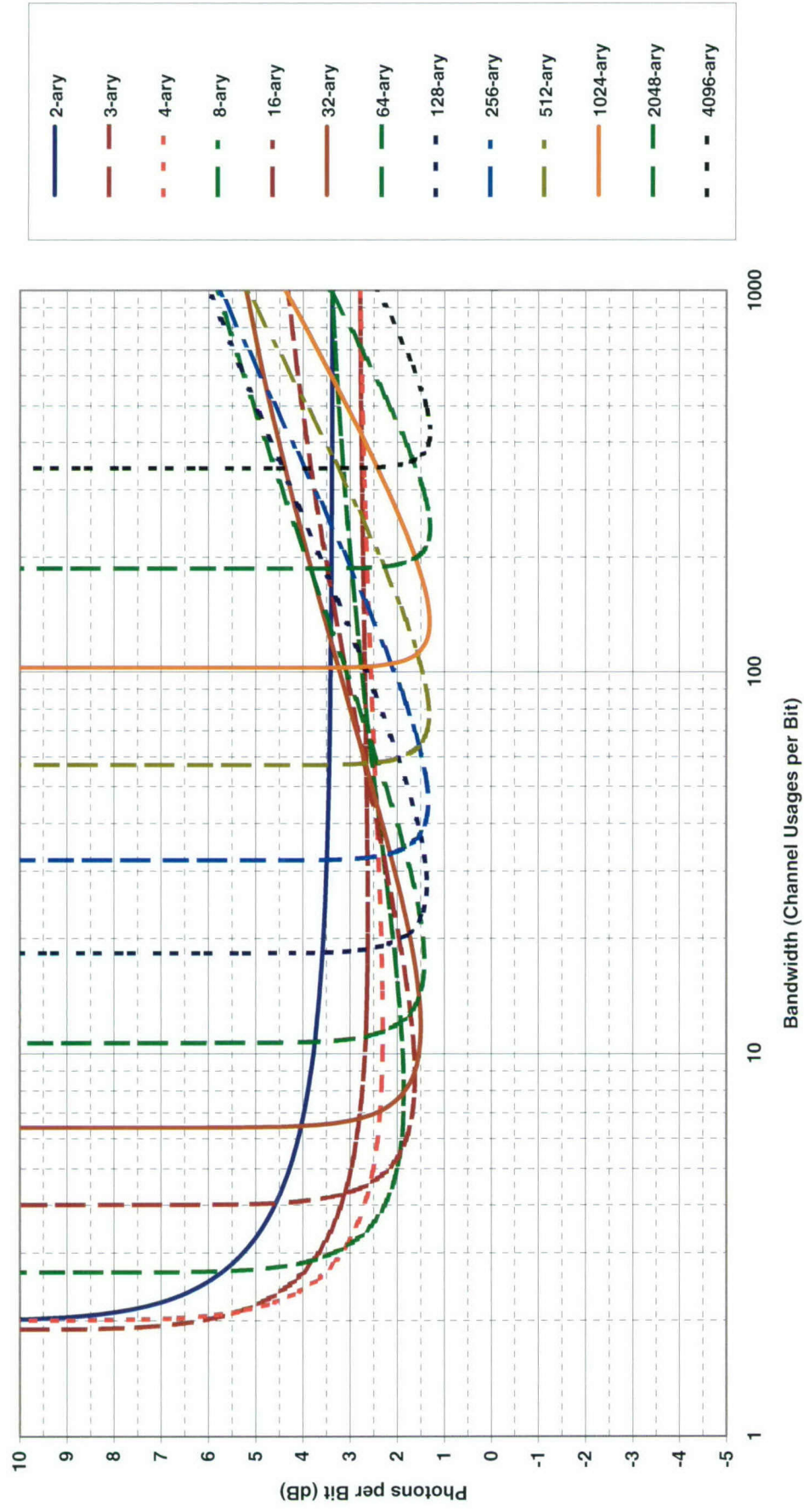


Chart 70. Efficiency at classical cutoff: orthogonal homodyne coherent hard decision.

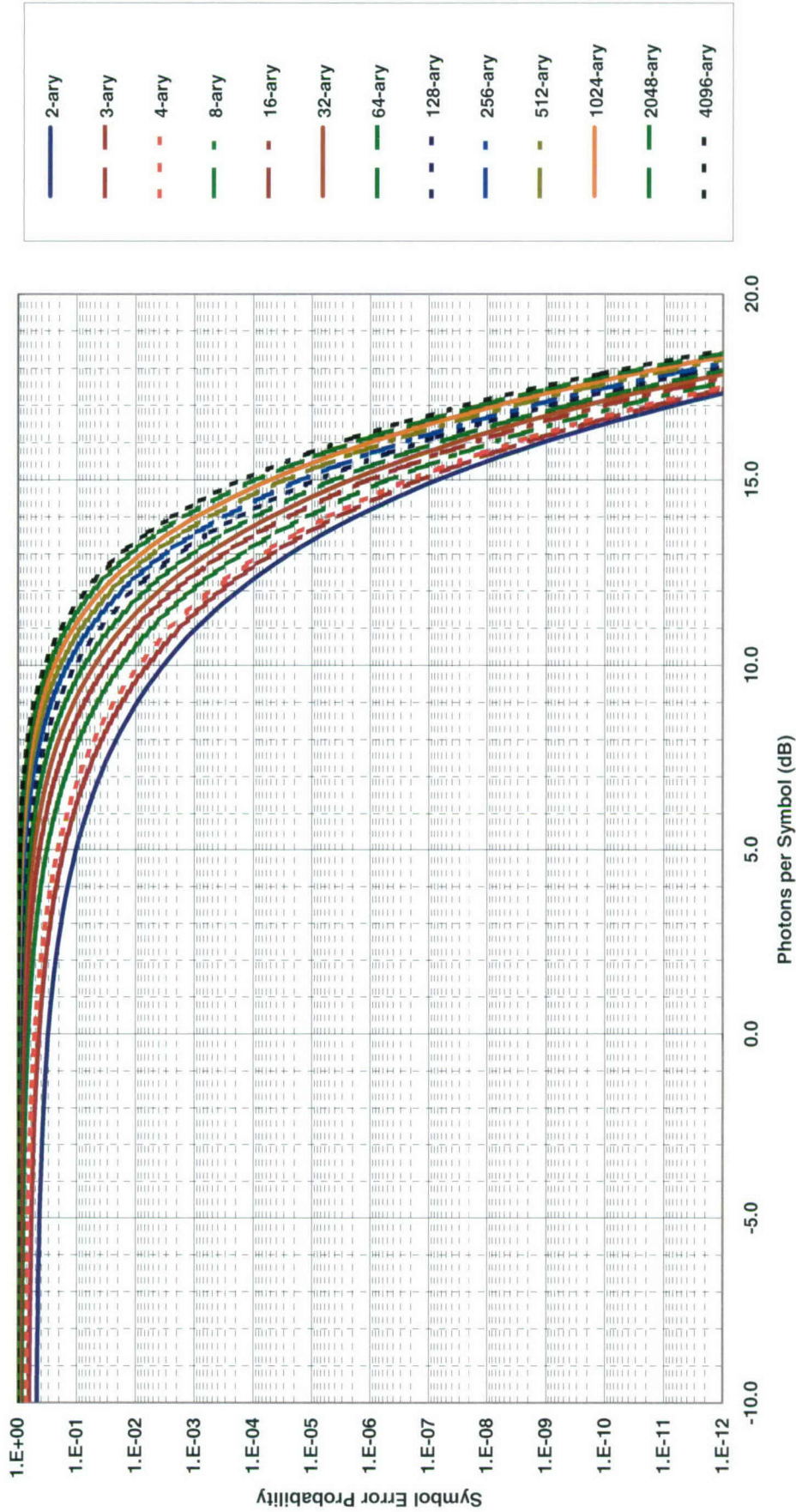


Chart 71. Symbol error probability: orthogonal heterodyne or preamplified noncoherent.

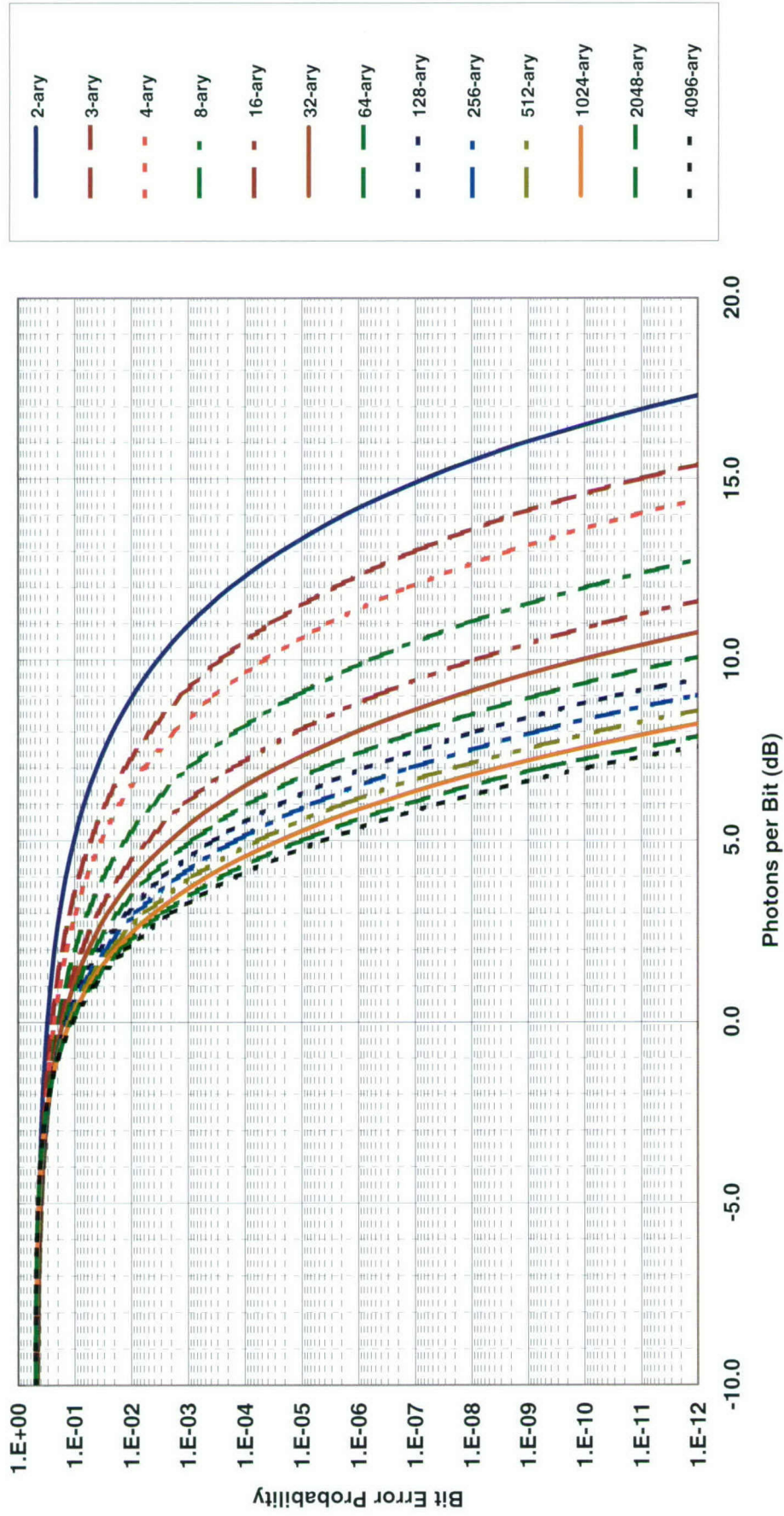


Chart 72. Bit-error probability: orthogonal heterodyne or preamplified noncoherent.

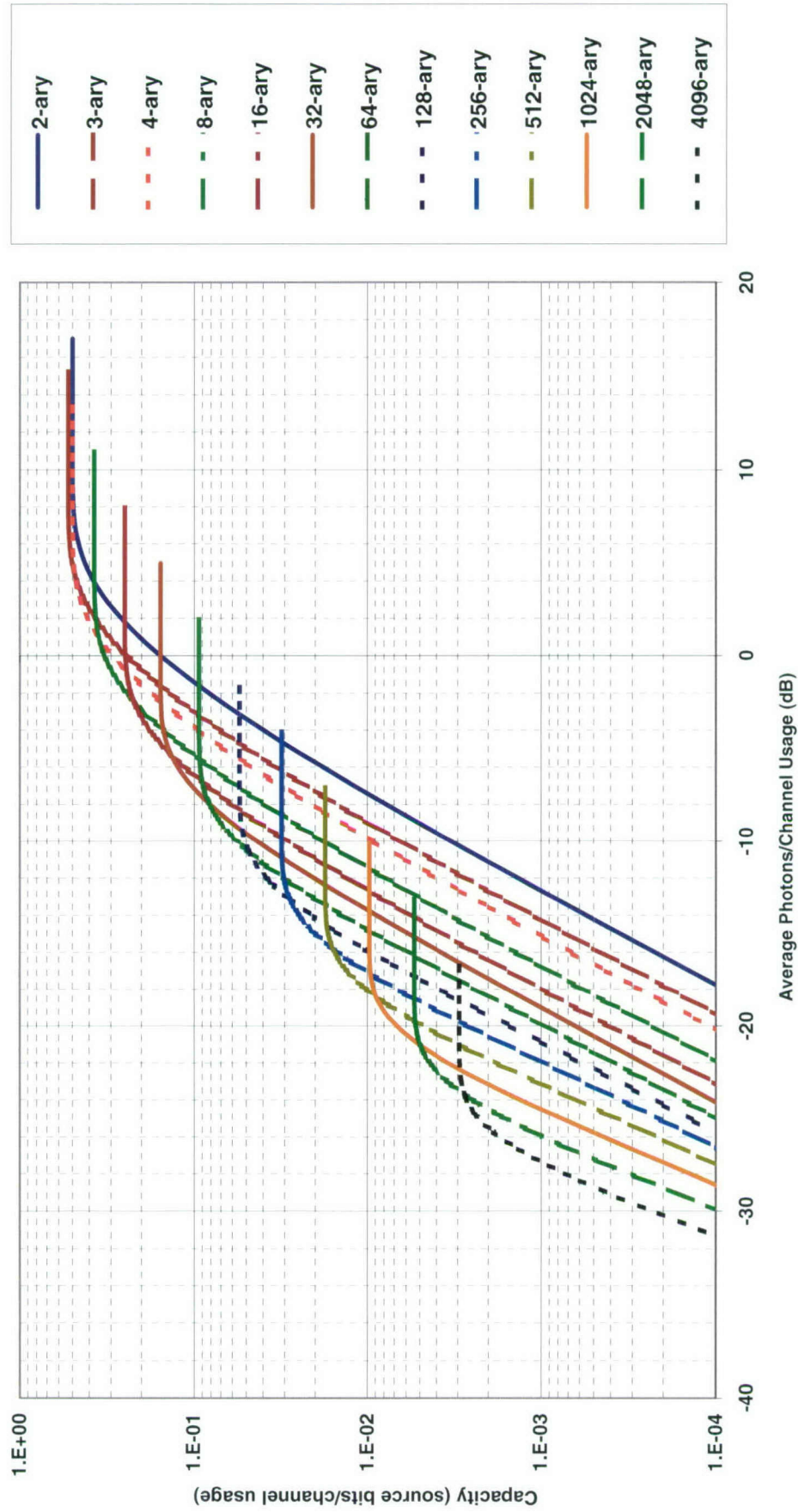


Chart 73. Classical capacity: orthogonal heterodyne or preamplified noncoherent hard decision.

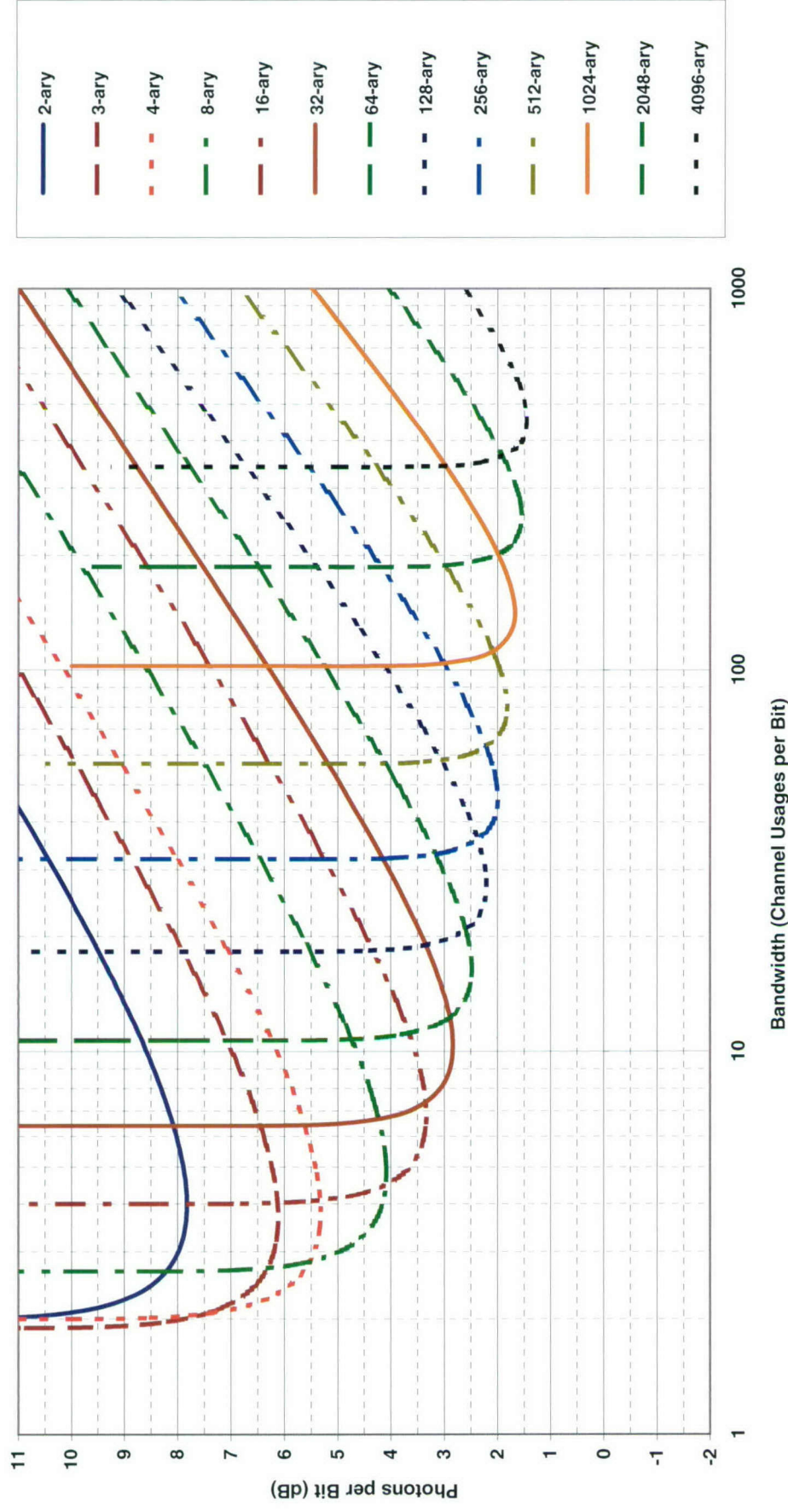


Chart 74. Efficiency at classical capacity: orthogonal heterodyne or preamplified noncoherent hard decision.

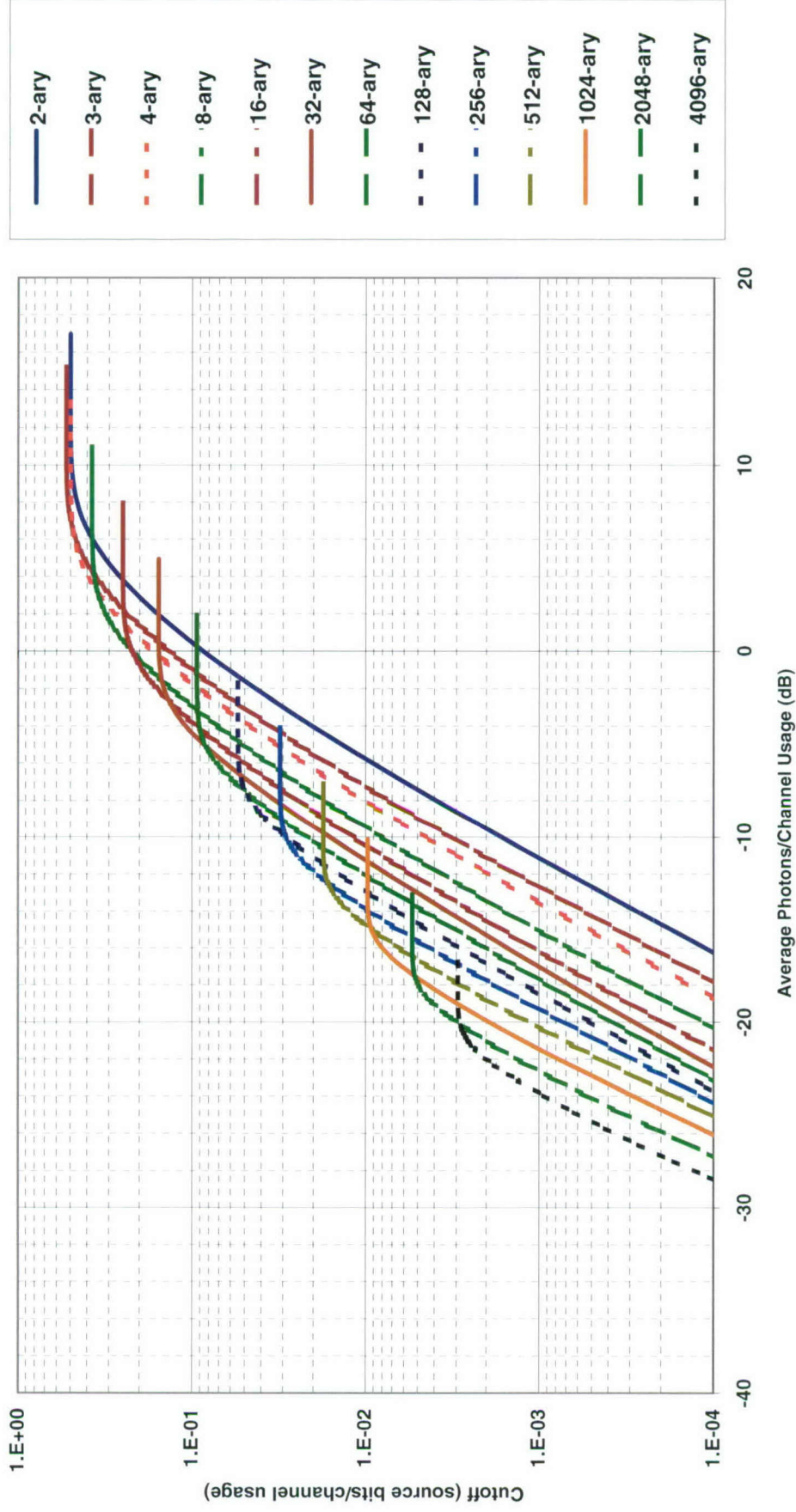


Chart 75. Classical cutoff: orthogonal heterodyne or preamplified noncoherent hard decision.

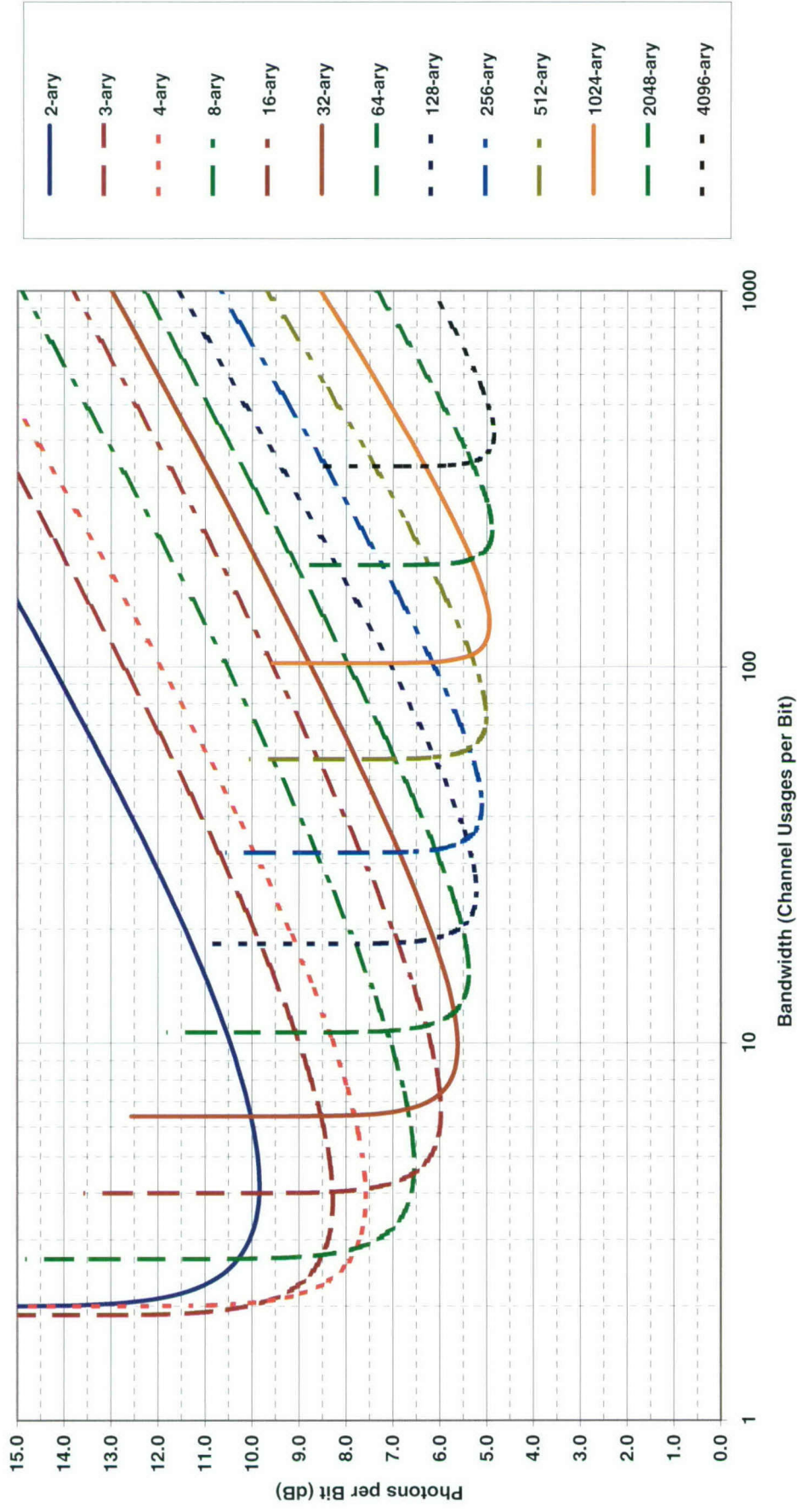


Chart 76. Efficiency at classical cutoff: orthogonal heterodyne or preamplified noncoherent hard decision.

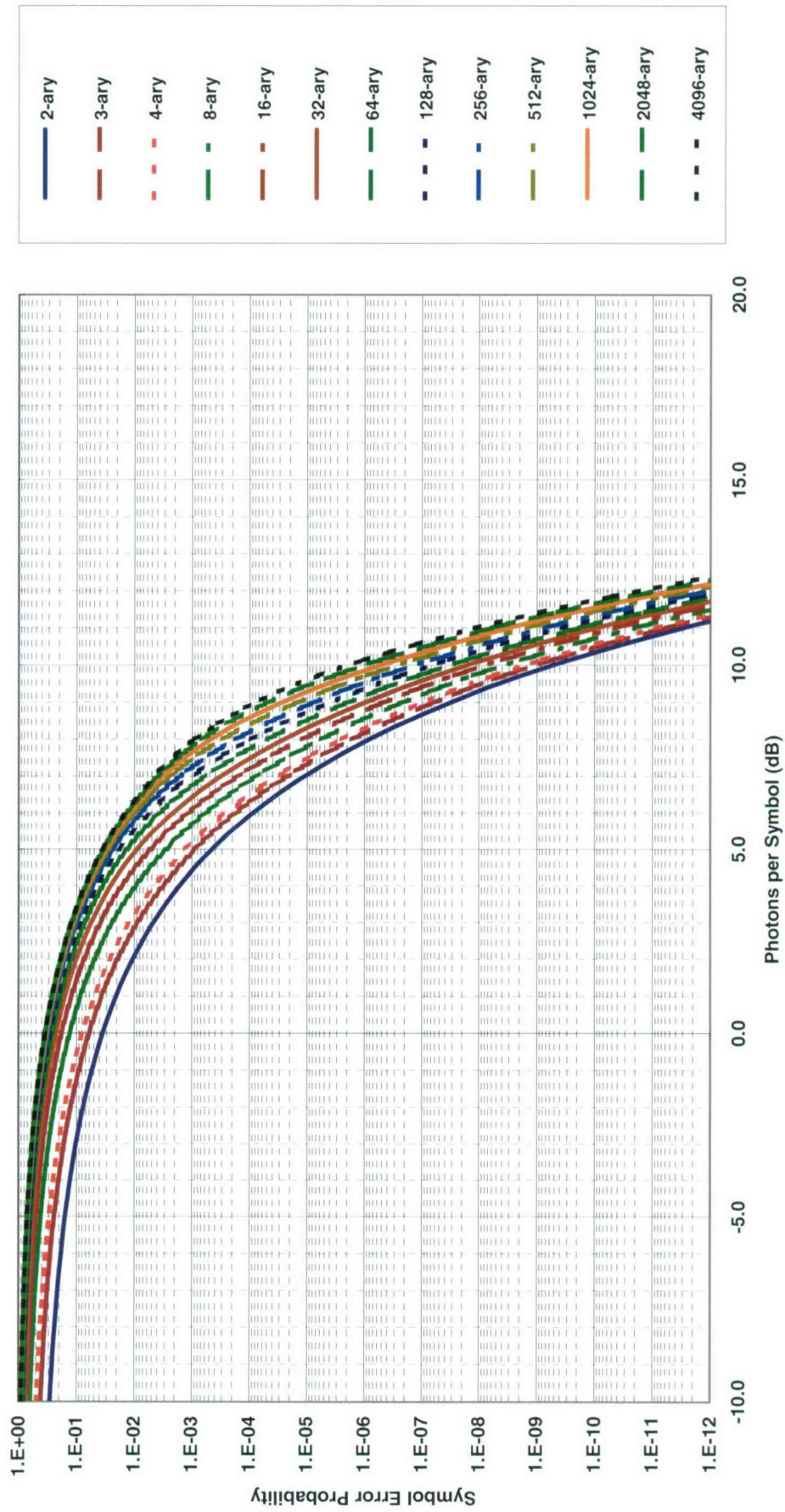


Chart 77. Symbol error probability: orthogonal quantum hard decision (semiclassical).

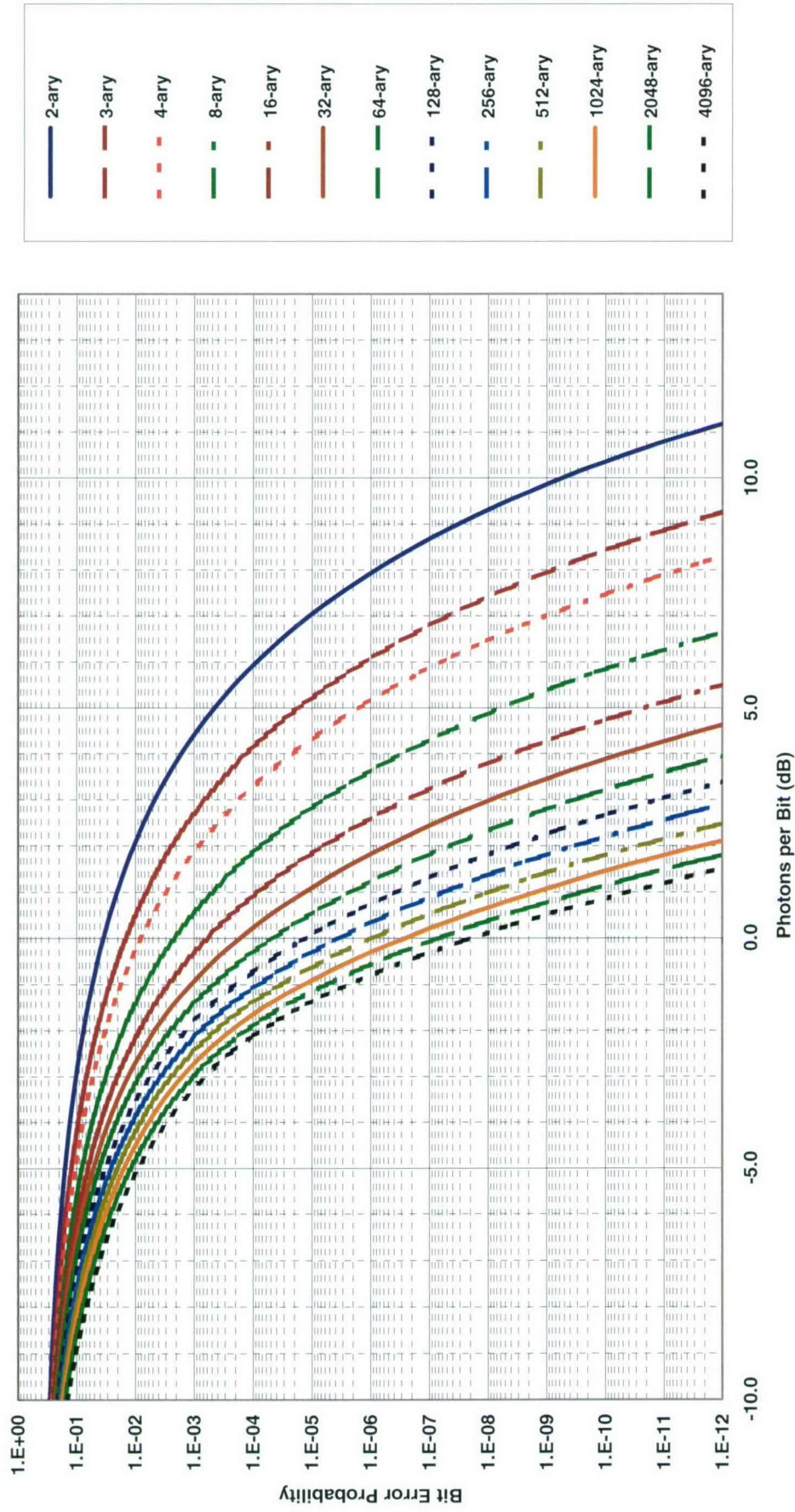


Chart 78. Bit-error probability: orthogonal quantum hard decision (semiclassical).

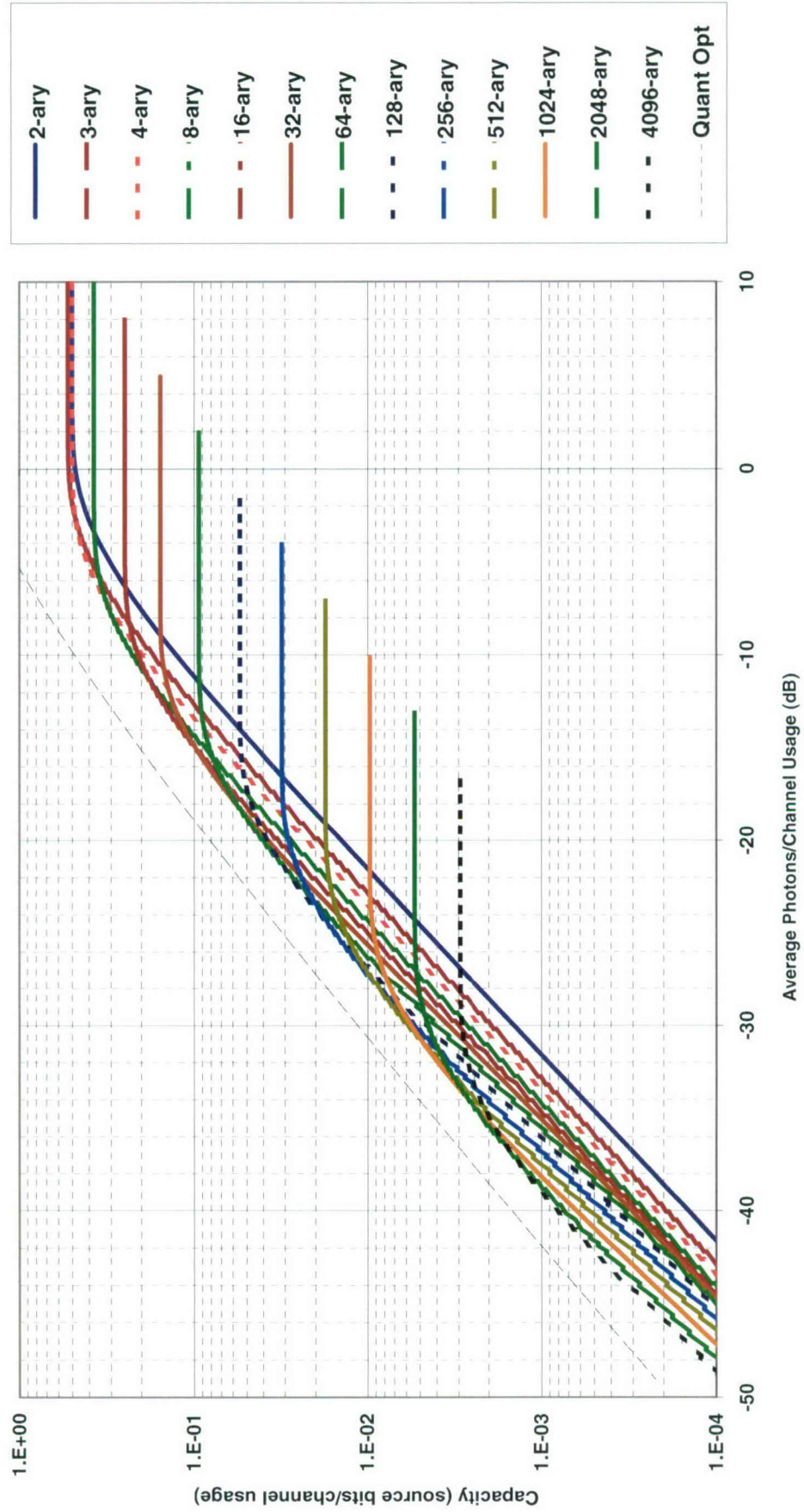


Chart 79. Classical capacity: orthogonal quantum hard decision (semiclassical).

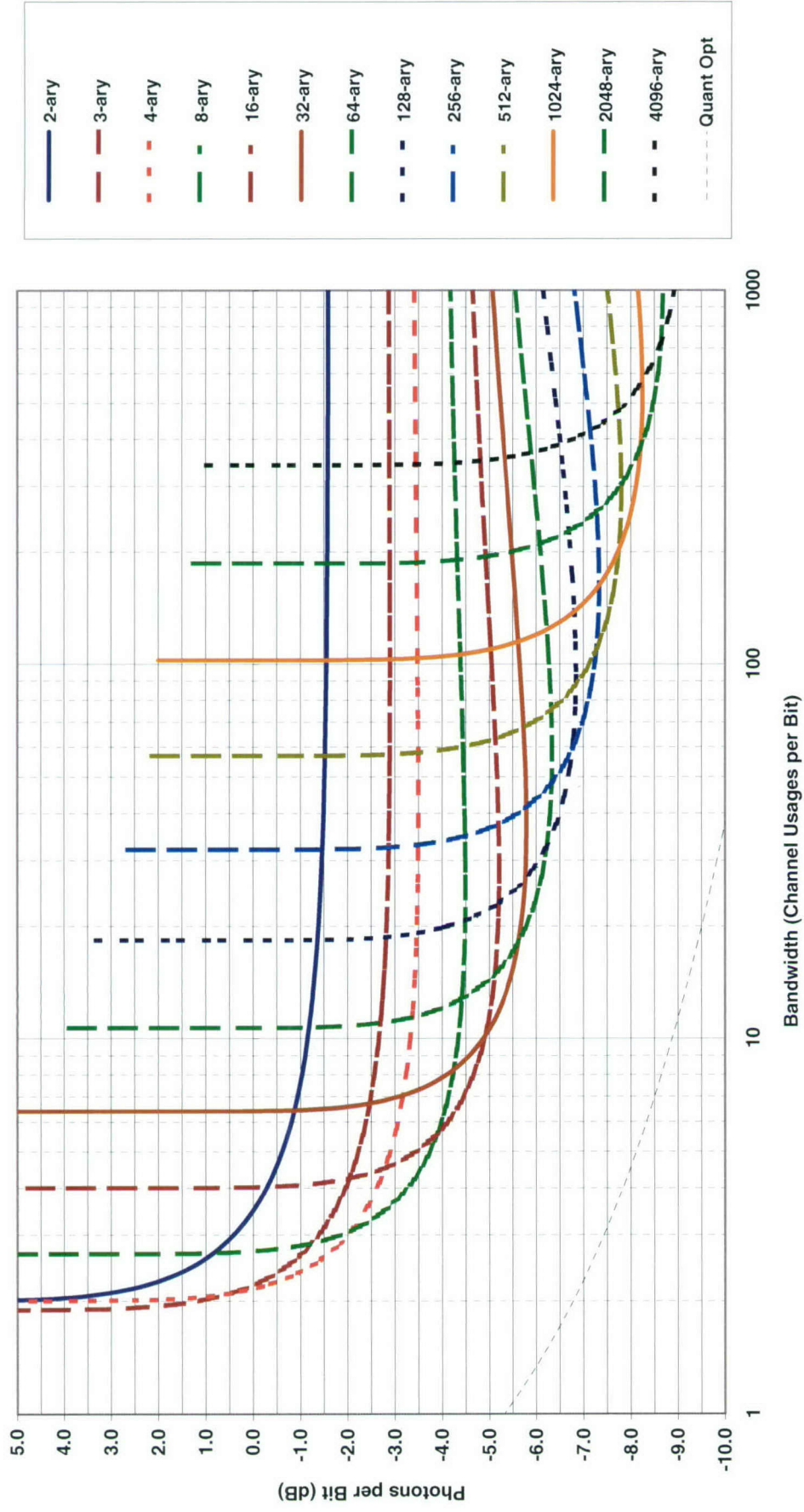


Chart 80. Efficiency at classical capacity: orthogonal quantum hard decision (semiclassical).

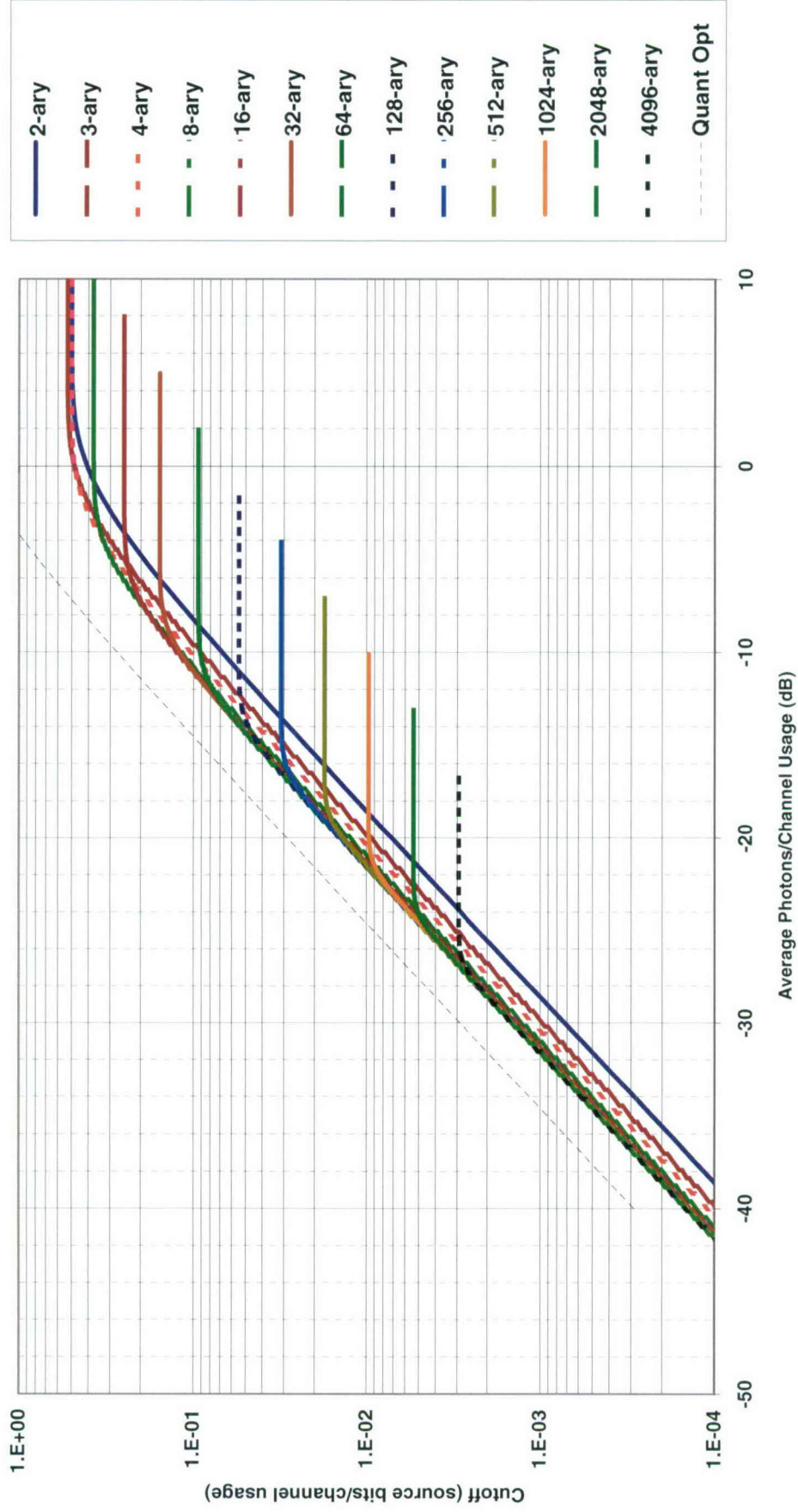


Chart 81. Classical cutoff: orthogonal quantum hard decision (semiclassical).

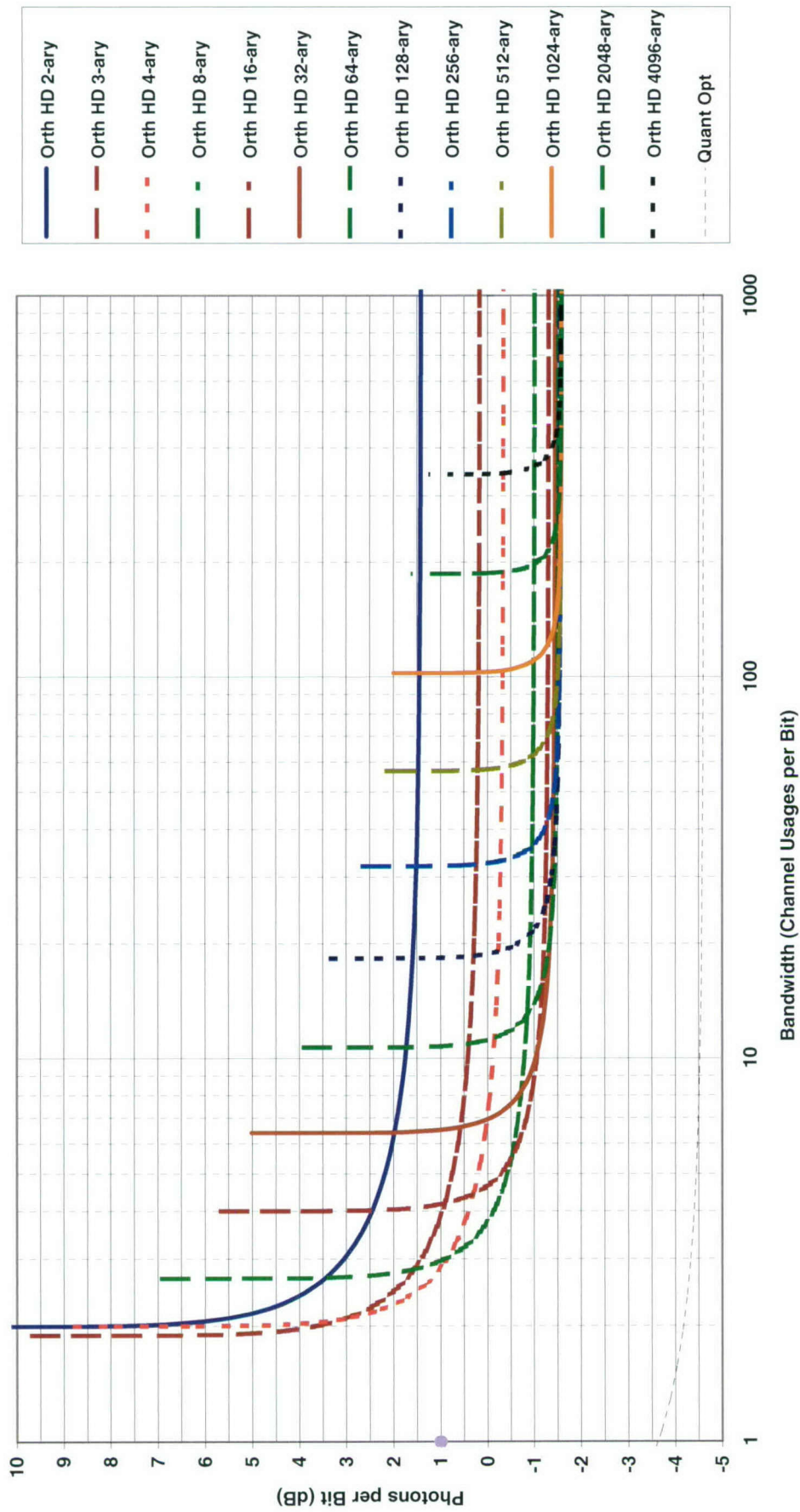


Chart 82. Efficiency at classical cutoff: orthogonal quantum hard decision (semiclassical).

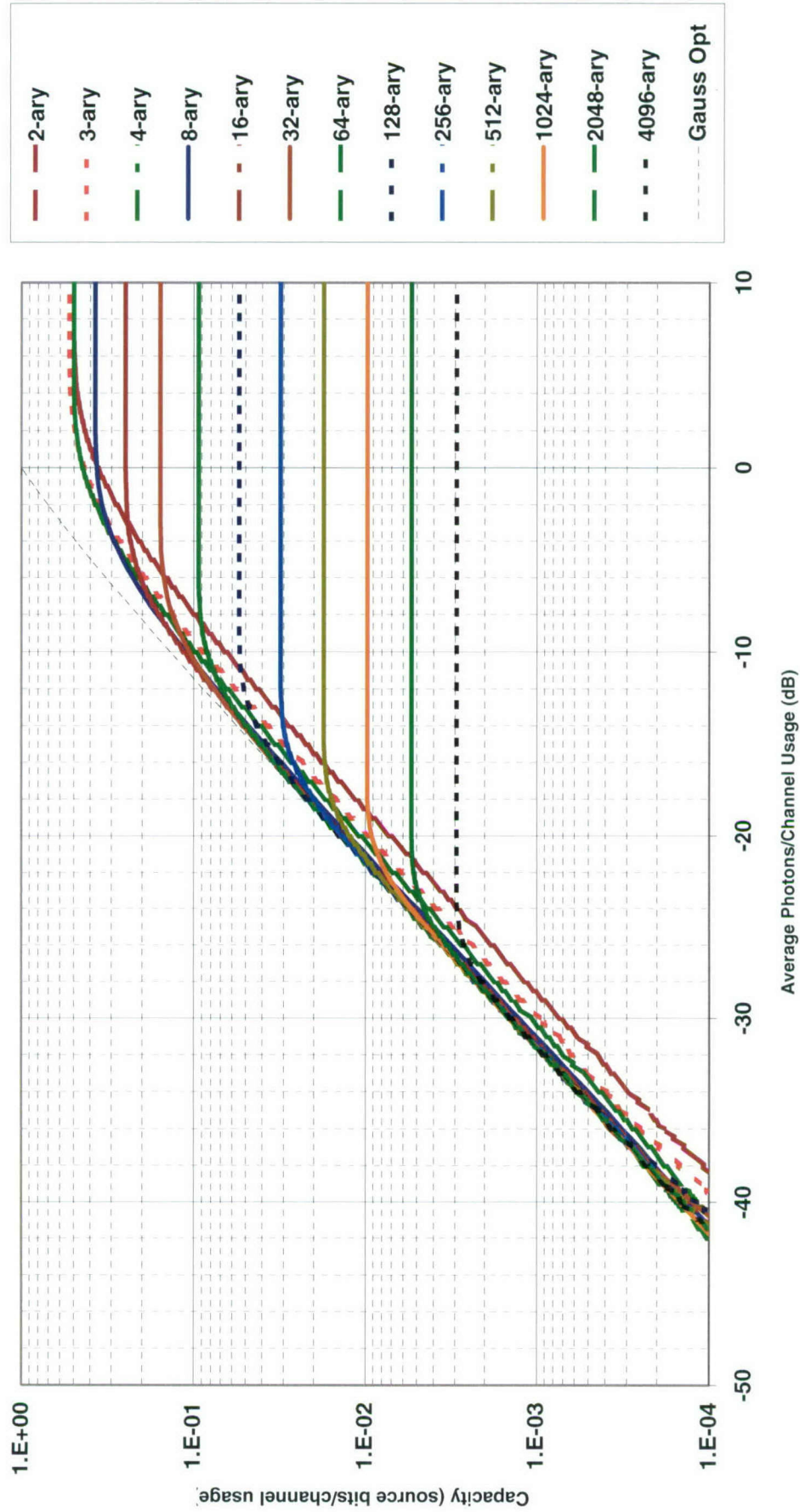


Chart 83. Classical capacity: orthogonal heterodyne or preamplified coherent soft decision.

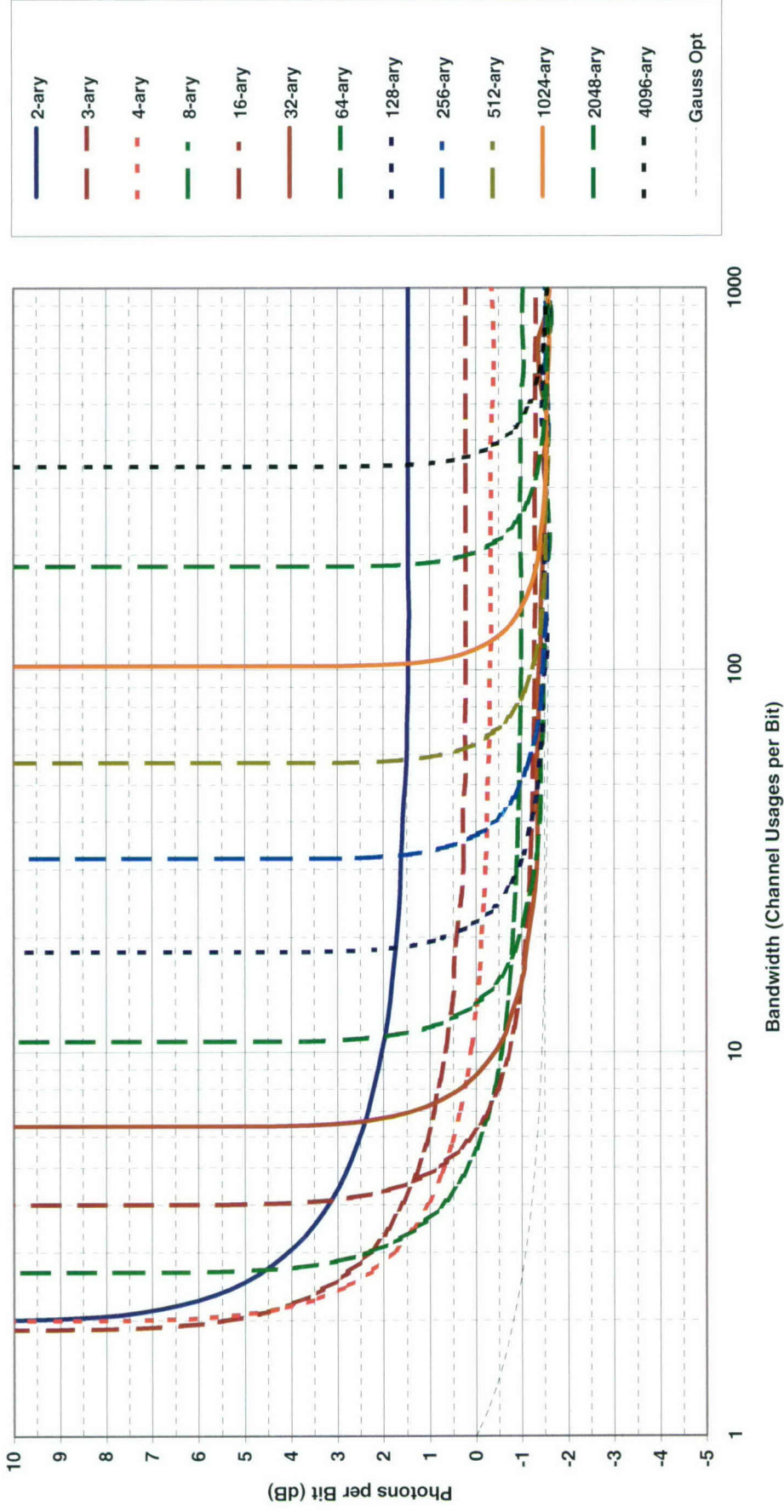


Chart 84. Efficiency at classical capacity: orthogonal heterodyne or preamplified coherent soft decision.

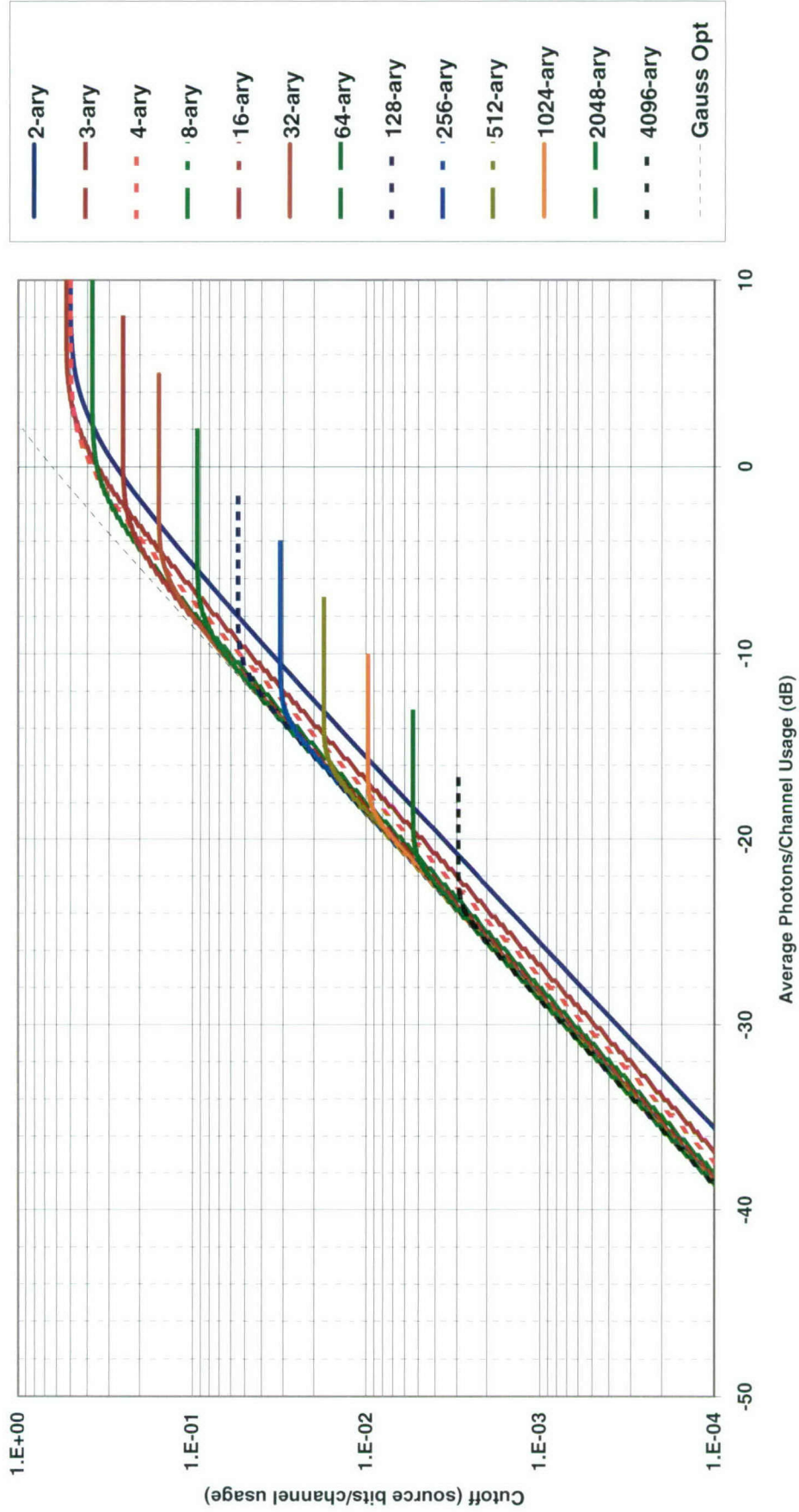


Chart 85. Classical cutoff: orthogonal heterodyne or preamplified coherent soft decision.

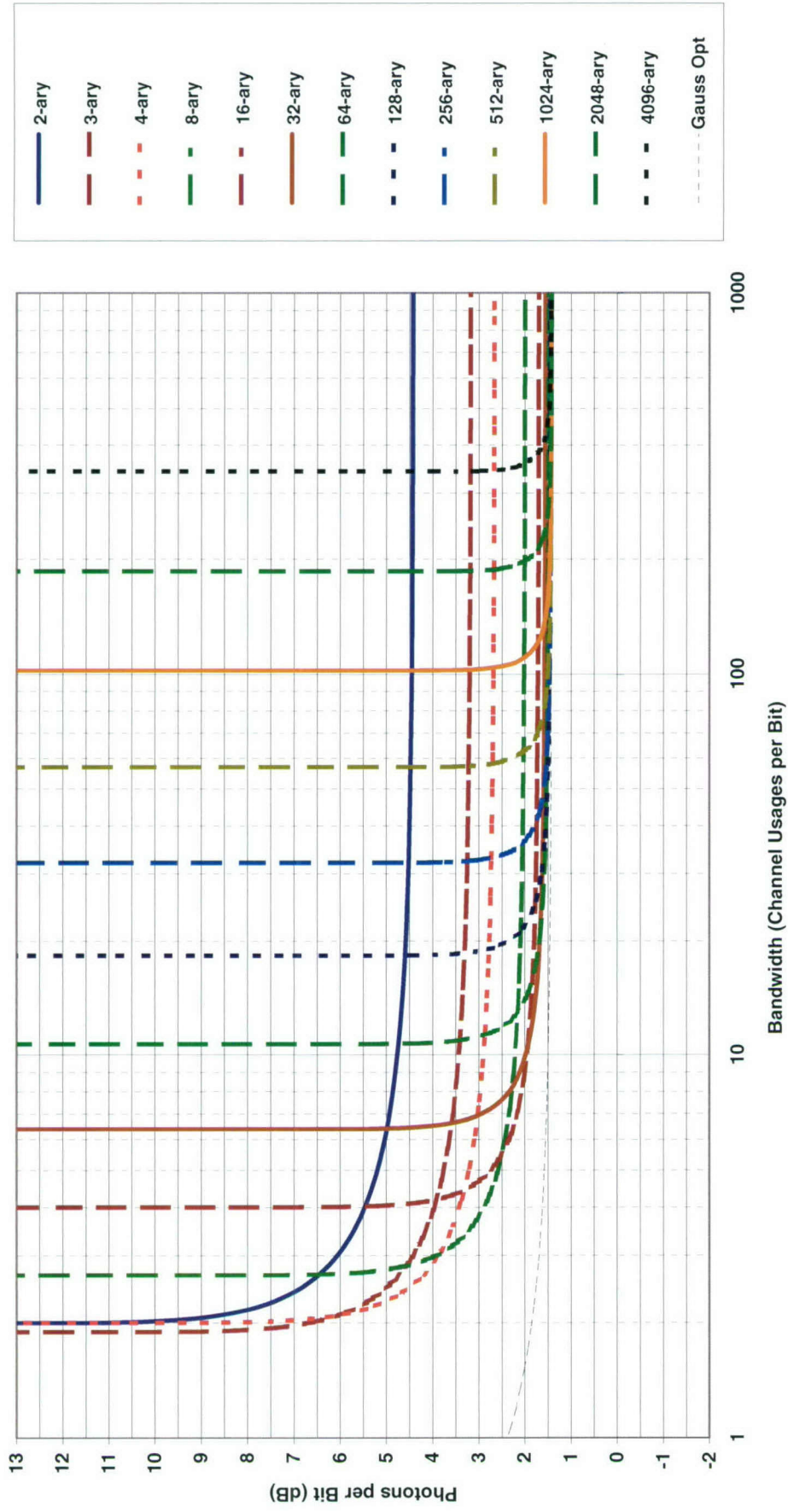


Chart 86. Efficiency at classical cutoff: orthogonal heterodyne or preamplified coherent soft decision.

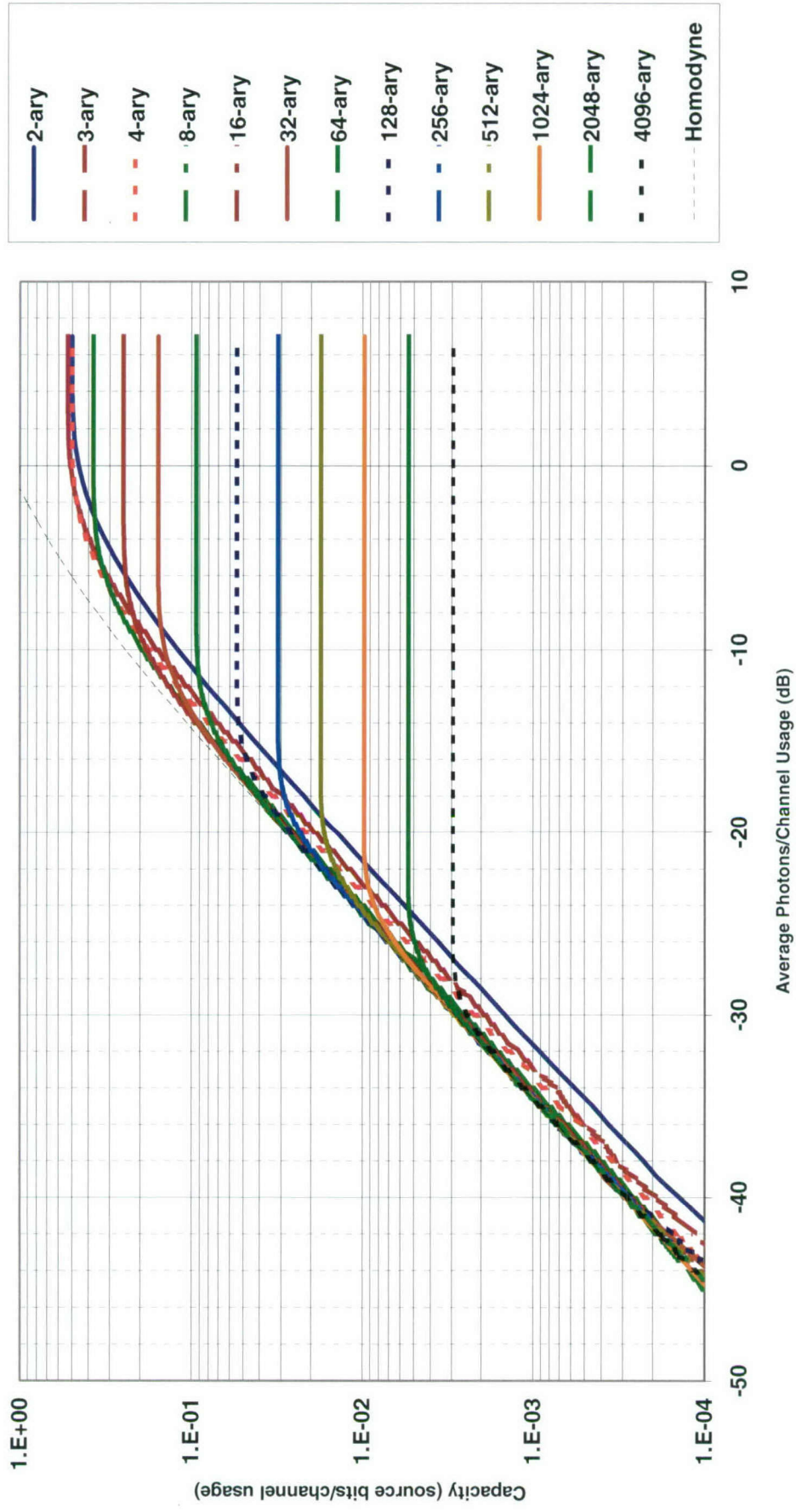


Chart 87. Classical capacity: orthogonal homodyne coherent soft decision.

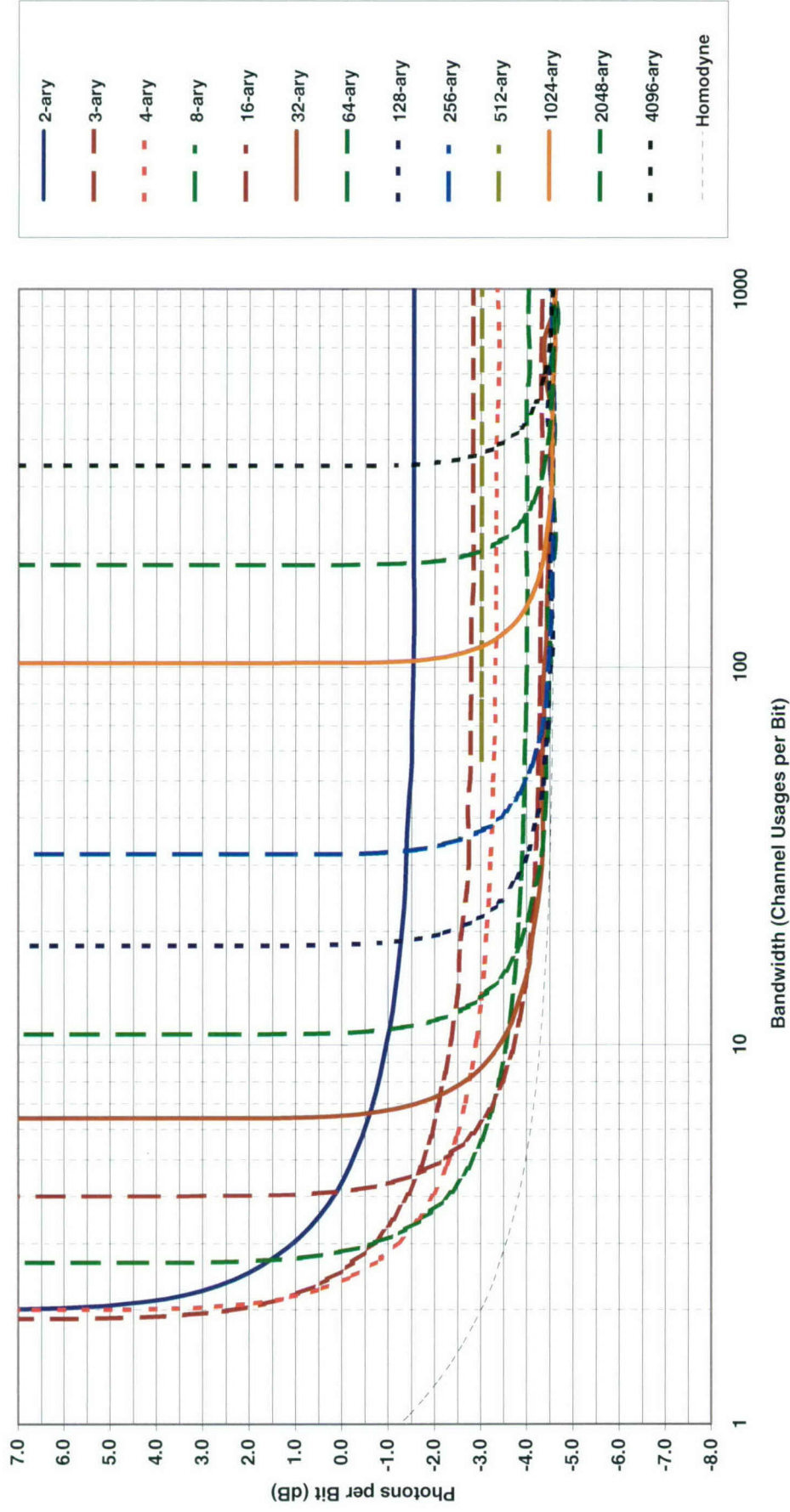


Chart 88. Efficiency at classical capacity: orthogonal homodyne coherent soft decision.

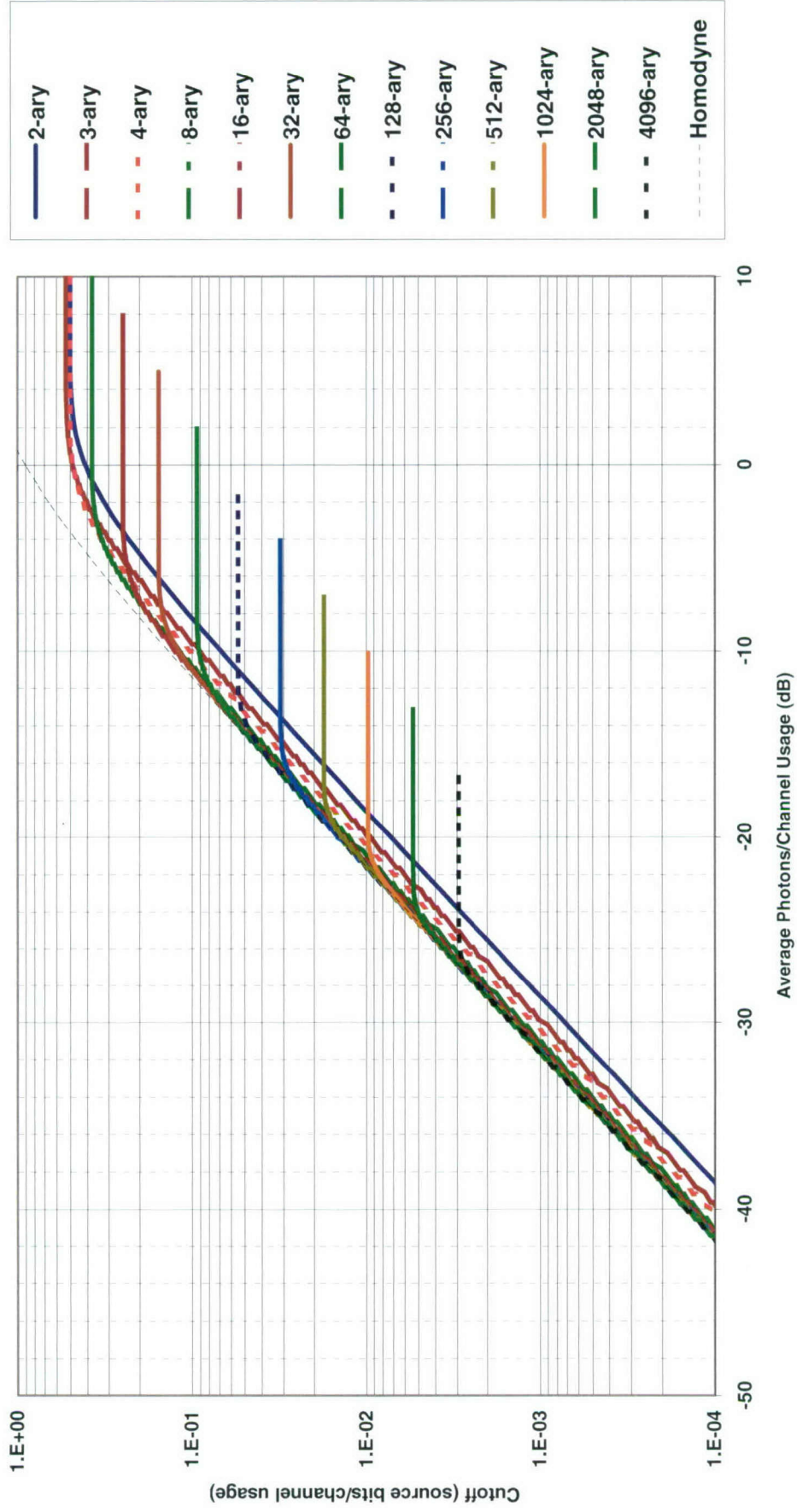


Chart 89. Classical cutoff: orthogonal homodyne coherent soft decision.

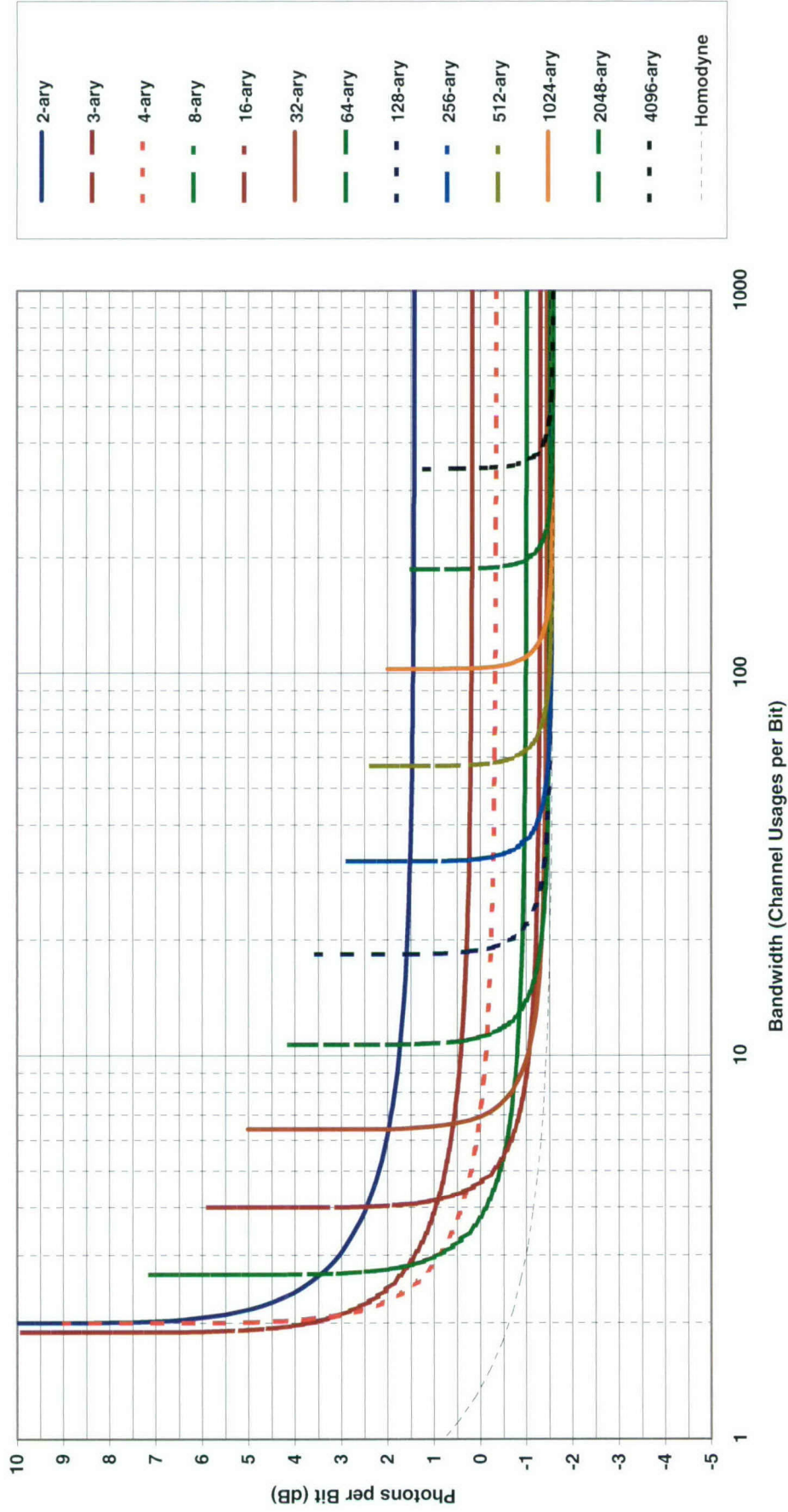


Chart 90. Efficiency at classical cutoff: orthogonal homodyne coherent soft decision.

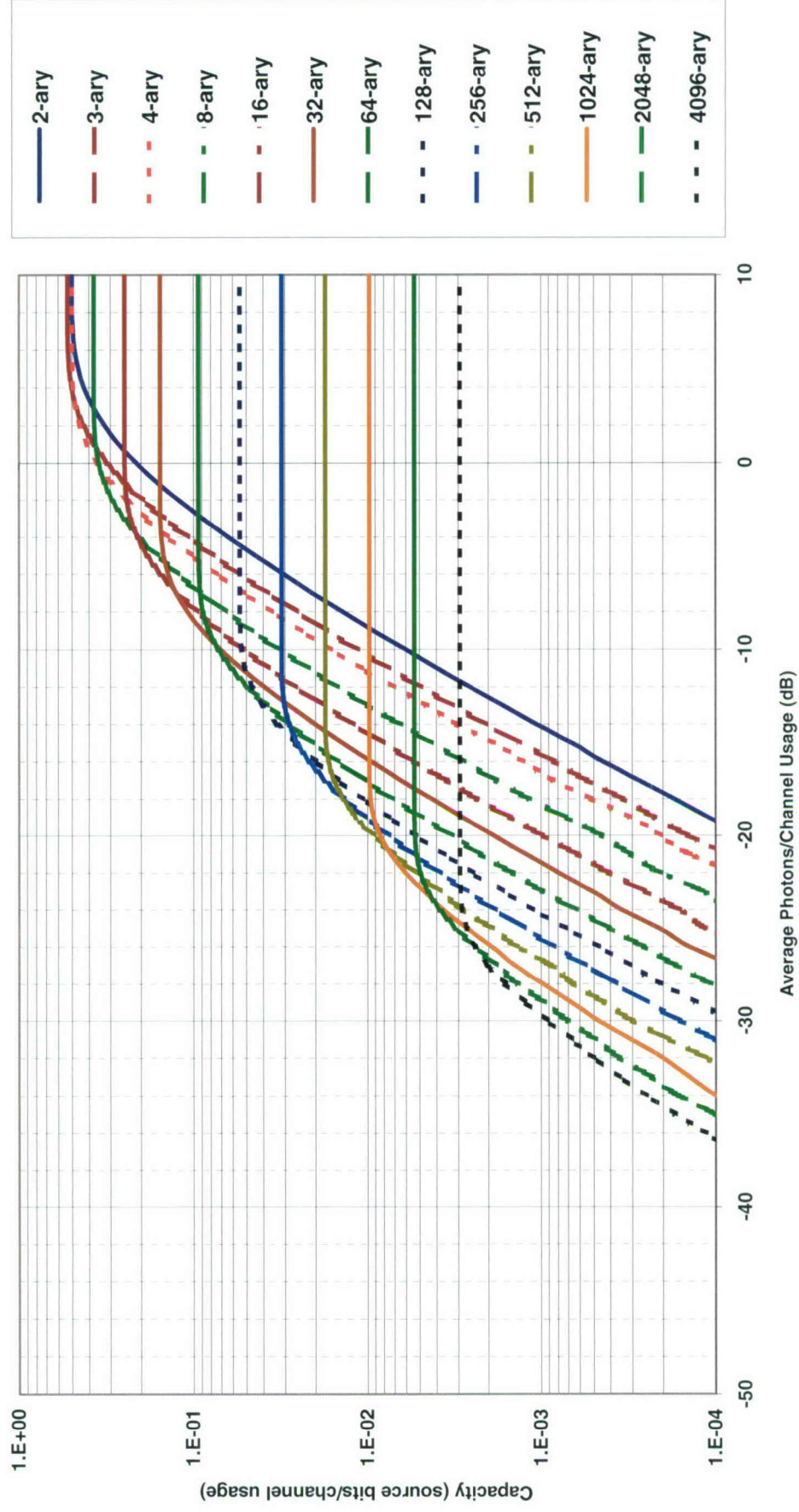


Chart 91. Classical capacity: orthogonal heterodyne or preamplified noncoherent soft decision.

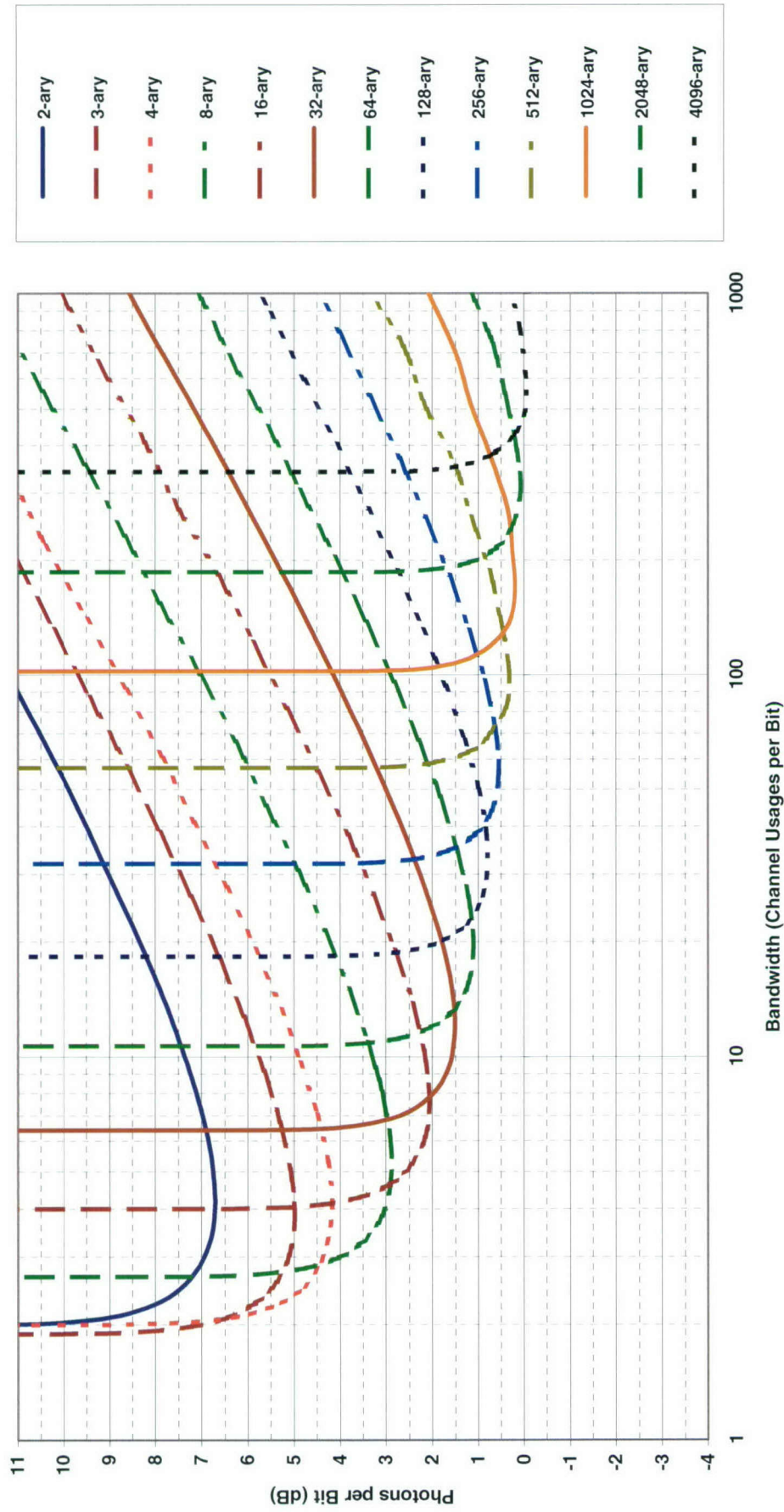


Chart 92. Efficiency at classical capacity: orthogonal heterodyne or preamplified noncoherent soft decision.

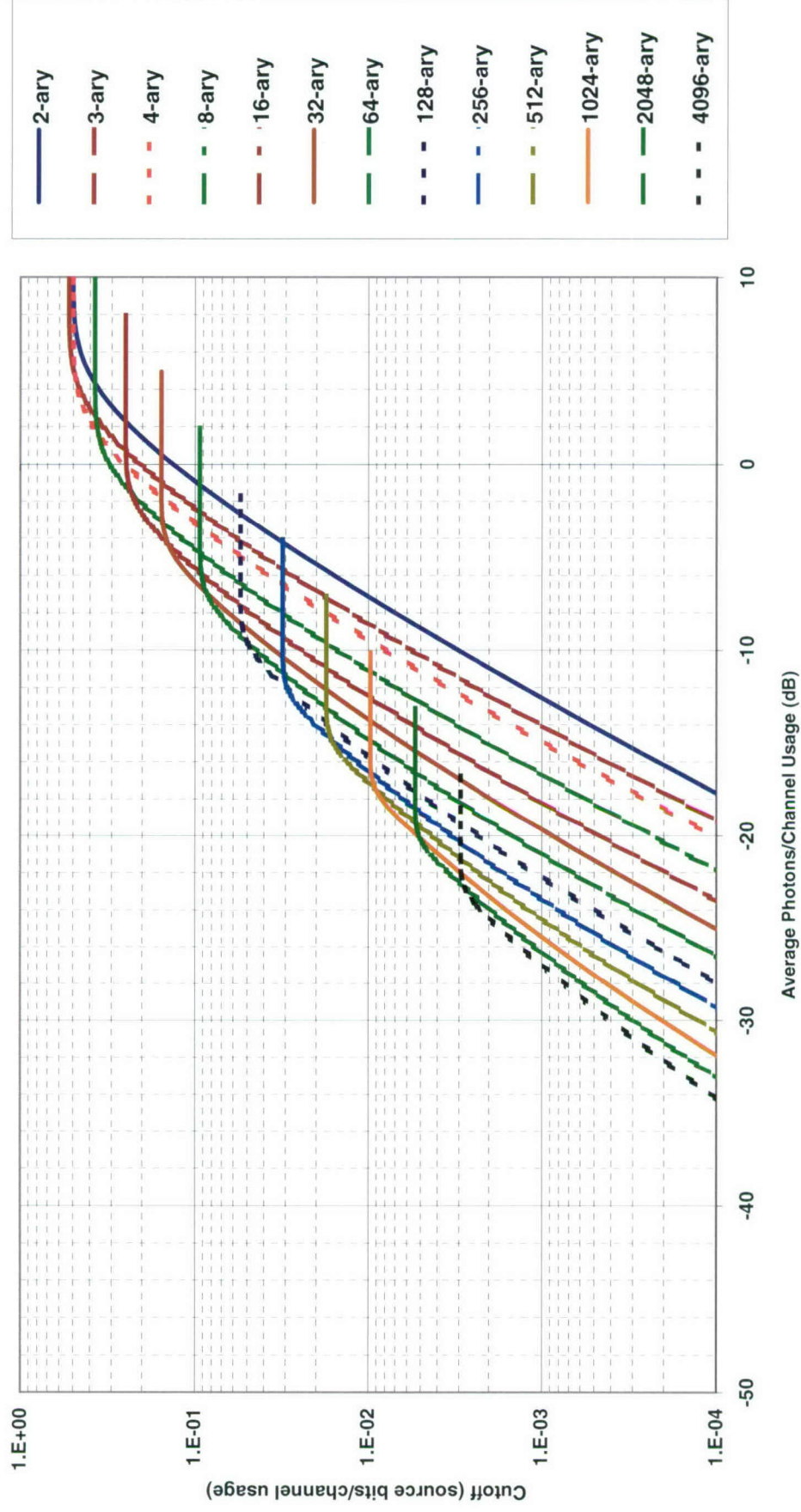


Chart 93. Classical cutoff: orthogonal heterodyne or preamplified noncoherent soft decision.

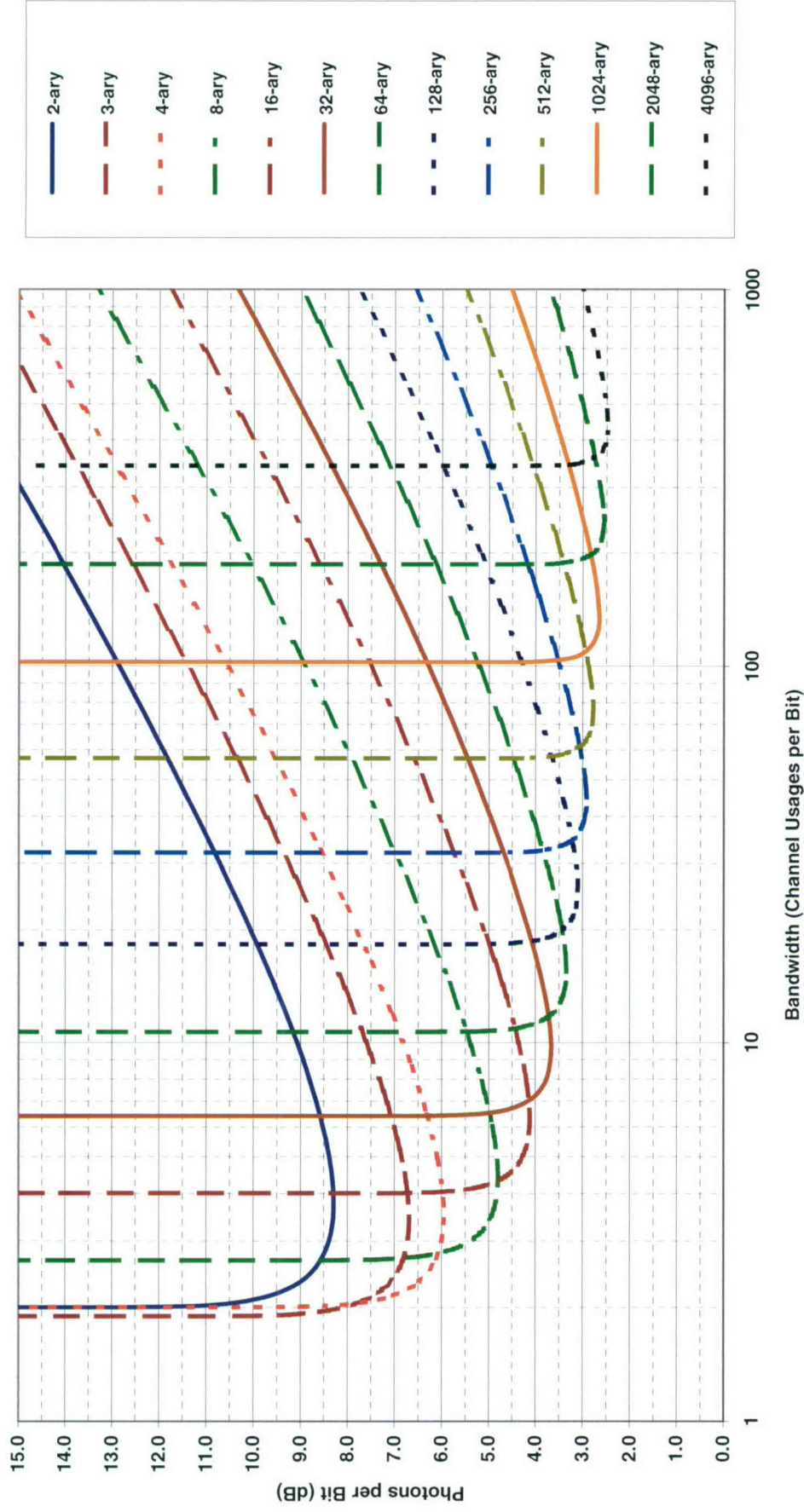


Chart 94. Efficiency at classical cutoff: orthogonal heterodyne or preamplified noncoherent soft decision.

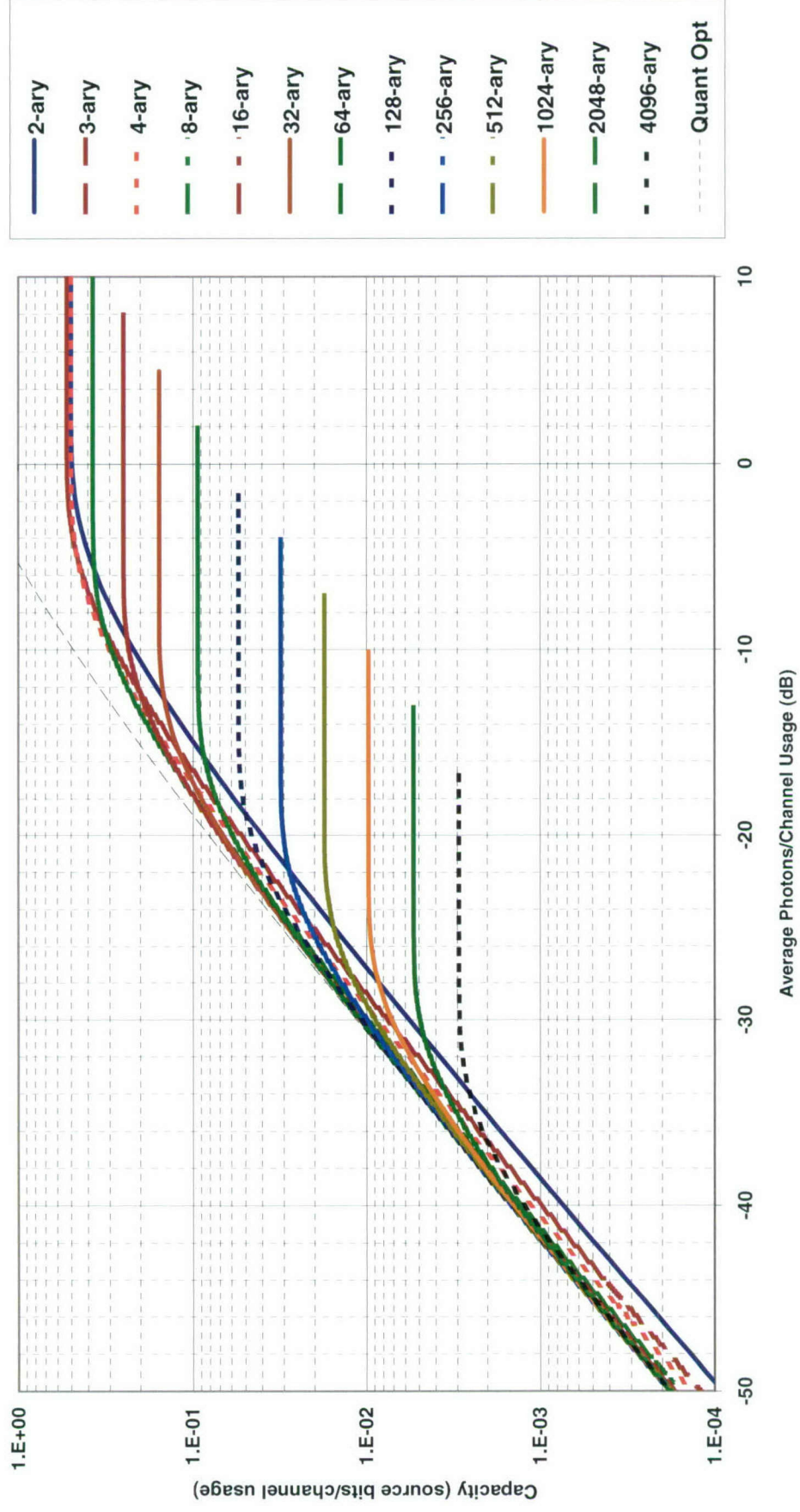


Chart 95. Quantum capacity: orthogonal.

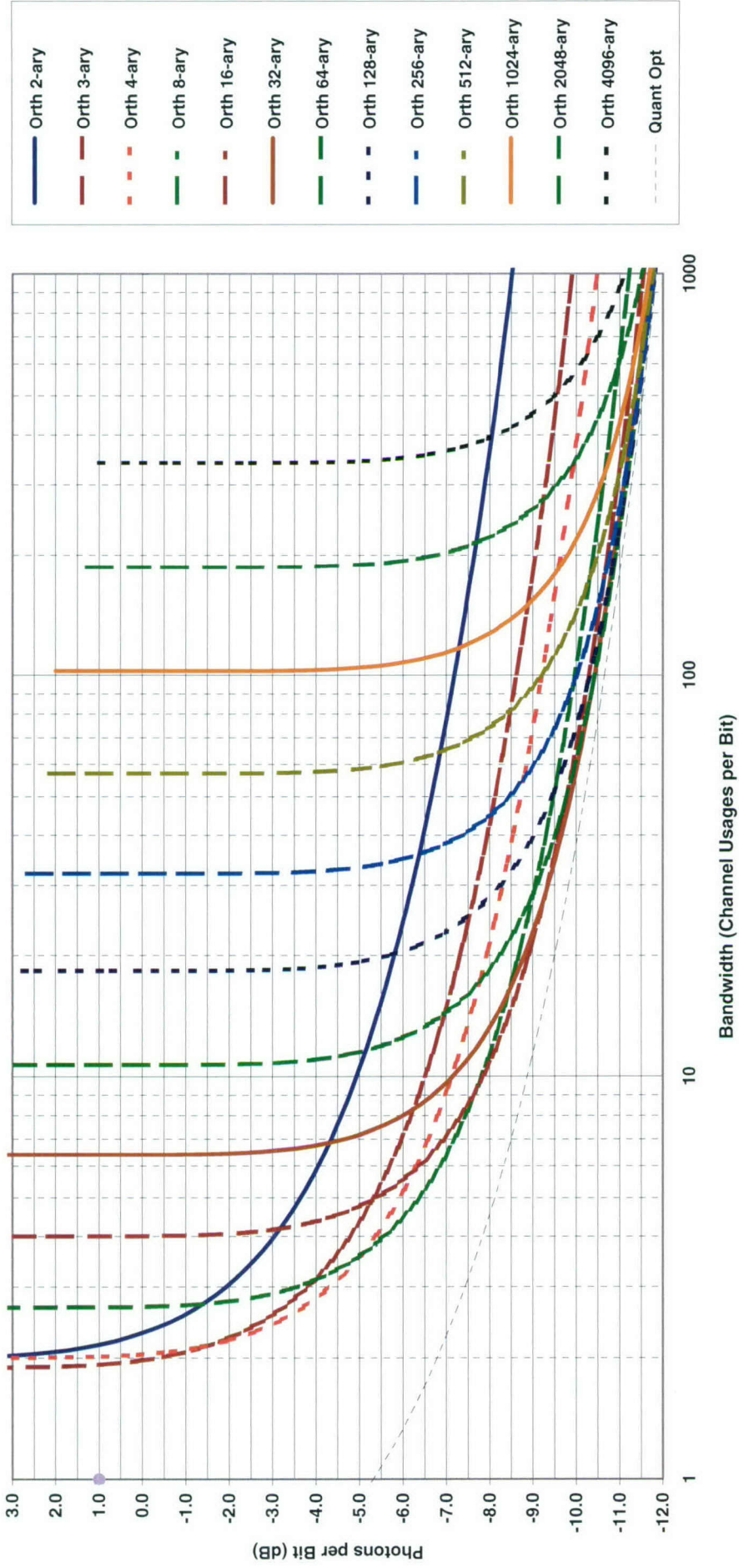


Chart 96. Efficiency at quantum capacity: orthogonal.

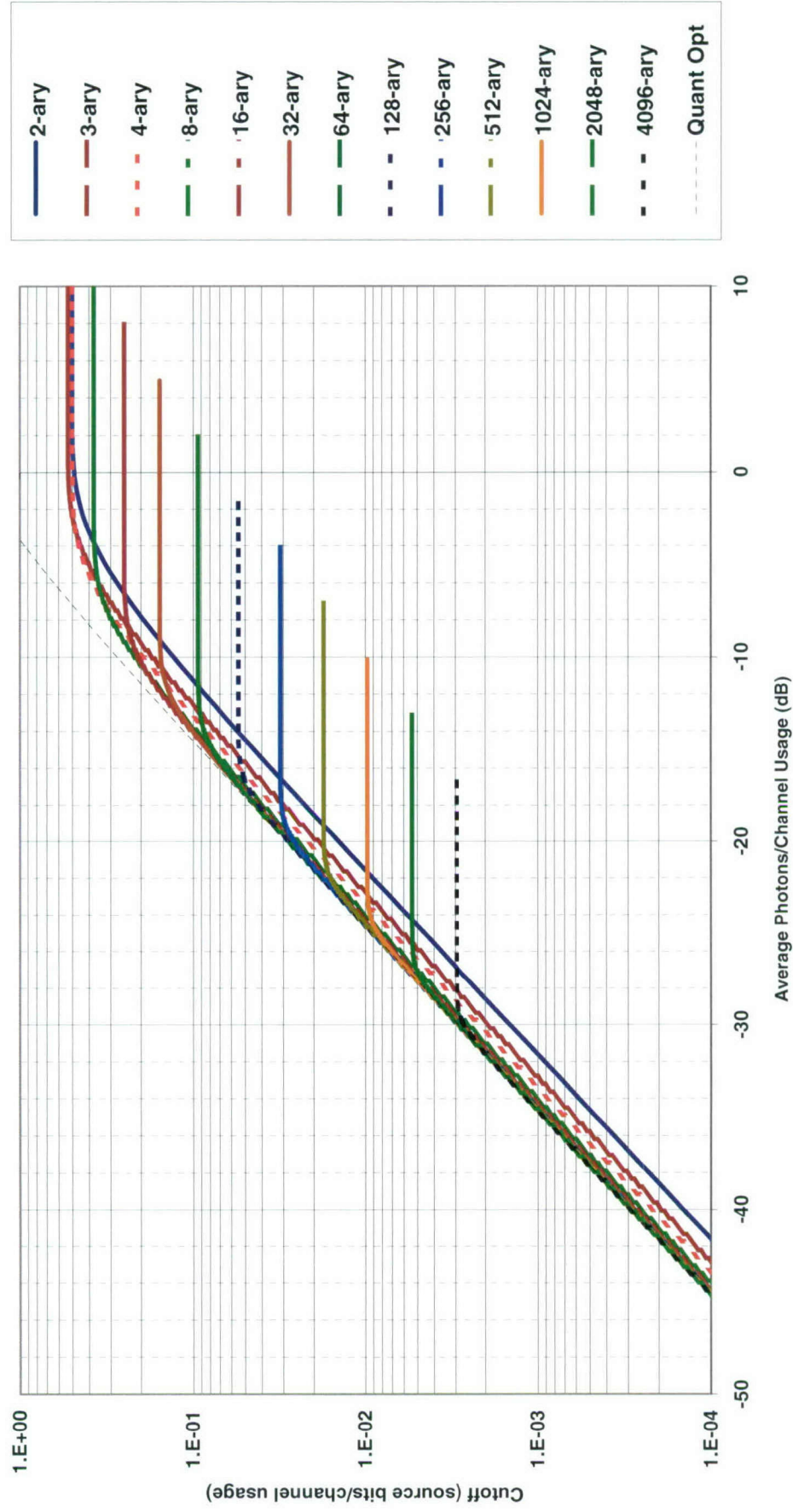


Chart 97. Quantum cutoff: orthogonal.

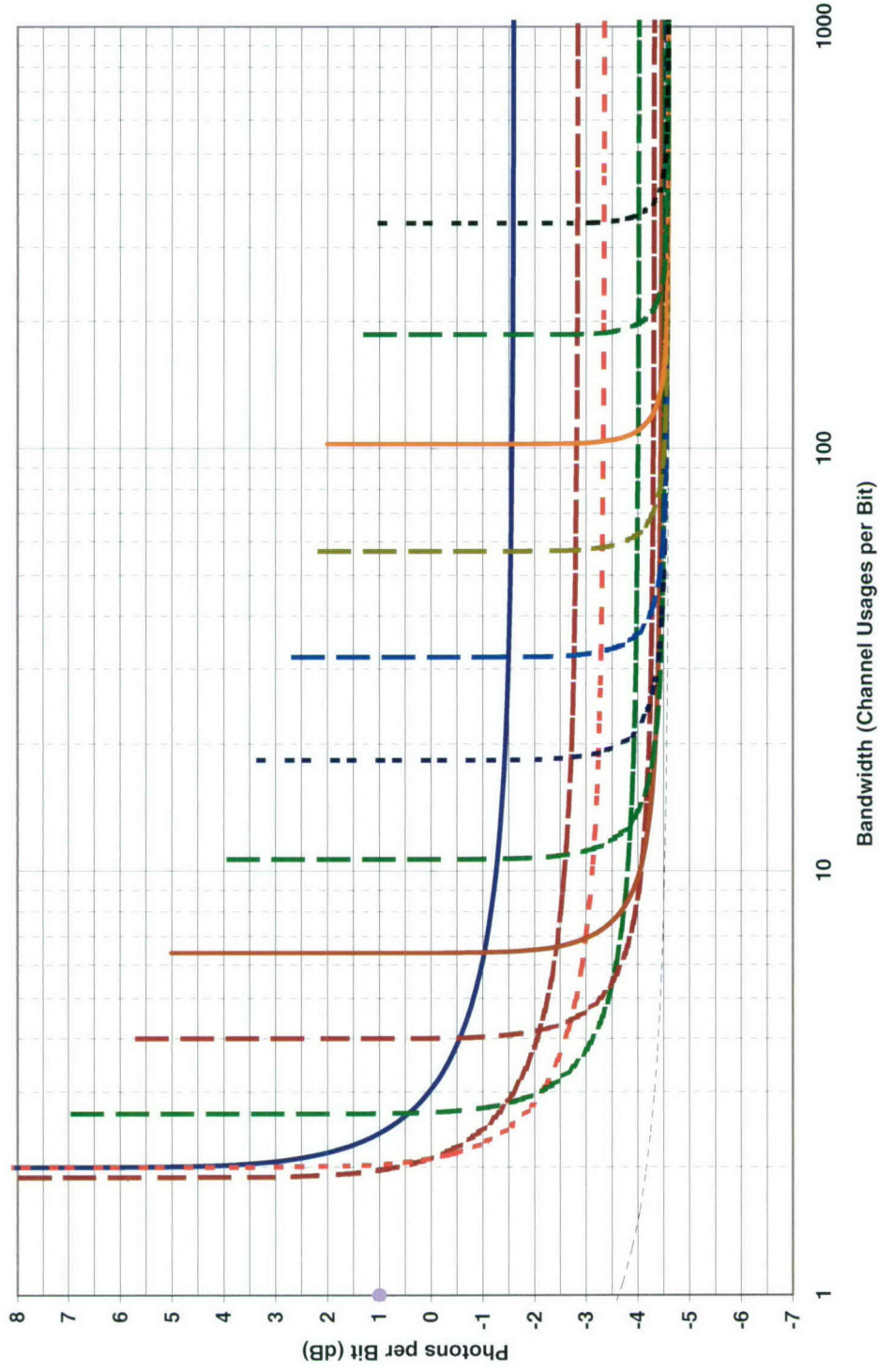


Chart 98. Efficiency at quantum cutoff: orthogonal.

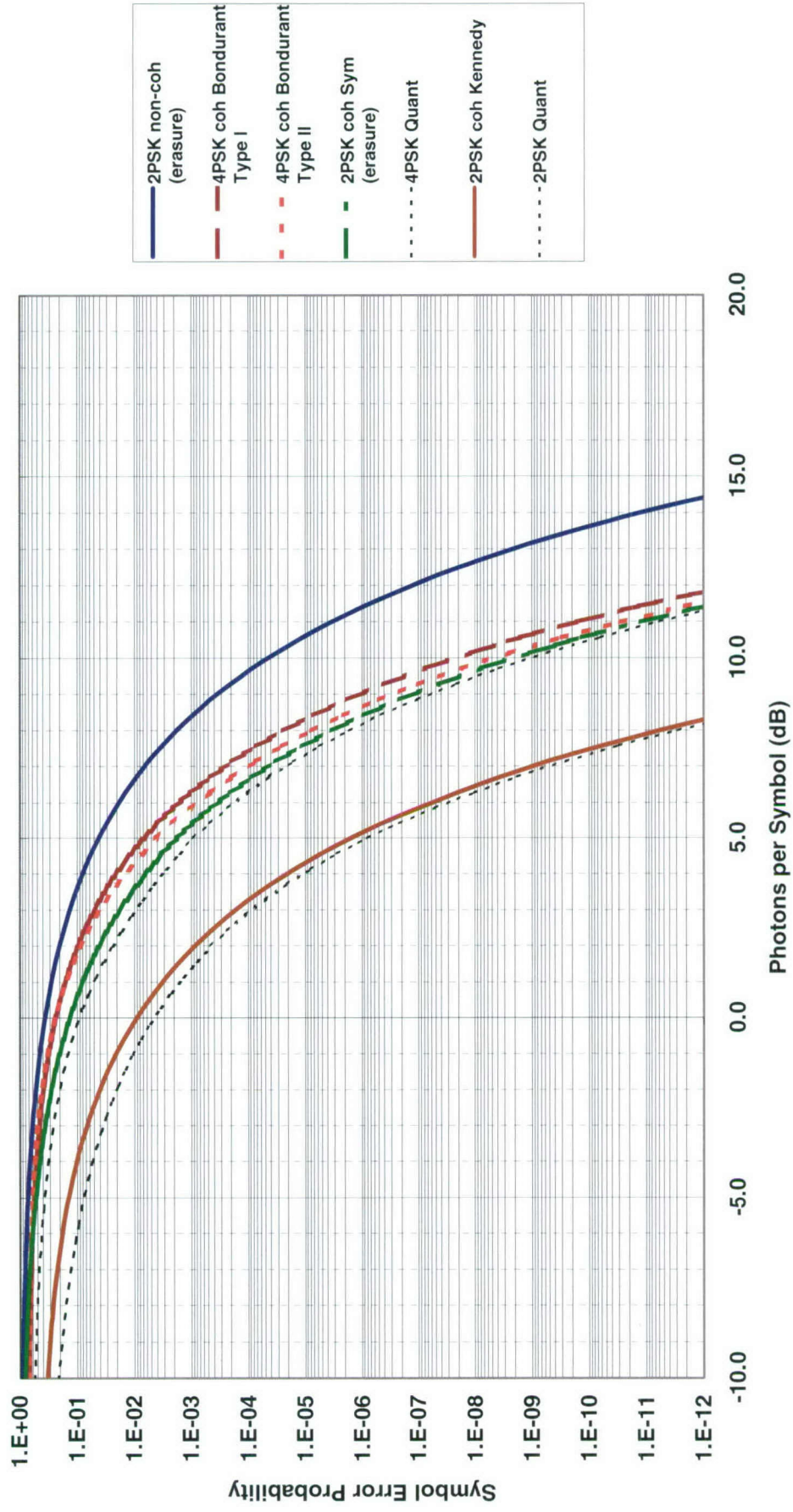


Chart 99. Symbol error probability: MPSK photon counting.

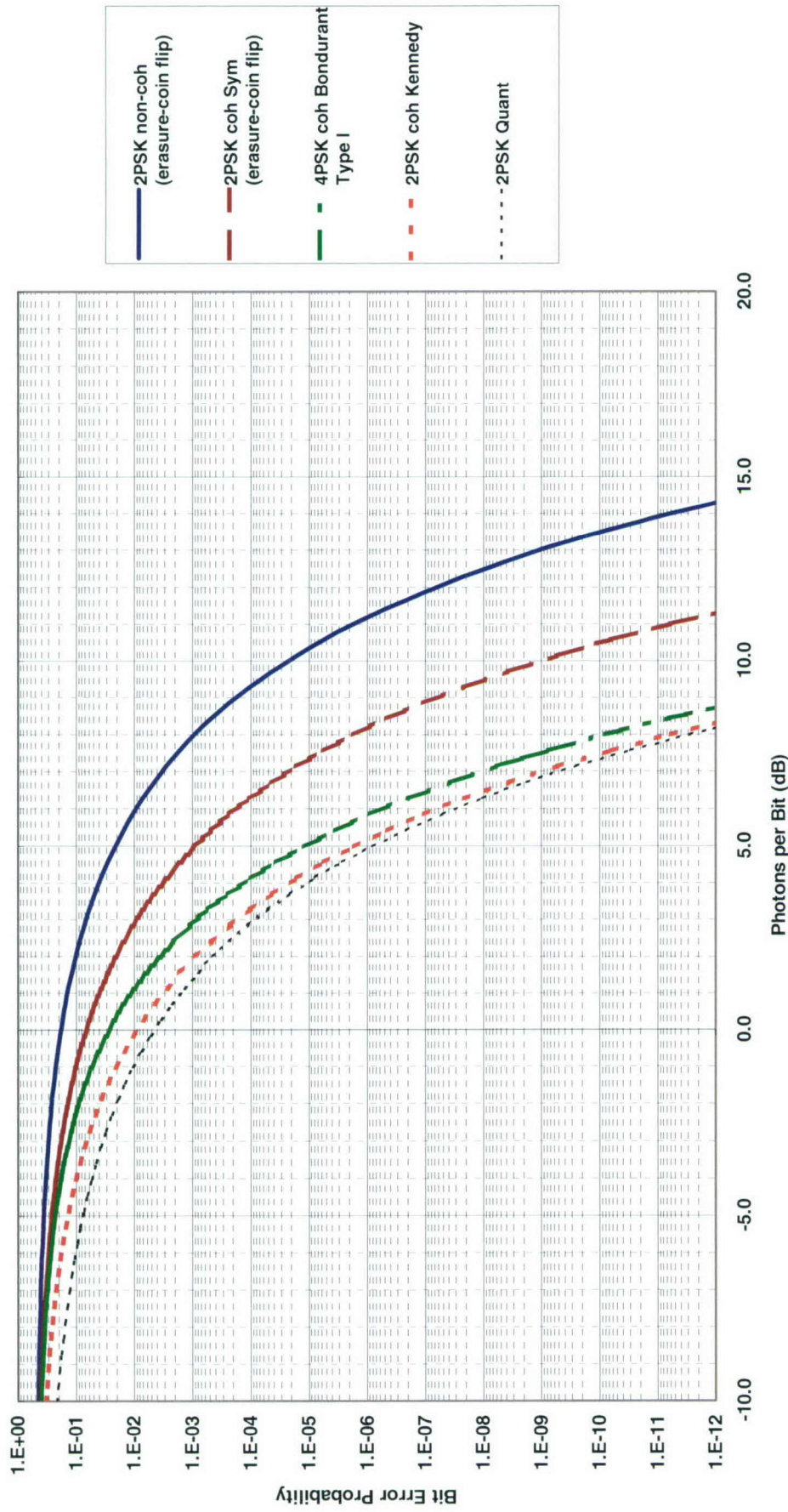


Chart 100. Bit-error probability: MPSK photon counting.

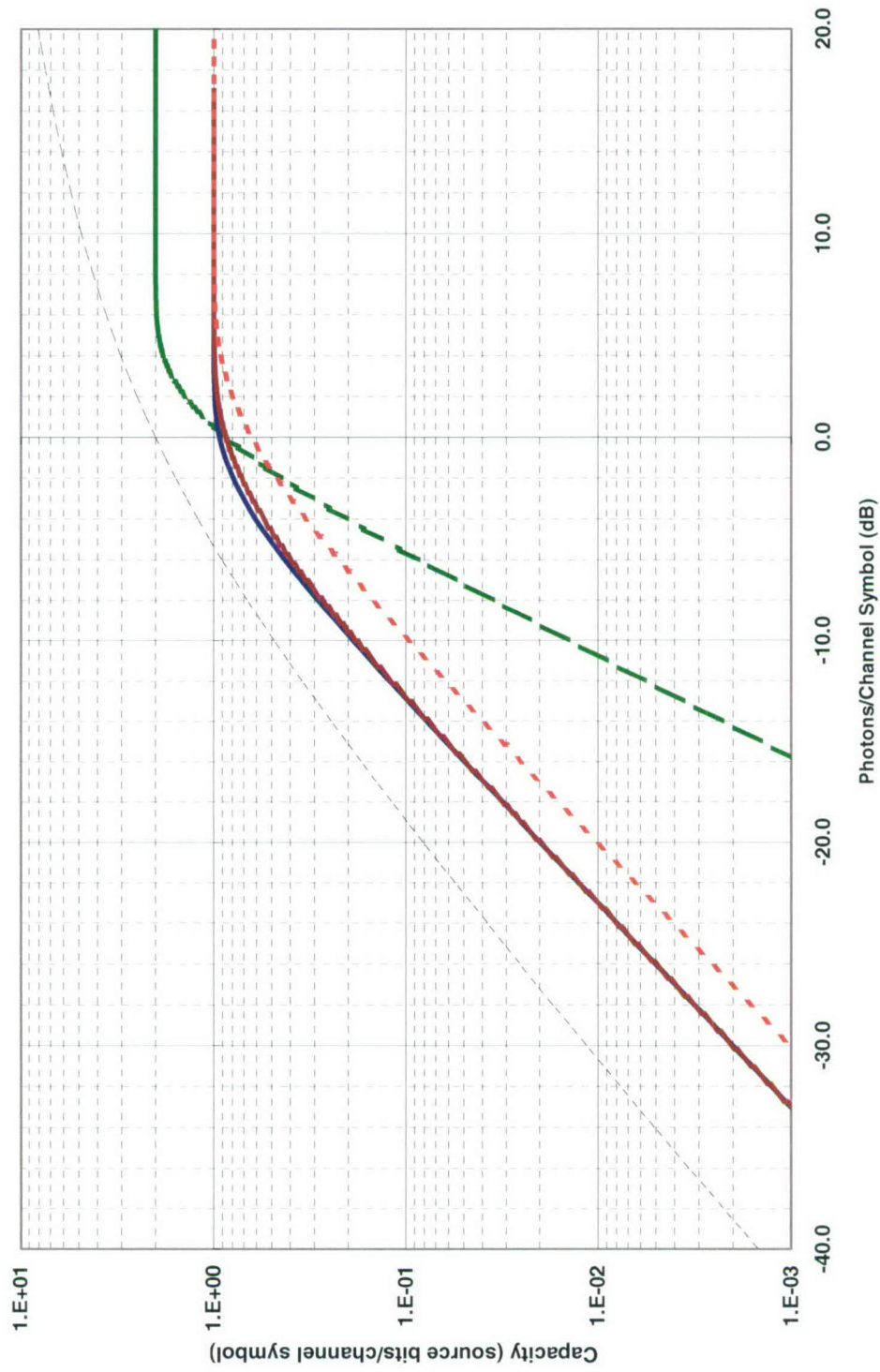


Chart 101. Classical capacity: MPSK photon counting hard decision.

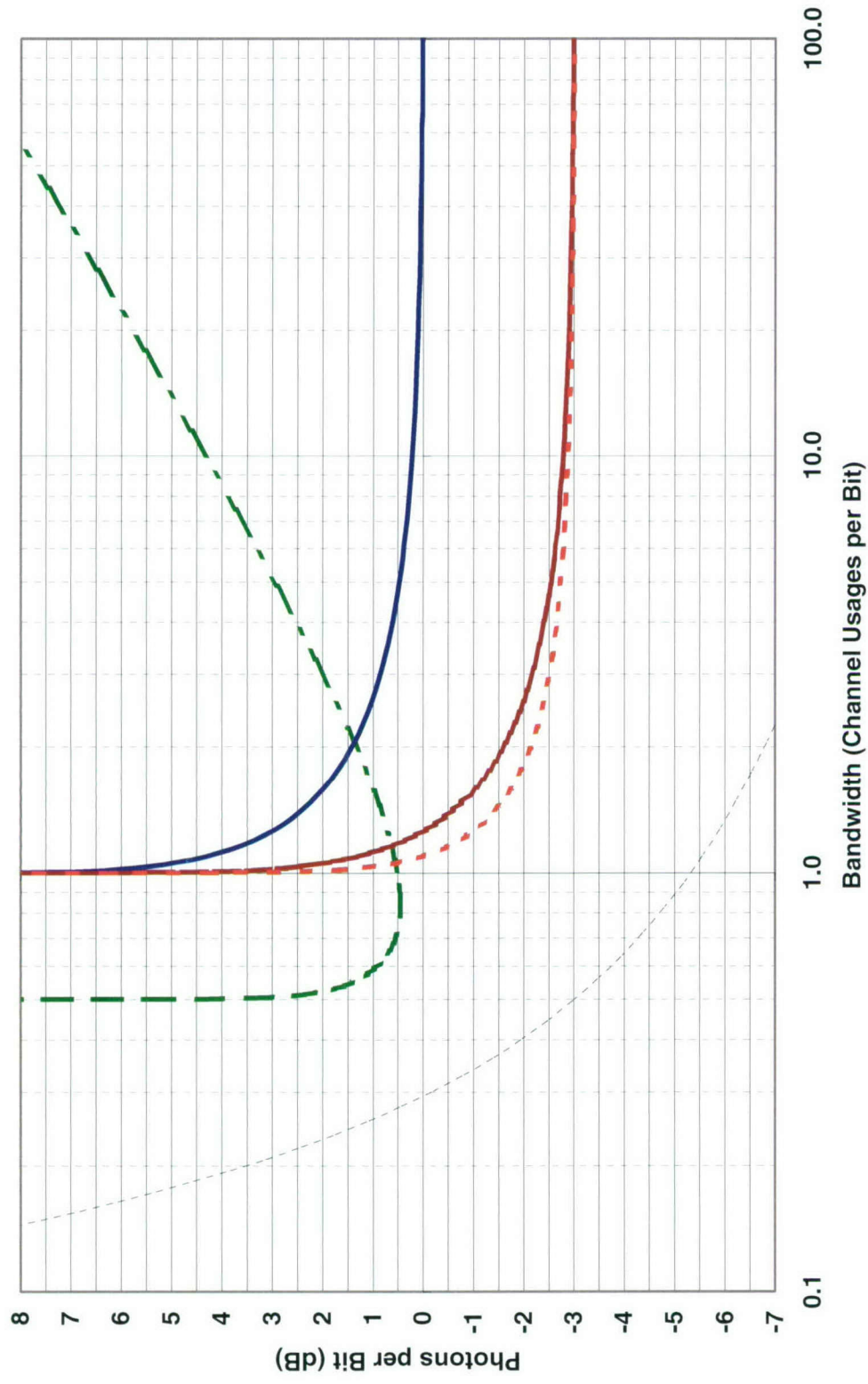


Chart 102. Efficiency at classical capacity: MPSK photon counting hard decision.

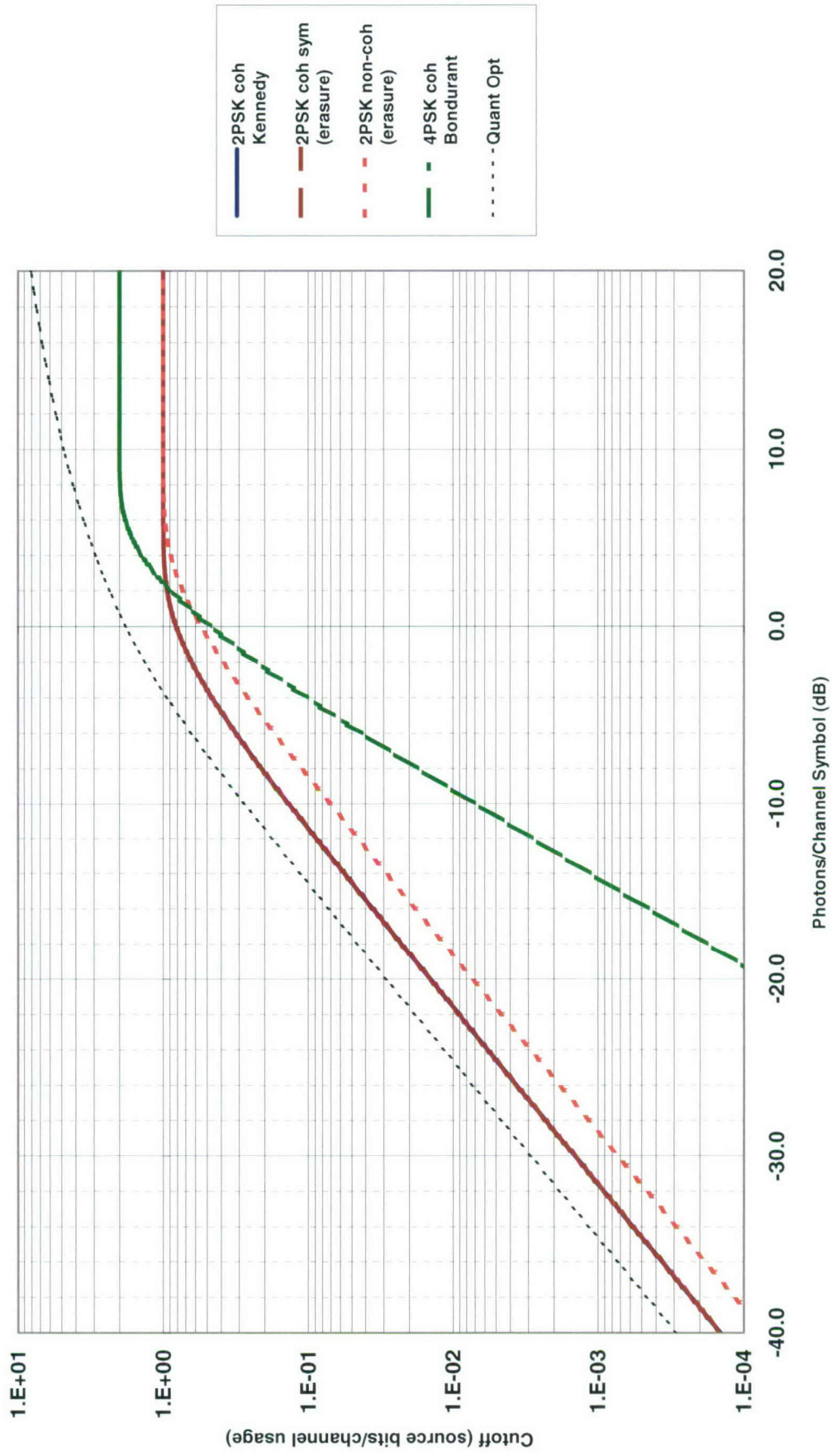


Chart 103. Classical cutoff: MPSK photon counting hard decision.

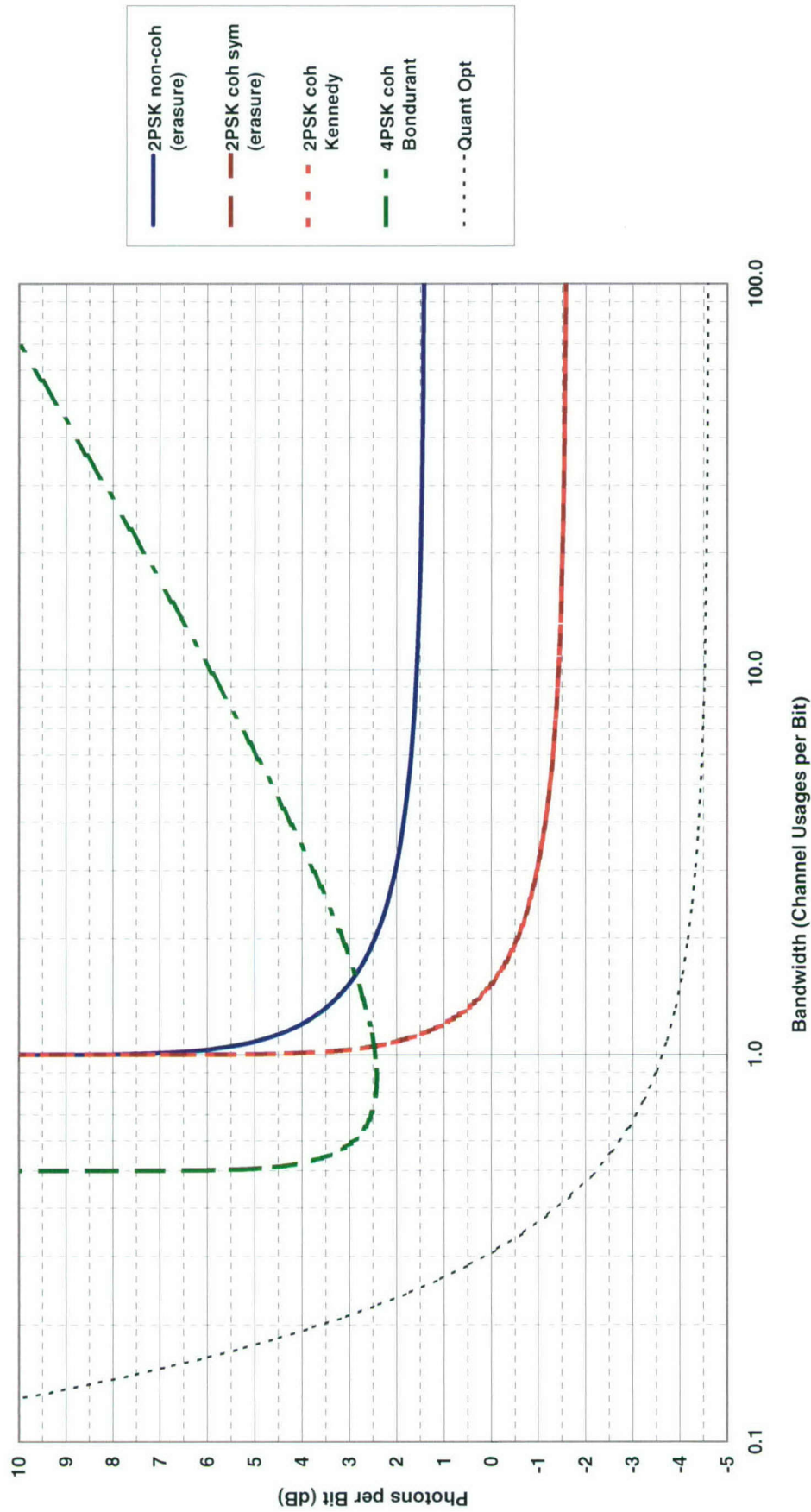


Chart 104. Efficiency at classical cutoff: MPSK photon counting hard decision.

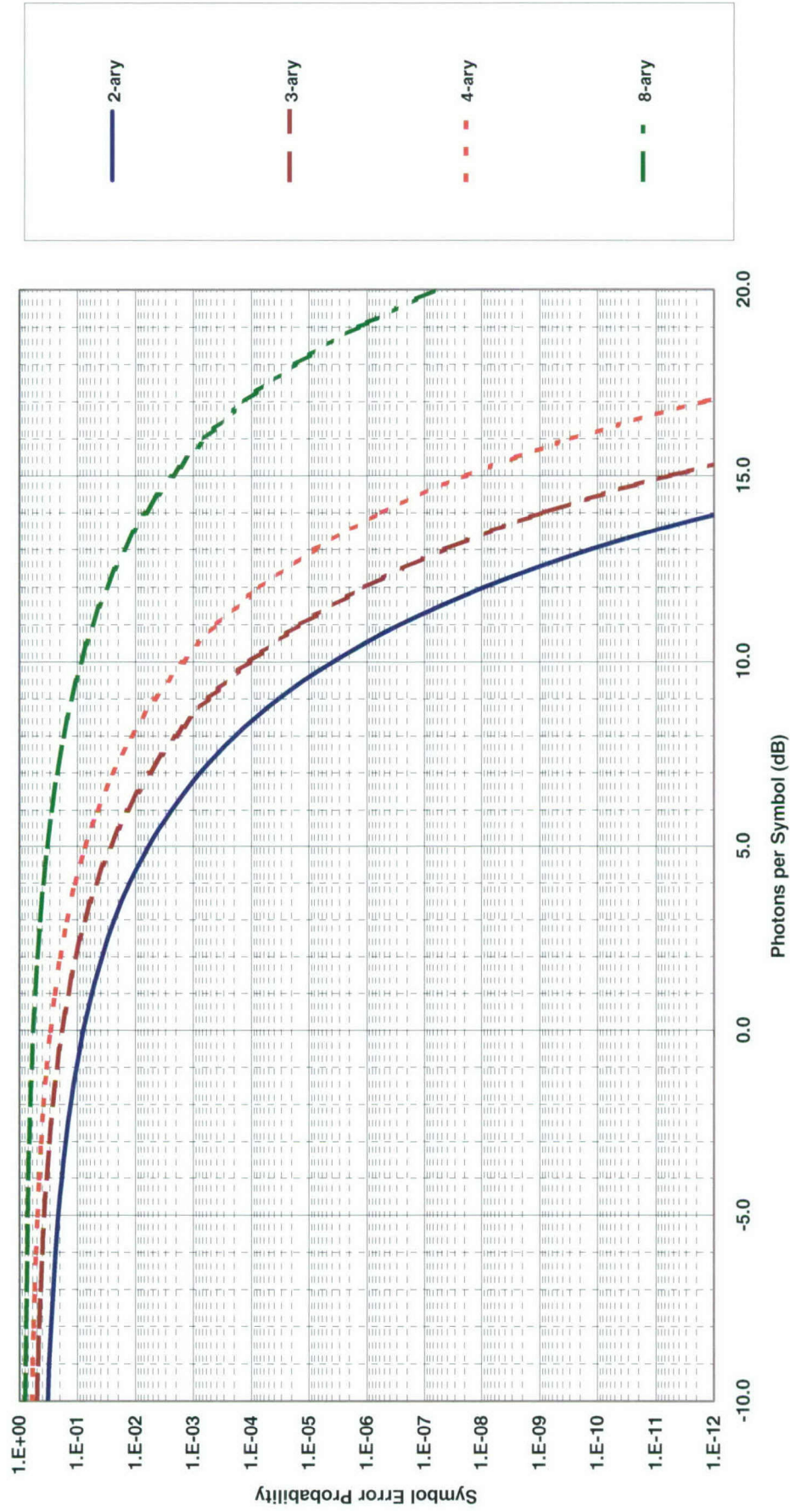


Chart 105. Symbol error probability: MPSK heterodyne or preamplified coherent.

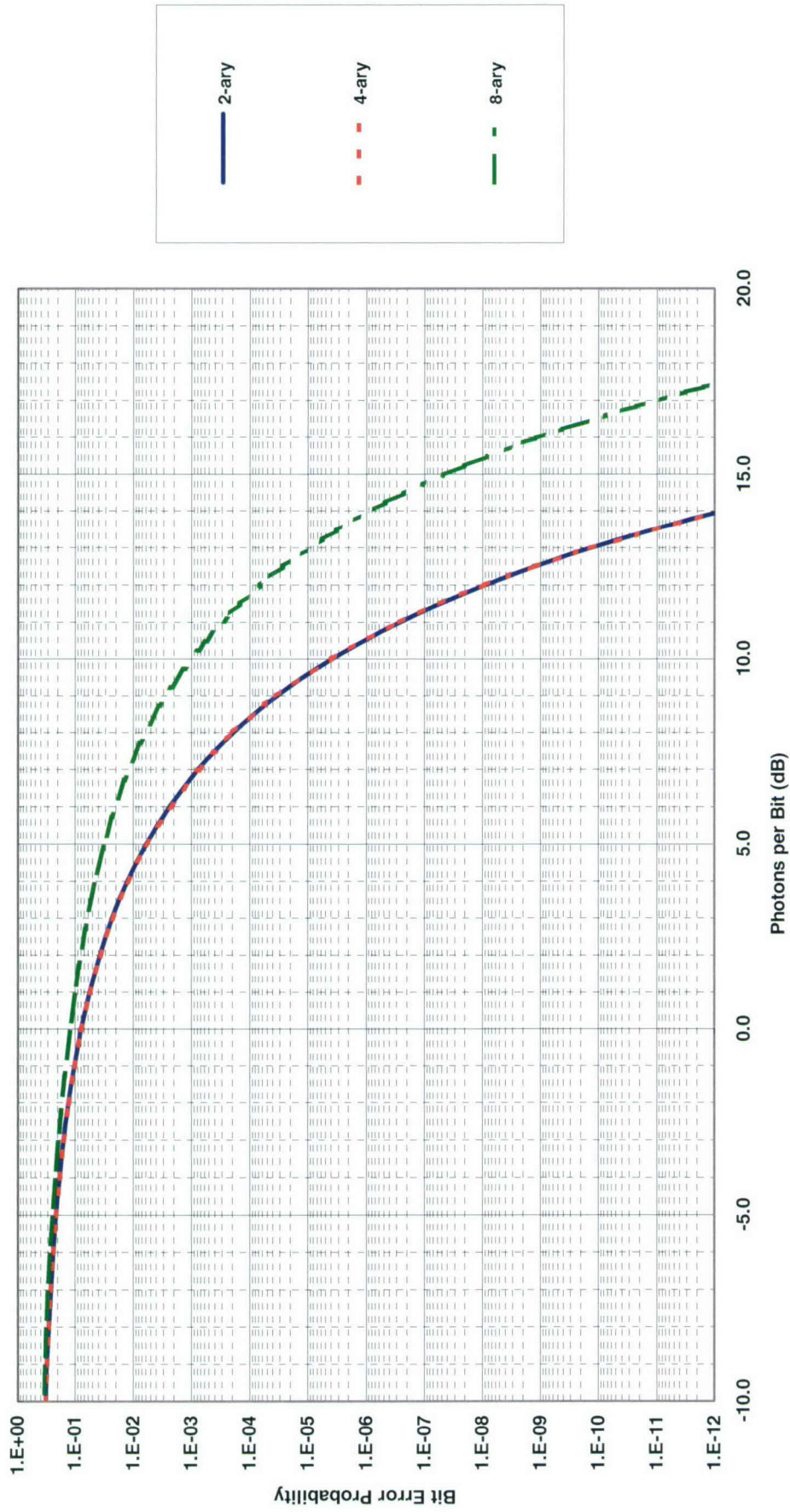


Chart 106. Bit-error probability: MPSK heterodyne or preamplified coherent.

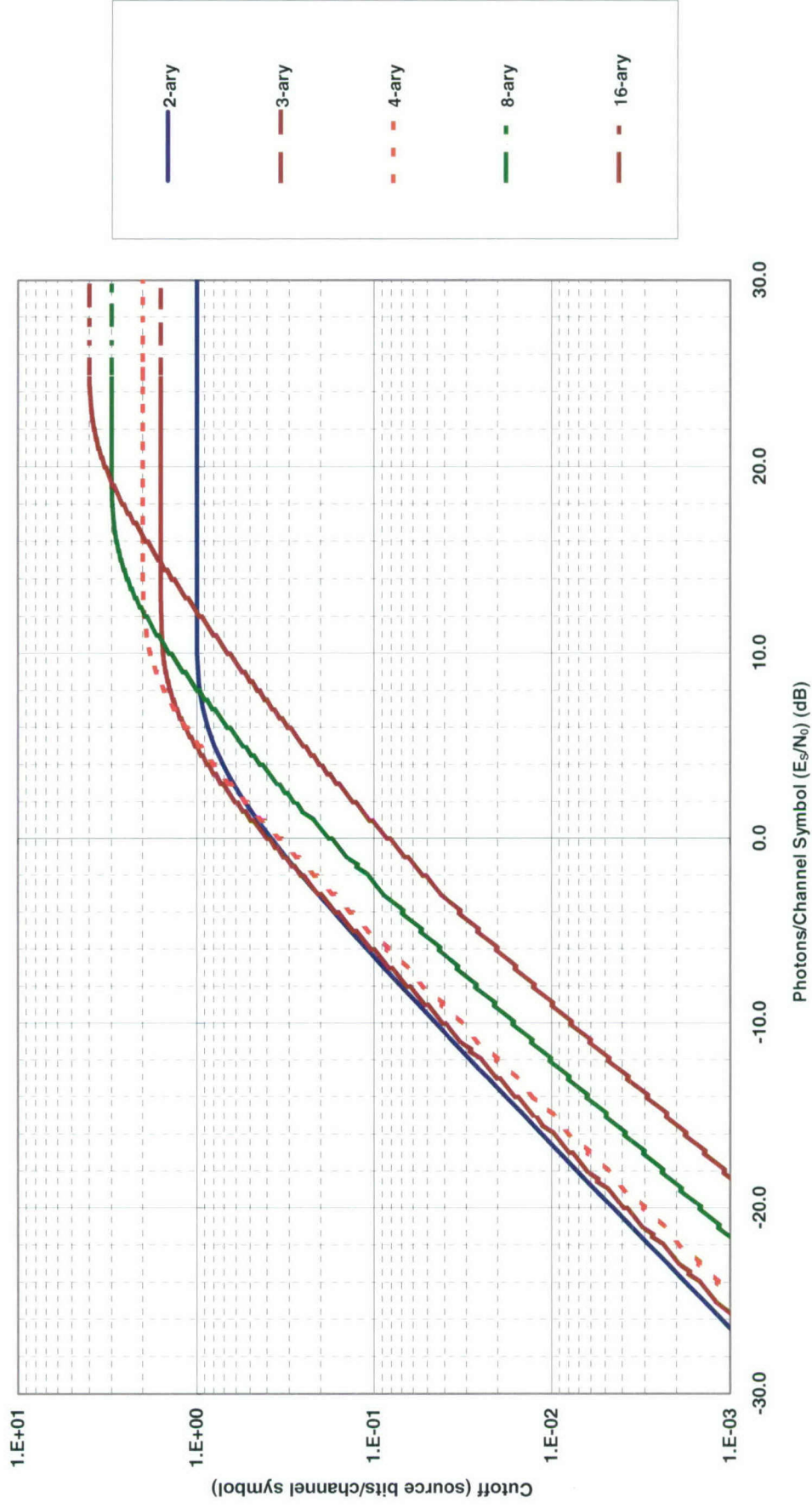


Chart 107. Classical cutoff: MPSK heterodyne or preamplified coherent pure hard decision.

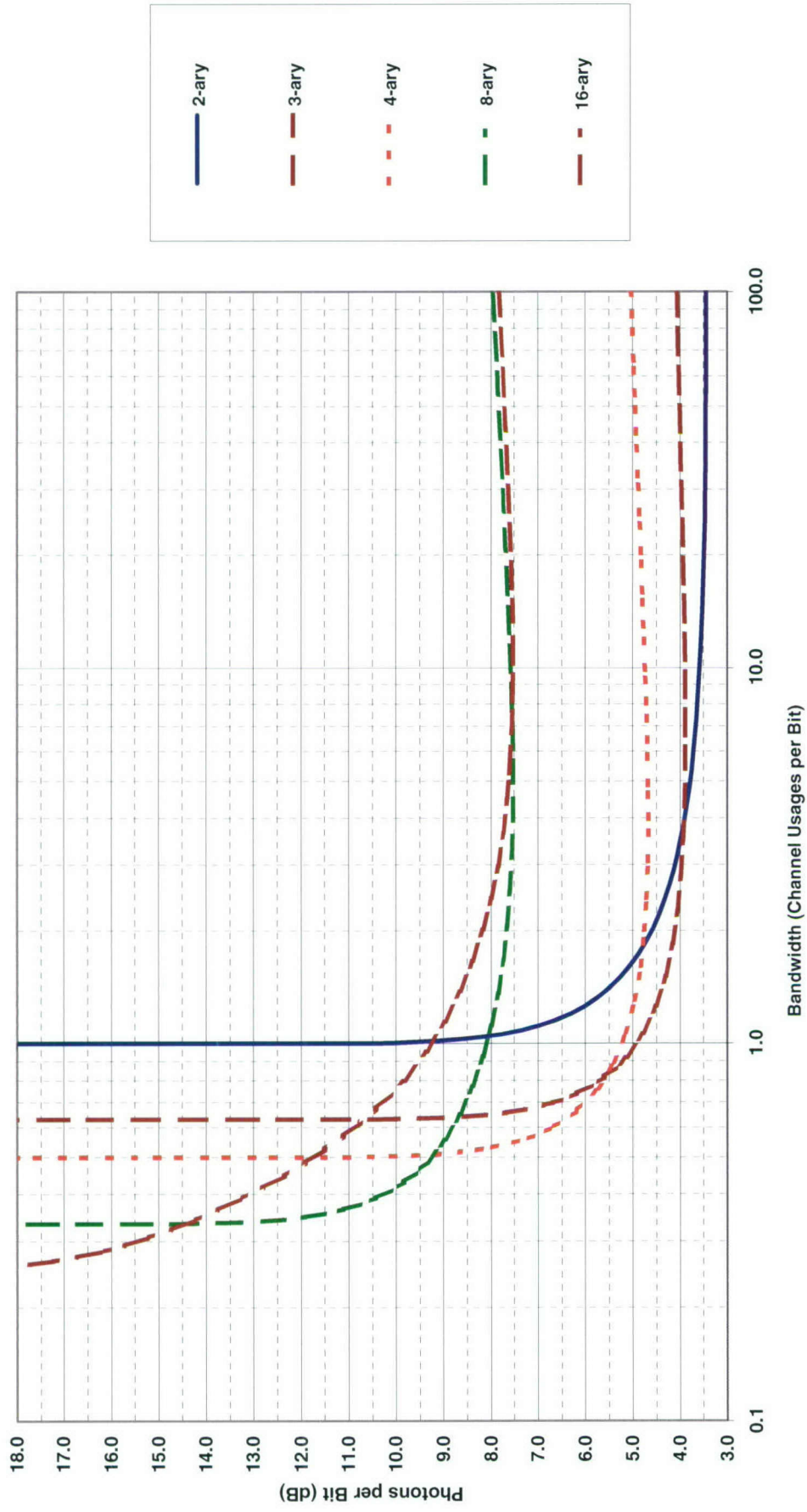


Chart 108. Efficiency at classical cutoff: MPSK heterodyne or preamplified coherent pure hard decision.

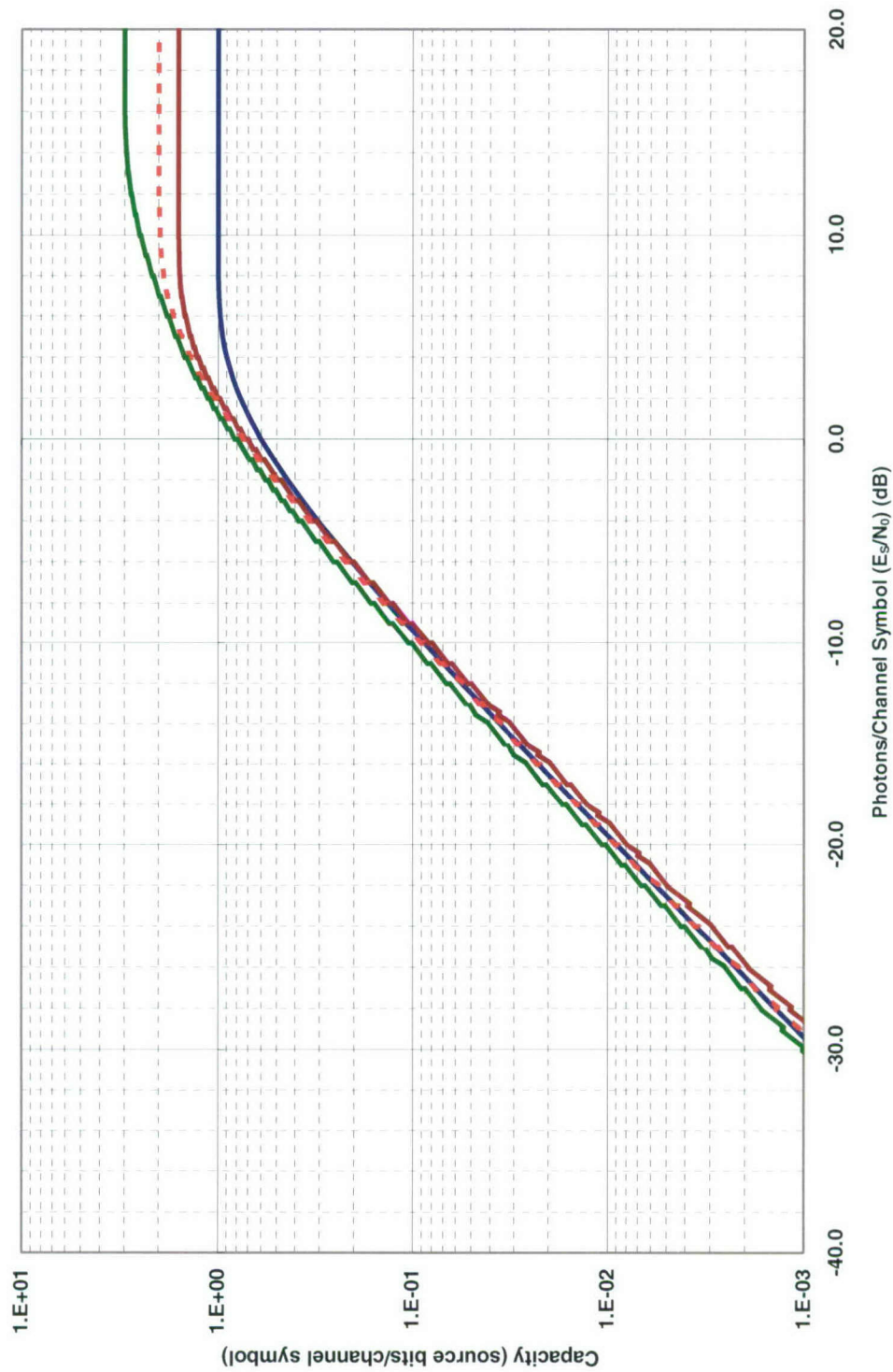


Chart 109. Classical capacity: MPSK heterodyne or preamplified coherent hard decision with ML decoding.

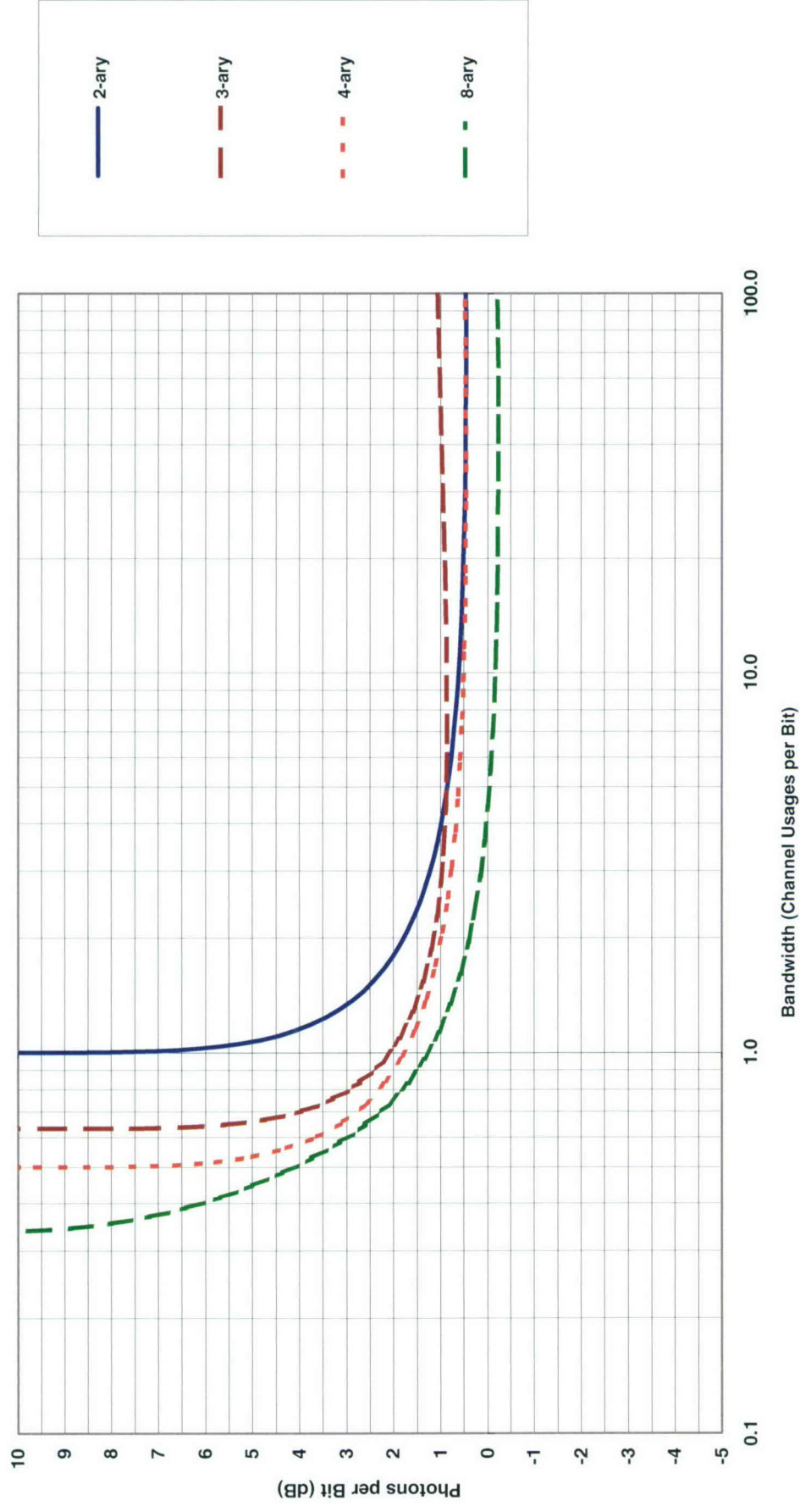


Chart 110. Efficiency at classical capacity: MPSK heterodyne or preamplified coherent hard decision with ML decoding.

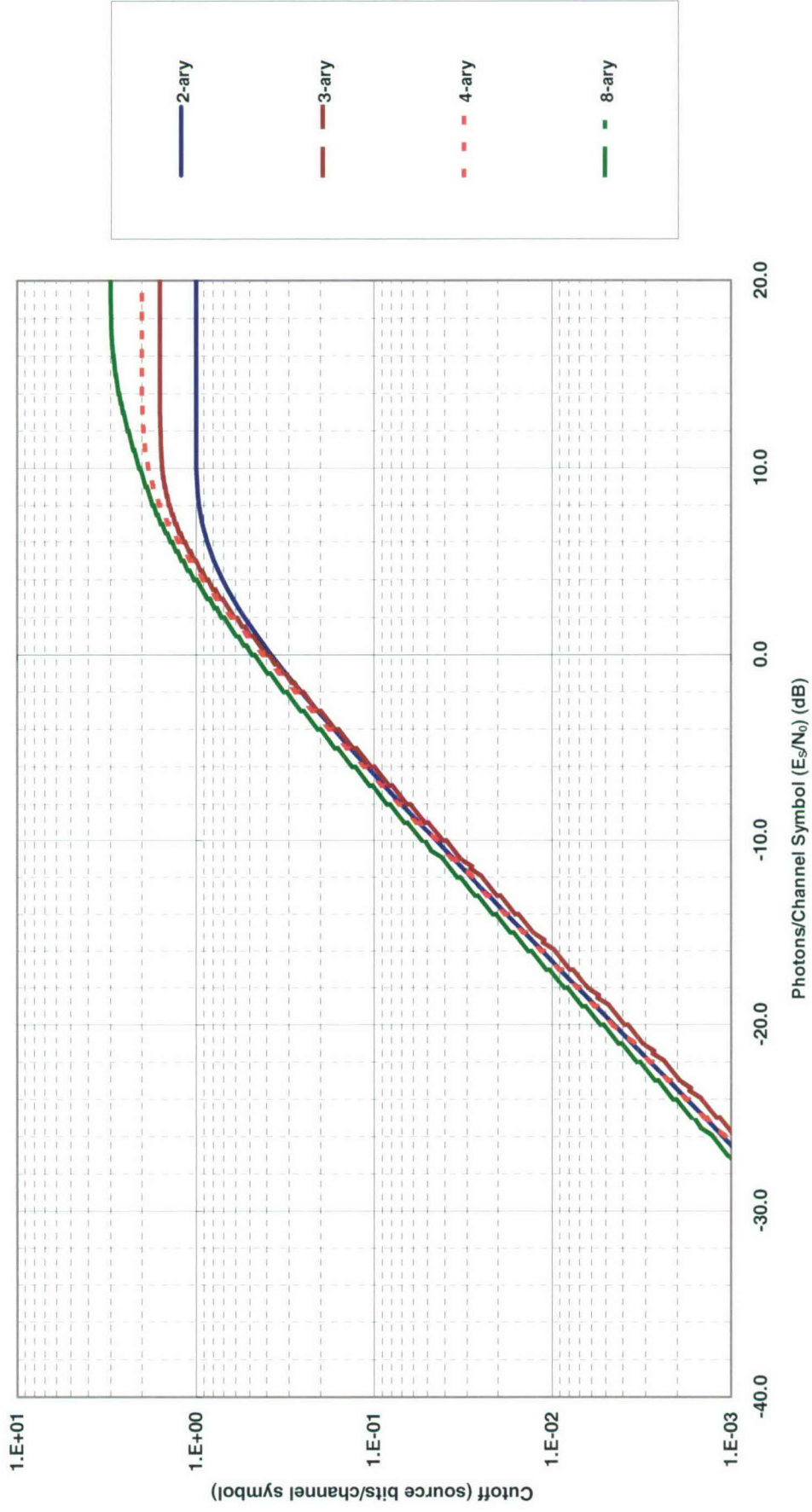


Chart 111. Classical cutoff: MPSK heterodyne or preamplified coherent hard decision with ML decoding.

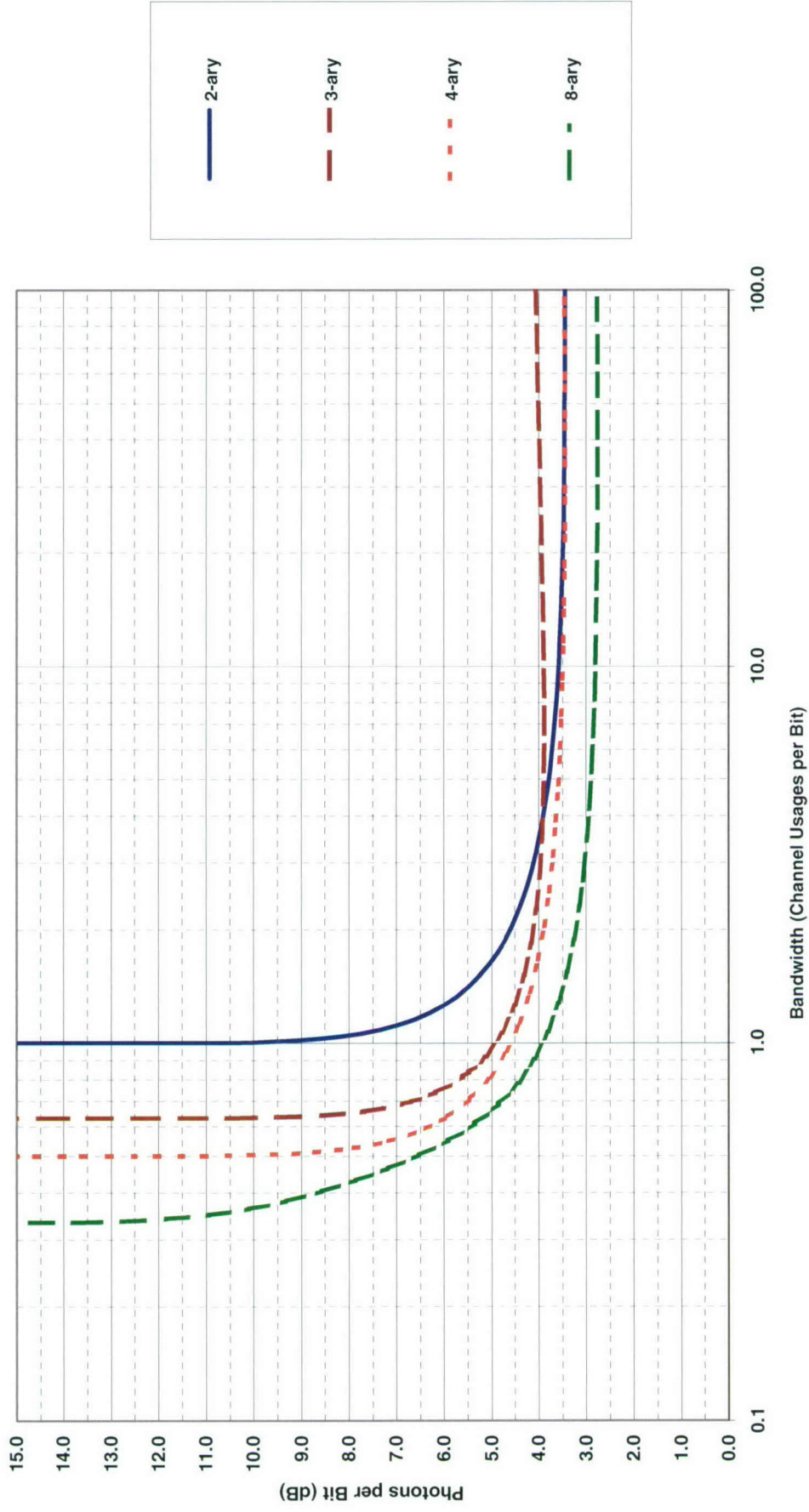


Chart 112. Efficiency at classical cutoff: MPSK heterodyne or preamplified coherent hard decision with ML decoding.

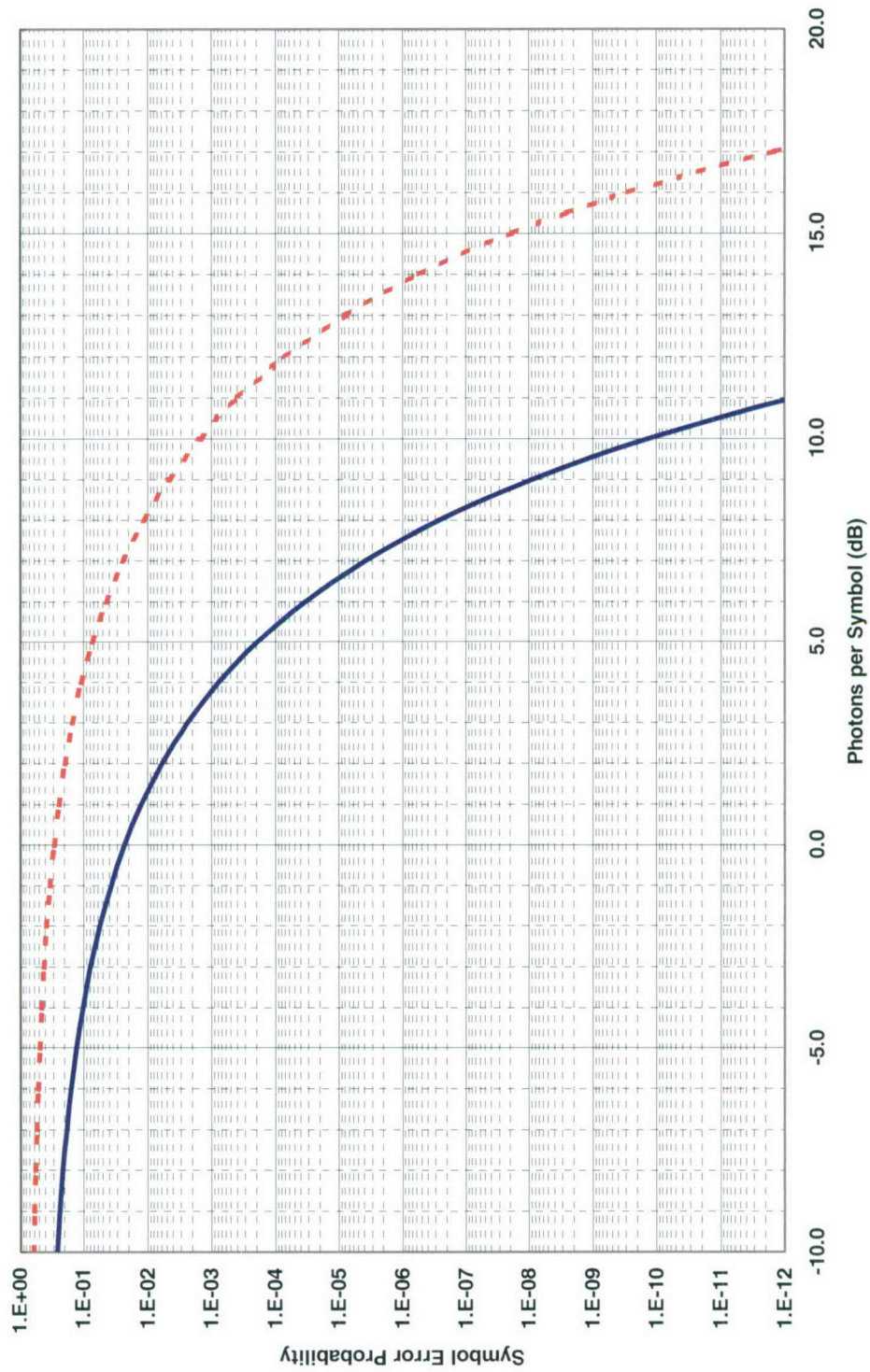


Chart 113. Symbol error probability: MPSK homodyne coherent.

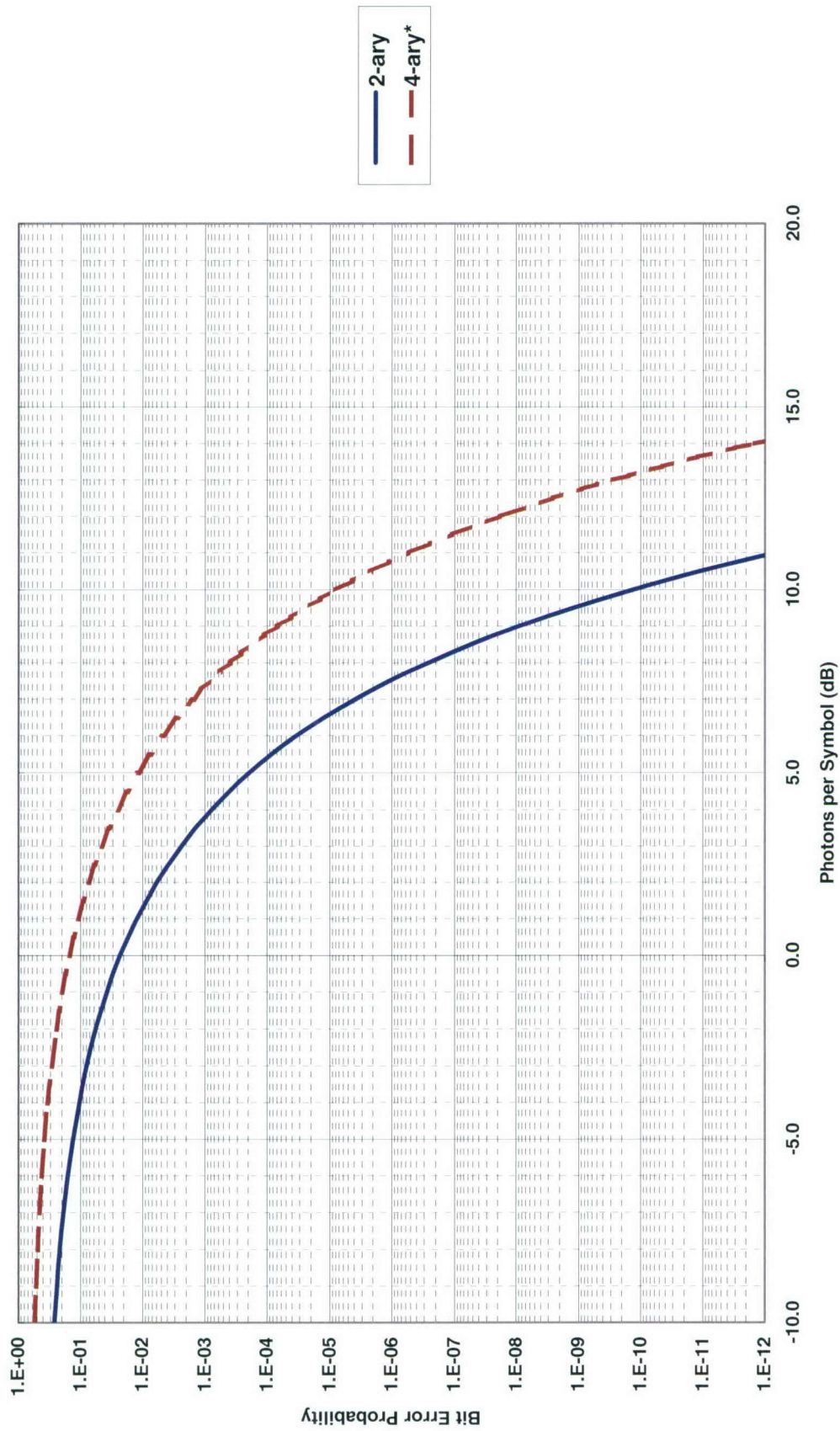


Chart 114. Bit-error probability: MPSK homodyne coherent.

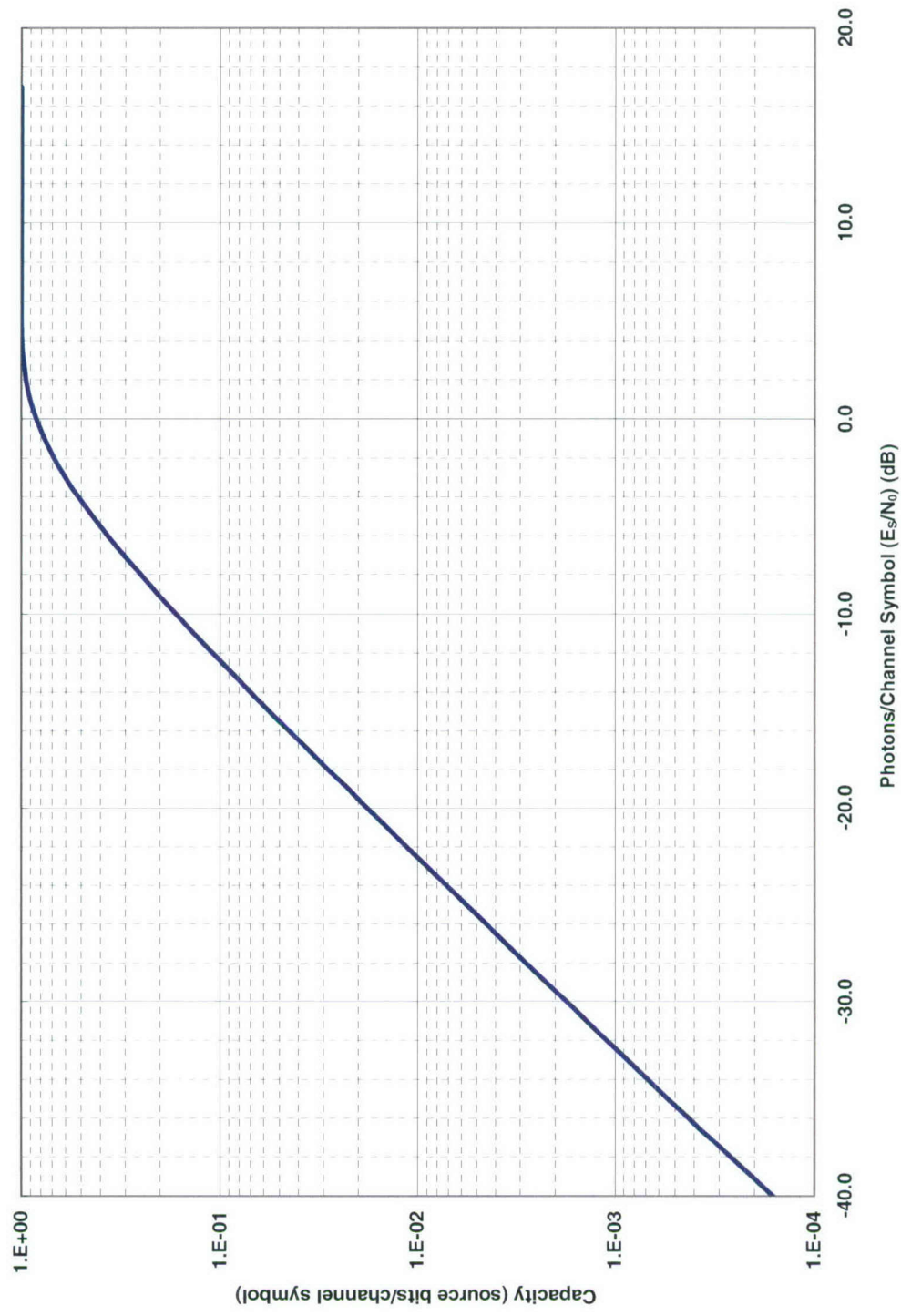


Chart 115. Classical capacity: MPSK homodyne coherent hard decision.

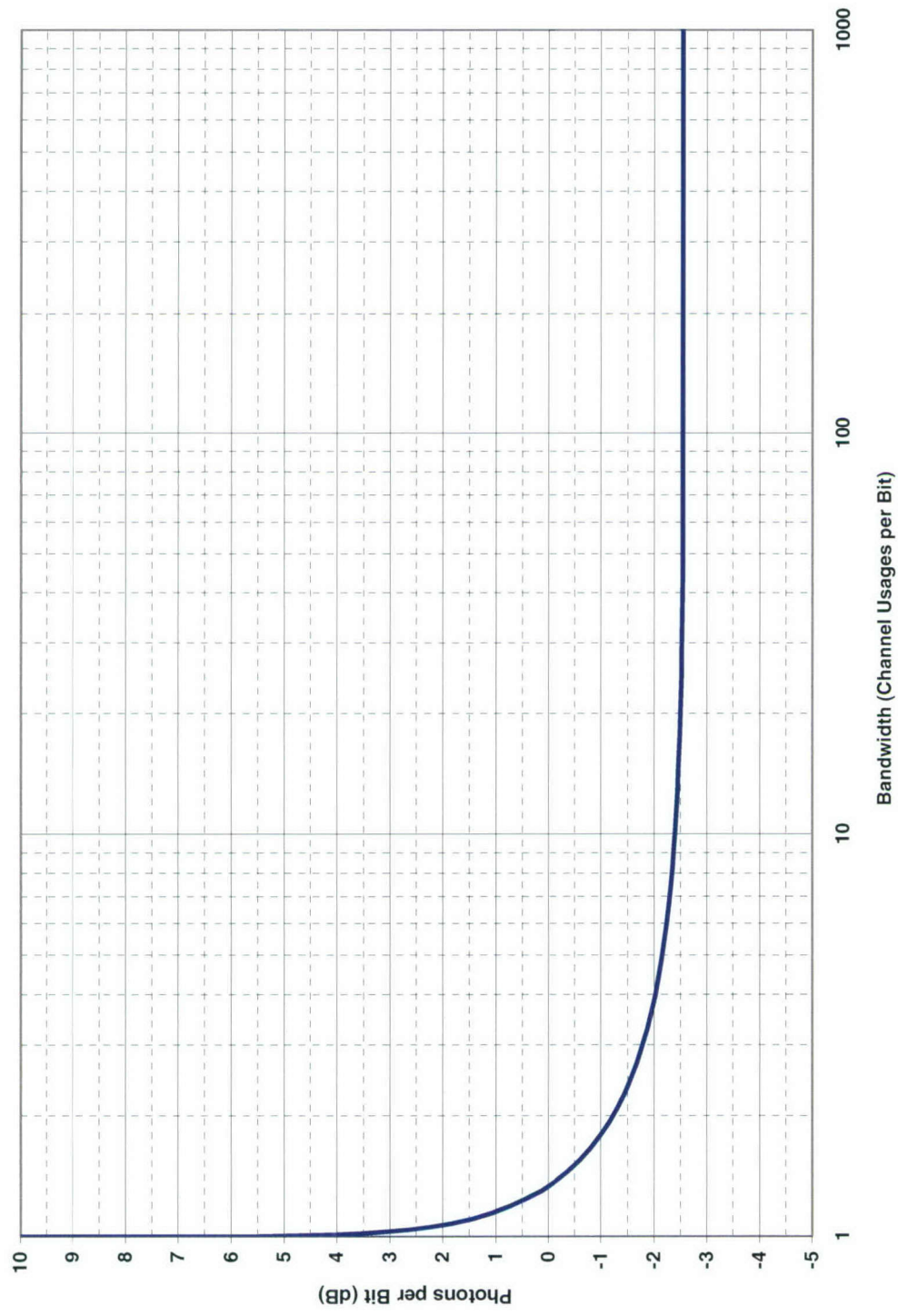


Chart 116. Efficiency at classical capacity: MPSK homodyne coherent hard decision.

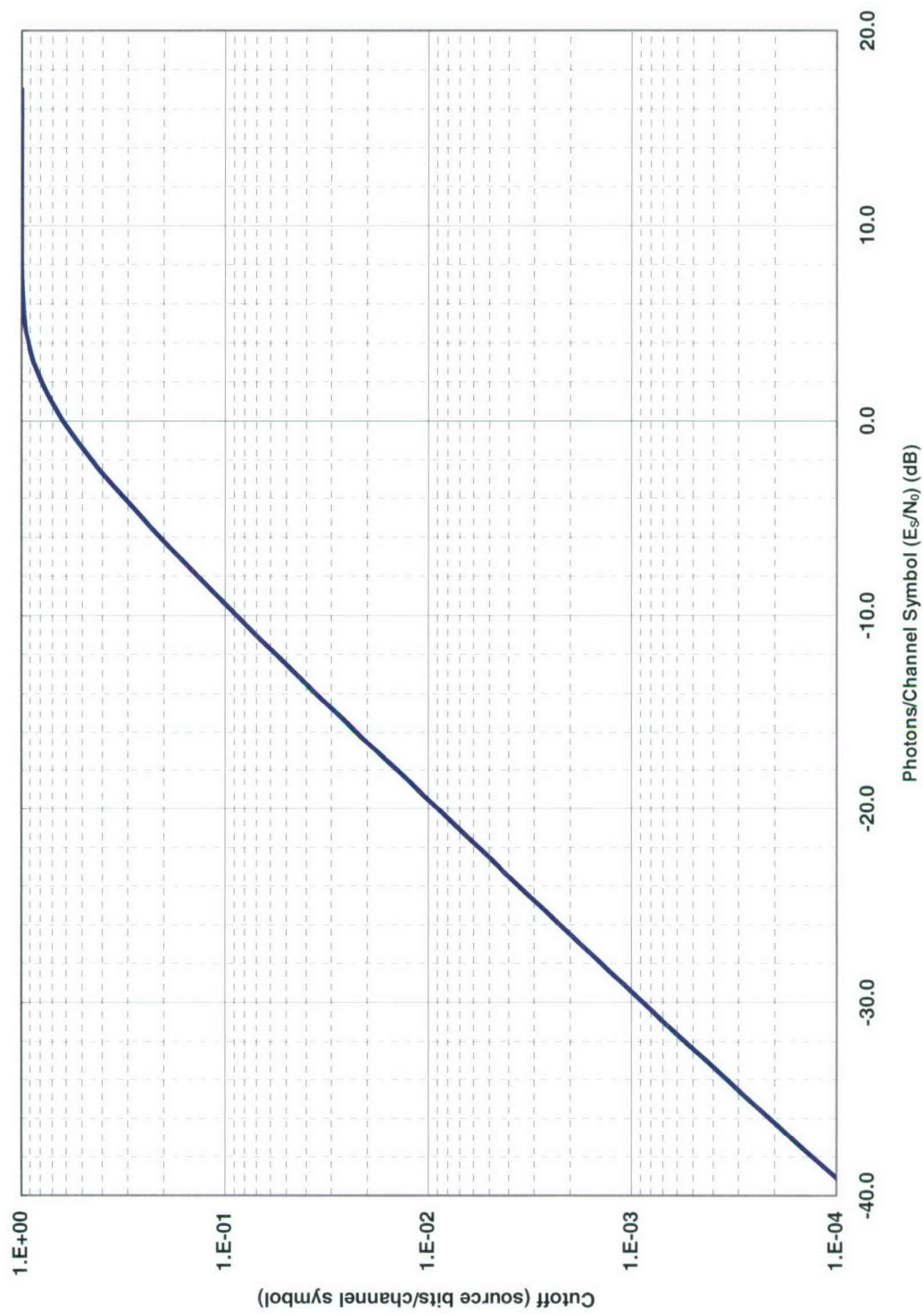


Chart 117. Classical cutoff: MPSK homodyne coherent hard decision.

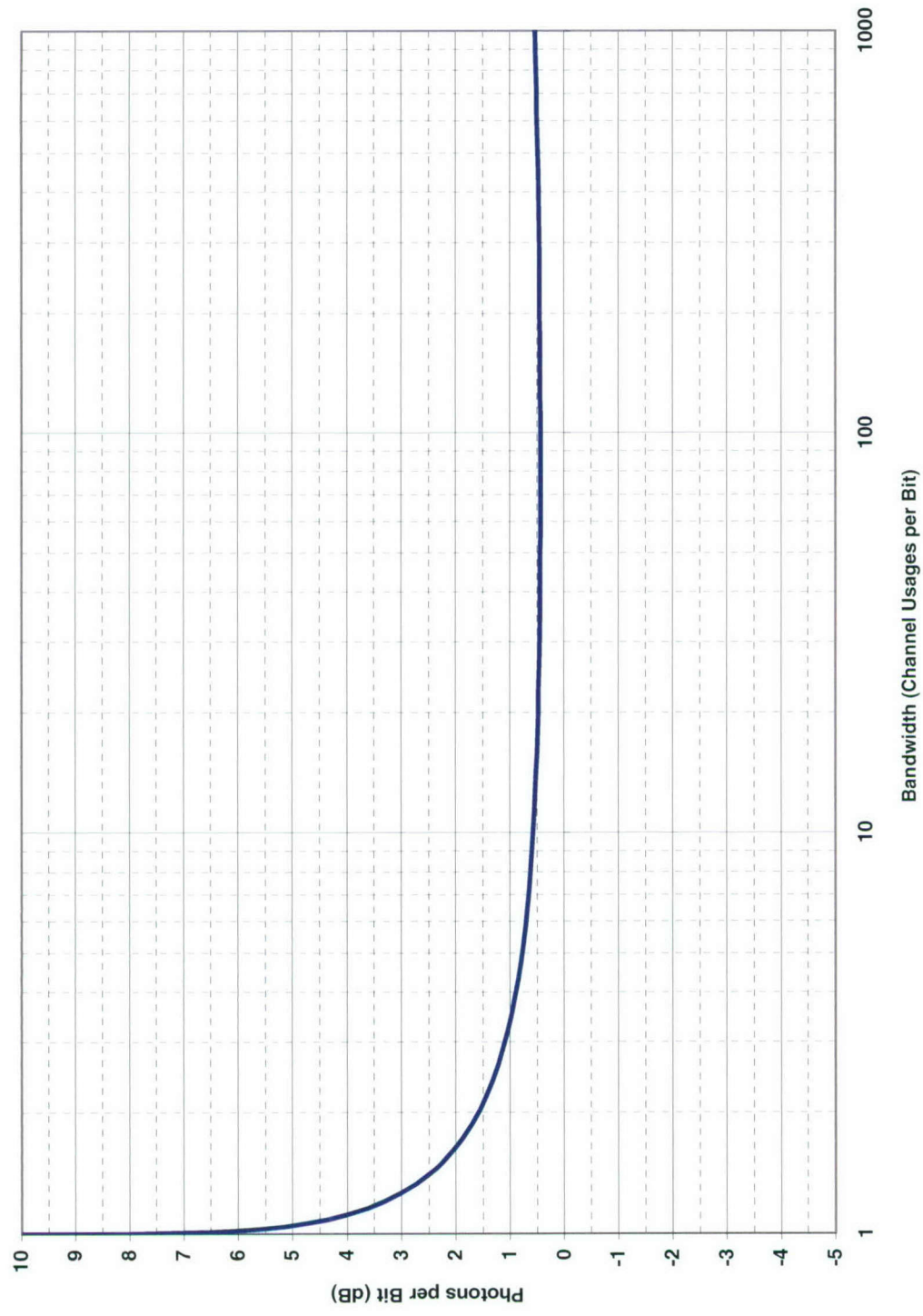


Chart 118. Efficiency at classical cutoff: MPSK homodyne coherent hard decision.

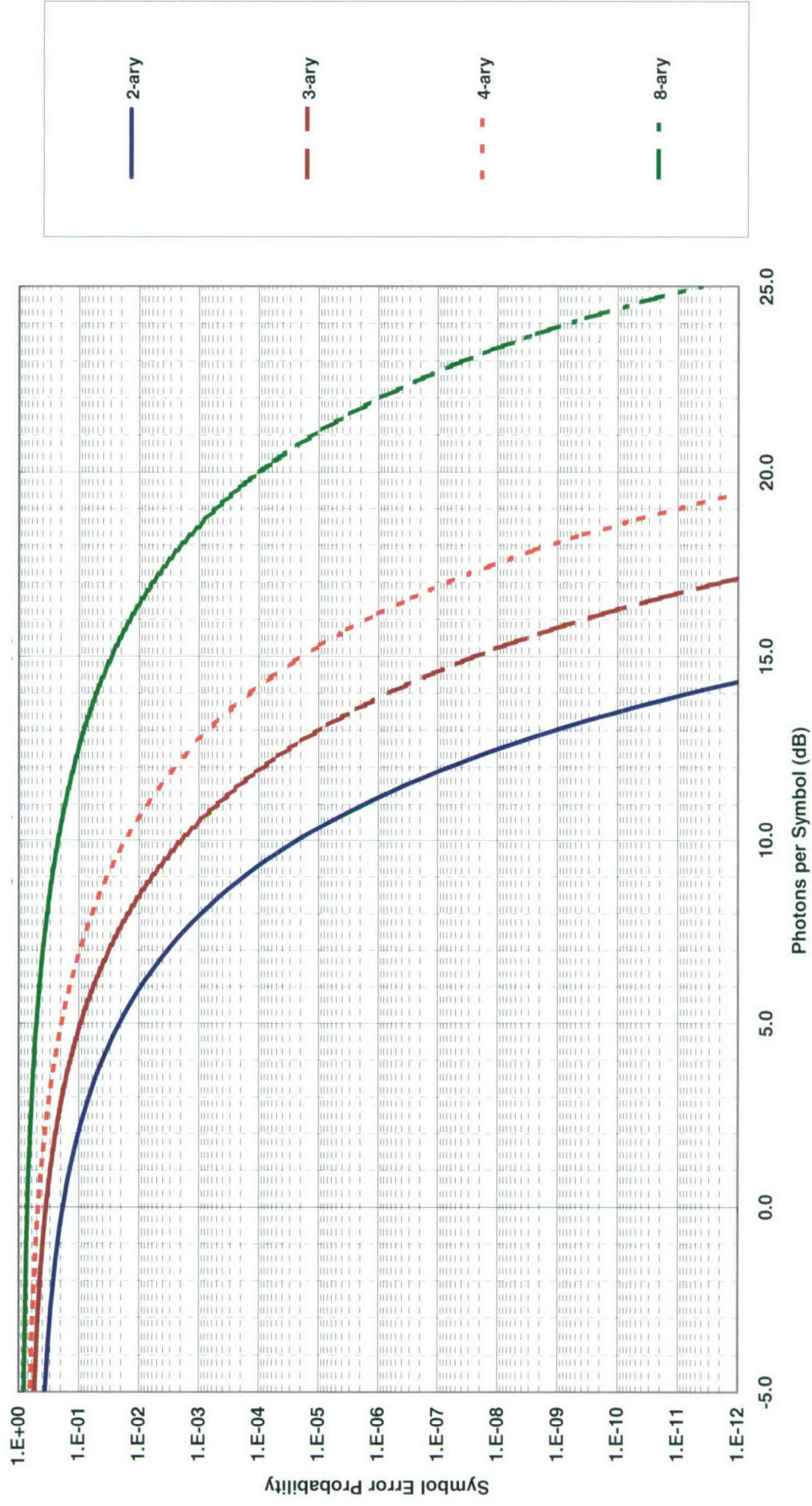


Chart 119. Symbol error probability: MPSK heterodyne or preamplified noncoherent.

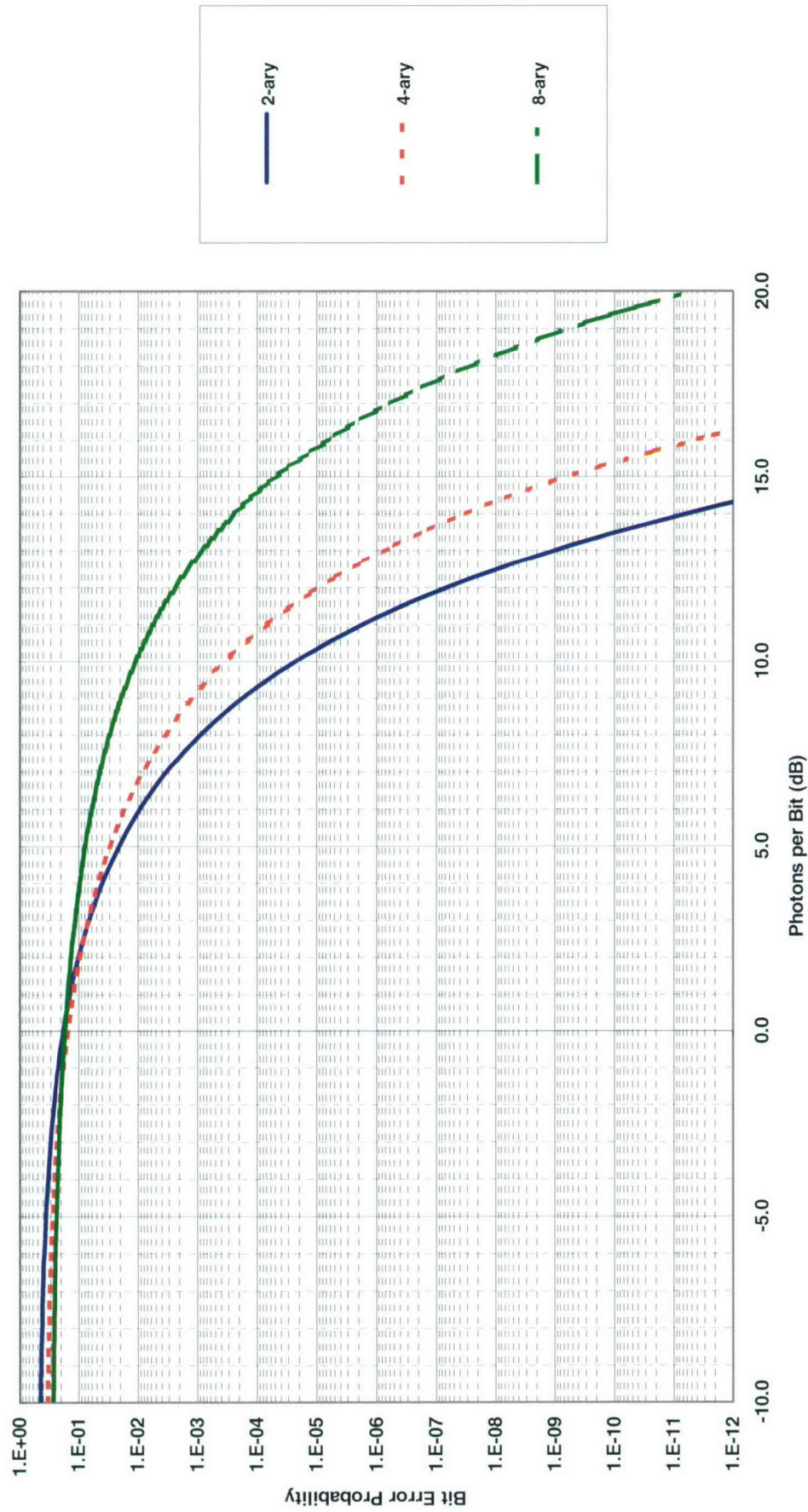


Chart 120. Bit-error probability: MPSK heterodyne or preamplified noncoherent.

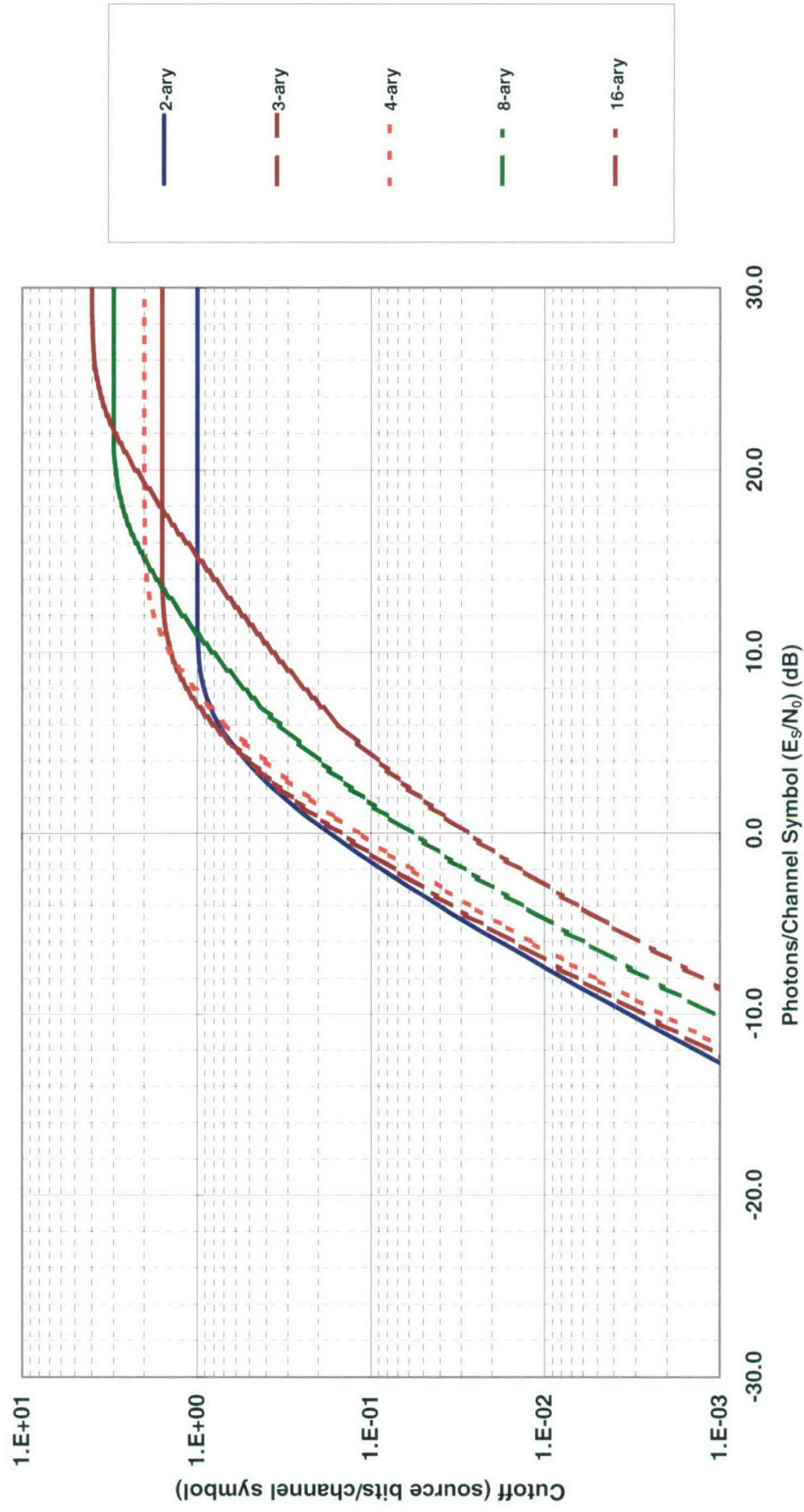


Chart 121. Classical cutoff: MPSK heterodyne or preamplified noncoherent hard decision pure hard decision.

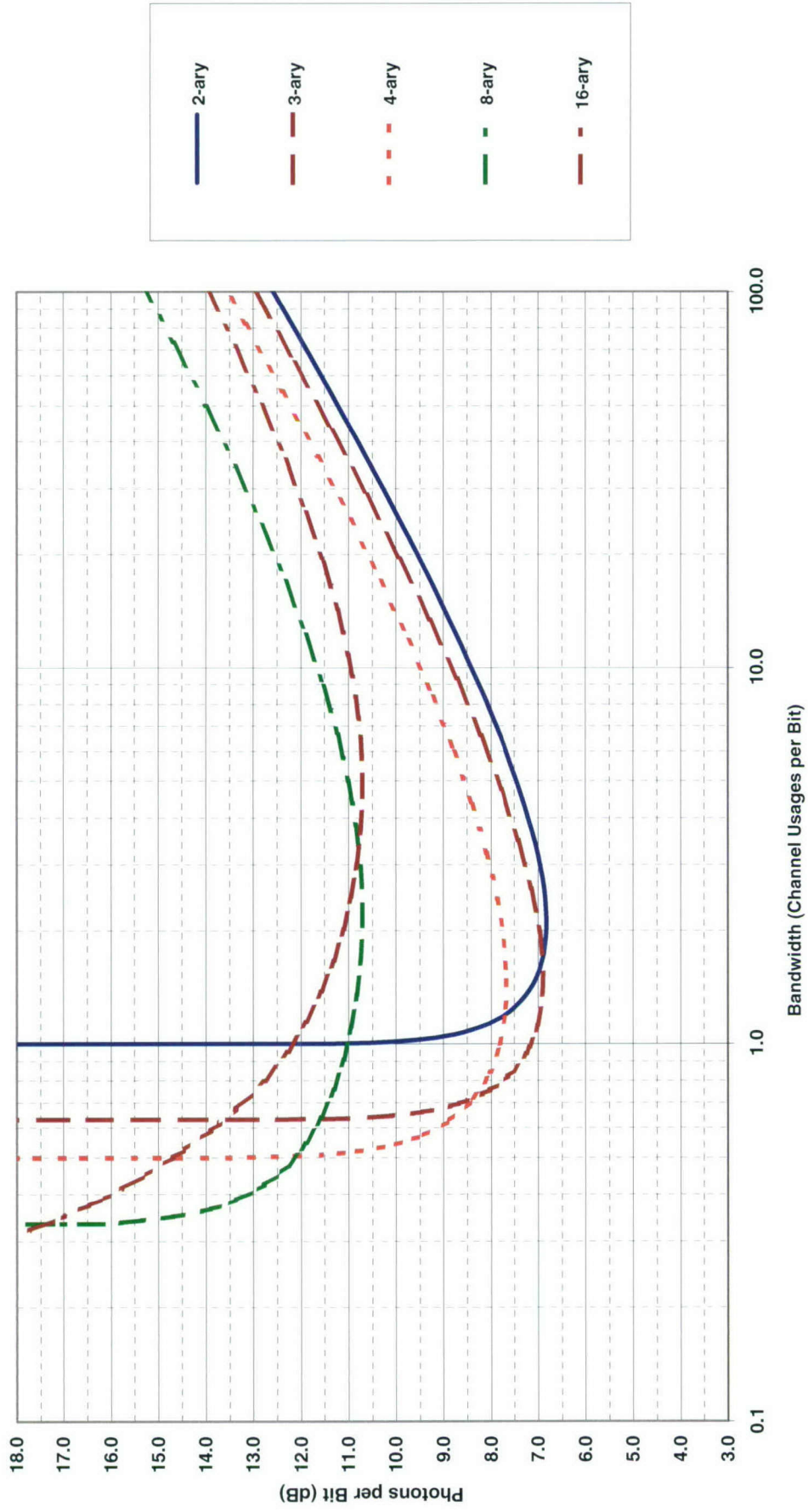


Chart 122. Efficiency at classical cutoff: MPSK heterodyne or preamplified noncoherent hard decision pure hard decision.

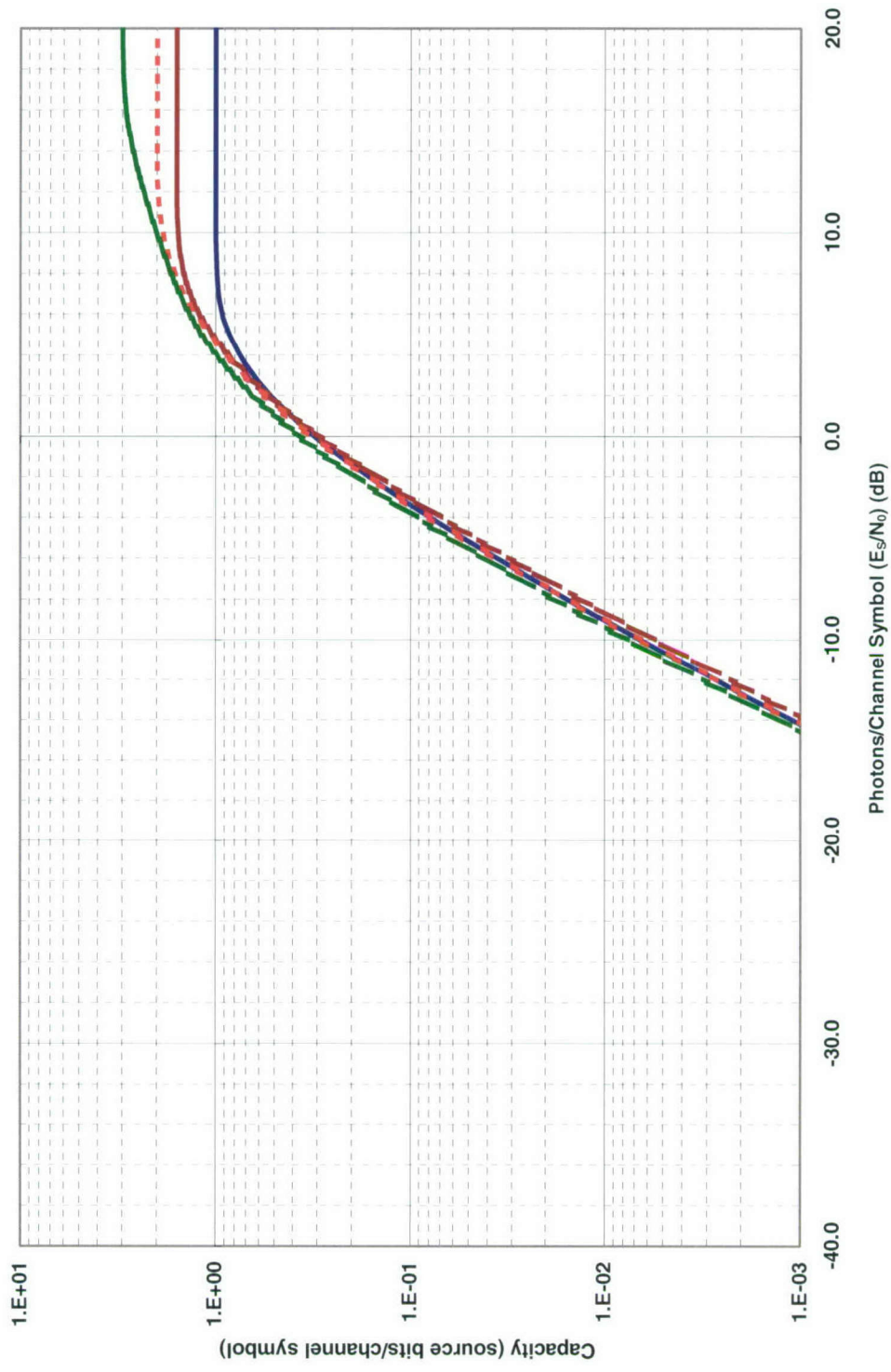


Chart 123. Classical capacity: MPSK heterodyne or preamplified noncoherent hard decision with ML decoding.

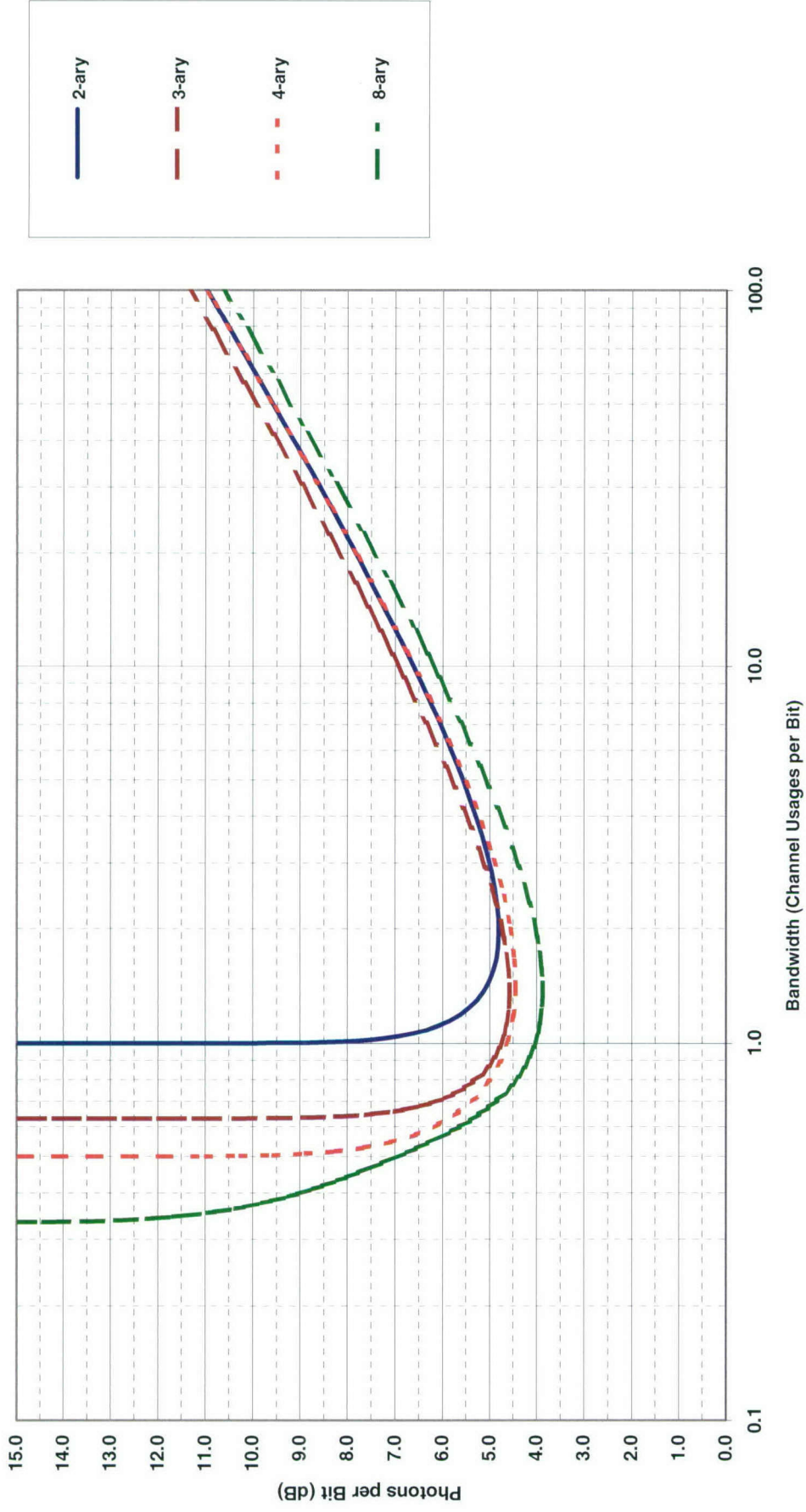


Chart 124. Efficiency at classical capacity: MPSK heterodyne or preamplified noncoherent hard decision with ML decoding.

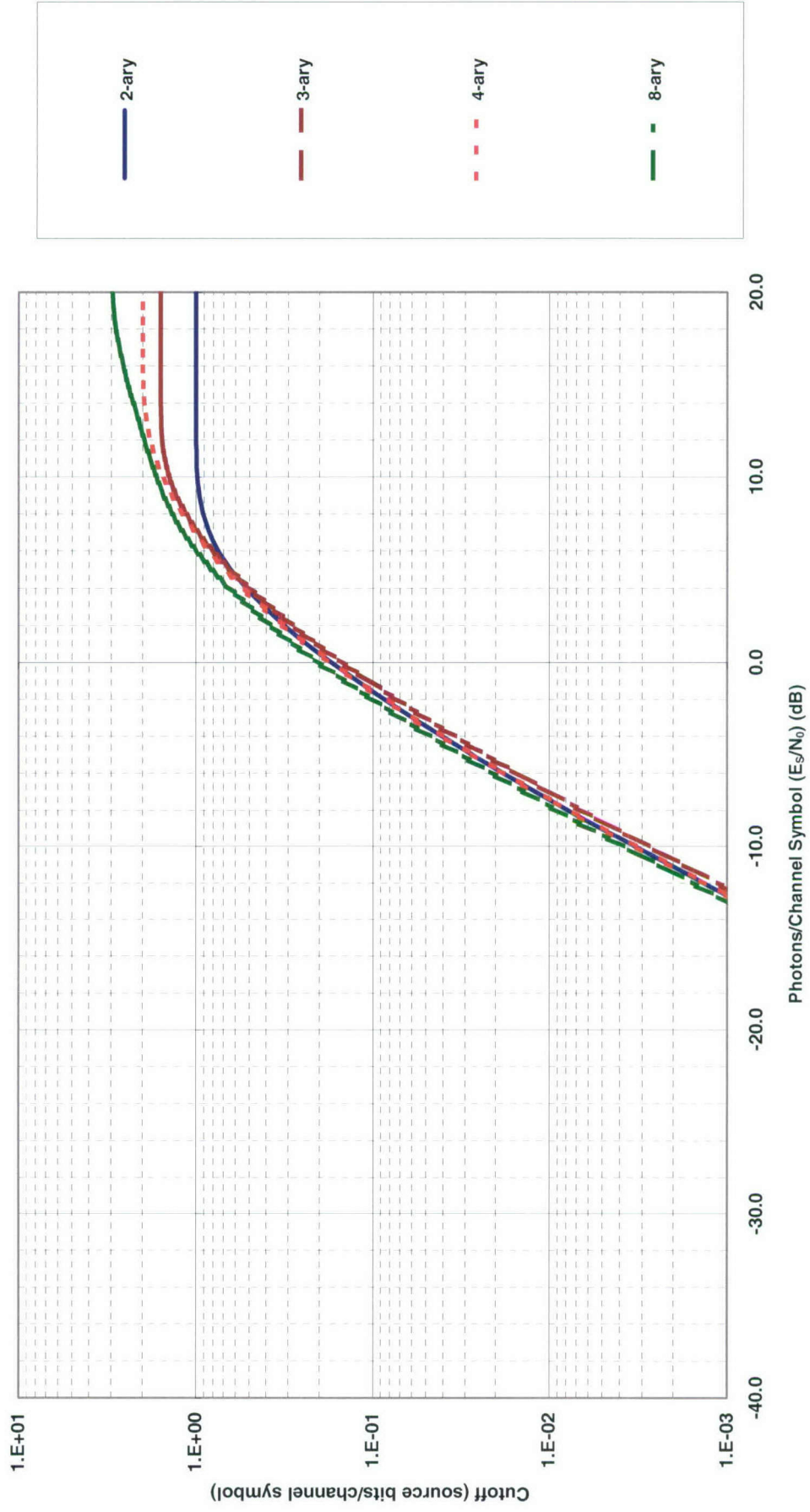


Chart 125. Classical cutoff: MPSK heterodyne or preamplified noncoherent hard decision with ML decoding.

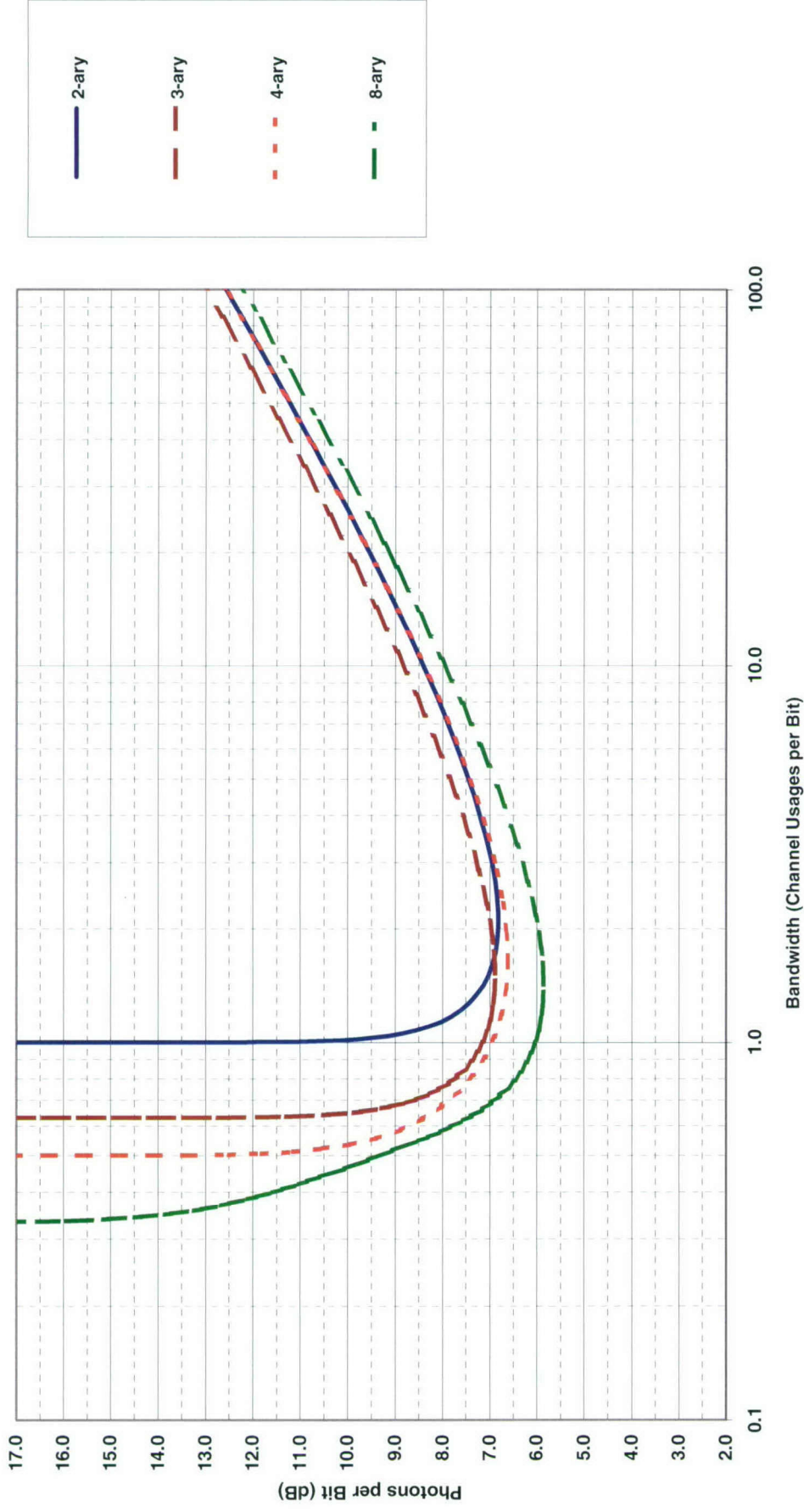


Chart 126. Efficiency at classical cutoff: MPSK heterodyne or preamplified noncoherent hard decision with ML decoding.

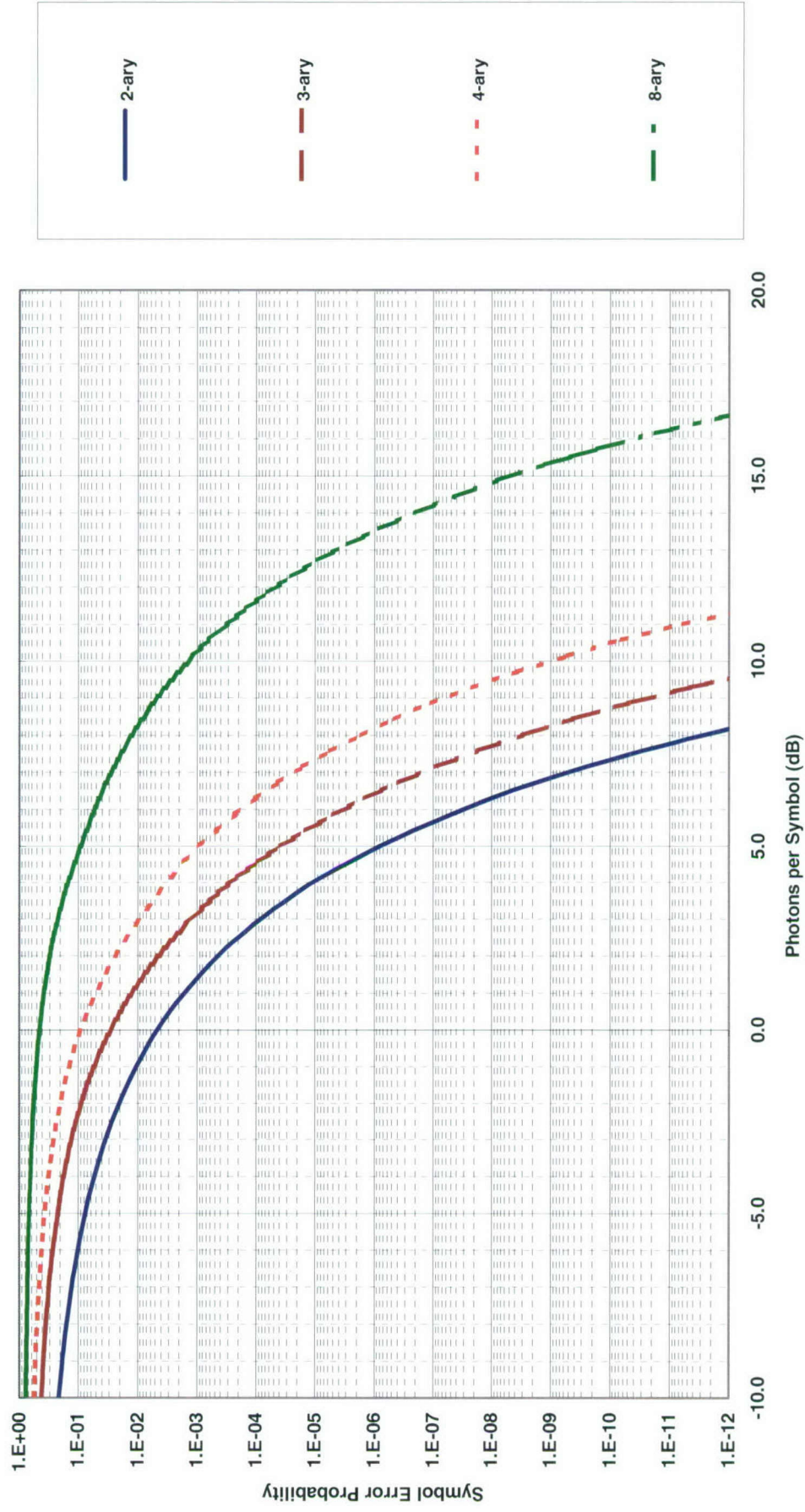


Chart 127. Symbol error probability: MPSK quantum hard decision (semiclassical).

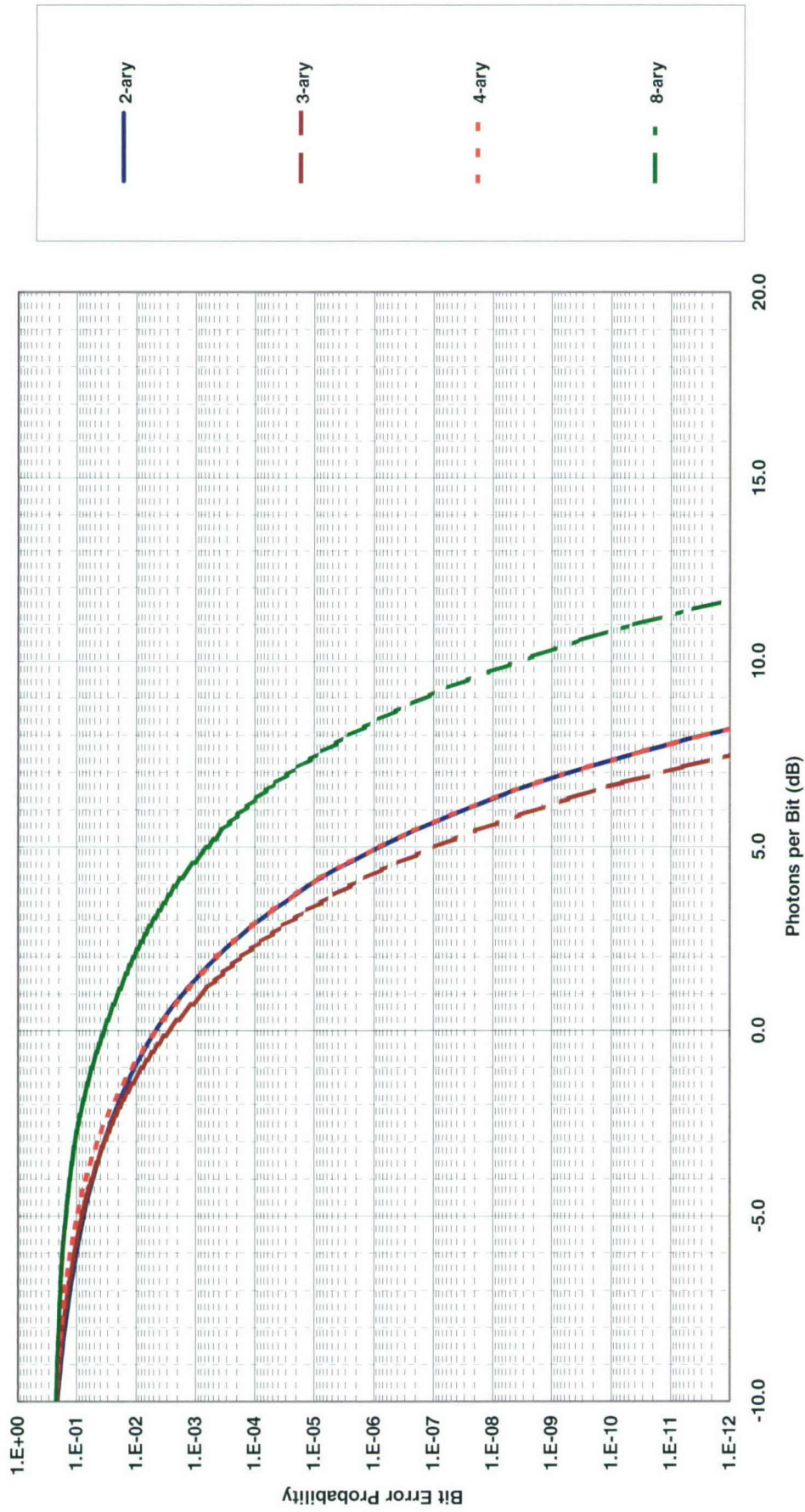


Chart 128. Bit-error probability: MPSK quantum hard decision (semiclassical).

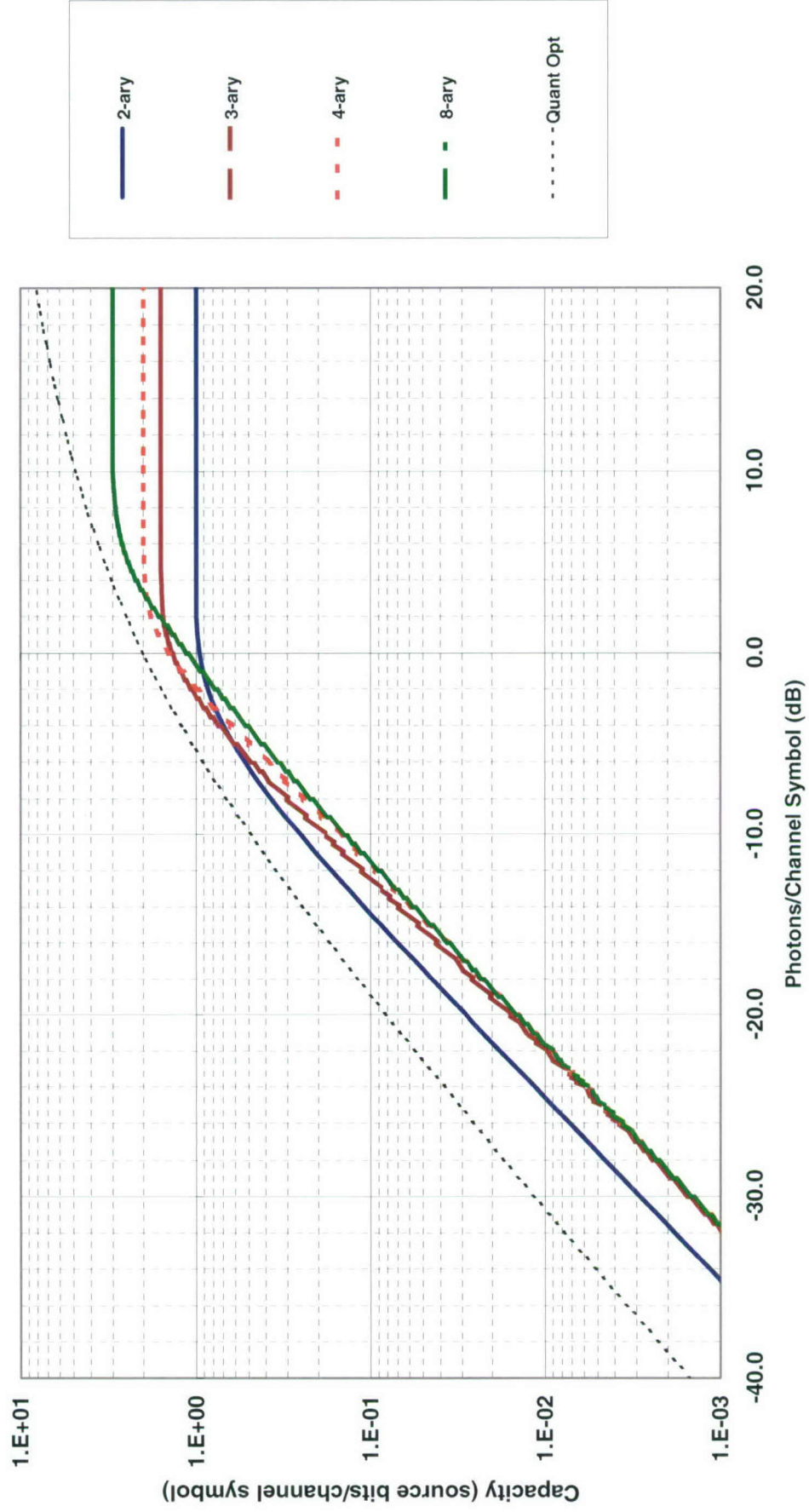


Chart 129. Classical capacity: MPSK quantum hard decision (semiclassical) with ML decoding.

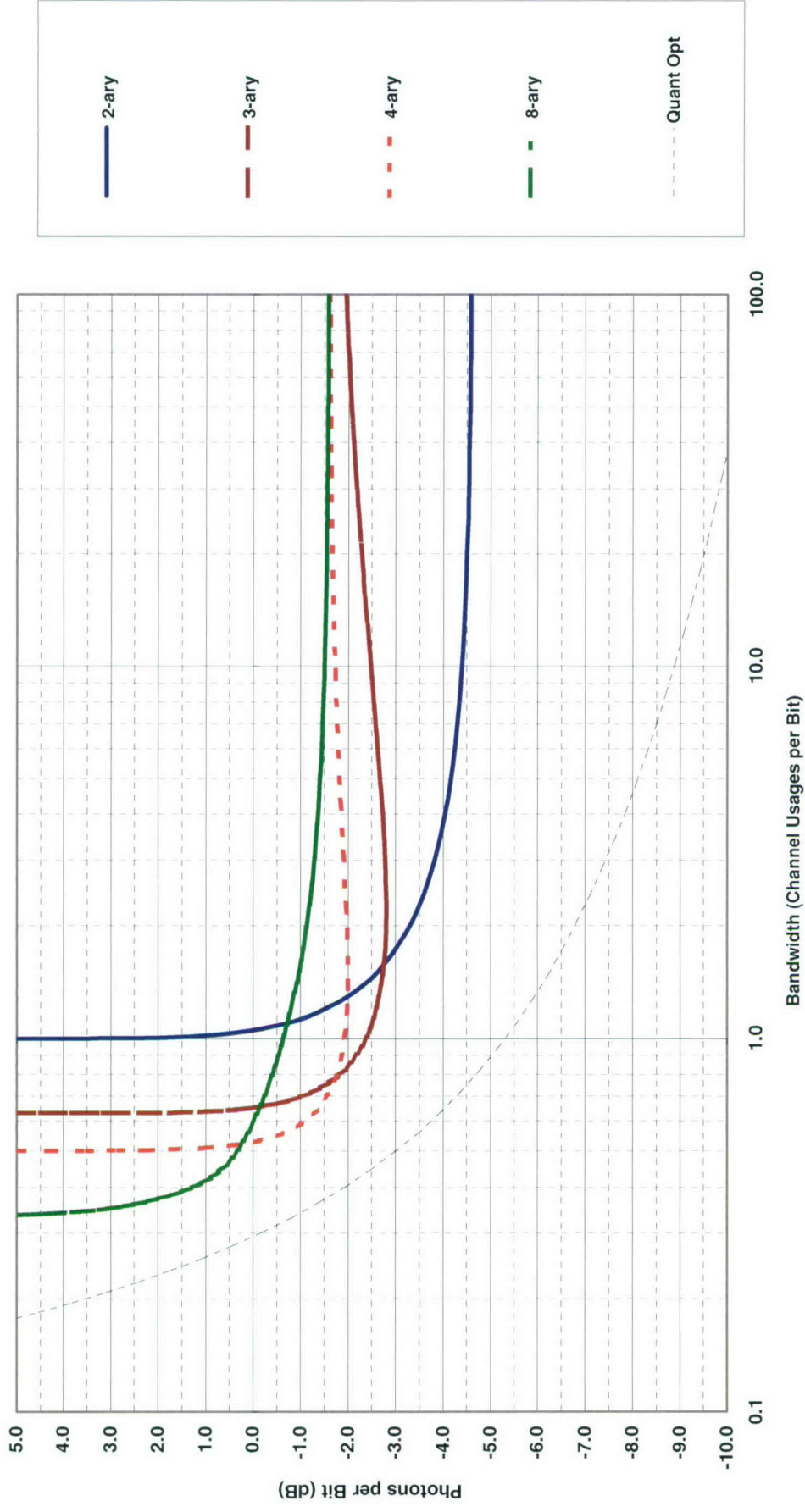


Chart 130. Efficiency at classical capacity: MPSK quantum hard decision (semiclassical) with ML decoding.

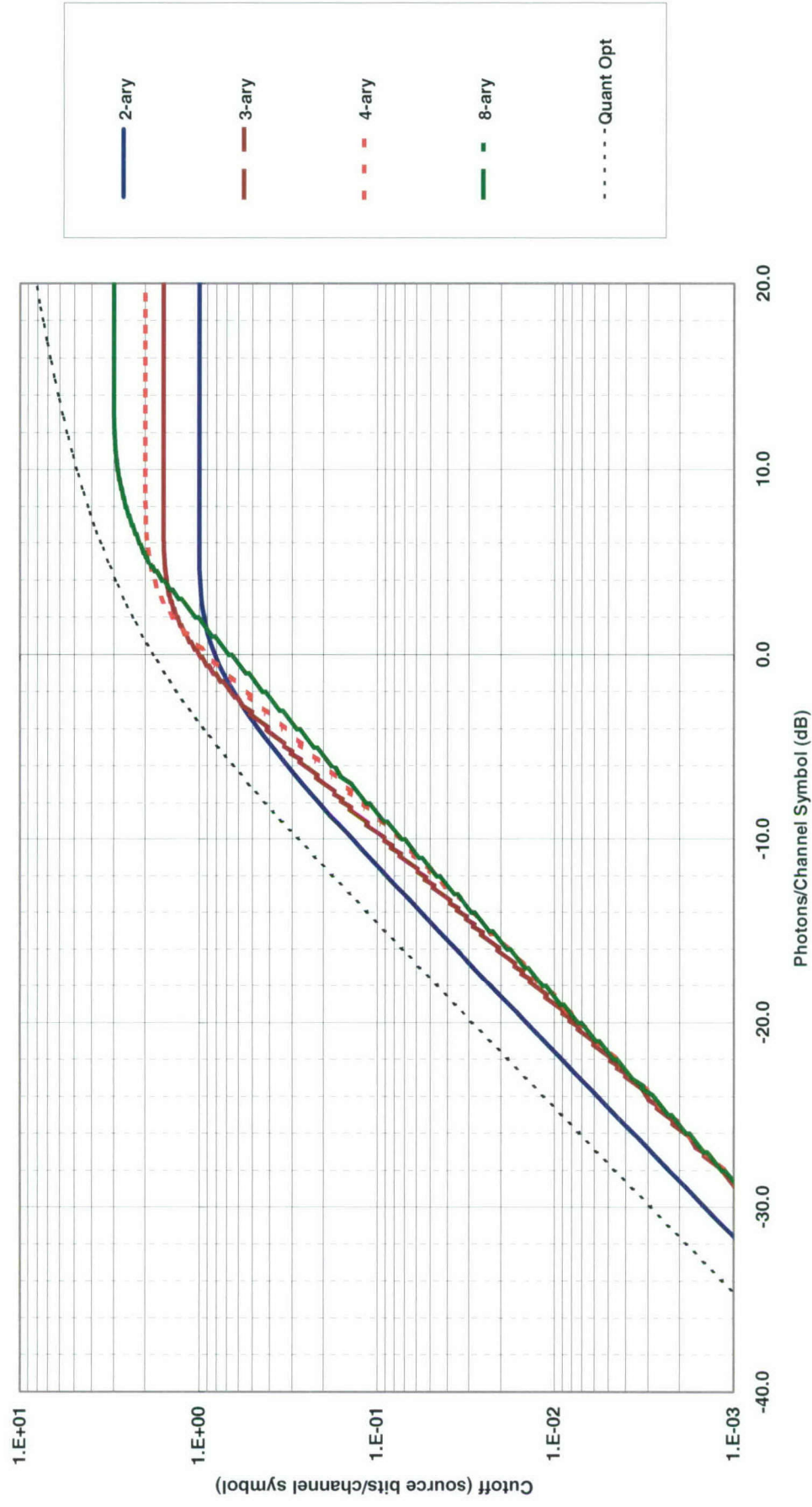


Chart 131. Classical cutoff: MPSK quantum hard decision (semiclassical) with ML decoding.

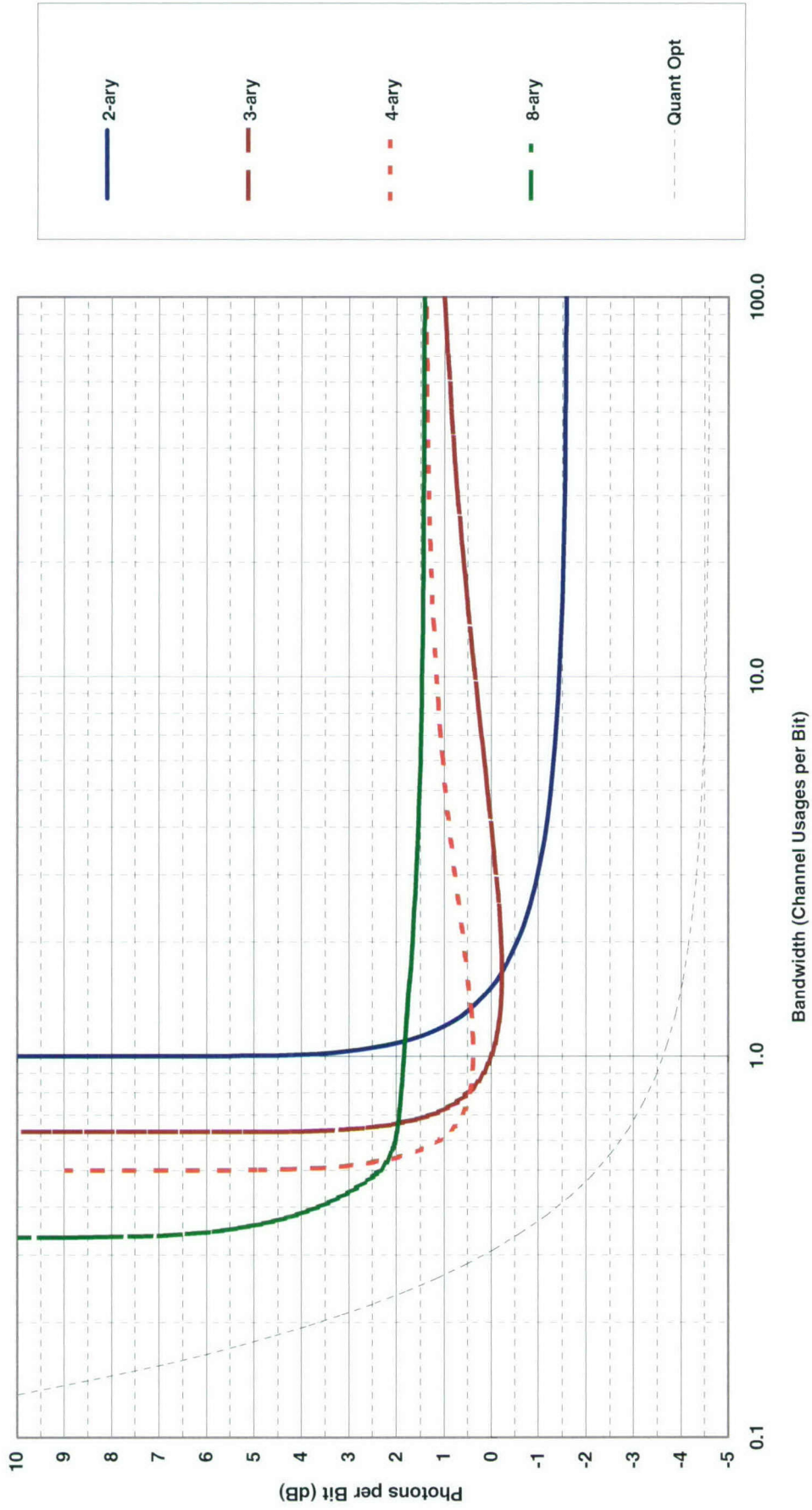


Chart 132. Efficiency at classical cutoff: MPSK quantum hard decision (semiclassical) with ML decoding.

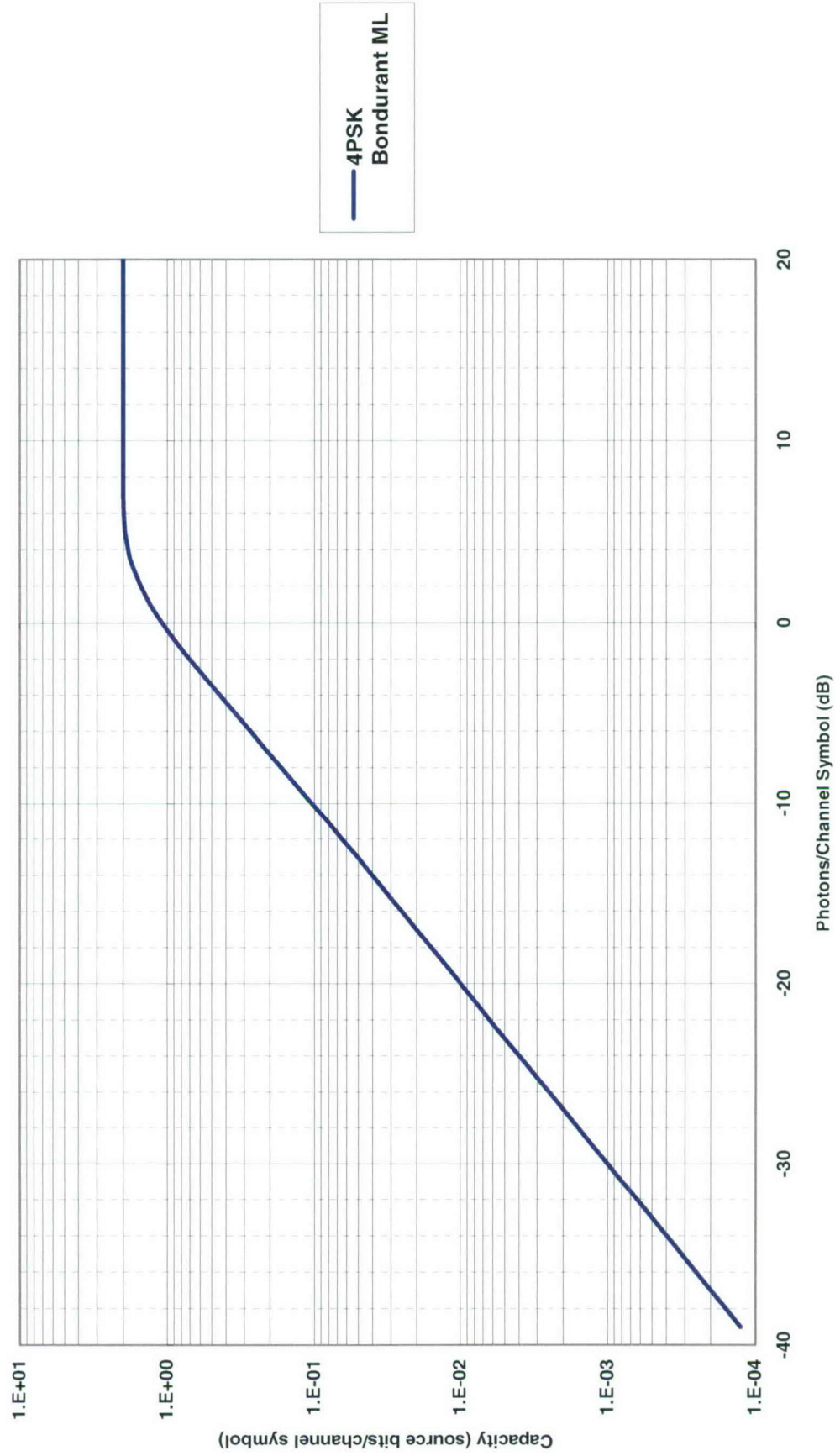


Chart 133. Classical capacity: 4PSK photon counting hard decision with ML decoding.

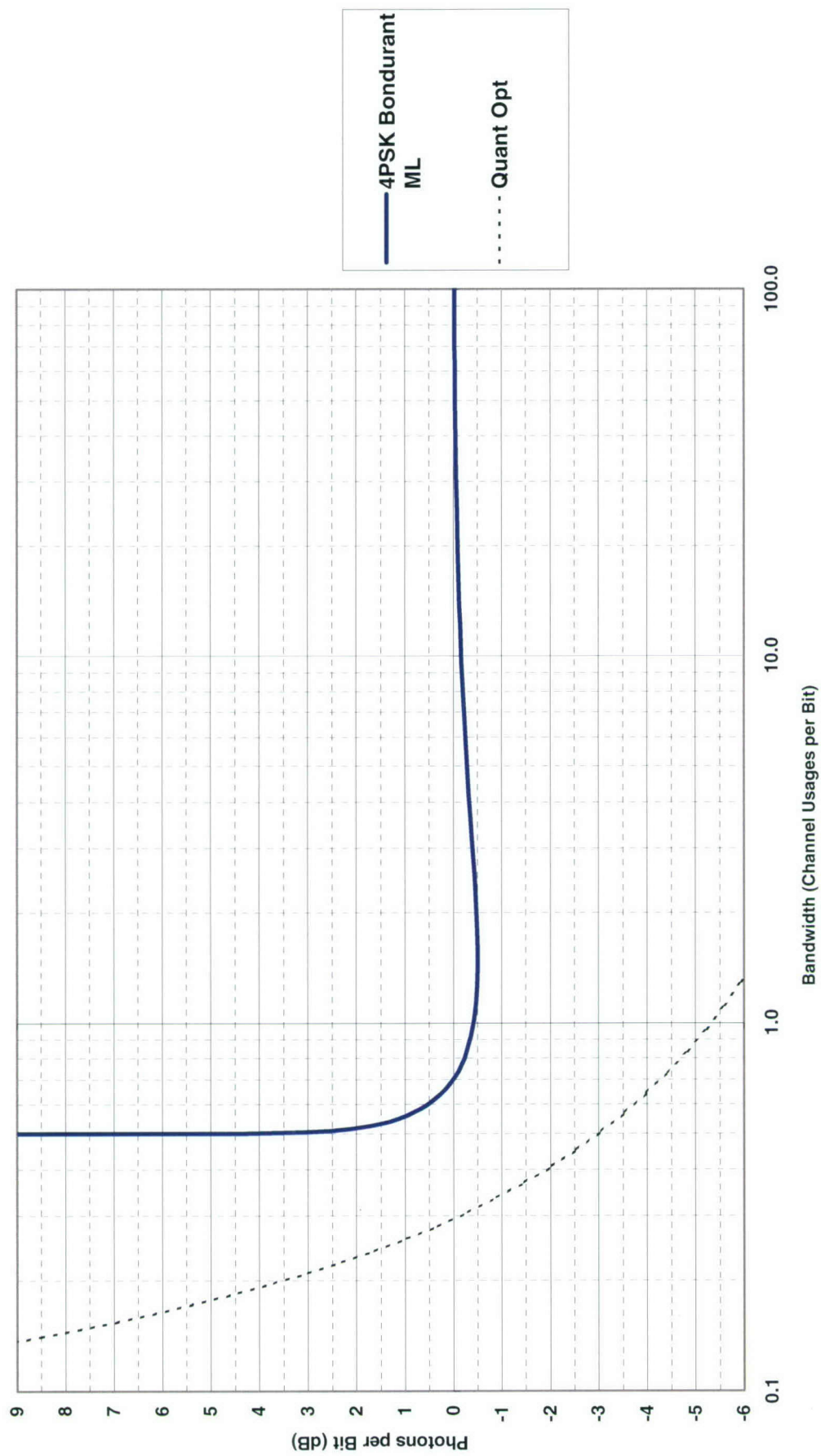


Chart 134. Efficiency at classical capacity: 4PSK photon counting hard decision with ML decoding.

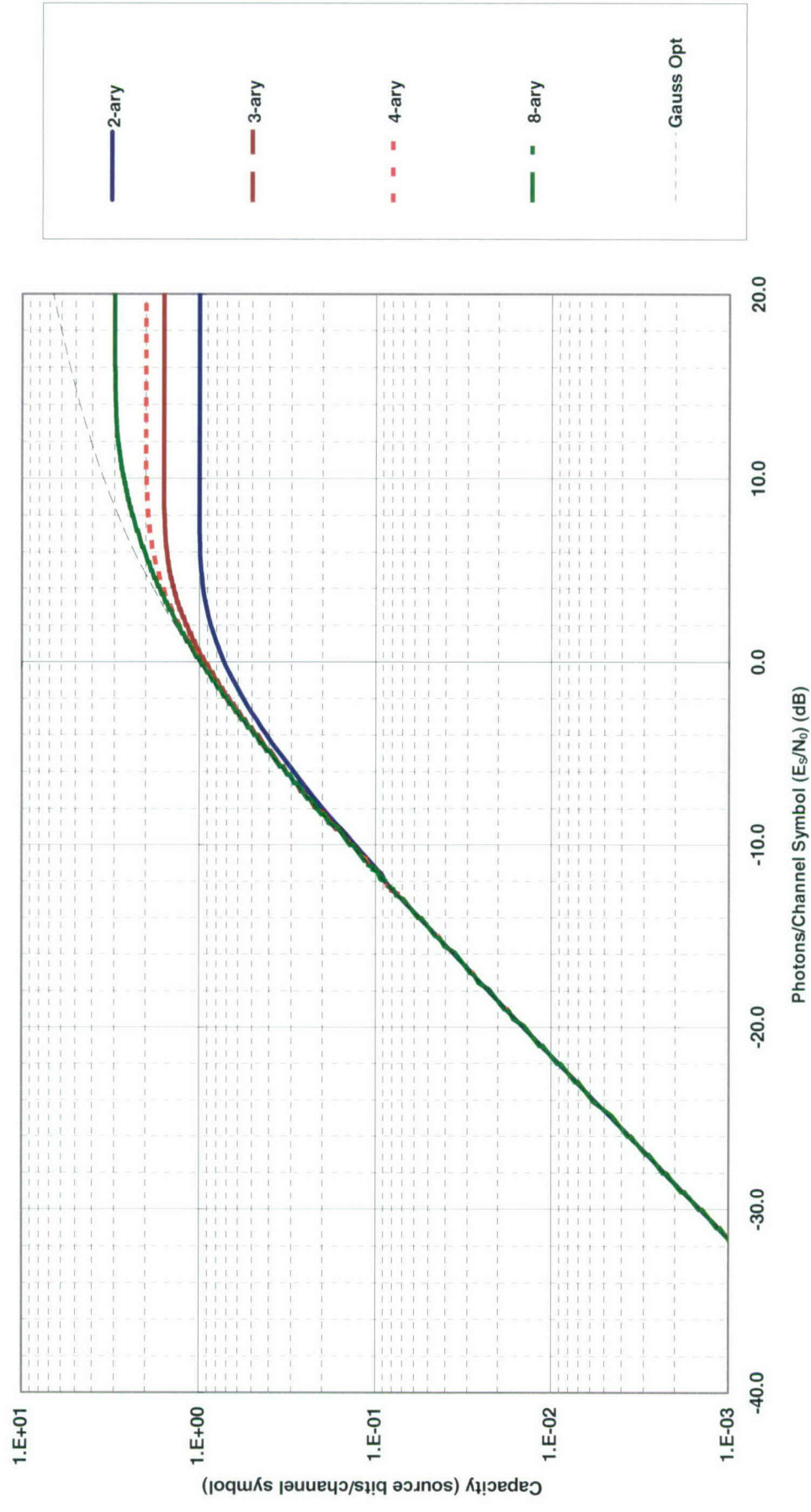


Chart 135. Classical capacity: MPSK heterodyne or preamplified coherent soft decision.

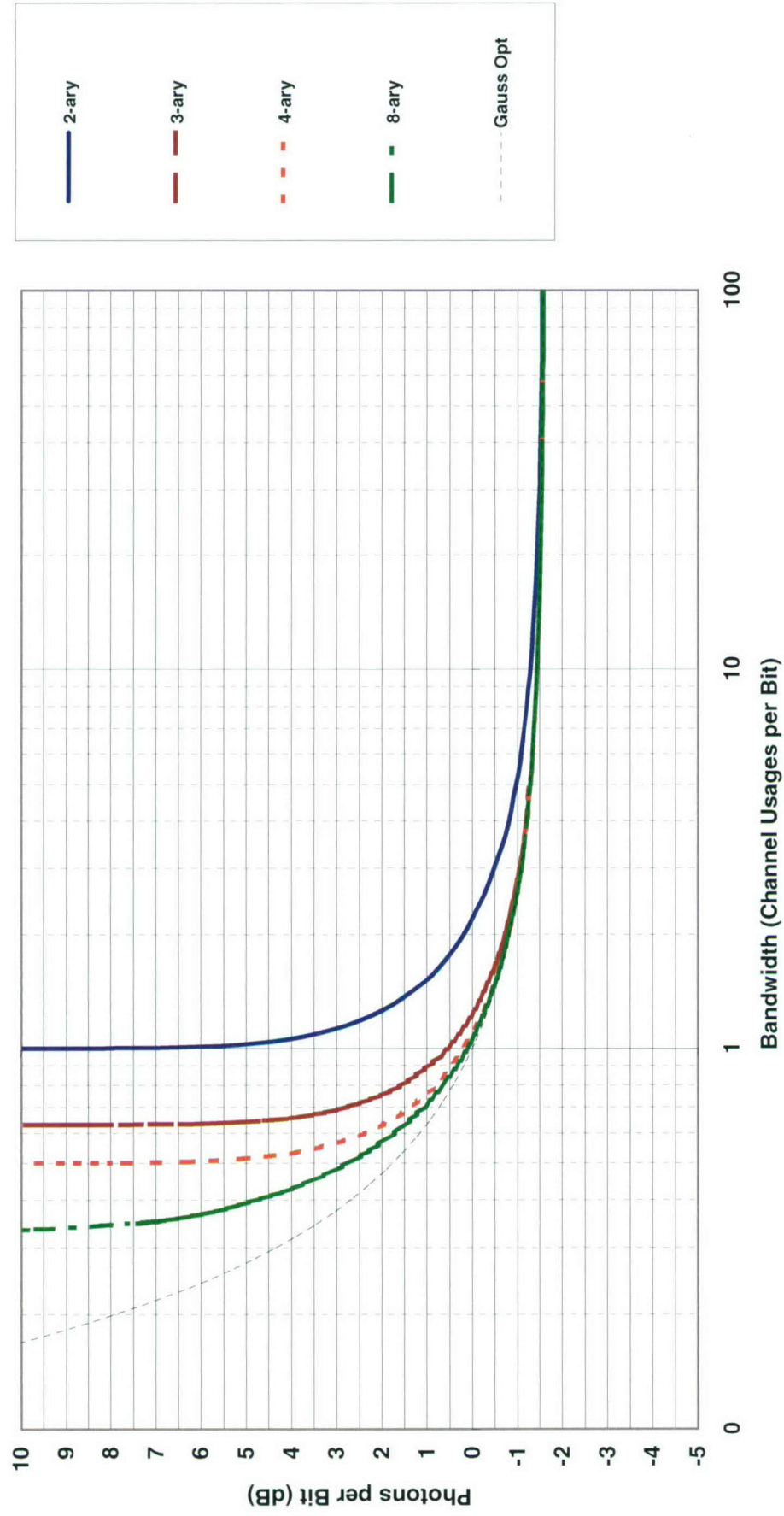


Chart 136. Efficiency at classical capacity: MPSK heterodyne or preamplified coherent soft decision.

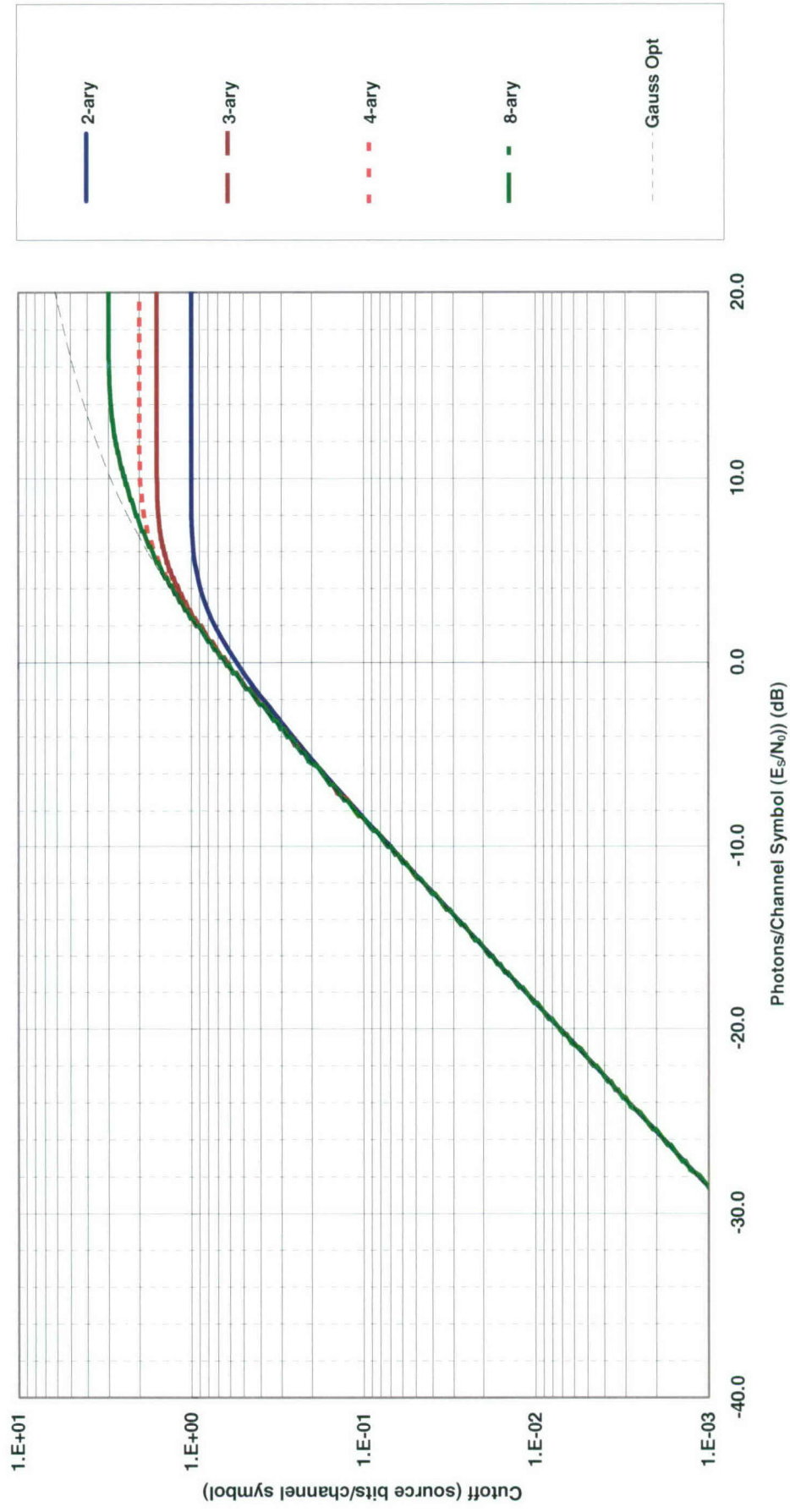


Chart 137. Classical cutoff: MPSK heterodyne or preamplified coherent soft decision.

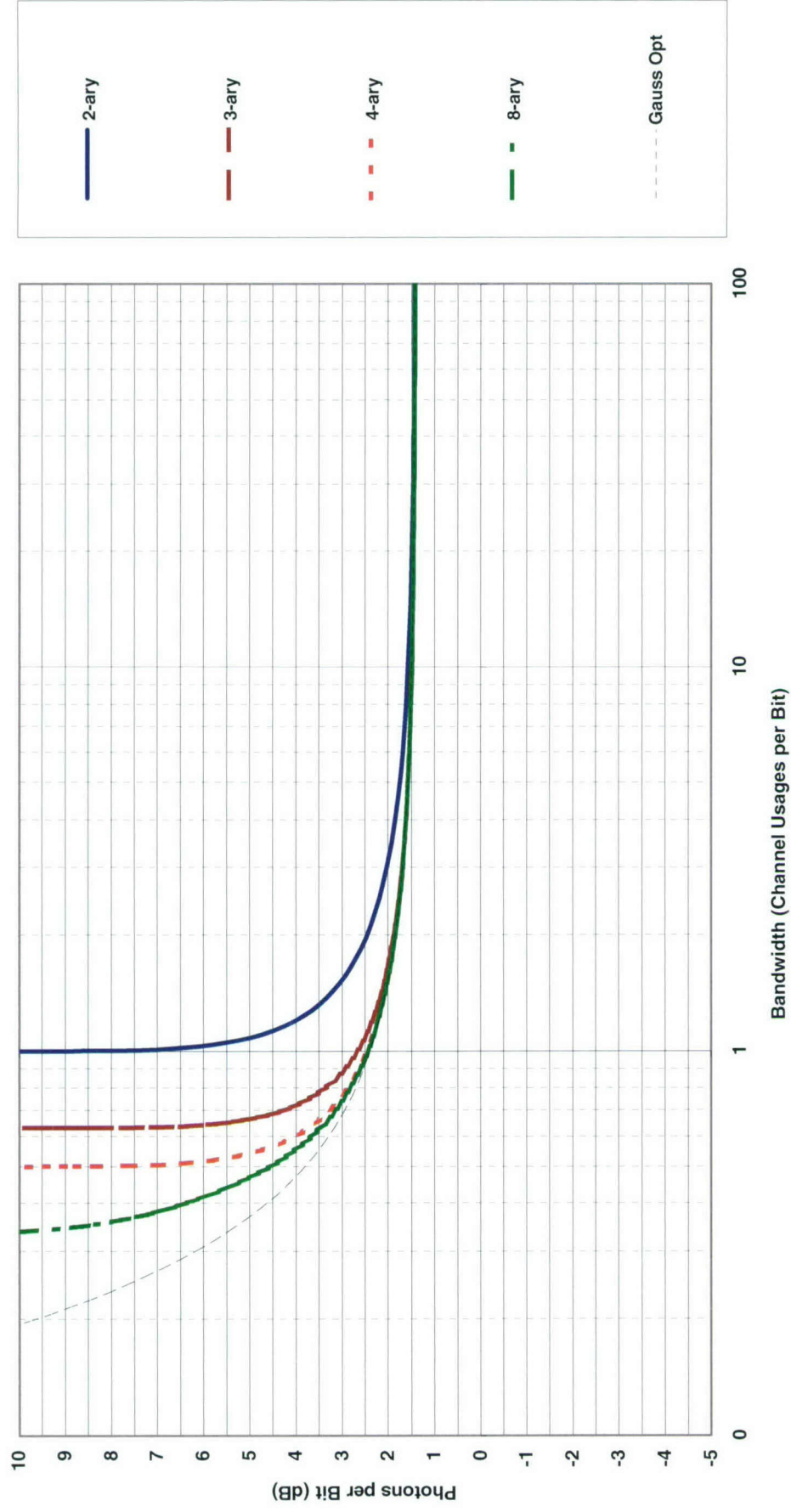


Chart 138. Efficiency at classical cutoff: MPSK heterodyne or preamplified coherent soft decision.

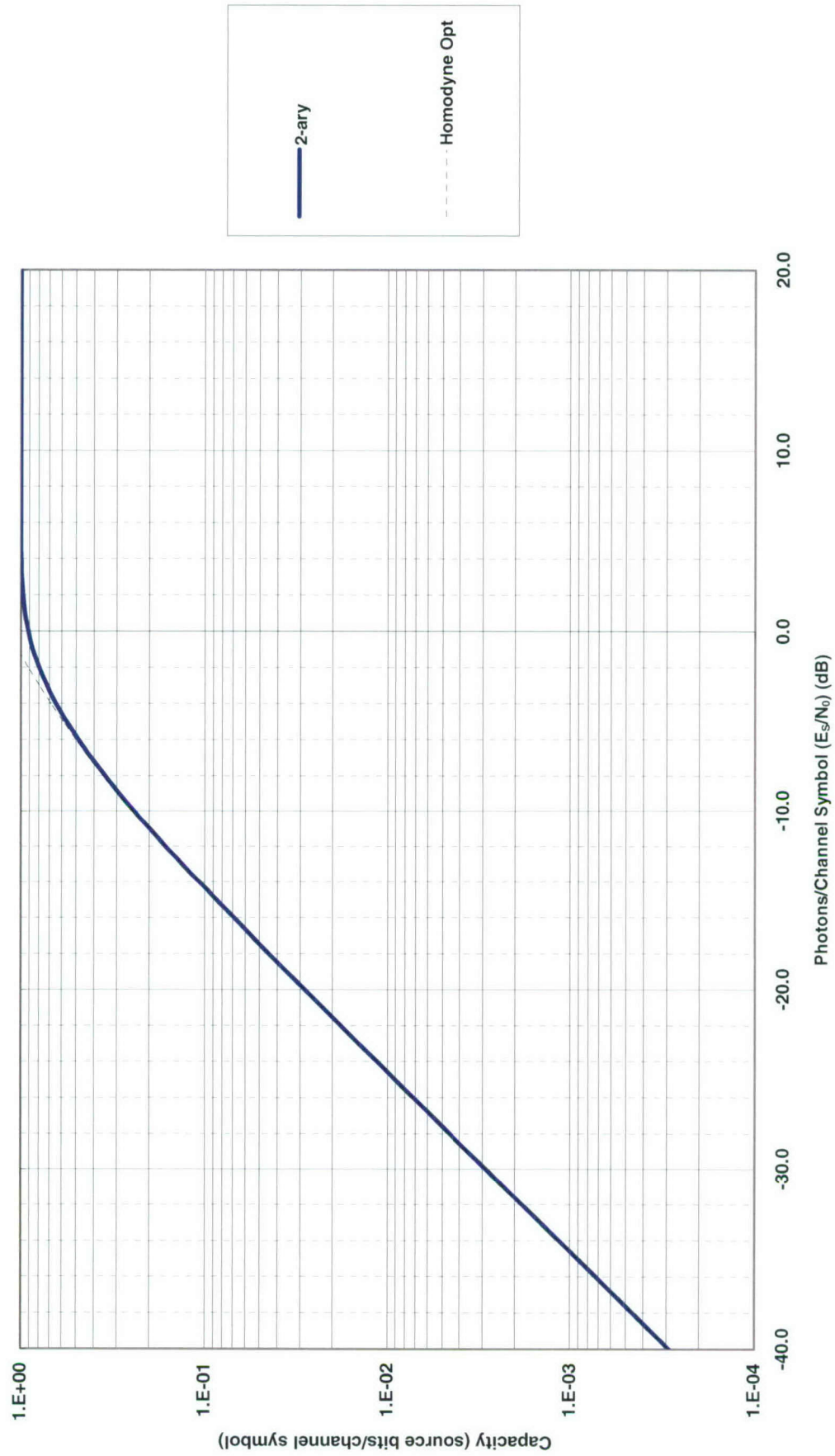


Chart 139. Classical capacity: MPSK homodyne coherent soft decision.

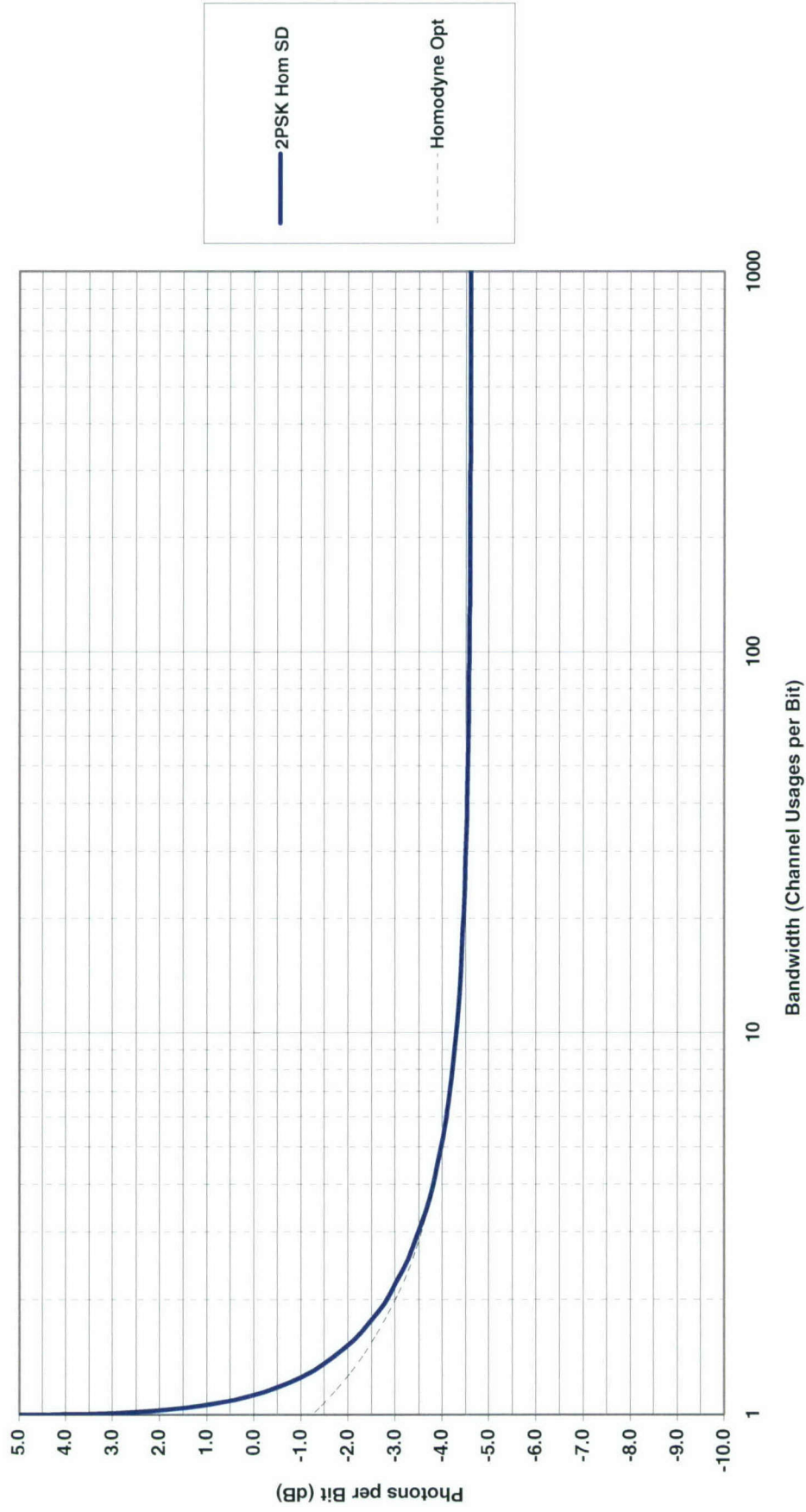


Chart 140. Efficiency at classical capacity: MPSK homodyne coherent soft decision.

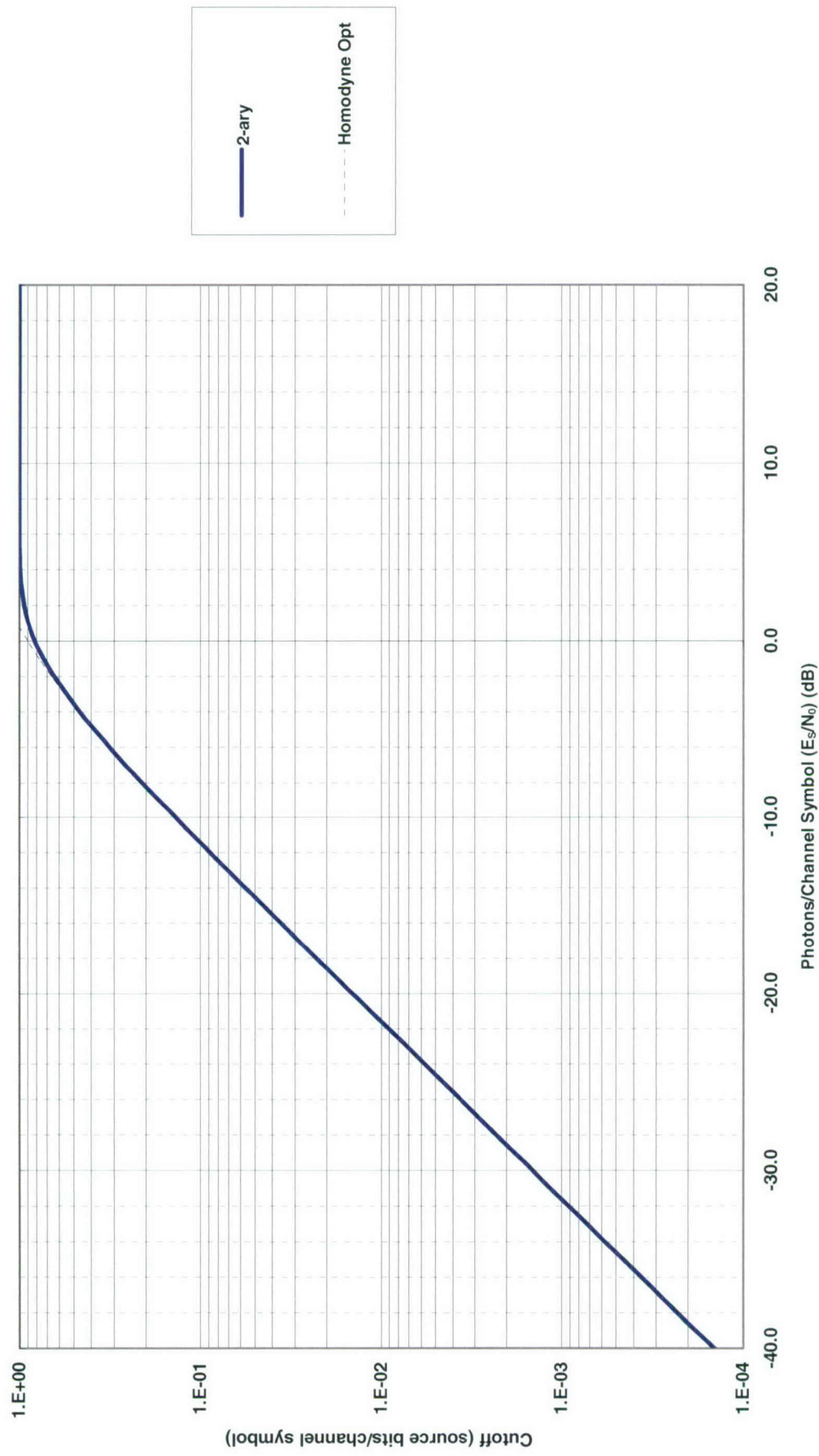


Chart 141. Classical cutoff: MPSK homodyne coherent soft decision.

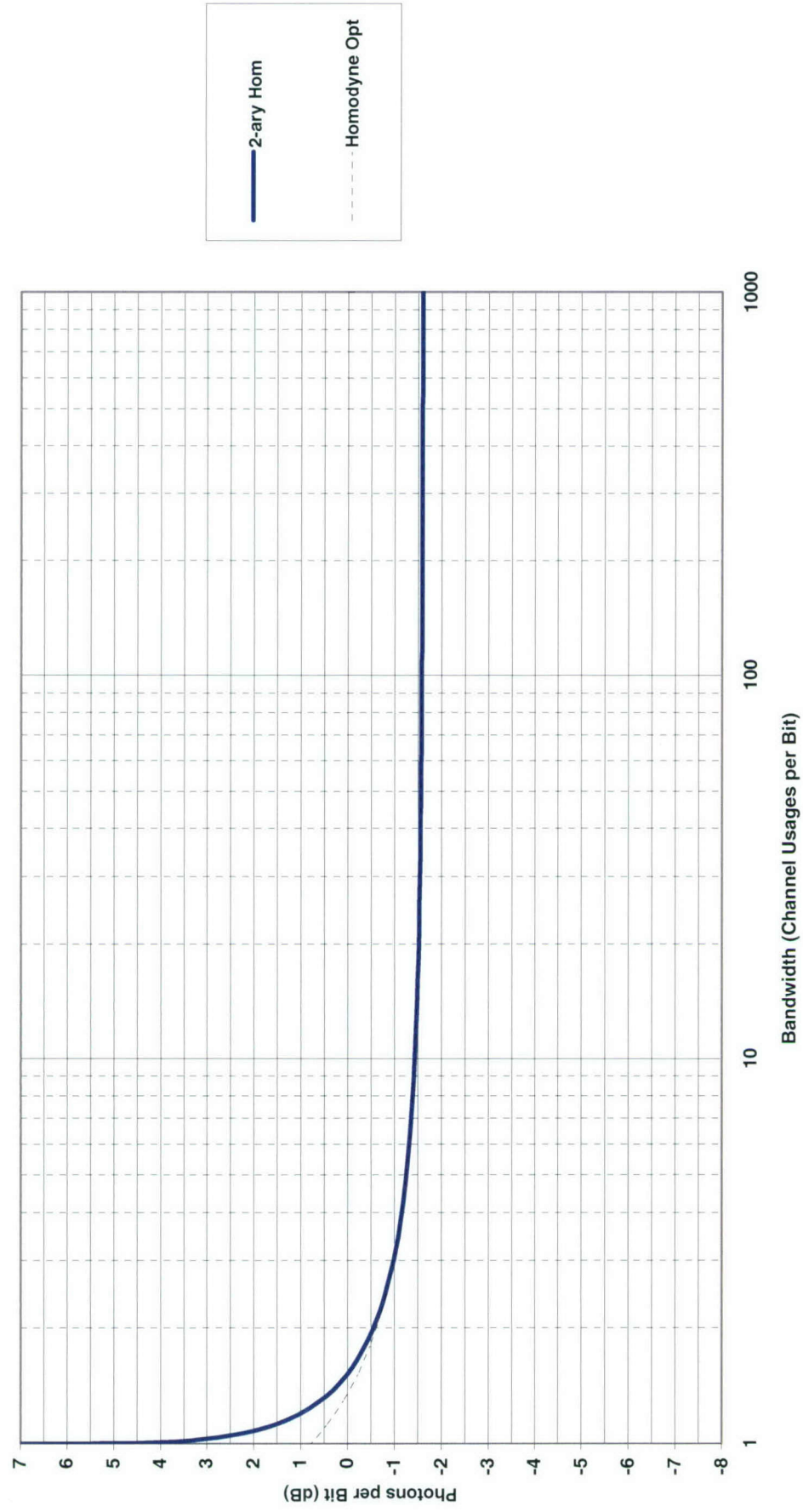


Chart 142. Efficiency at classical cutoff: MPSK homodyne coherent soft decision.

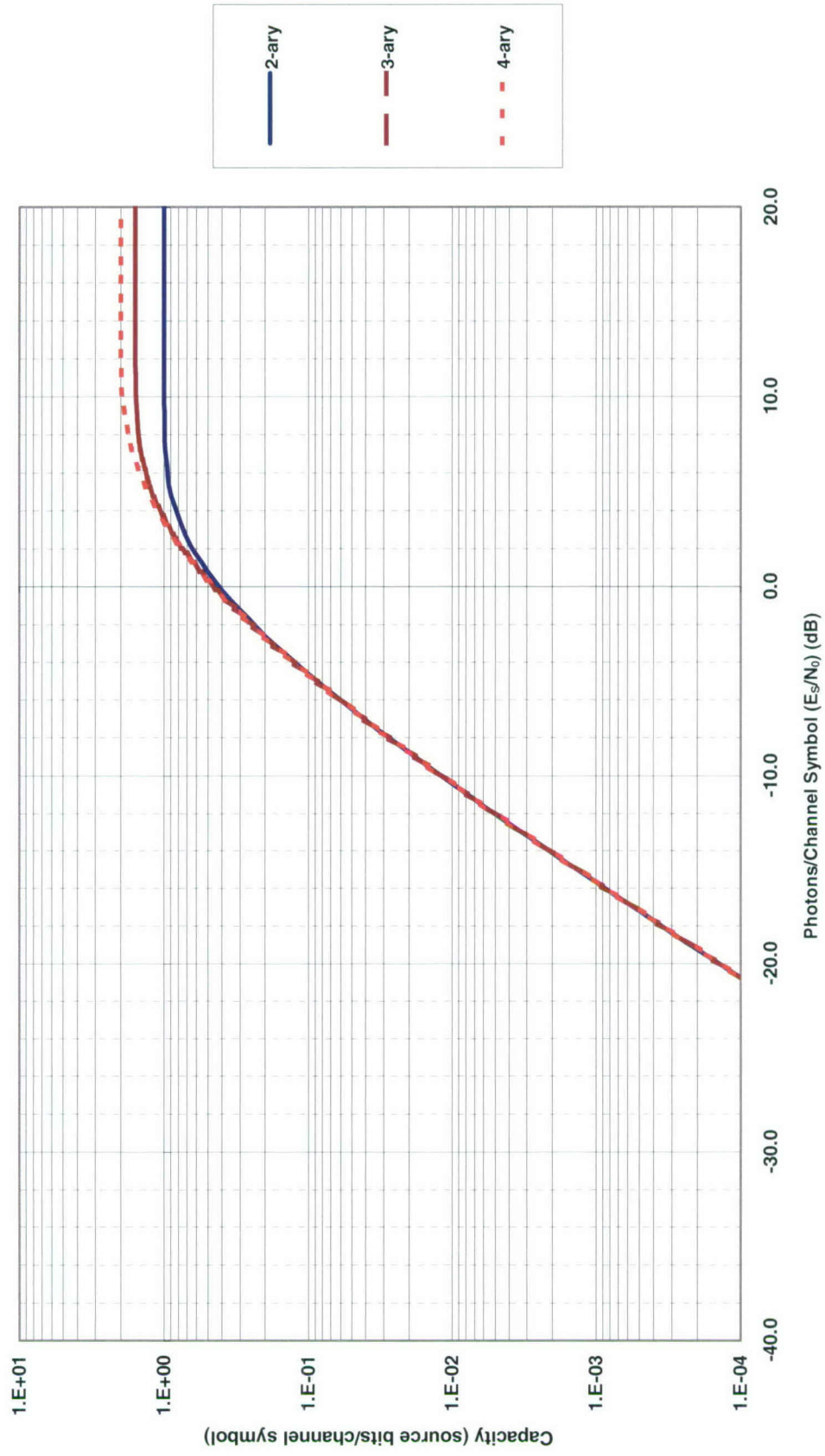


Chart 143. Classical capacity: MPSK heterodyne or preamplified noncoherent soft decision.

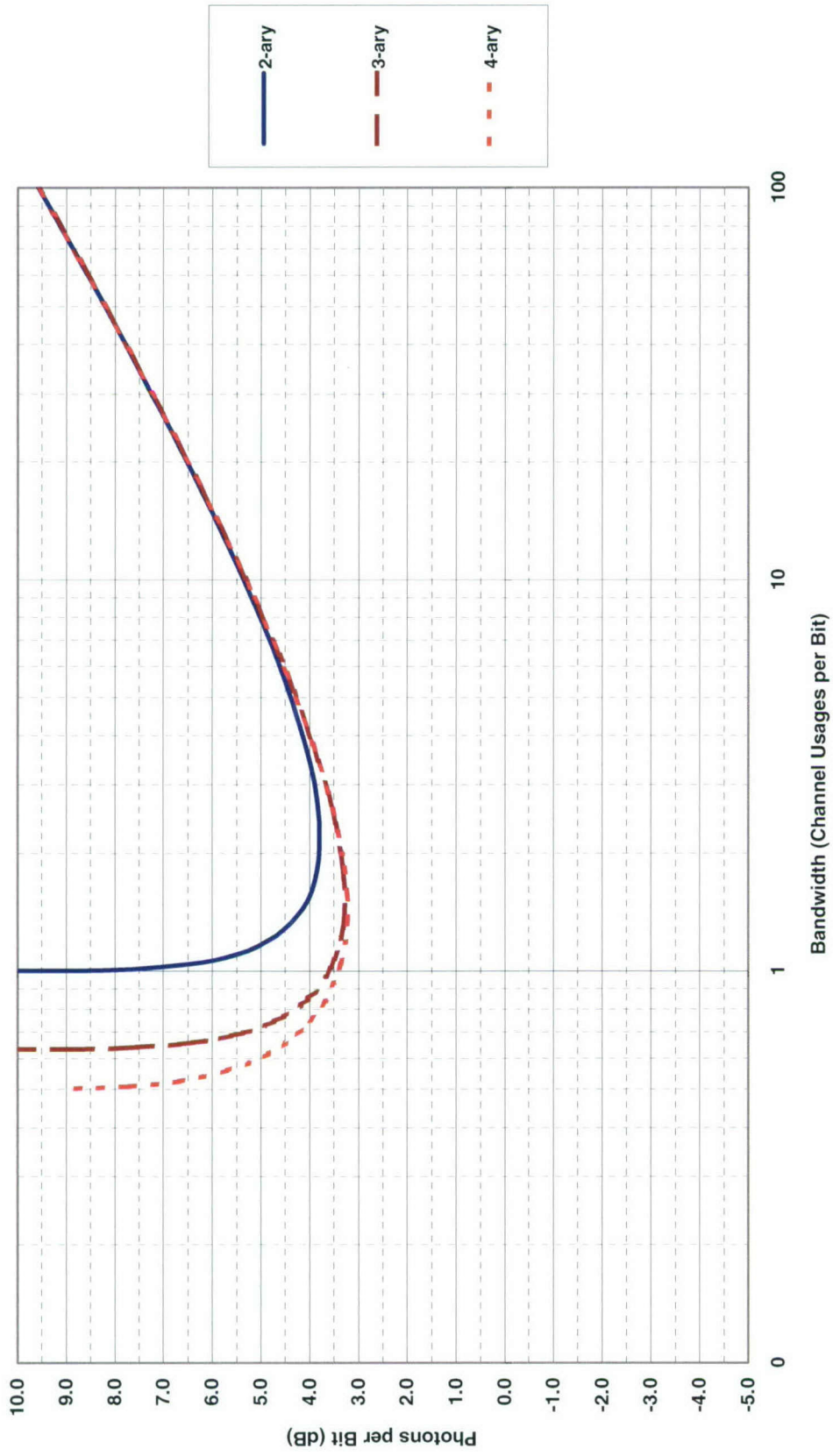


Chart 144. Efficiency at classical capacity: MPSK heterodyne or preamplified noncoherent soft decision.

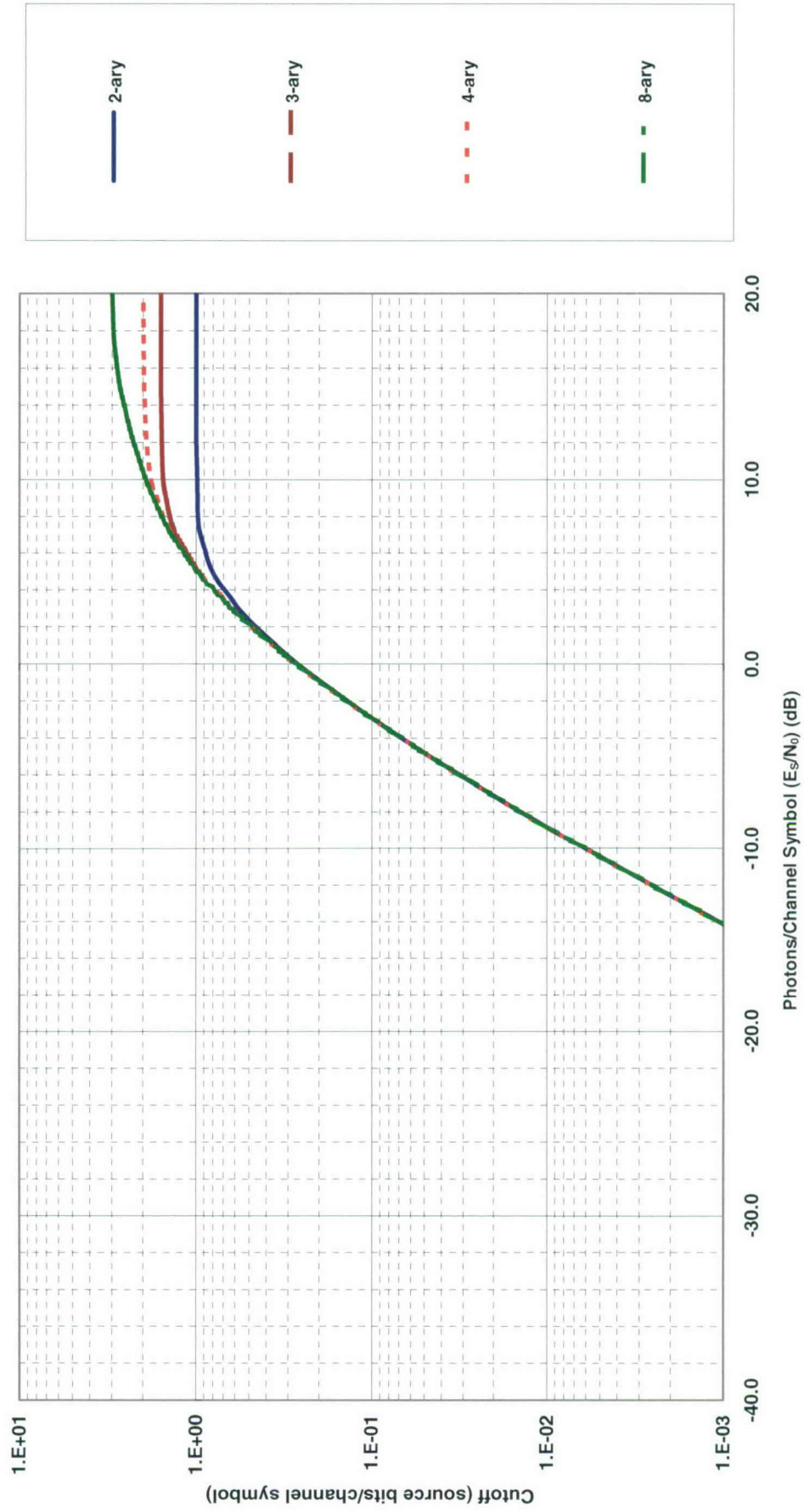


Chart 145. Classical cutoff: MPSK heterodyne or preamplified noncoherent soft decision.

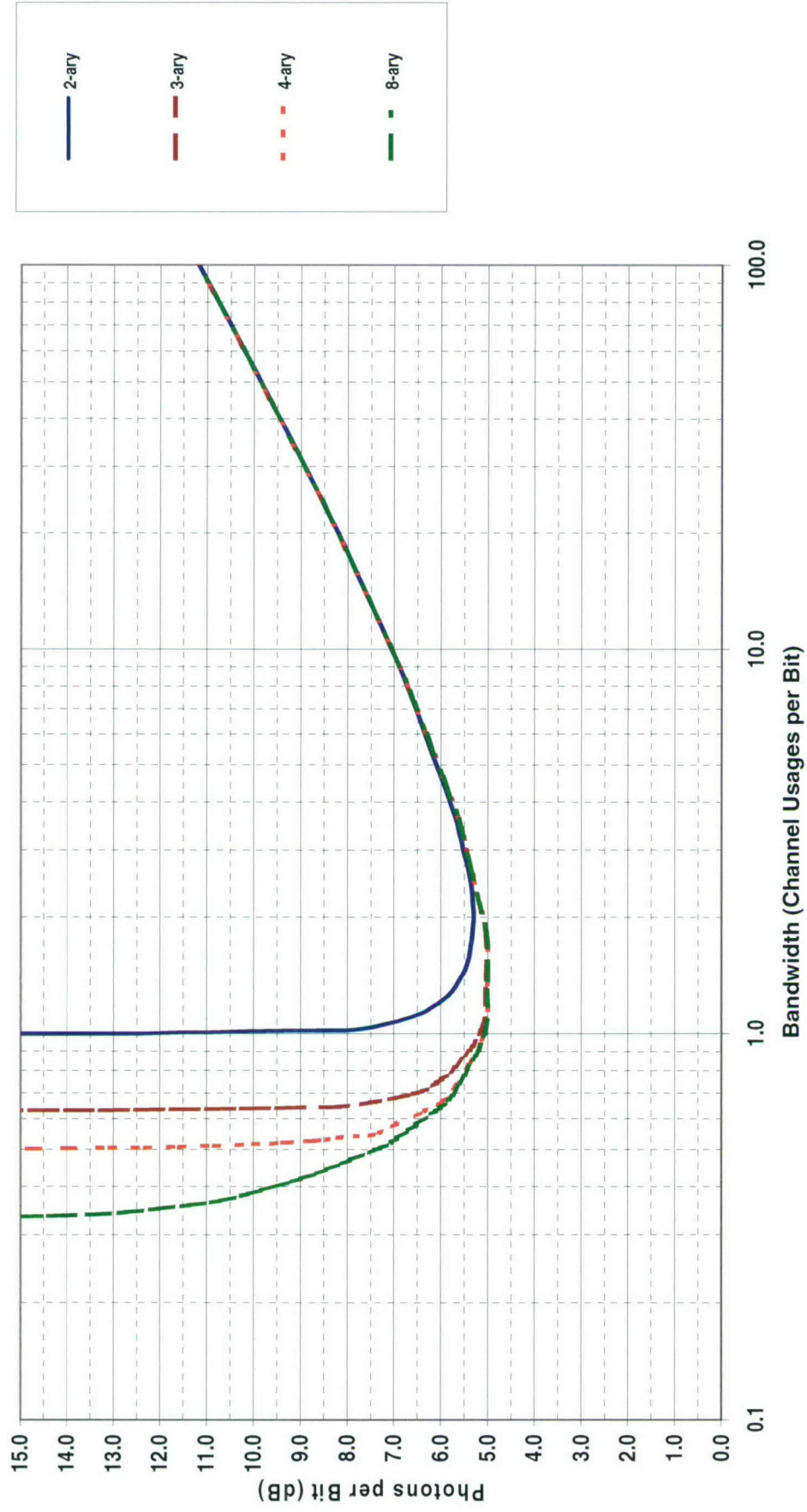


Chart 146. Efficiency at classical cutoff: MPSK heterodyne or preamplified noncoherent soft decision.

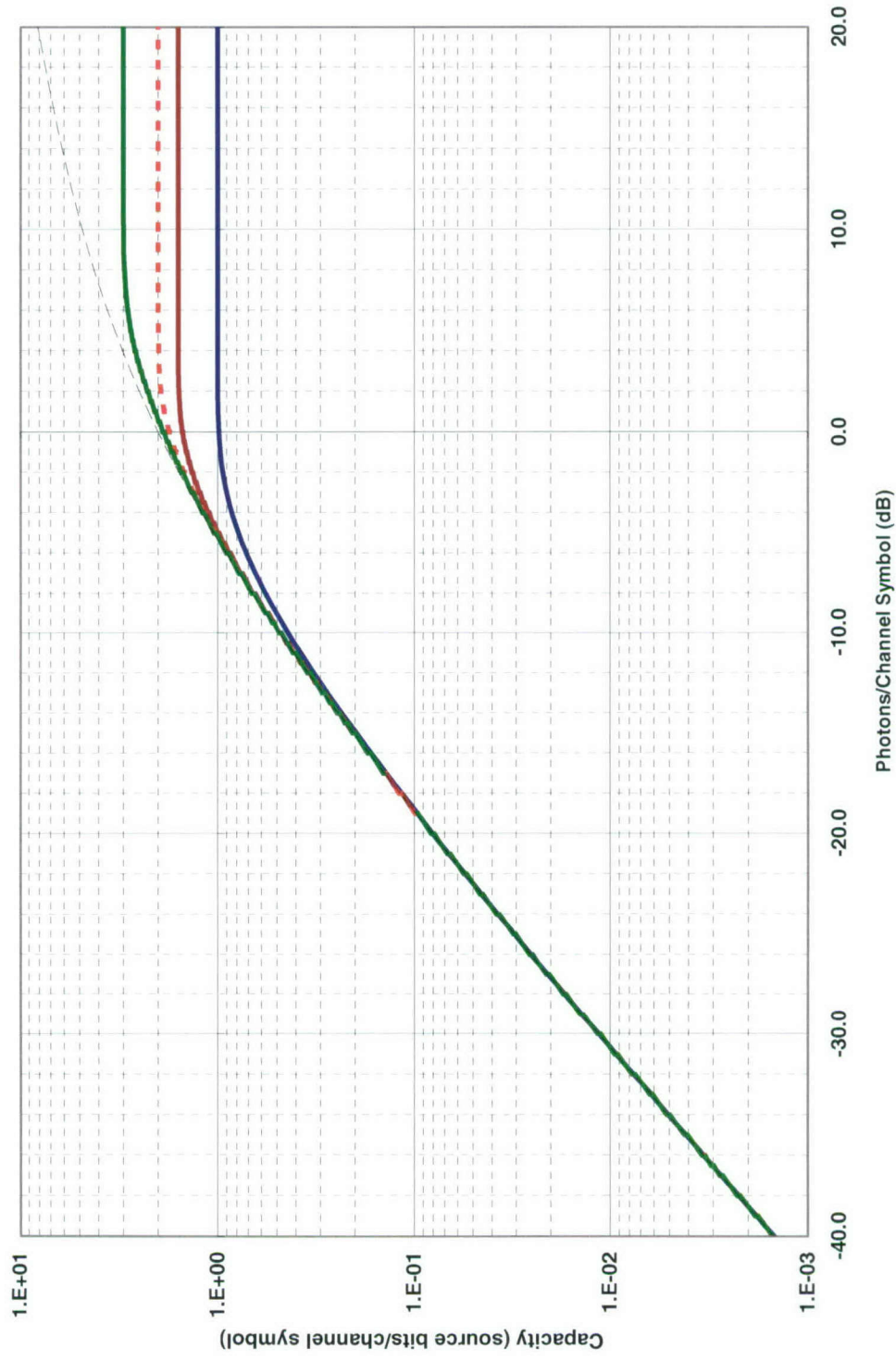


Chart 147. Quantum capacity: MPSK.

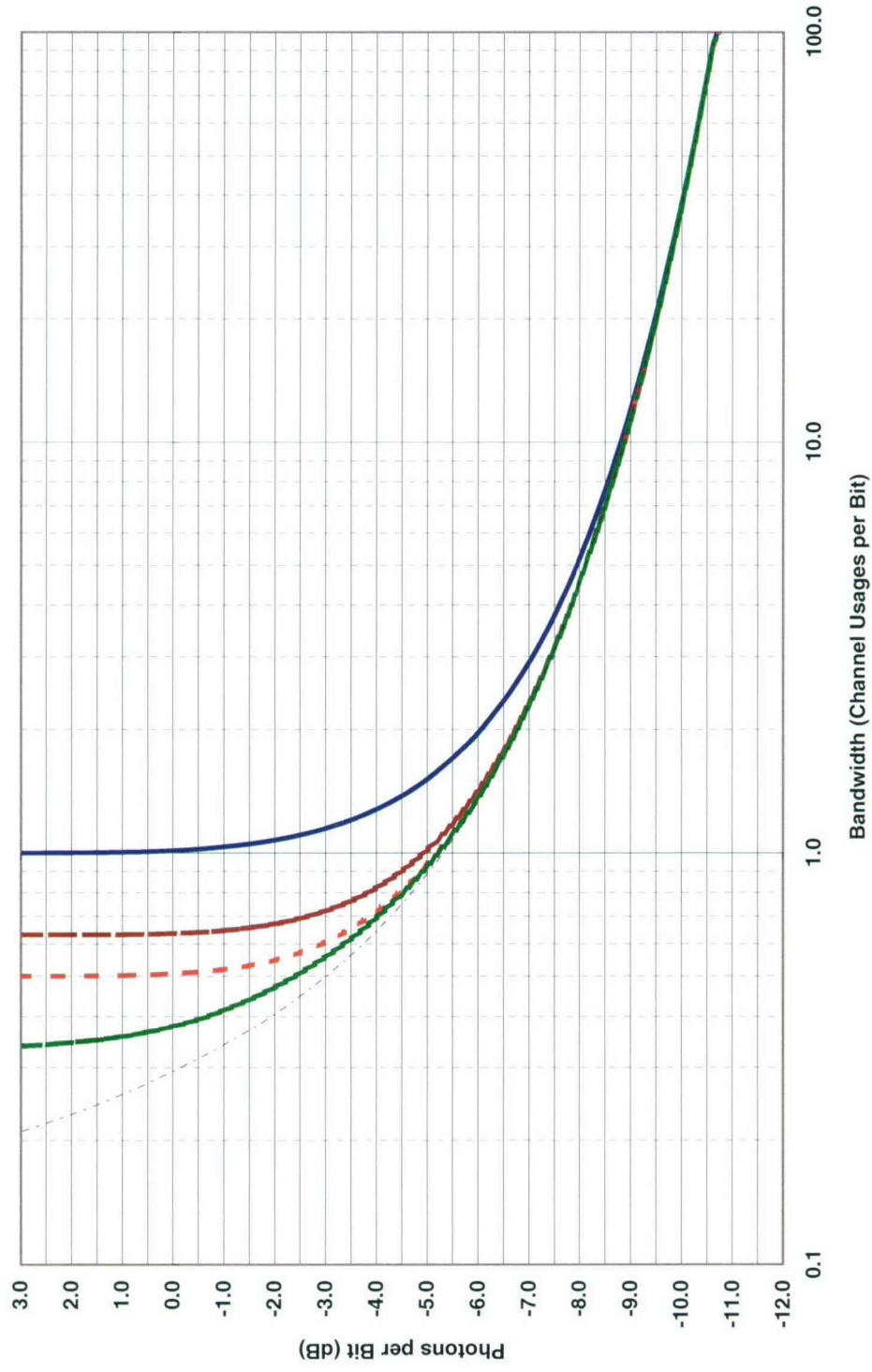


Chart 148. Efficiency at quantum capacity: MPSK.

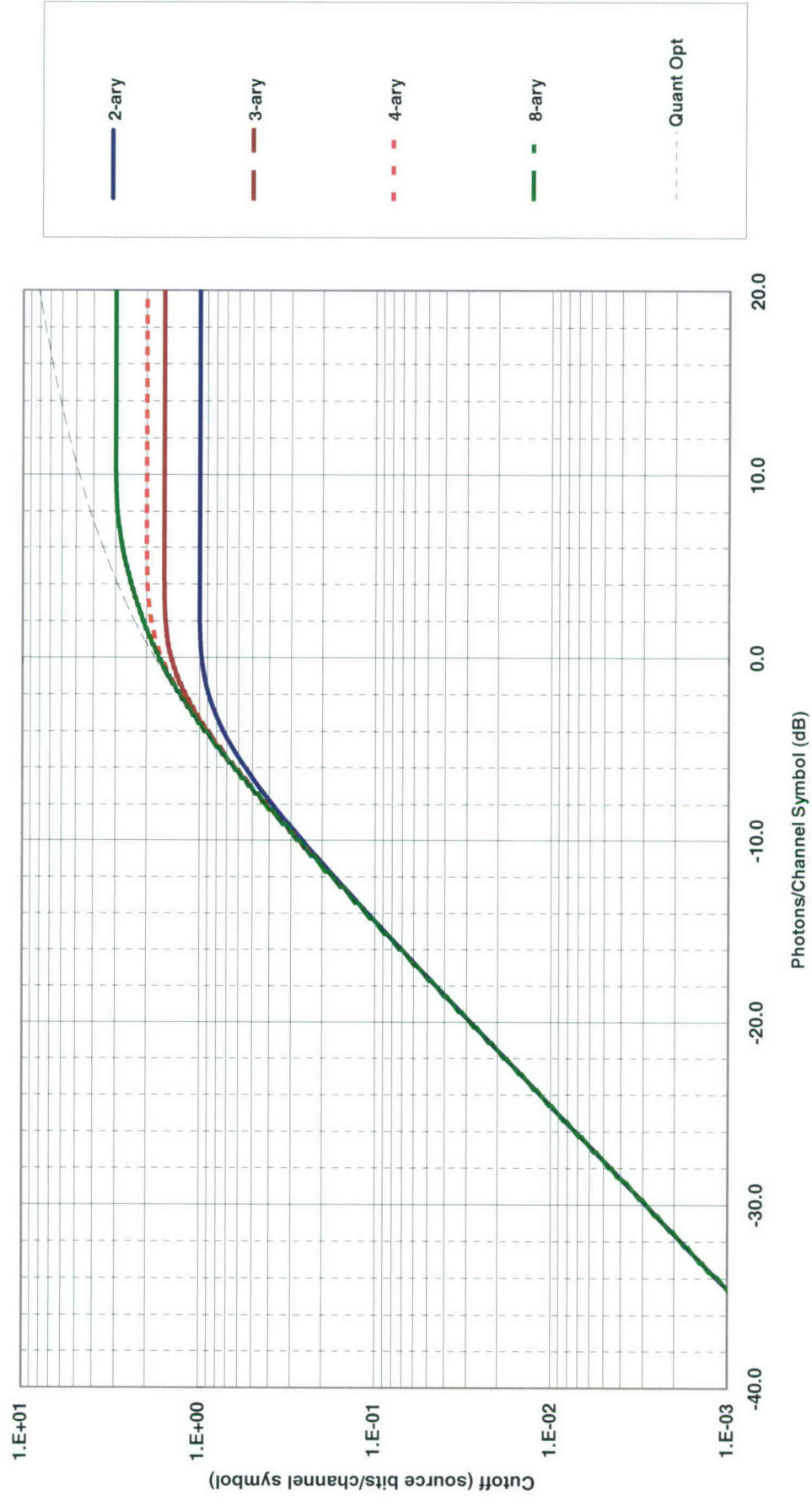


Chart 149. Quantum cutoff: MPSK.

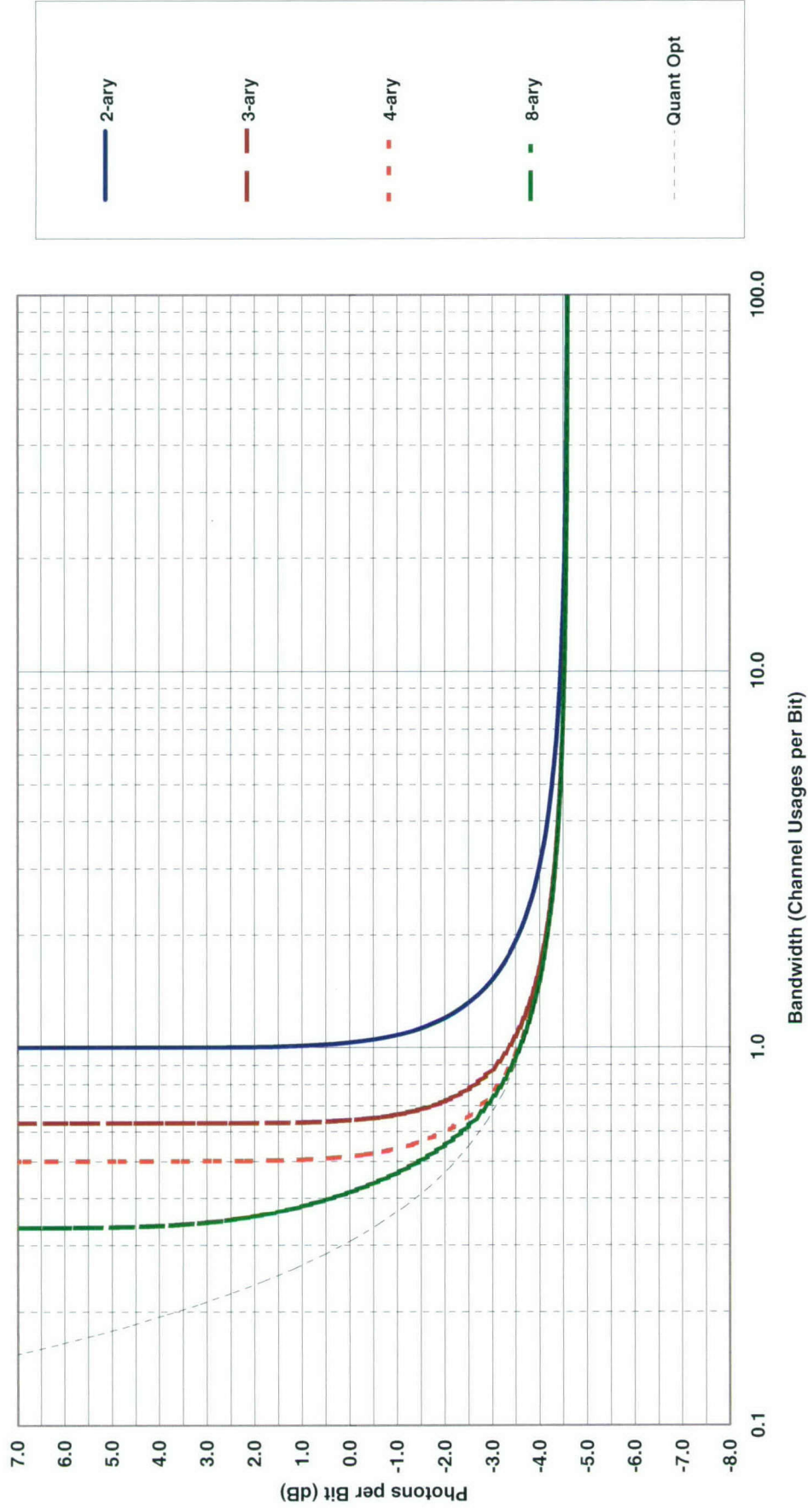


Chart 150. Efficiency at quantum cutoff: MPSK.

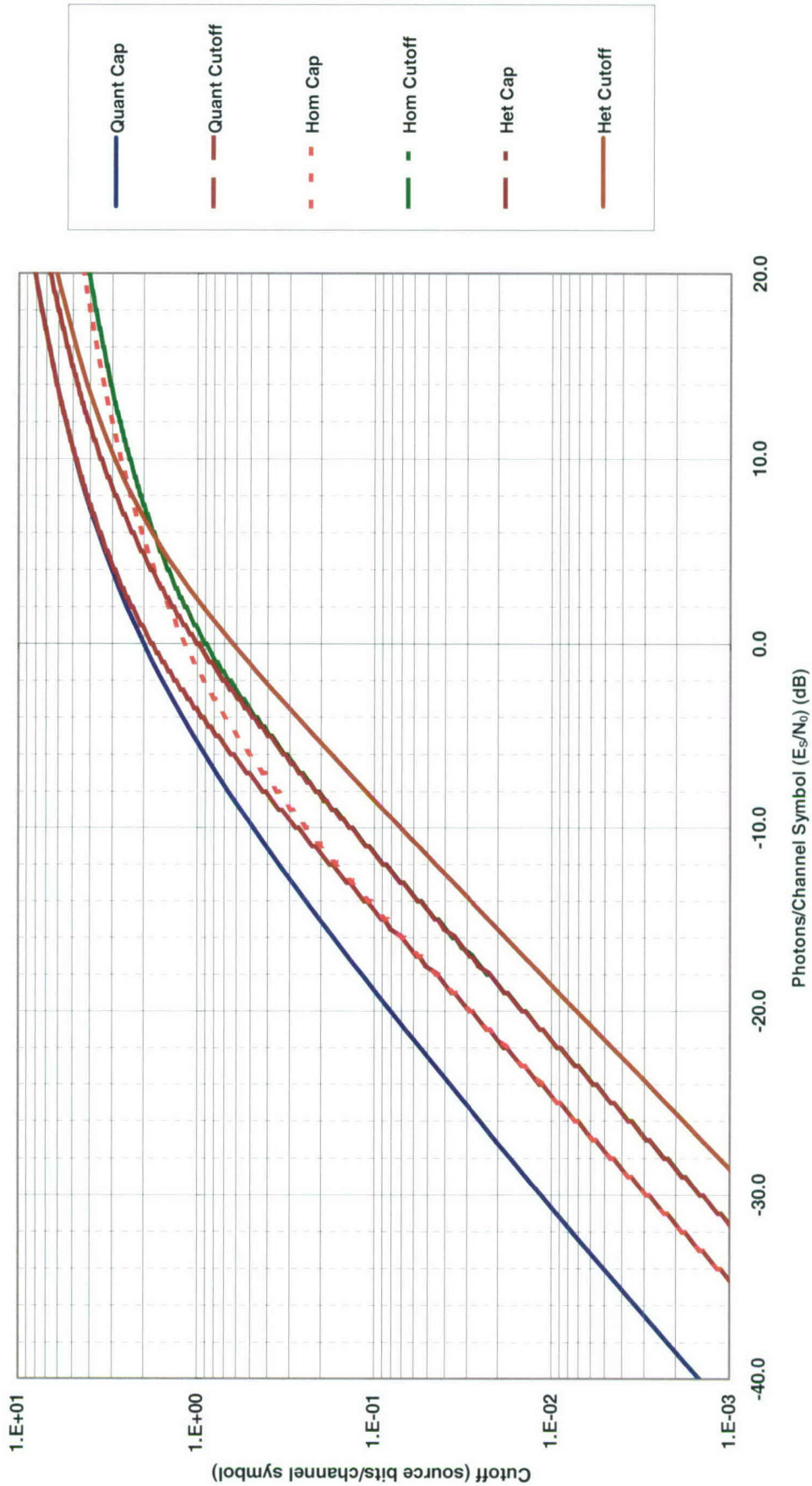


Chart 151. Comparison: Capacity and cutoff: classical and quantum Gaussian.

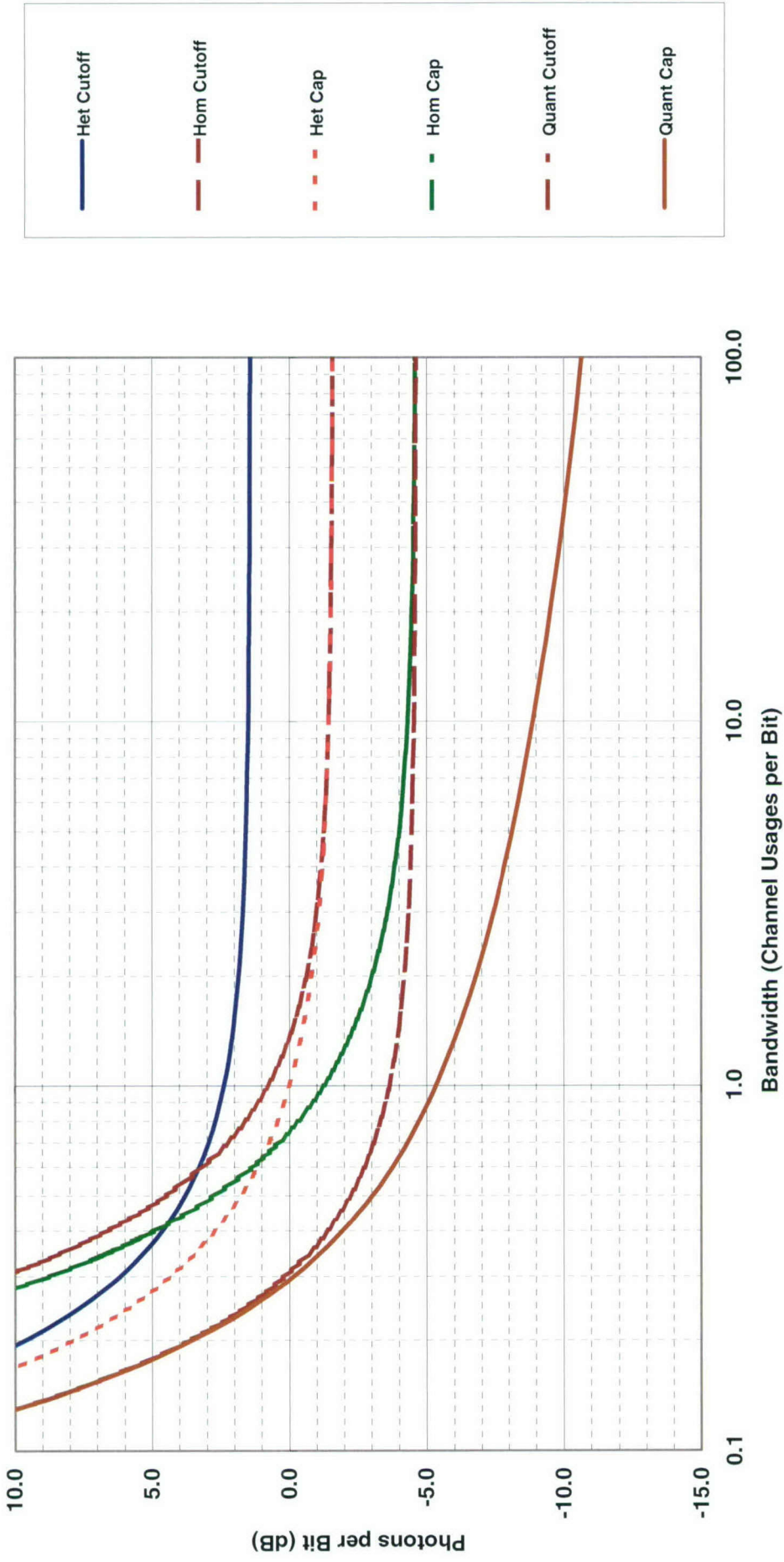


Chart 152. Comparison: Efficiencies at classical Gaussian capacity, classical Gaussian cutoff, quantum Gaussian capacity, quantum Gaussian cutoff.

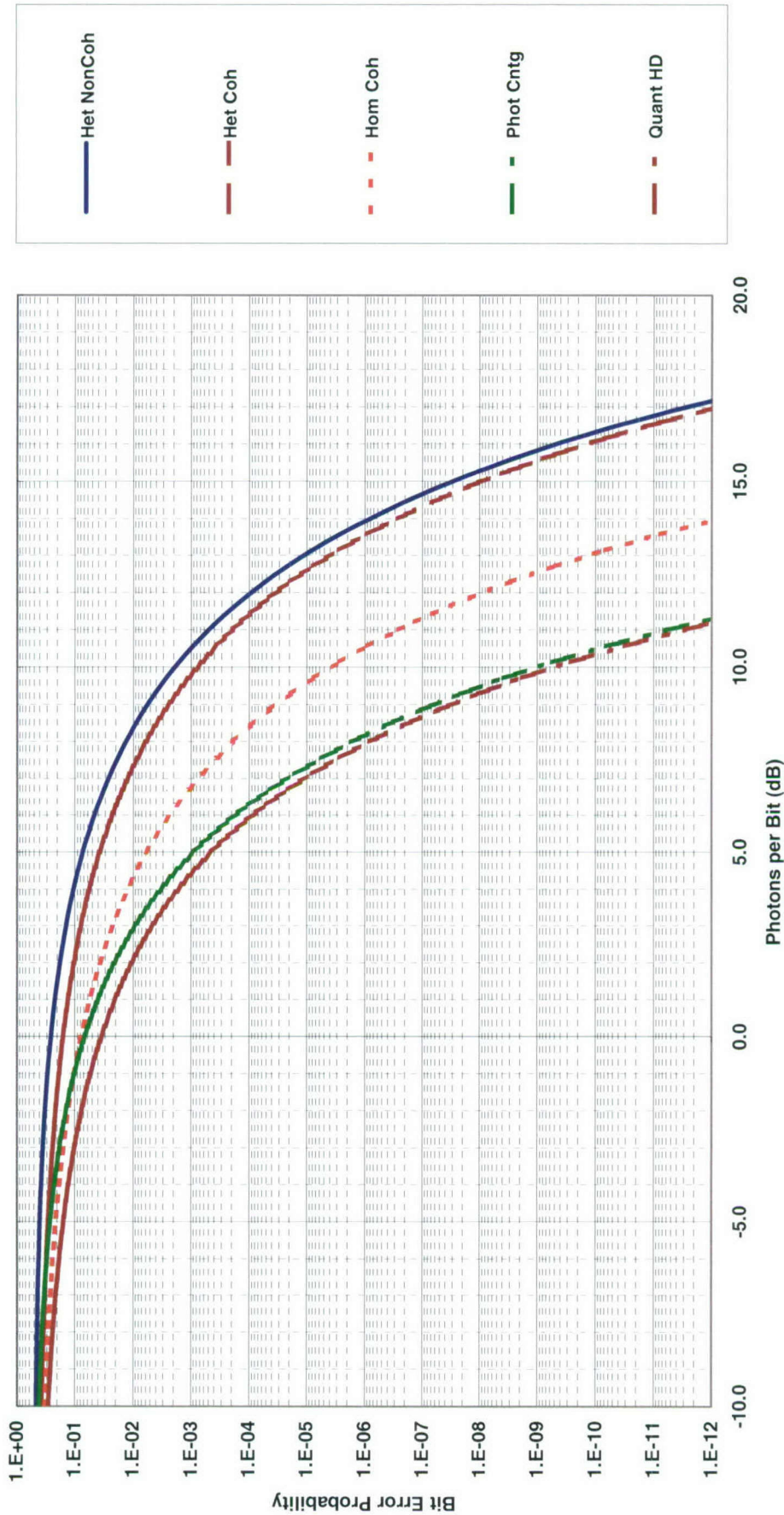


Chart 153. Comparison: BER, OOK ($p_1 = 1/2$)—preamplified noncoherent, heterodyne or preamplified coherent, homodyne coherent, photon counting, quantum.

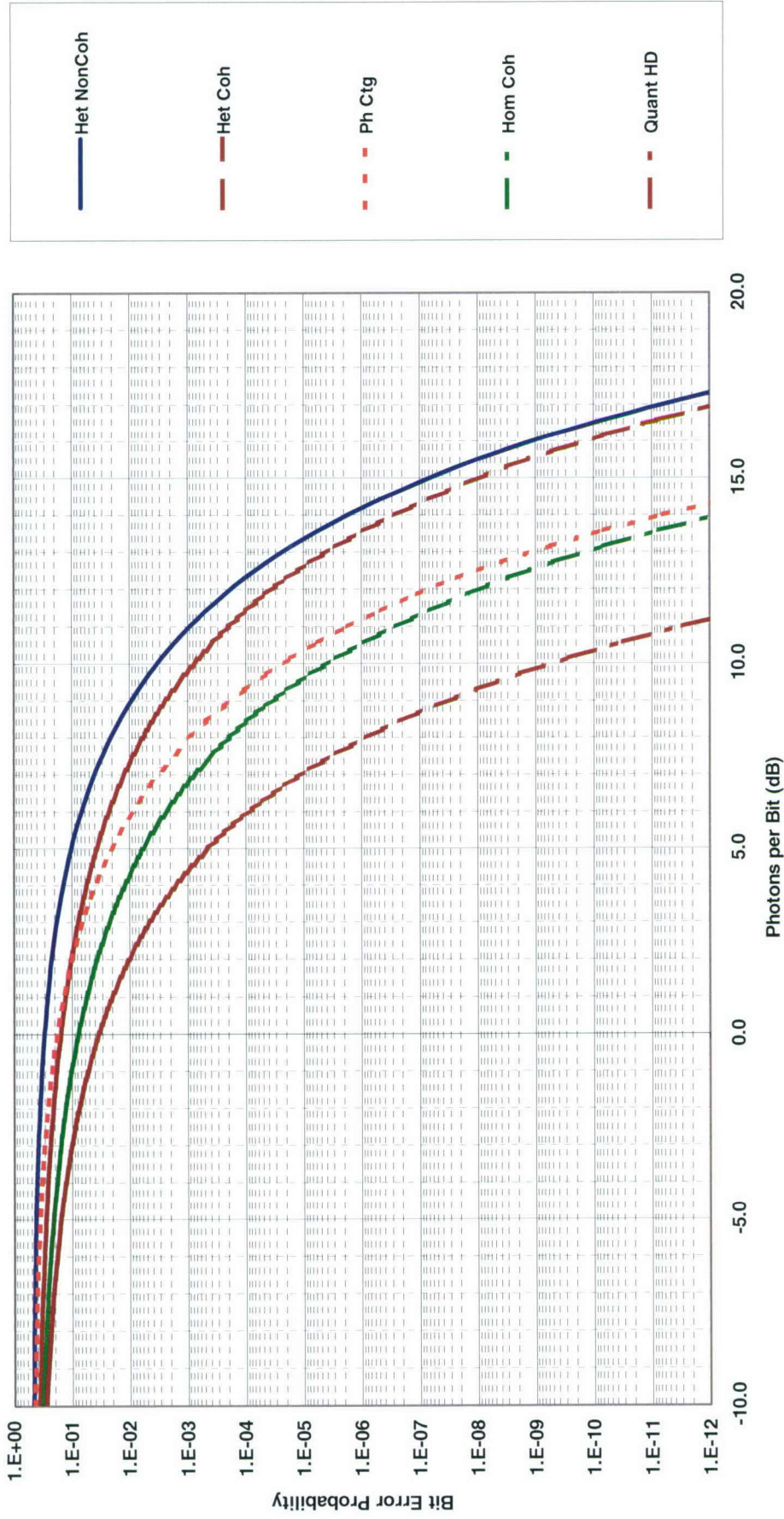


Chart 154. Comparison: BER, orthogonal ($M = 2$)—preamplified noncoherent, heterodyne or preamplified coherent, homodyne coherent, photon counting, quantum.

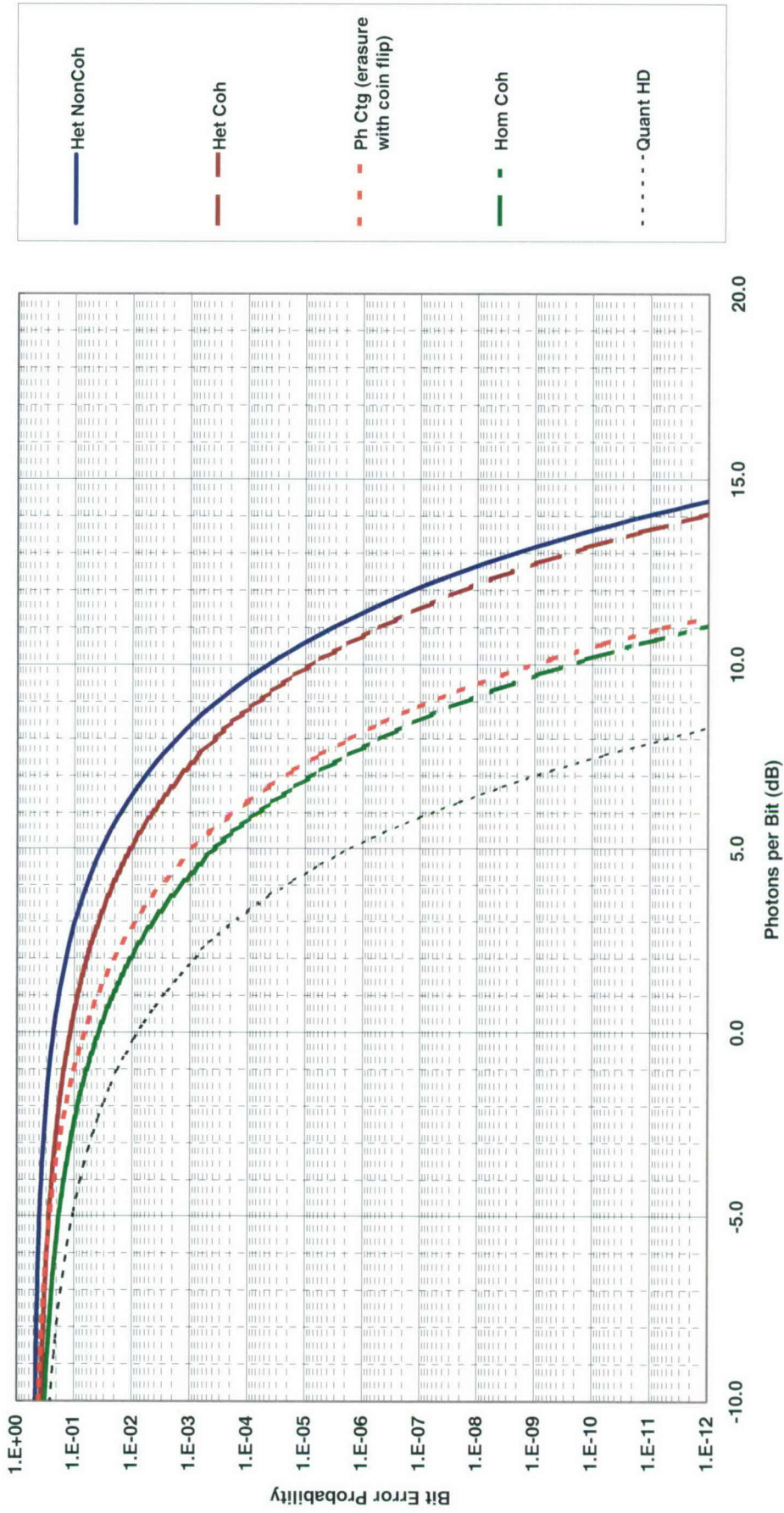


Chart 155. Comparison: BER, orthogonal ($M = 4$)—preamplified noncoherent, heterodyne or. preamplified coherent, homodyne coherent, photon counting, quantum.

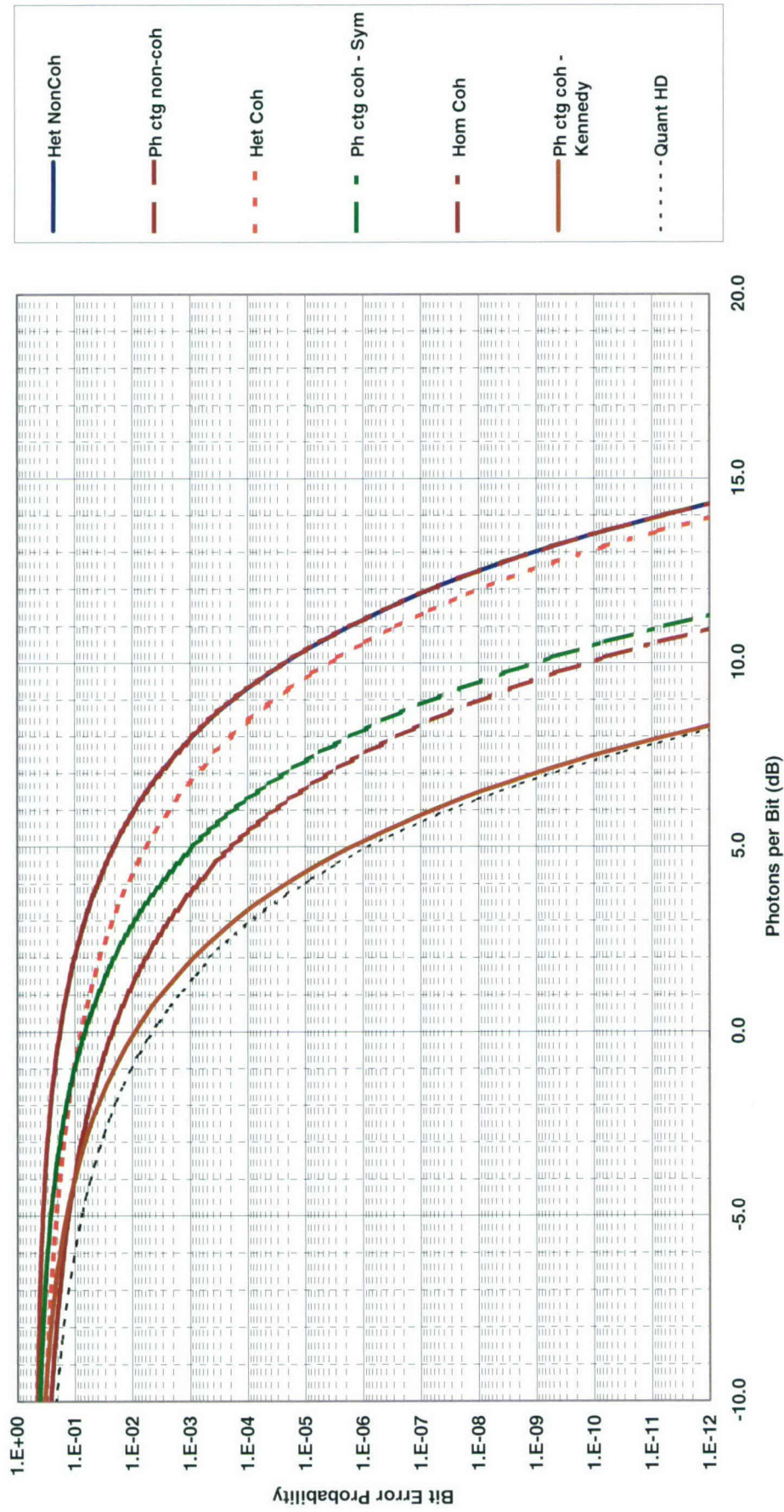


Chart 156. Comparison: BER, PSK ($M = 2$)—preamplified noncoherent (DPSK), heterodyne or preamplified coherent, homodyne coherent, photon counting, quantum.

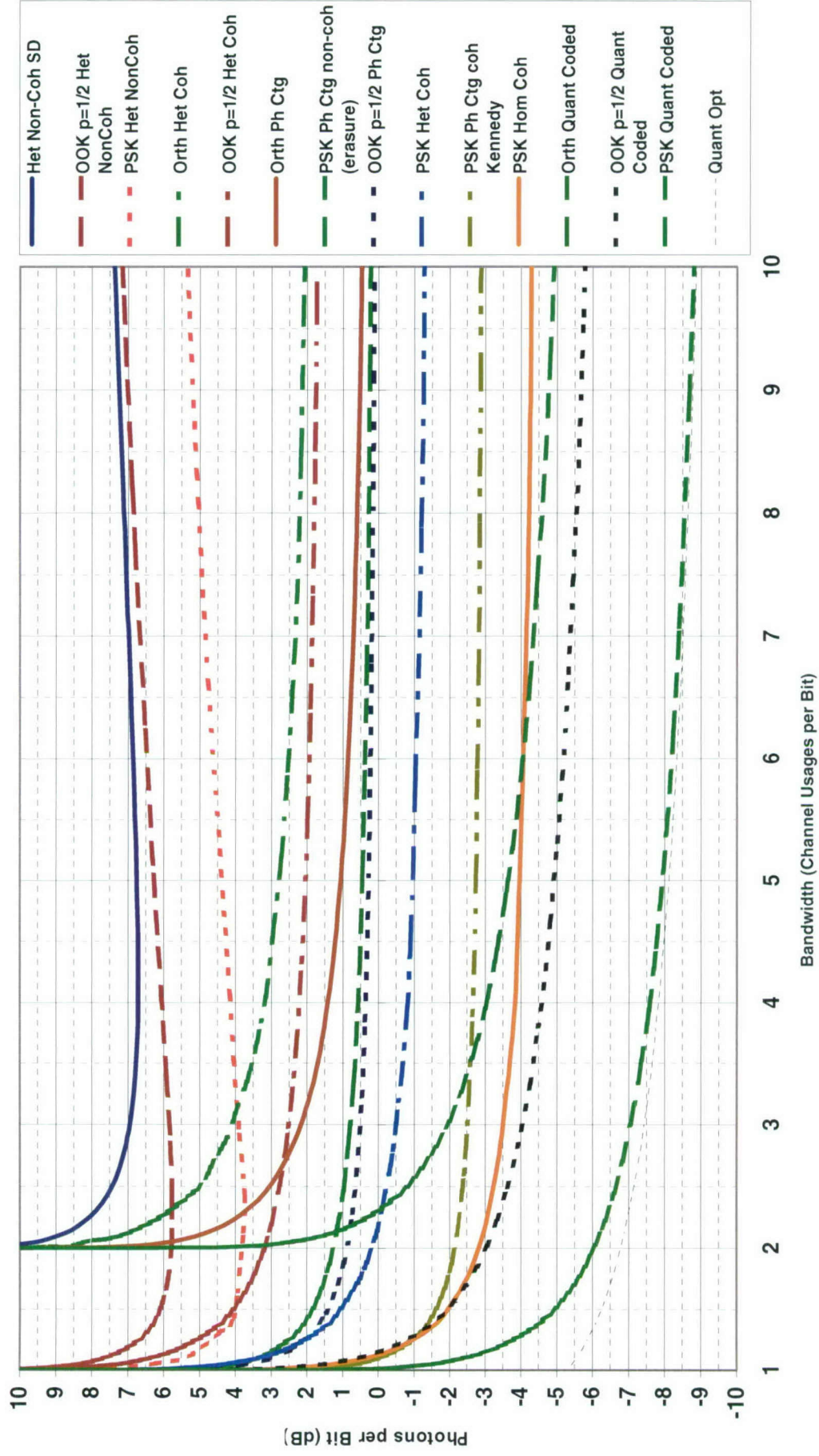


Chart 157. Comparison: Efficiency at capacity, binary modulations—OOK ($p_1 = 1/2$), PPM, and PSK, each at preamplified noncoherent, heterodyne or preamplified coherent, and quantum, or Gaussian quantum.

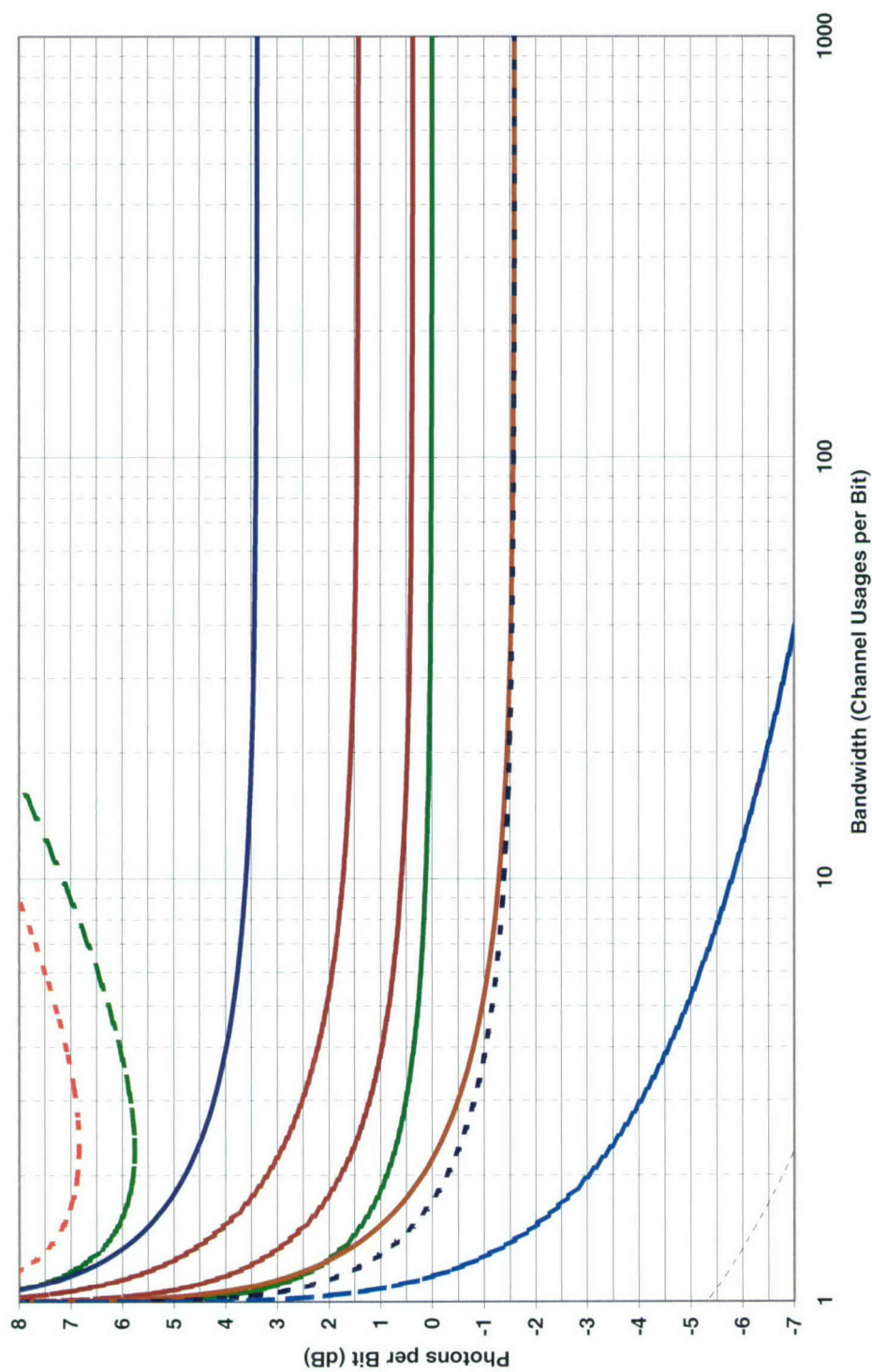


Chart 158. Comparison: Efficiency at capacity, OOK, $p_1 = 1/2$, soft and hard decisions, preamplified noncoherent, heterodyne or preamplified coherent, homodyne coherent, photon counting, quantum, or Gaussian quantum.

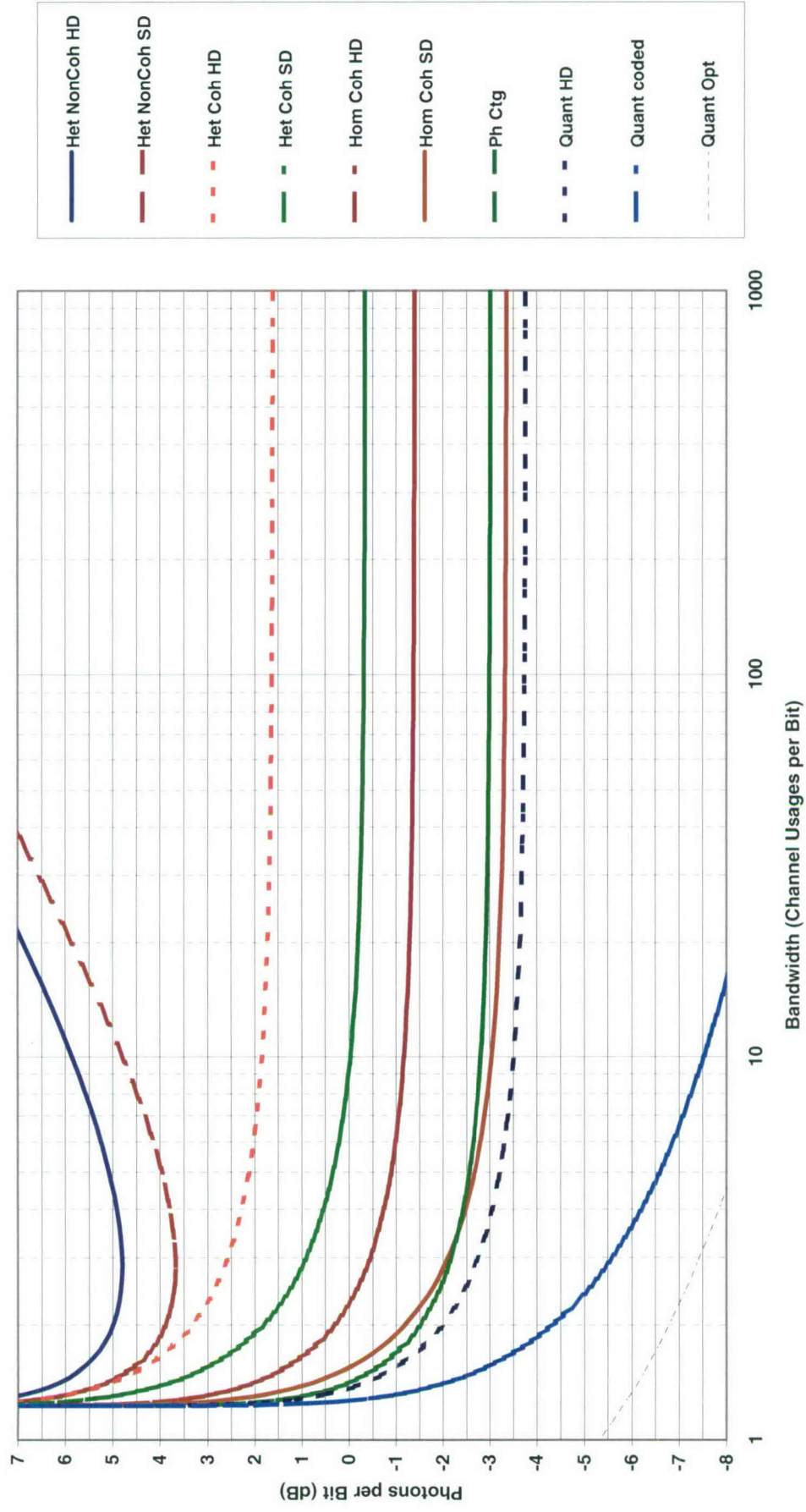


Chart 159. Comparison: Efficiency at capacity, OOK, $p_1 = 1/4$, soft and hard decisions, preamplified noncoherent, heterodyne or preamplified coherent, homodyne coherent, photon counting, quantum, or Gaussian quantum.

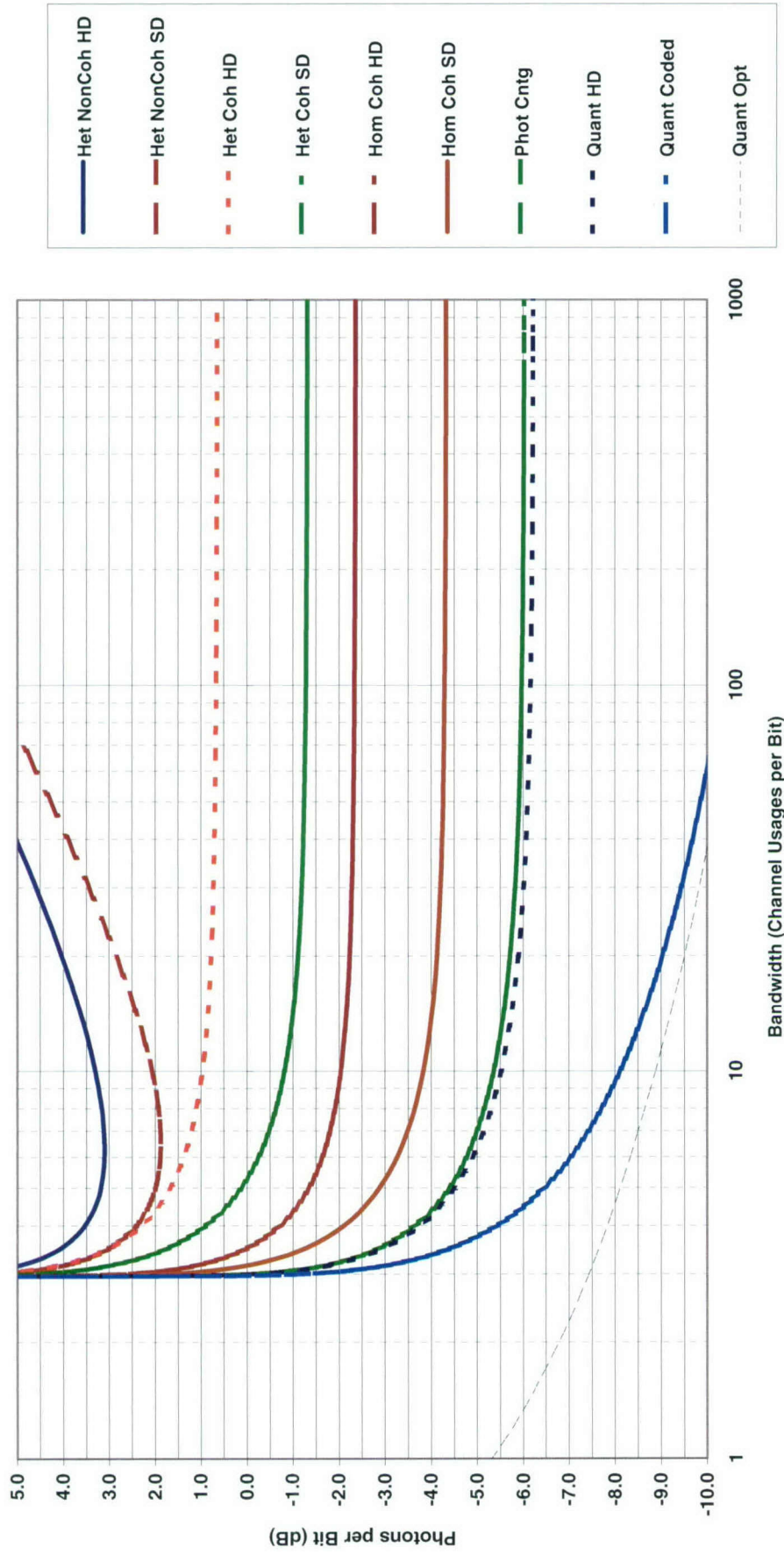


Chart 160. Comparison: Efficiency at capacity, OOK, $p_1 = 1/16$, soft and hard decisions, preamplified noncoherent, heterodyne or preamplified coherent, homodyne coherent, photon counting, quantum, or Gaussian quantum.

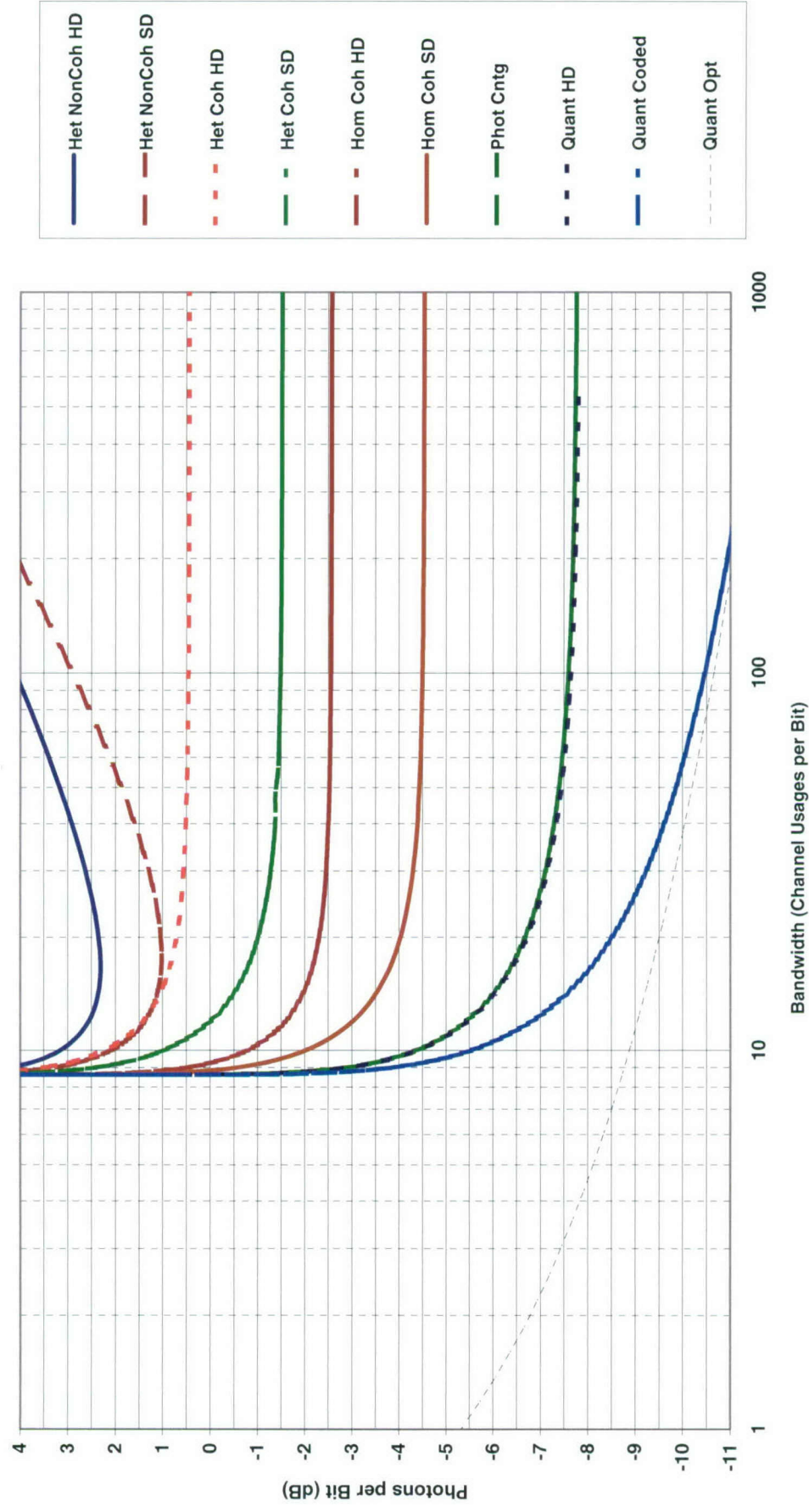


Chart 161. Comparison: Efficiency at capacity, OOK, $p_1 = 1/64$, soft and hard decisions, preamplified noncoherent, heterodyne or preamplified coherent, homodyne coherent, photon counting, quantum, or Gaussian quantum.

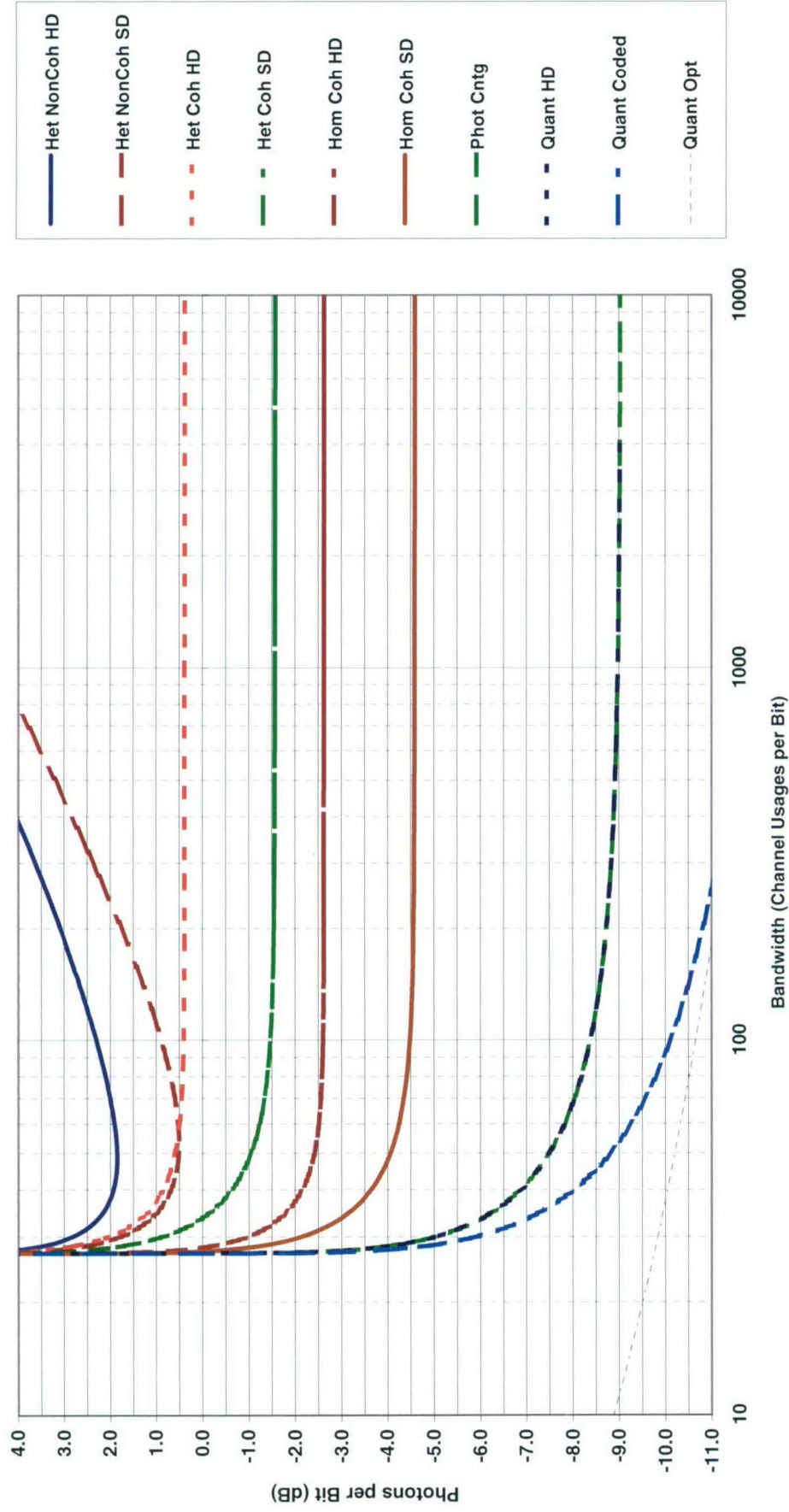


Chart 162. Comparison: Efficiency at capacity, OOK, $p_1 = 1/256$, soft and hard decisions, preamplified noncoherent, heterodyne or preamplified coherent, homodyne coherent, photon counting, quantum, or Gaussian quantum.

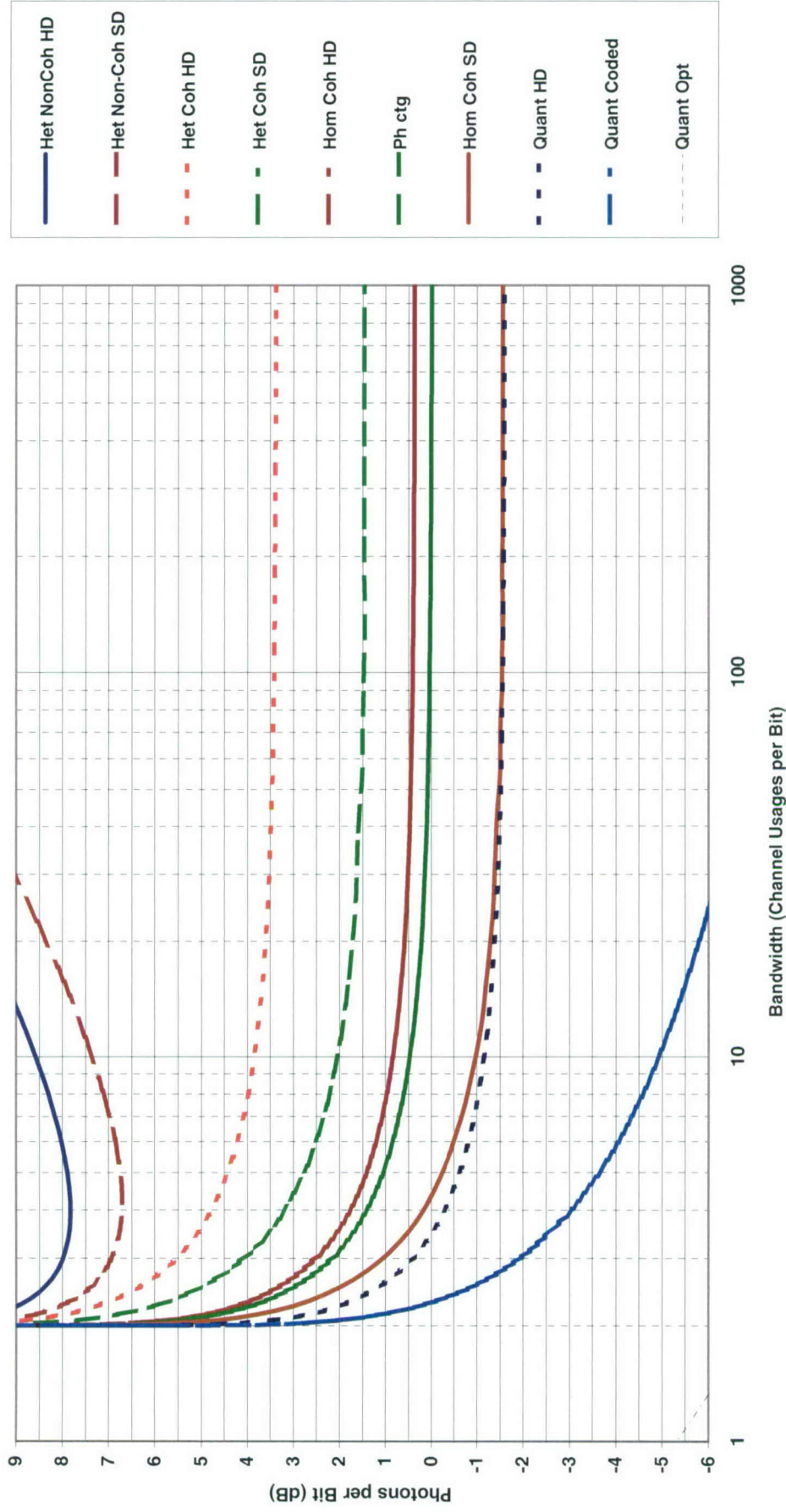


Chart 163. Comparison: Efficiency at capacity, orthogonal, $M = 2$, soft and hard decisions, preamplified noncoherent, heterodyne or preamplified coherent, homodyne coherent, photon counting, quantum, or Gaussian quantum.

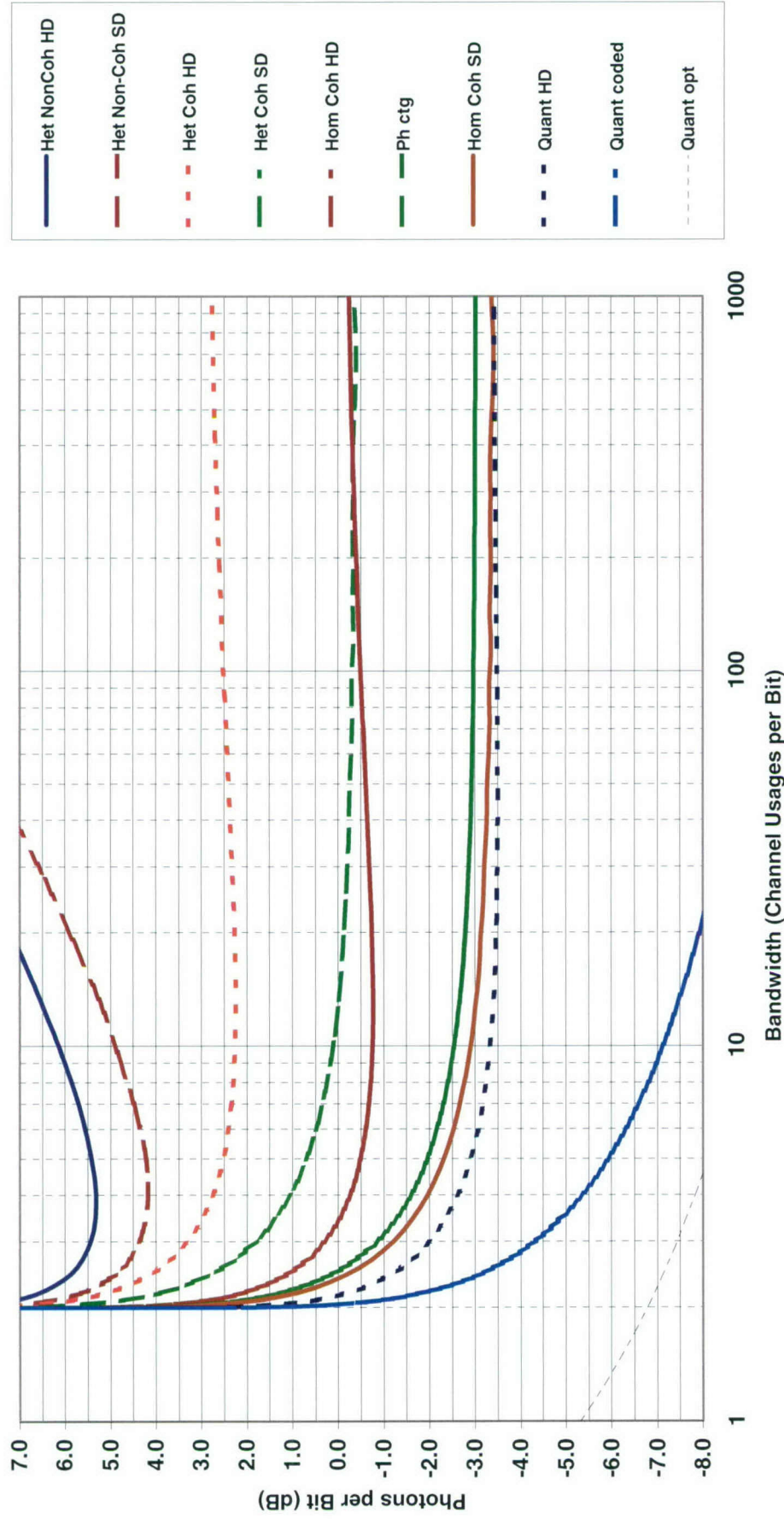


Chart 164. Comparison: Efficiency at capacity, orthogonal, $M = 4$, soft and hard decisions, preamplified noncoherent, heterodyne or preamplified coherent, homodyne coherent, photon counting, quantum, or Gaussian quantum.

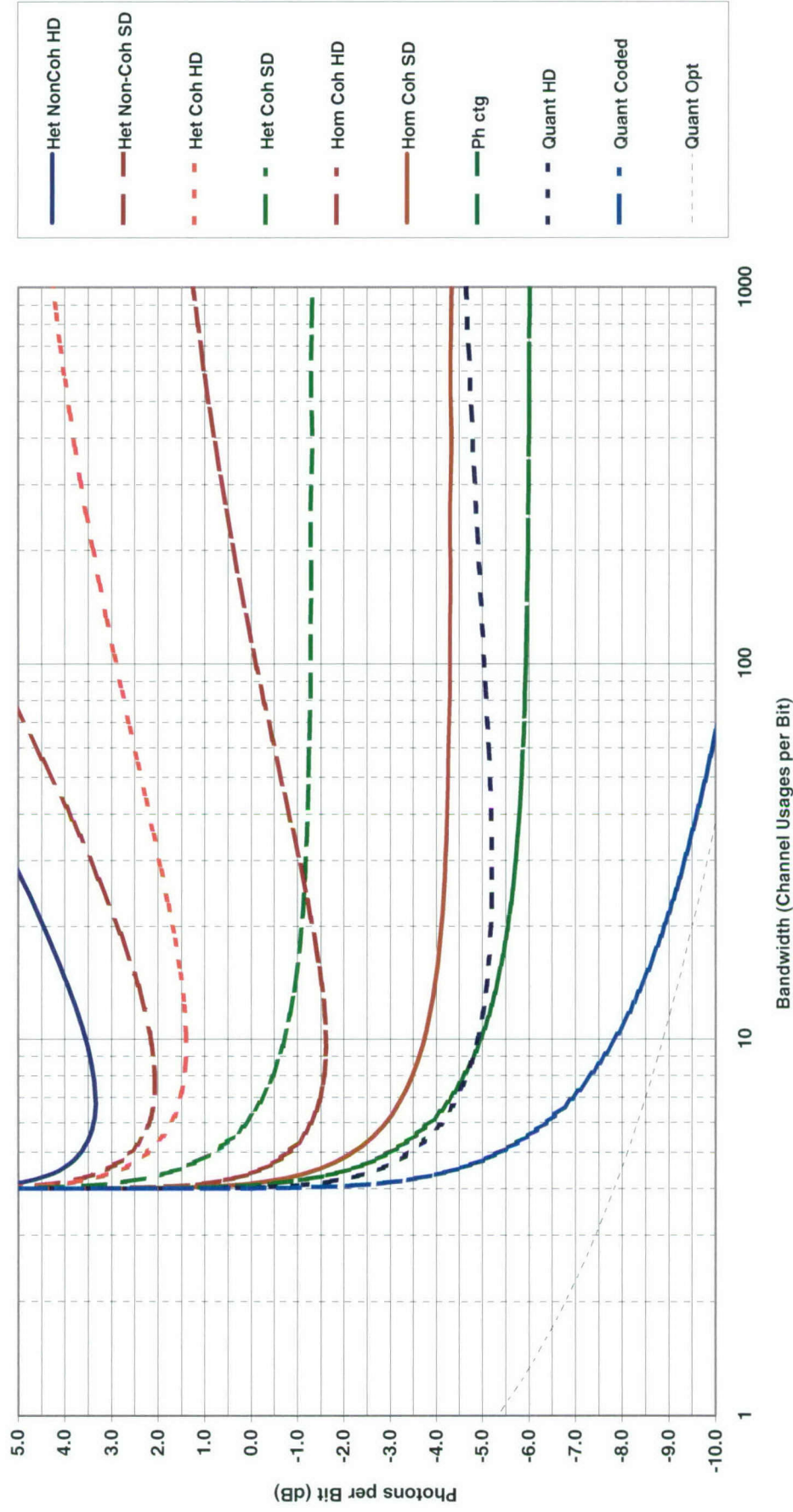


Chart 165. Comparison: Efficiency at capacity, orthogonal, $M = 16$, soft and hard decisions, preamplified noncoherent, heterodyne or preamplified coherent, homodyne coherent, photon counting, quantum, or Gaussian quantum.

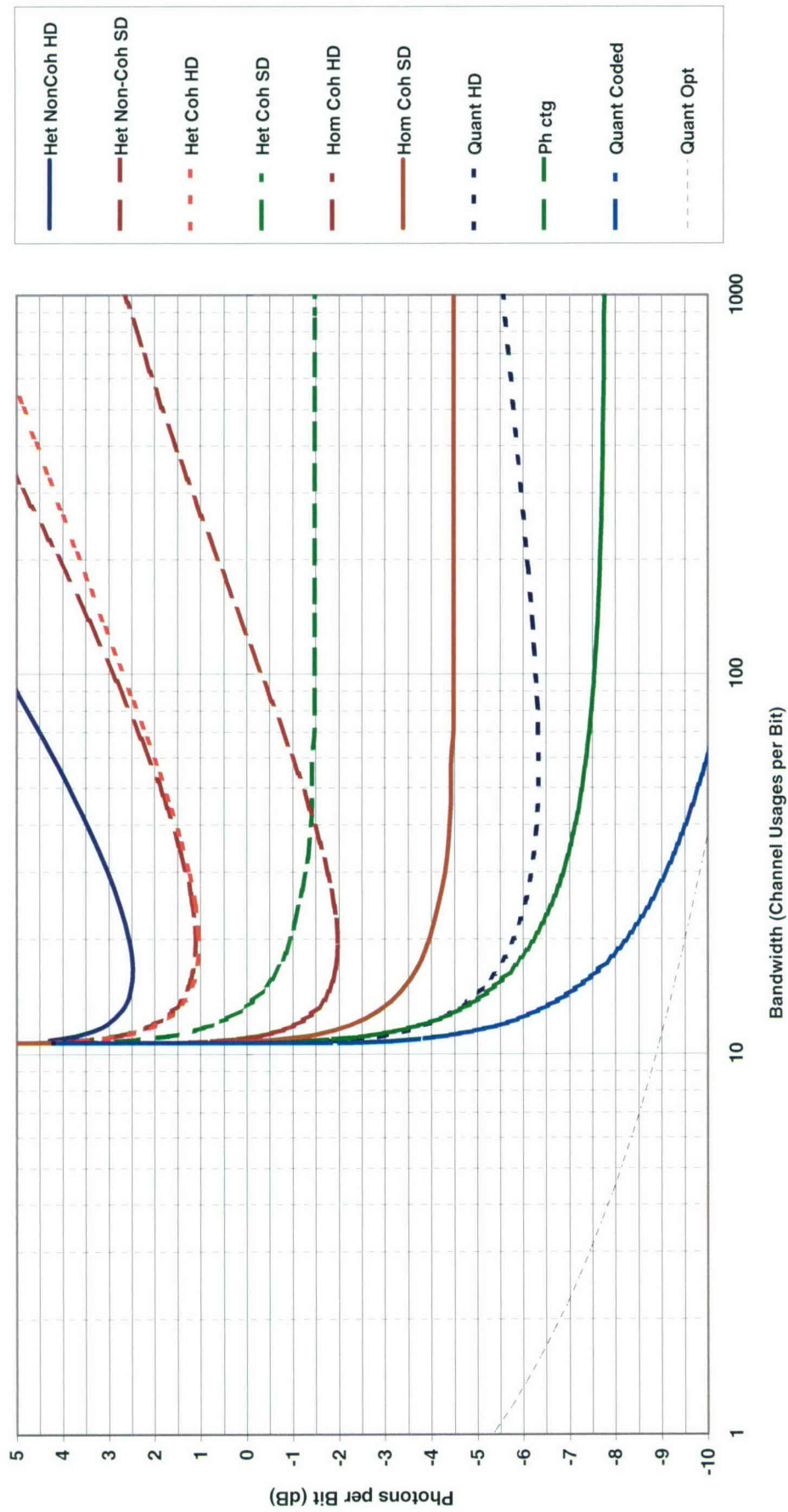


Chart 166. Comparison: Efficiency at capacity, orthogonal, $M = 64$, soft and hard decisions, preamplified noncoherent, heterodyne or preamplified coherent, homodyne coherent, photon counting, quantum, or Gaussian quantum.

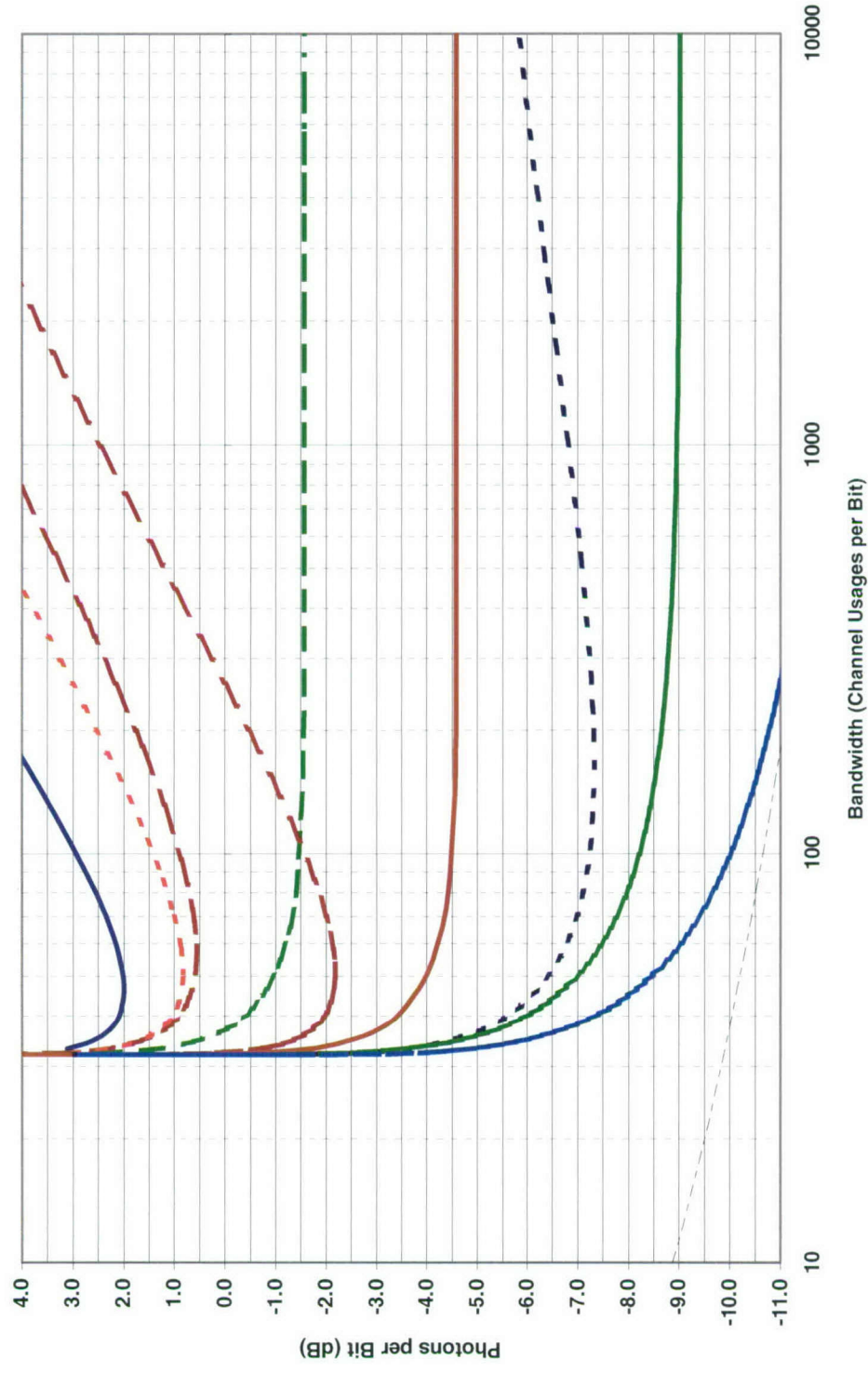


Chart 167. Comparison: Efficiency at capacity, orthogonal, $M = 256$, soft and hard decisions, preamplified noncoherent, heterodyne or preamplified coherent, homodyne coherent, photon counting, quantum, or Gaussian quantum.

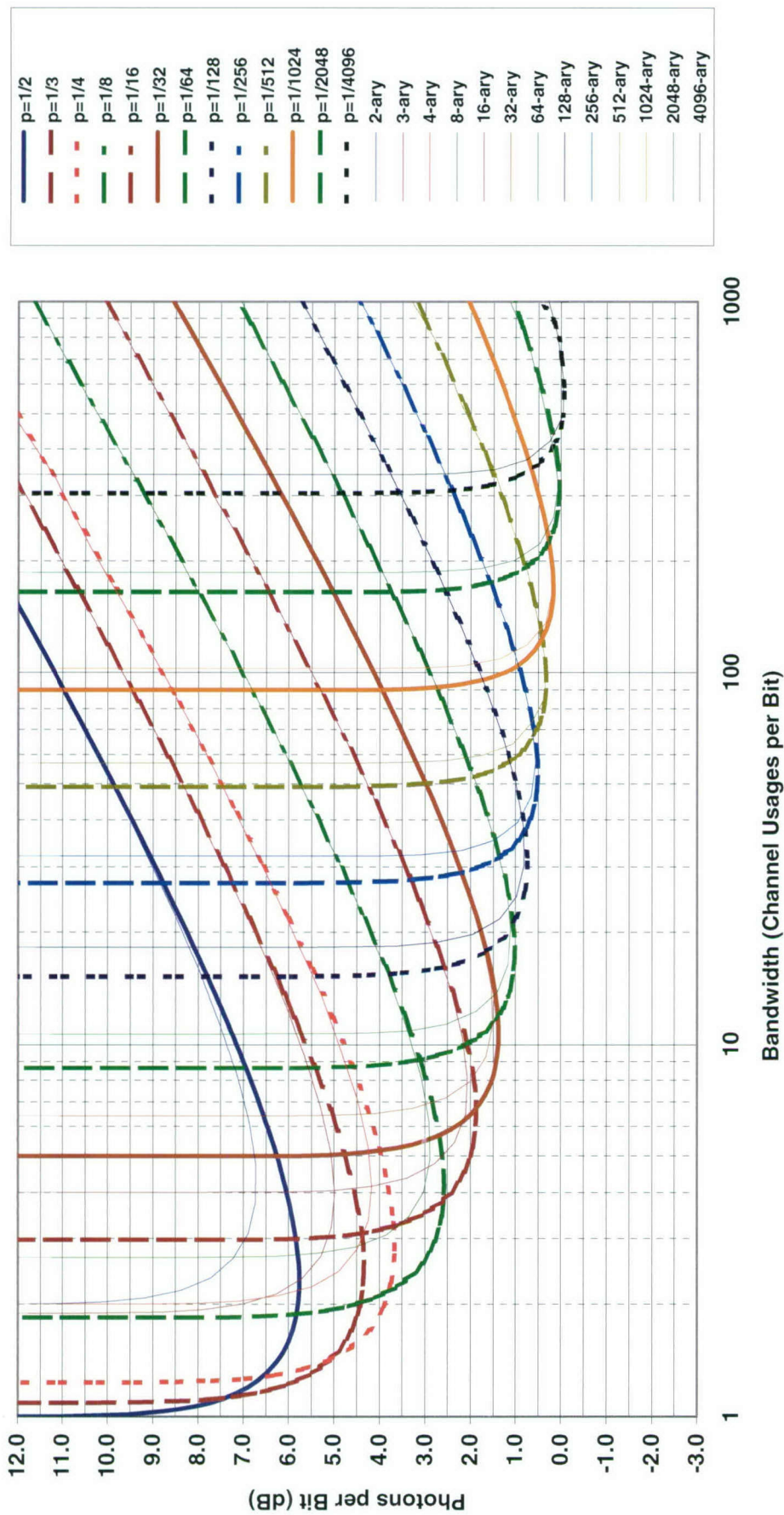


Chart 168. Comparison: Efficiency at capacity, OOK and orthogonal— $M(1/p_1) = 2, 3, 4, 8, 16, 32, 64, 128, 256, 512, 1024$, soft decision, preamplified noncoherent.

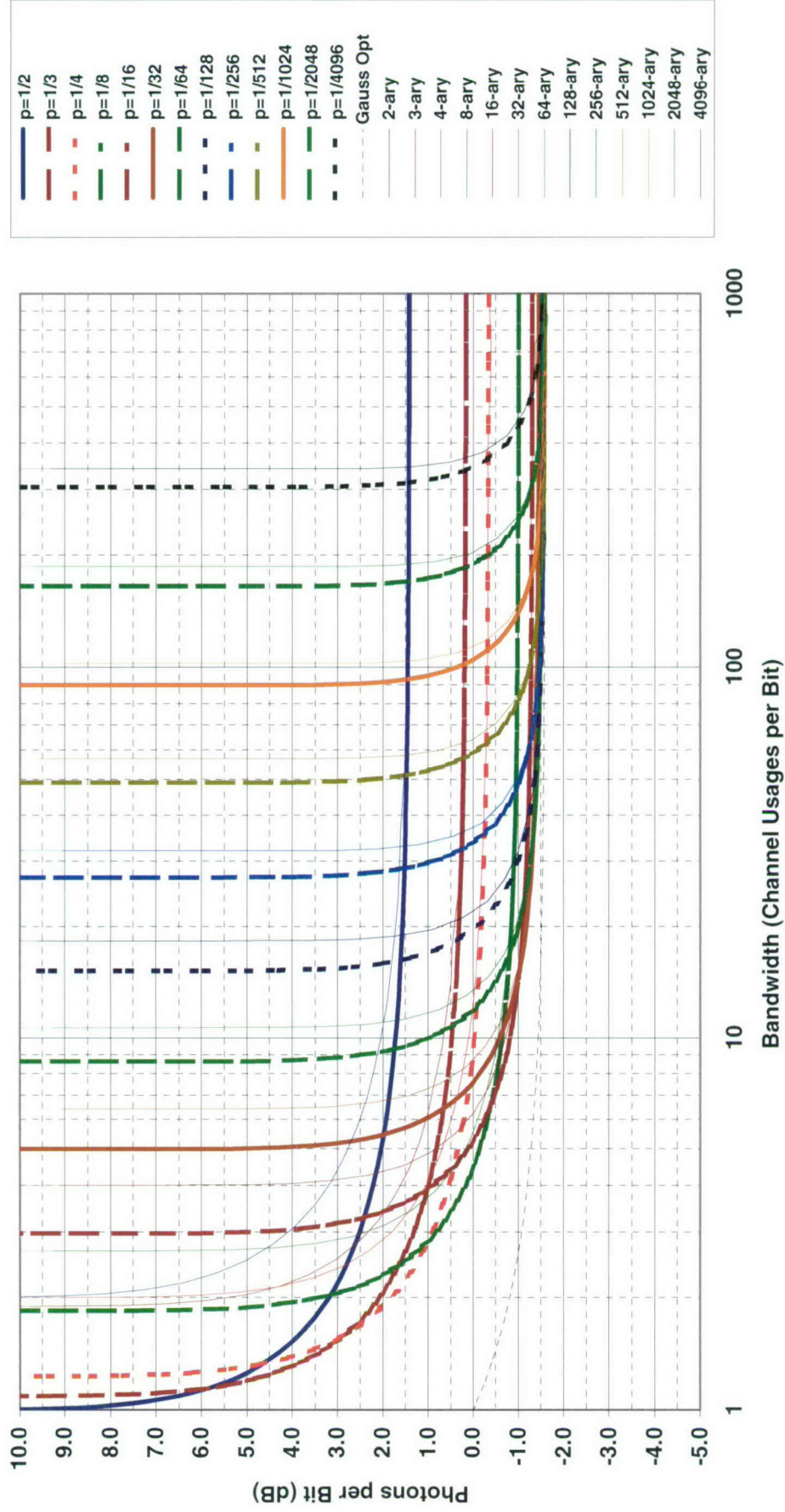


Chart 169. Comparison: Efficiency at capacity, OOK and orthogonal— $M(1/p) = 2, 3, 4, 8, 16, 32, 64, 128, 256, 512, 1024$, soft decision—heterodyne or preamplified coherent, or classical Gaussian.

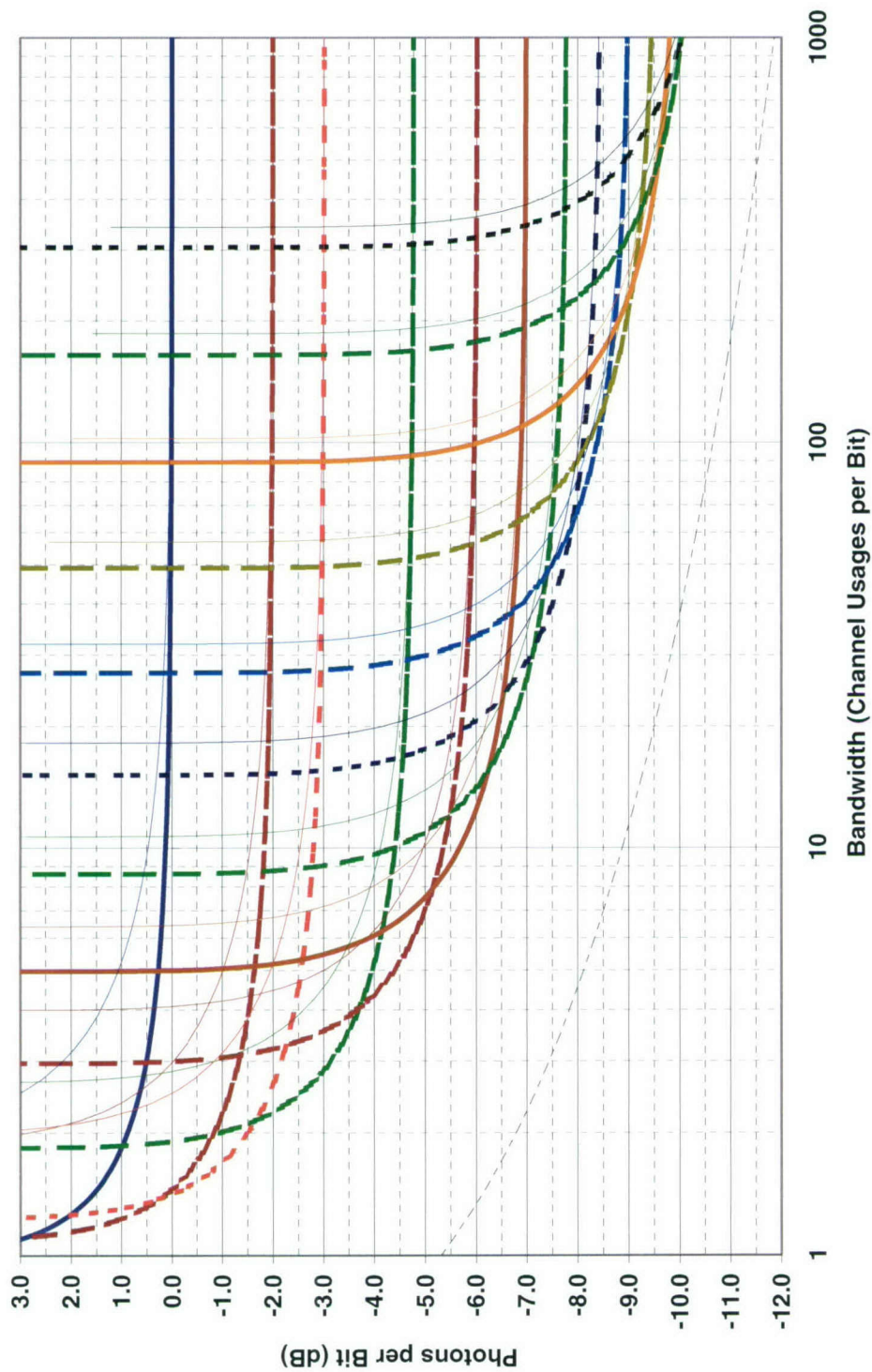


Chart 170. Comparison: Efficiency at capacity, OOK and orthogonal— $M(1/p_1) = 2, 3, 4, 8, 16, 32, 64, 128, 256, 512, 1024$, soft decision—photon counting, or Gaussian quantum.

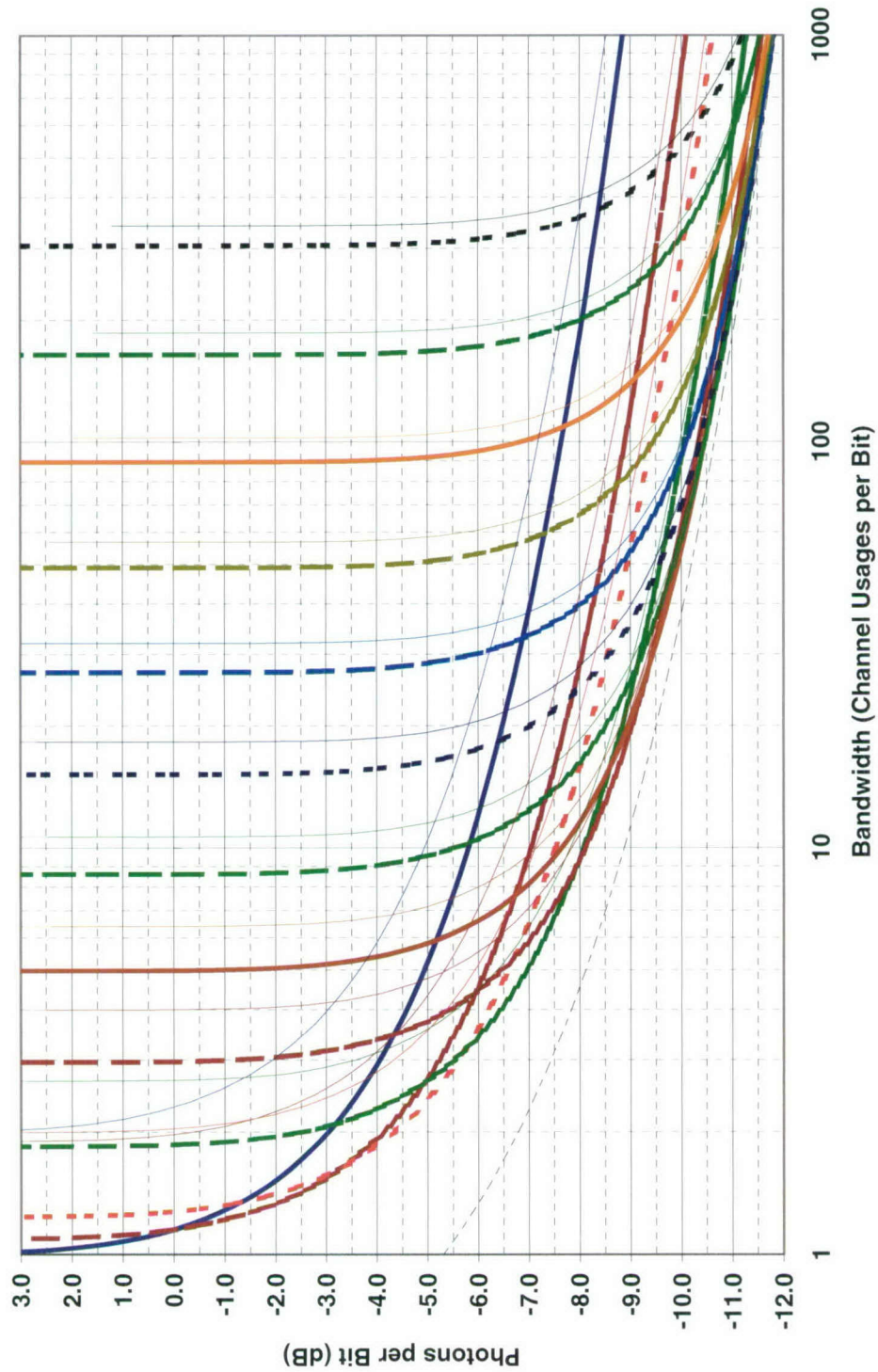


Chart 171. Comparison: Efficiency at capacity, OOK and orthogonal— $M(1/p_1) = 2, 3, 4, 8, 16, 32, 64, 128, 256, 512, 1024$, soft decision—quantum ML, or Gaussian quantum.

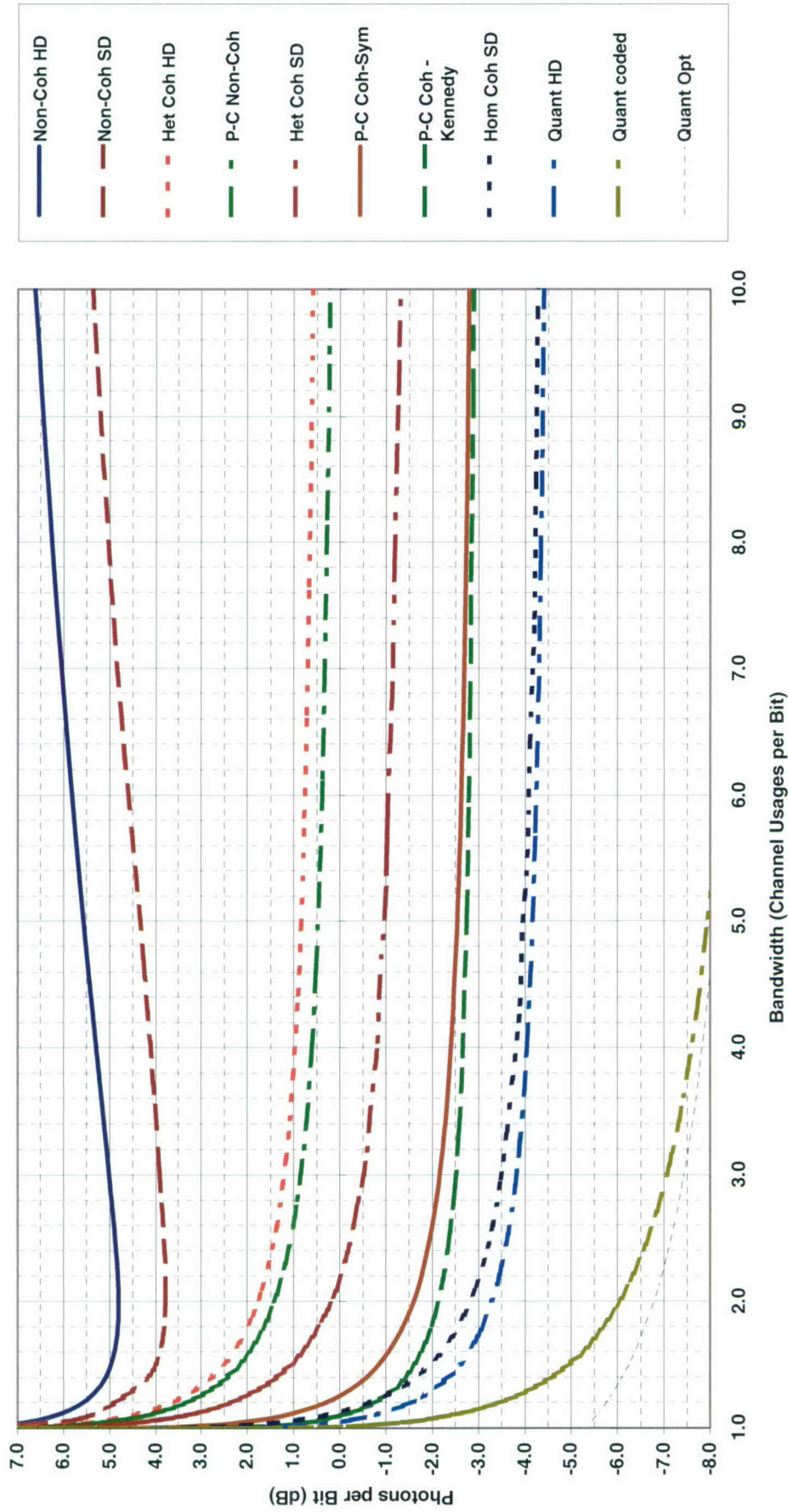


Chart 172. Comparison: Efficiency at capacity, MPSK, $M = 2$, soft decision—preamplified DPSK, heterodyne or preamplified coherent, homodyne coherent, photon counting, quantum, or Gaussian quantum.

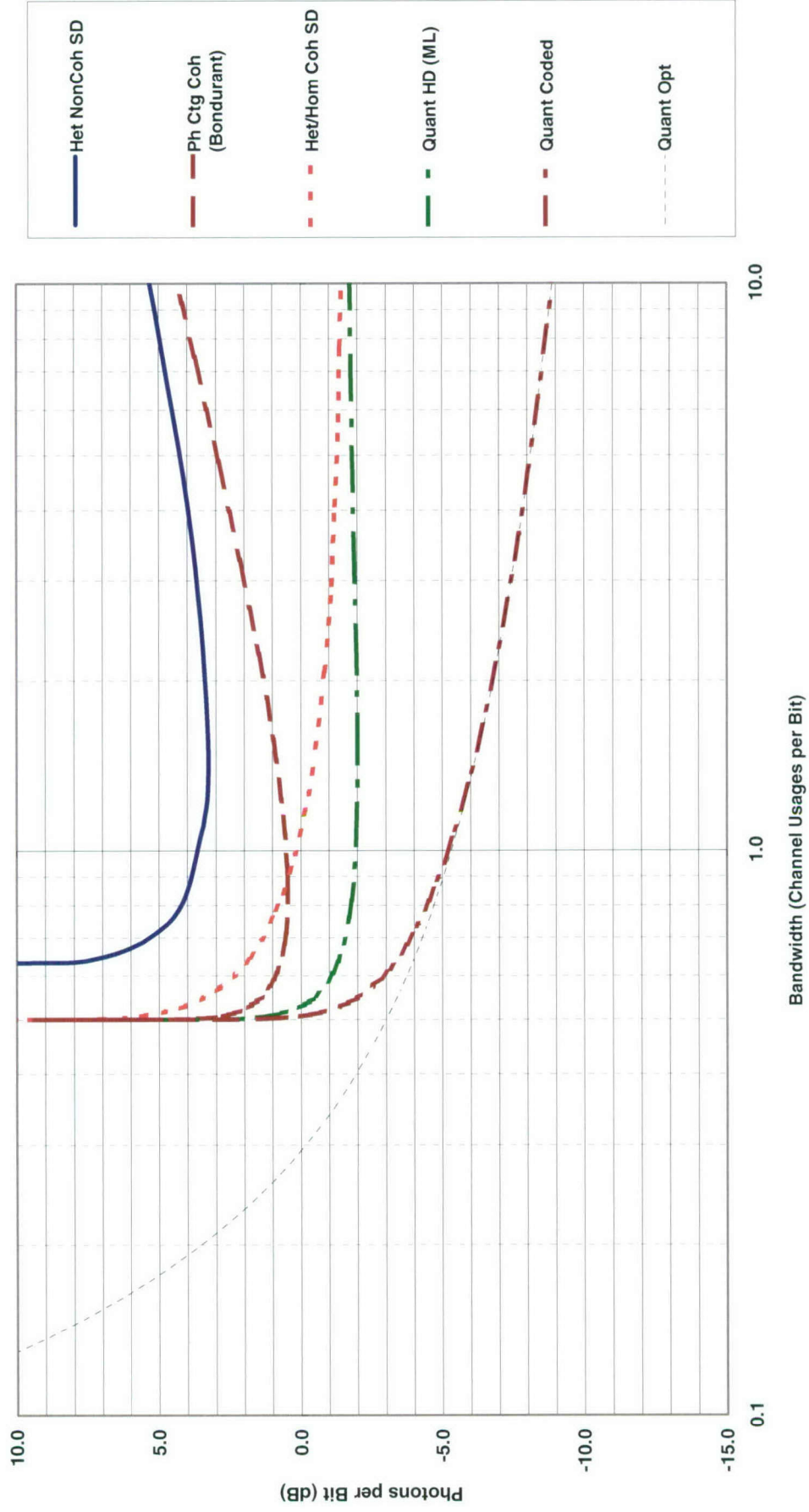


Chart 173. Comparison: Efficiency at capacity, MPSK, $M = 4$, soft decision—preamplified DQPSK, heterodyne or preamplified coherent, Bondurant photon counting, quantum HD, Gaussian coded, or Gaussian quantum.

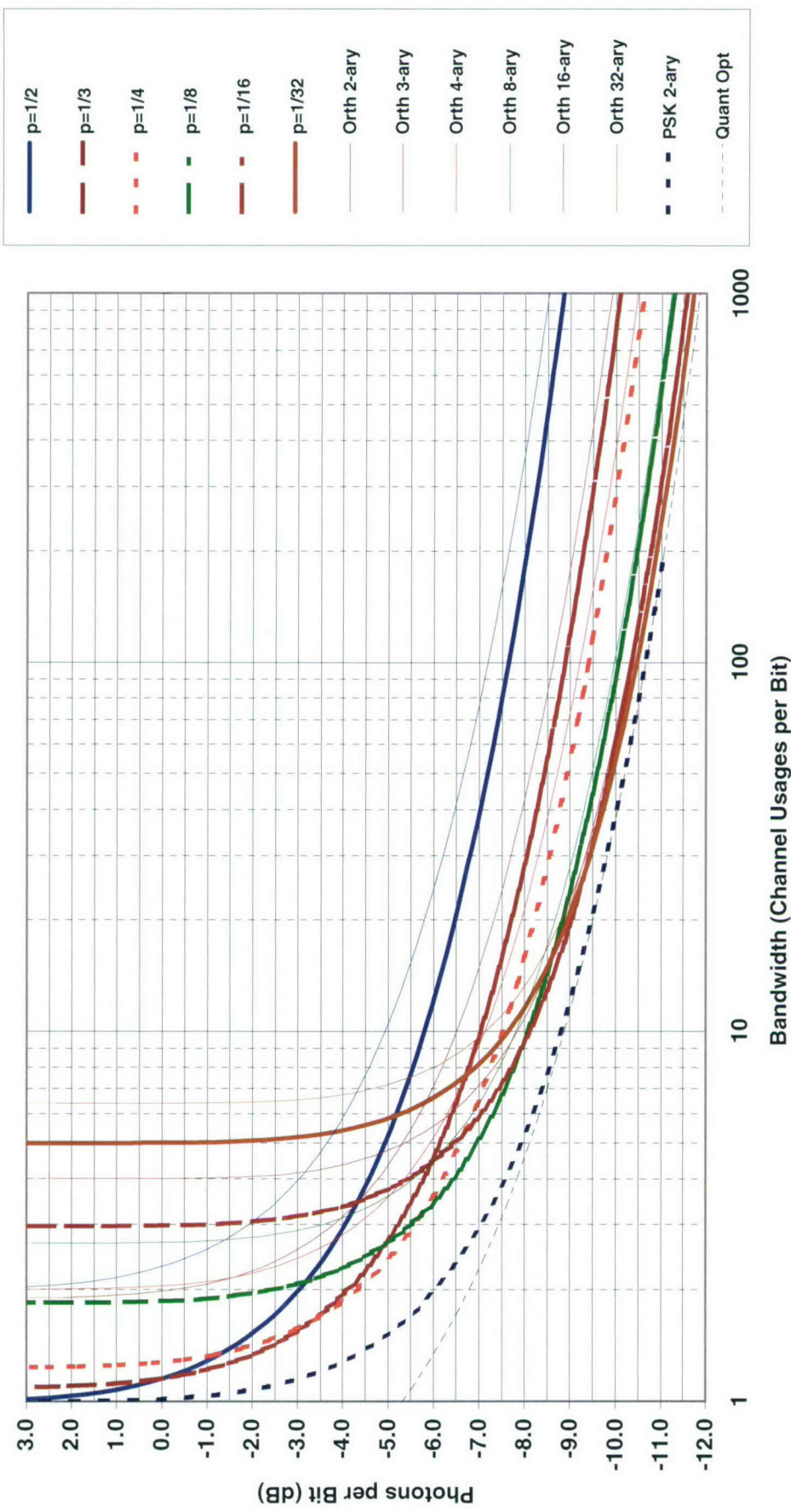
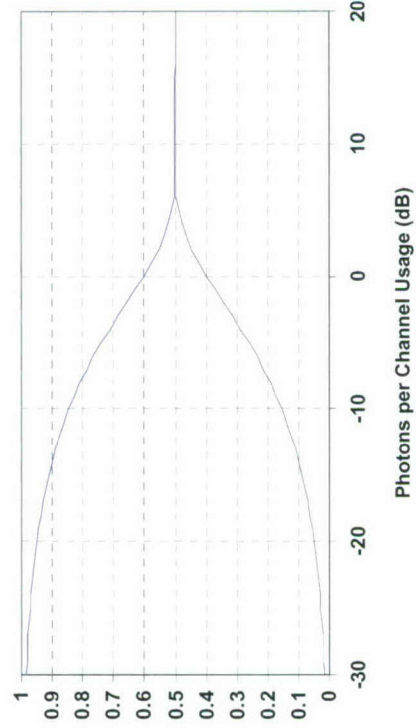
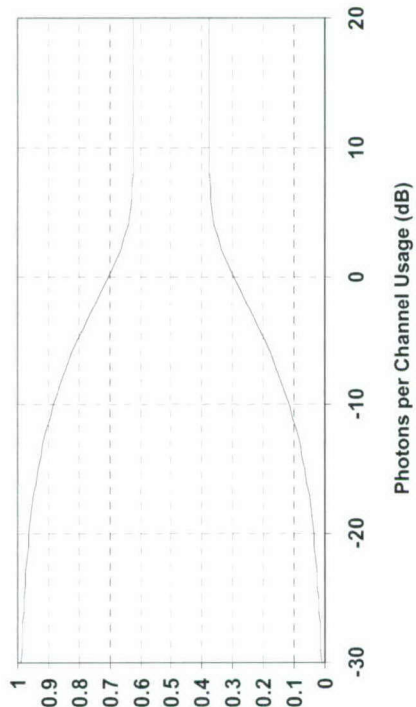


Chart 174. Comparison: Efficiency at capacity, quantum coded.

Quantum Eigenvalues
OOK $p=1/2$



Quantum Eigenvalues
OOK $p=1/4$



Quantum Eigenvalues
OOK $p=1/8$

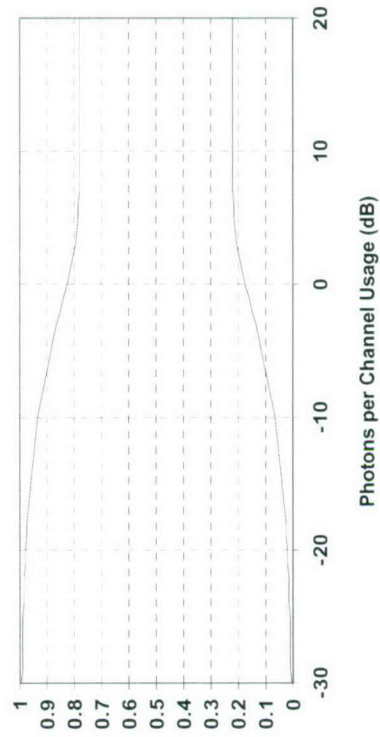
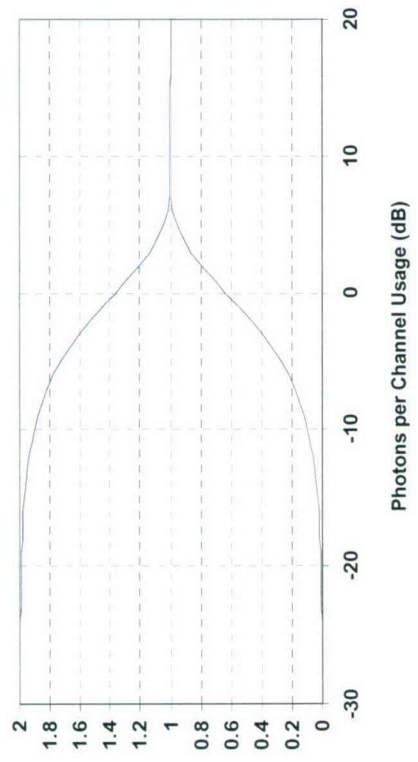
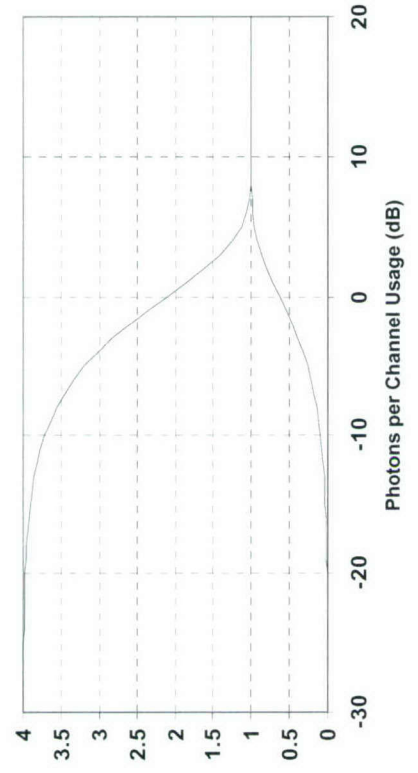


Chart 175. Quantum eigenvalues (λ_k): OOK.

Quantum Eigenvalues
2 Orth



Quantum Eigenvalues
4 Orth



Quantum Eigenvalues
8 Orth

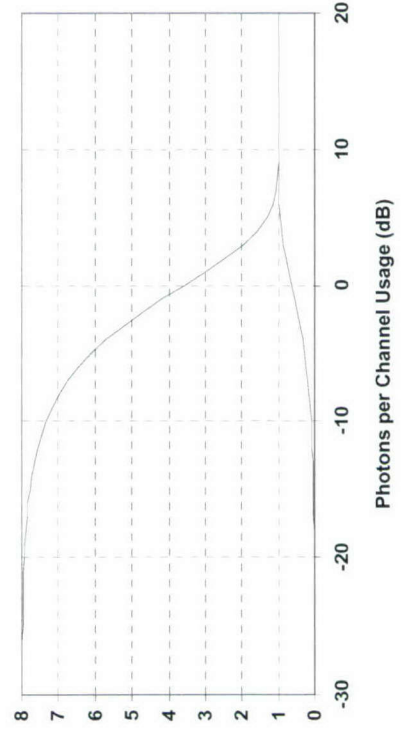
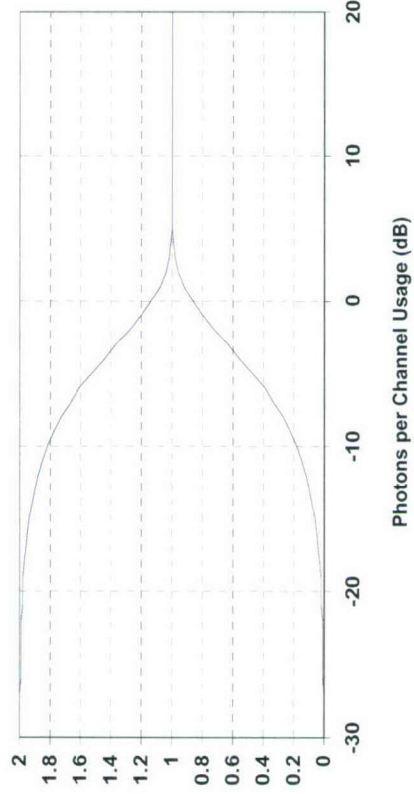
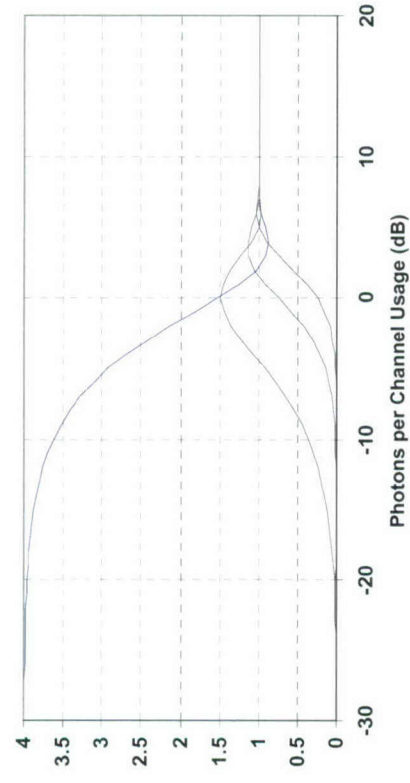


Chart 176. Quantum eigenvalues (v_k): Orthogonal.

Quantum Eigenvalues
2PSK



Quantum Eigenvalues
4PSK



Quantum Eigenvalues
8PSK

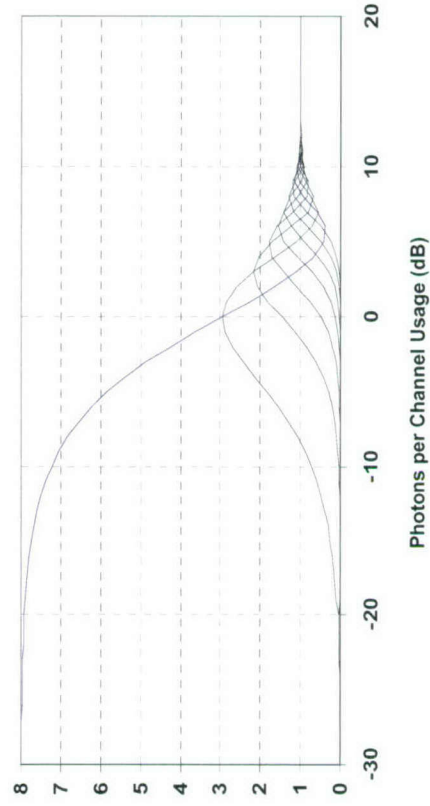


Chart 177. Quantum eigenvalues (ν_k): PSK.

REPORT DOCUMENTATION PAGE

Form Approved
OMB No. 0704-0188

Public reporting burden for this collection of information is estimated to average 1 hour per response, including the time for reviewing instructions, searching existing data sources, gathering and maintaining the data needed, and completing and reviewing this collection of information. Send comments regarding this burden estimate or any other aspect of this collection of information, including suggestions for reducing this burden to Department of Defense, Washington Headquarters Services, Directorate for Information Operations and Reports (0704-0188), 1215 Jefferson Davis Highway, Suite 1204, Arlington, VA 22202-4302. Respondents should be aware that notwithstanding any other provision of law, no person shall be subject to any penalty for failing to comply with a collection of information if it does not display a currently valid OMB control number. **PLEASE DO NOT RETURN YOUR FORM TO THE ABOVE ADDRESS.**

1. REPORT DATE (DD-MM-YYYY) 9 September 2005			2. REPORT TYPE Special Report		3. DATES COVERED (From - To)	
4. TITLE AND SUBTITLE Optical Communications: A Compendium of Signal Formats, Receiver Architectures, Analysis Mathematics, and Performance Comparisons					5a. CONTRACT NUMBER FA8721-05-C-0002	
					5b. GRANT NUMBER	
					5c. PROGRAM ELEMENT NUMBER	
6. AUTHOR(S) Don M. Boroson					5d. PROJECT NUMBER	
					5e. TASK NUMBER	
					5f. WORK UNIT NUMBER	
7. PERFORMING ORGANIZATION NAME(S) AND ADDRESS(ES) MIT Lincoln Laboratory 244 Wood Street Lexington, MA 02420-9108					8. PERFORMING ORGANIZATION REPORT NUMBER 60-1054	
9. SPONSORING / MONITORING AGENCY NAME(S) AND ADDRESS(ES) NASA Goddard Building 19, Room S028 Greenbelt, MD 20771					10. SPONSOR/MONITOR'S ACRONYM(S)	
					11. SPONSOR/MONITOR'S REPORT NUMBER(S) ESC-TR-2005-060	
12. DISTRIBUTION / AVAILABILITY STATEMENT Approved for public release; distribution is unlimited.						
13. SUPPLEMENTARY NOTES						
14. ABSTRACT There are a number of options for modulation formats in optical fiber and free-space lasercom systems. There are a seemingly even greater number of options for receiver architectures. Although most of these possibilities and combinations have been analyzed in journal publications and textbooks, there does not seem to be a <i>single</i> place to look for all relevant results concerning these options. Furthermore, comparisons of the options do not seem to have been methodically tabulated. In this work, then, we will present, describe, analyze, and compare the theoretical communications performance metrics of the most common optical modulation formats paired with the basic classes of receiver types.						
15. SUBJECT TERMS						
16. SECURITY CLASSIFICATION OF:			17. LIMITATION OF ABSTRACT Same as Report	18. NUMBER OF PAGES 268	19a. NAME OF RESPONSIBLE PERSON	
a. REPORT Unclassified	b. ABSTRACT Unclassified	c. THIS PAGE Unclassified			19b. TELEPHONE NUMBER (include area code)	